

**SPATIAL ANALYSIS OF GROUNDWATER QUALITY  
USING GEOPHYSICAL AND GEOCHEMICAL  
APPROACH IN UTHAL, BALOCHISTAN**



SHAISTA MAHMUD  
02-283161-003

A thesis submitted in fulfilment of the  
requirements for the award of the degree of  
Doctor of Philosophy (Geophysics)

Department of Earth and Environmental Sciences

BAHRIA UNIVERSITY KARACHI CAMPUS

OCTOBER 2023

## **Approval for Examination**

**Scholar's Name:** Shaista Mahmud

**Registration No:** 31406

**Programme of Study:** Geophysics

**Thesis Title:** “Spatial Analysis of Groundwater Quality using Geophysical and Geochemical approach in Uthal, Balochistan”

It is to certify that the above scholar's thesis has been completed to my satisfaction and, to my belief, its standard is appropriate for submission for examination. I have also conducted plagiarism test of this thesis using HEC prescribed software and found similarity index 19% that is within the permissible limit set by HEC for the PhD degree thesis. I have also found the thesis in a format recognized by the BU for the PhD thesis.

### **Principal Supervisor**

Dr. Salma Hamza  
HOD/Senior Associate Professor  
Department of Earth & Environmental Sciences

**Signature:**



**Date:** 25 October 2023

## **AUTHOR'S DECLARATION**

I, Shaista Mahmud hereby state that my Ph.D. thesis titled “Spatial Analysis of Groundwater Quality using Geophysical and Geochemical approach in Uthal, Balochistan” is my own work and has not been submitted previously by me for taking any degree from Bahria University (Karachi Campus) or anywhere else in the country/world. At any time if my statement is found to be incorrect even after my graduation, the University has the right to withdraw/cancel my Ph.D. degree.



Name of Scholar: Shaista Mahmud

Date: 25 October 2023

## **PLAGIARISM UNDERTAKING**

I, solemnly declare that the research work presented in the thesis titled “Spatial Analysis of Groundwater Quality using Geophysical and Geochemical approach in Uthal, Balochistan” is solely my research work with no significant contribution from any other person. Small contribution / help wherever taken has been duly acknowledged and that complete thesis has been written by me.

I understand the zero tolerance policy of the HEC and Bahria University towards plagiarism. Therefore, I as an author of the above titled thesis declare that no portion of my thesis has been plagiarized and any material used as reference is properly referred/cited.

I undertake that if I am found guilty of any formal plagiarism in the above titled thesis even after award of Ph.D. degree, the university reserves the right to withdraw / revoke my Ph.D. degree and that HEC and the University have the right to publish my name on the HEC /University website on which names of scholars are placed who submitted plagiarized thesis.

**Scholar / Author’s Sign:**



**Name of the Scholar:** Shaista Mahmud



## **ACKNOWLEDGMENT**

Firstly, I am very thankful to The God Almighty, the most benevolent and merciful, for the completion of my research work. I acknowledge the generous and intellectual support of my supervisor Dr. Salma Hamza for her support, motivation, and immense knowledge. Her guidance helped me throughout the time of research and writing of this thesis. I acknowledge the guidance provided by my Co-supervisor, Dr. Anwar Qadir with whose guidance I was able to complete my thesis work. I am thankful to the Principal Bahria School of Engineering and Applied Science, Dr. Sohaib Ahmed and Principal Bahria School of Maritime and applied Sciences Dr. Asif Inam for their continuous support, guidance and encouragement. I am grateful to my family members, my friends & colleagues, Mr. Muhammad Irfan, Ms. Ayla Wajahat, Mr. Ahsan Majeed Qureshi, and Dr. Syed Nawaz Ul Huda for supporting me throughout my research work. I am grateful to the support extended to me by the Director General and Director Bahria University Karachi campus. This thesis is part of the National Research Program for Universities project (HEC-NRPU # 5250), Higher Education Commission of Pakistan. I would like to thank the HEC funding and research support.

## **DEDICATION**

I dedicate this research work to my parents who are not there to see this but had made me what I am today, to my daughters, my husband, and my friends for their immense support and encouragement.

## ABSTRACT

Uthal is located in Lasbela District in Pakistan's Balochistan province. It has an arid to semi-arid climate, and the main source of fresh water for domestic and agricultural purposes is groundwater. To determine the spatial distribution of groundwater and its quality, an electrical resistivity survey was carried out using the schlumberger array. The PASI Electrical Resistivity Imaging System was utilized to examine 25 stations in the study area, to investigate a depth of 150 meter. IPI2win software was used for curve matching to assess the measured geoelectrical characteristics. The Dar Zarrouk parameters were computed after identifying five geoelectrical layers. The resistivity of the topmost, thinnest layer of unconsolidated material ranged from 600 to 2600  $\Omega\text{m}$ . The resistivity of the second layer of unconsolidated sand and gravel ranged from 50 to 11500  $\Omega\text{m}$ ; that of the third layer of dry sand and clay was up to 200  $\Omega\text{m}$ ; that of the fourth layer showed a thick freshwater zone with a resistivity between 75 and 100  $\Omega\text{m}$ ; and that of the layer after that showed a thick layer of sand and clay with fresh water had a resistivity of between 48 and 90  $\Omega\text{m}$ . The Dar Zarrouk parameters estimated for longitudinal unit conductance (S), ranges from 0.1 to 1.65 mho, transverse unit resistance (T), which is larger than 25000  $\Omega\text{m}^2$ , longitudinal resistance ( $R_S$ ), which ranges from 50 to 1350  $\Omega\text{m}$ , and transverse resistivity ( $R_T$ ), which ranges from 22 to 1150  $\Omega\text{m}$ . The ERS data and Dar Zarrouk characteristics identified the freshwater zones in the subsurface. Small pockets of saline water were found in few near surface zones due to evaporation owing to the arid and semi-arid surface conditions. There has been no indication of seawater intrusion, from the ERS data and Dar Zarrouk characteristics. To confirm the findings of electrical resistivity data, groundwater samples from 100 sites were collected from the study area. Chemical analyses were performed for major cations and anions present in water. In addition, to study the

characteristic of water, trace element analysis was also performed on the samples. The major cations and anions of the study area are, Sodium (Na) (50.7 to 1858 mg/l), Chloride (Cl) (6.2 to 2150 mg/l), Potassium (K) (1 to 34 mg/l), Calcium (Ca) (19 to 857 mg/l), Magnesium (Mg) (5.77 to 281 mg/l), Bicarbonates ( $\text{HCO}_3$ ) (58 to 860 mg/l), Sulfate ( $\text{SO}_4$ ) (44 to 4411 mg/l) &  $\text{NO}_3$  (48 to 854). The trace elements are, Aluminum (Al) (5 to 756  $\mu\text{g/l}$ ), Chromium (Cr) (0.5 to 114  $\mu\text{g/l}$ ), Cadmium (Cd) (0 to 24  $\mu\text{g/l}$ ), Chromium (Cu) (0.05 to 354  $\mu\text{g/l}$ ), Manganese (Mn) (2 to 675  $\mu\text{g/l}$ ), Nickel (Ni) (0 to 412  $\mu\text{g/l}$ ), Lead (Pb) (1.5 to 79  $\mu\text{g/l}$ ), Zinc (Zn) (5 to 801  $\mu\text{g/l}$ ) and Arsenic (As), Cobalt (Co), & Titanium (Ti) below detection limits. Estimates were made for the physical parameters; alkalinity, total dissolved solids, and electric conductance parameters. The concentration of main cations, anions, and trace elements are within the permissible limits as per WHO standards, except for a few sample points. The sedimentary rocks and the mineralization of the Bela Ophiolites exposed in the study area are the main sources of these cations, anions, and trace elements. The study integrated the Dar zarrouk parameters, as calculated from the electrical resistivity values ( $\rho$ ), and the corresponding Total Dissolved Salts (TDS) values. The study area has been divided into four zones namely, very good potential (TDS < 500 mg/l &  $\rho$  from 200 to 1500  $\Omega\text{m}$ ), good potential (TDS from 501 to 1000 mg/l &  $\rho$  from 100 to 200  $\Omega\text{m}$ ), fair potential (TDS from 1001 to 2000 mg/l & 20 to 100  $\Omega\text{m}$ ) and poor potential zones (TDS > 2000 mg/l &  $\rho$  < 20  $\Omega\text{m}$ ). The current study has provided the quantitative legend of the area. This legend can be quantified and applied to surrounding semi-arid to arid of the area. This is valid for reservoir modeling and changes in hydrofacies and trend analysis for good water management practices.

## TABLE OF CONTENT

<b>AUTHOR’S DECLARATION</b>	<b>iii</b>
<b>PLAGIARISM UNDERTAKING</b>	<b>iv</b>
<b>ACKNOWLEDGMENT</b>	<b>v</b>
<b>DEDICATION</b>	<b>vi</b>
<b>ABSTRACT</b>	<b>vii</b>
CHAPTER 1 .....	1
1.1 Introduction .....	1
1.2 Spatial Dimensions and groundwater quality .....	3
1.3 Previous Work .....	4
1.4 Gap Analysis .....	5
1.5 Problem Statement.....	6
1.6 Significance of the Study.....	7
1.7 Objectives of the study .....	8
1.8 Description of the Study Area .....	9
1.8.1 Population .....	11
1.8.2 Climate.....	11
1.8.3 Physical Structure .....	12
1.8.4 Hills.....	12
1.8.5 Plains.....	13
1.8.6 Coastal Area.....	13
1.9 Drainage System.....	13
1.10 Geology of the Study Area .....	15
1.10.1 Ferozabad Group.....	15
1.10.2 Sembar Formation.....	15
1.10.3 Bela Ophiolite .....	16
1.11 Soil.....	16
1.12 Agriculture.....	16

1.13 Vegetation and Forest.....	17
CHAPTER 2 LITERATURE REVIEW .....	18
2.1 Introduction .....	18
2.2 Spatial study of groundwater.....	19
2.3 Geophysical technique and groundwater quality.....	20
2.4 Geology of the Study Area.....	22
2.4.1 Ferozabad Group.....	23
2.4.2 Sembar Formation.....	28
2.4.3 Bela volcanic group .....	29
2.5 Rocks and Soil Contribution .....	30
CHAPTER 3 RESEARCH METHODOLOGY.....	32
3.1 Introduction .....	32
3.2 Study Area.....	35
3.3 Electrical Resistivity Survey .....	35
3.4 Water Sampling Guidelines.....	45
3.5 Preparation of collected samples for geochemical analyses.....	47
3.6 Geochemical analysis of water samples .....	47
3.6.1 Alkalinity/acidity .....	48
3.6.2 Titrimetry .....	48
3.6.3 Flame photometry .....	51
3.6.4 ICP-MS .....	53
3.6.5 Gravimetry .....	55
3.7 Precision and accuracy .....	56
3.7.1 Water Sample Preparation .....	56
3.7.2 Presentation of Results.....	57
3.8 Supporting software.....	61
3.8.1 Microsoft Excel.....	61
3.8.2 Google Earth Engine.....	62
3.8.3 IPI 2 Win.....	62
3.8.4 Global Mapper .....	65
3.8.5 ArcGIS .....	65
3.8.6 Grapher .....	67
3.9 Statistical Analysis.....	67
3.9.1 Measure of Central Tendency and Dispersion.....	68
3.9.2 Principal Component Analysis.....	69
CHAPTER 4 .....	71

4.1 Introduction .....	71
4.2 Geochemistry.....	74
4.2.1 pH and Alkalinity of groundwater .....	80
4.2.2 Electrical Conductivity (EC) and Total Dissolved Solids (TDS) .....	82
4.2.3 Sodium (Na) and Potassium (K).....	84
4.2.4 Calcium (Ca) and Magnesium (Mg) .....	86
4.2.5 Sulphate (SO <sub>4</sub> ) & Chloride (Cl) .....	88
4.2.6 Bicarbonate .....	91
4.2.7 Nitrate .....	92
4.3 Ionic Composition .....	94
4.4 Hydrofacies.....	94
4.5 Analysis of Stiff pattern.....	96
4.6 Trace Elements .....	110
4.6.1 Cadmium.....	110
4.6.2 Chromium .....	112
4.6.3 Copper.....	112
4.6.4 Iron.....	113
4.6.5 Manganese .....	113
4.6.6 Nickel.....	113
4.6.7 Lead.....	114
4.6.8 Zinc .....	114
CHAPTER 5 .....	117
5.1 Introduction .....	117
5.2 Basic Principle.....	118
5.2.1 Vertical Electrical Sounding (VES).....	119
5.2.2 Electrode Configurations .....	120
5.3 Electrical Resistivity of study area .....	124
5.4 Interpretation of VES Points .....	127
5.5 Spatial Distribution of geoelectrical layers, thickness and depth .....	152
5.6 Estimation of (D-Z) Dar Zarrouk Parameters from the Electrical Resistivity data .....	164
5.7 Well log Data.....	170
CHAPTER 6 .....	171
6.1 Introduction .....	171
6.2 Hydro geochemical Data .....	174
6.2.1 Elemental Analysis of Groundwater Samples.....	174
6.2.2 Correlation Matrix .....	178

6.2.3 Principal Component Analysis (PCA) .....	178
6.2.4 Trace Element Analysis .....	180
6.3 Rock-water Interaction .....	184
6.4 Electrical Resistivity Sounding Data.....	185
6.4.1 Geoelectrical Layers .....	185
6.4.2 The Dar Zarrouk (D-Z) Parameters .....	188
6.4.5 Subsurface Model .....	190
6.5 Integration of ERS and geochemical data .....	192
6.5.1 Geoelectrical layer 4 and geochemical parameters .....	192
6.5.2 Geoelectrical layer 5 and geochemical parameters .....	198
6.6 Groundwater Zones .....	204
CHAPTER 7 .....	206
RECOMMENDATIONS .....	210
REFERNCE .....	211



## LIST OF FIGURES

Figure 1.1 (a) The total water on earth and its distribution in saline and fresh water. (b) The total freshwater distribution. (c) Details of the fresh surface water as a pie chart Gupta (2021).....	2
Figure 1.2 Location of the Study Area- District Lasbela, Balochistan. ....	10
Figure 1.3 Average yearly temperature of Uthal shows high to warm weather.....	12
Figure 1.4 Drainage of the Study Area (Hamza, 2019). The important sites include towns and villages. ....	14
Figure 1.5 Distribution of banana crop, shrubs and grassland, other crops and bare soil in Uthal. ....	17
Figure 2.1 Generalized geological map of the study area, simplified after (Bashir et al., 2009; DeJong & Subhani, 1979).....	26
Figure 2.2 Generalized stratigraphy of the study area (Shah, 2009).....	27
Figure 2.3 A schematic diagram showing the elemental contribution from the geology of the study area (after Hamza, 2011).....	31
Figure 3.1 Flow chart showing the methodology of the thesis. ....	34
Figure 3.2 (a) An electric circuit with a battery and resistor. (b) An electric resistor depicting earth material having length $L$ , and area of cross-section $A$ . ....	37
Figure 3.3 Schematic diagram showing the current and equipotential lines in the subsurface (Robinson, 1988).....	38
Figure 3.4 Various electrode configurations used for electrical resistivity measurements (Robinson, 1988).....	39
Figure 3.5 Acquiring data using PASI 16GLN.....	41
Figure 3.6 Schlumberger electrode configuration used in resistivity measurements (Anomohanran, 2013).....	42
Figure 3.7 Earth Resistivity and the conductivity values for different subsurface materials.	

(Palacky, 1987). .....	44
Figure 3.8 Resistivity Curves of various types are shown in the figure from A to F: These types represent the number of the subsurface resistivity layers and their behavior in subsurface.(Sharma & Baranwal, 2005) .....	44
Figure 3.9 Titration for Ca and Mg.....	49
Figure 3.10 ICP-MS color analysis of elements. Groupings of elements that are typically identified by ICP-MS are color-coded. Alkali earth and alkaline earth are light blue; transition metals are yellow; other metals are orange; metalloids are magenta; halogens are dark blue; noble gases are red; and rare earth elements from the Lanthanide and Actinide families are pale green. (Calvete et al., 2017).....	53
Figure 3.11 The piper diagram used to represent the chemistry of water samples (Fetter, 2001)	58
Figure 3.12 Hydrochemical classification for natural water using the Piper diagram(Fetter, 2001) .....	60
Figure 3.13 Stiff pattern showing cation and anion distribution across the zero axis line (Stiff, 1951) .....	61
Figure 3.14 IPI2WIN Software curve window .....	64
Figure 3.15 IPI2WIN Software cross-section window .....	64
Figure 4.1 Location of water samples.....	73
Figure 4.2 pH distribution for the study area.....	81
Figure 4.3 Spatial distribution of Total Dissolved Salts TDS.....	83
Figure 4.4 Spatial distribution of electrical conductivity ( $\mu\text{s}/\text{cm}$ ) .....	83
Figure 4.5 Spatial Distribution of Sodium (mg/l) .....	85
Figure 4.6 Spatial distribution of Potassium (mg/l).....	86
Figure 4.7 Spatial distribution of Calcium (mg/l).....	87
Figure 4.8 Spatial distribution of Magnesium (mg/l) .....	88
Figure 4.9 Spatial distribution of $\text{SO}_4$ (mg/l) .....	90
Figure 4.10 Spatial distribution of Chlorides (mg/l).....	90
Figure 4.11 Spatial concentration of Bicarbonates (mg/l) .....	91
Figure 4.12 Spatial concentration of $\text{NO}_3$ (mg/l) .....	92
Figure 4.13 Piper diagram of groundwater chemistry in the Uthal.....	95
Figure 4.14 Stiff pattern of groundwater samples from the Uthal (samples 1 to10).....	100
Figure 4.15 Stiff pattern of groundwater samples from the Uthal (samples 11 to 20).....	101
Figure 4.16 Stiff pattern of groundwater samples from the Uthal (samples 21 to 30).....	102
Figure 4.17 Stiff pattern of groundwater samples from the Uthal (samples 31 to 40).....	103

Figure 4.18	Stiff pattern from groundwater samples from Uthal (41 to 50).....	104
Figure 4.19	Stiff pattern for groundwater samples of Uthal (51 to 60) .....	105
Figure 4.20	Stiff pattern from groundwater samples for Uthal (61 to 70).....	106
Figure 4.21	Stiff pattern for groundwater samples of Uthal (71 to 80) .....	107
Figure 4.22	Stiff pattern for groundwater samples for Uthal (81 to 90).....	108
Figure 4.23	Stiff pattern for groundwater samples for Uthal (91 to 100).....	109
Figure 4.24	Concentration of trace elements in the study area ( $\mu\text{g/l}$ ).....	115
Figure 4.25	Concentration of trace elements in the study area ( $\mu\text{g/l}$ ).....	116
Figure 5.1	Wenner Electrode Configuration.....	121
Figure 5.2	Schlumberger Electrode Configuration .....	122
Figure 5.3	Dipole- Dipole Electrode Configuration .....	122
Figure 5.4	Pole-Pole Electrode Configuration.....	123
Figure 5.5	Electrical Resistivity Ranges in ohm-m and conductivity in mS/m for various Earth materials (Palacky, 1987).....	123
Figure 5.6	Location of Electrical Resistivity Data points shown on the geologic map of the area. Well locations are also marked (Bashir et al., 2009). .....	125
Figure 5.7	The modeled resistivity curves using IPI2Win Software for UT-01.....	127
Figure 5.8	The modeled resistivity curves using IPI2Win Software for UT-02.....	128
Figure 5.9	The modeled resistivity curves using IPI2Win Software for UT-03.....	129
Figure 5.10	The modeled resistivity curves using IPI2Win Software for UT-04.....	130
Figure 5.11	The modeled resistivity curves using IPI2Win Software for UT-05.....	131
Figure 5.12	The modeled resistivity curves using IPI2Win Software for UT-06.....	132
Figure 5.13	The modeled resistivity curves using IPI2Win Software for UT-07.....	133
Figure 5.14	The modeled resistivity curves using IPI2Win Software for UT-08.....	134
Figure 5.15	The modeled resistivity curves using IPI2Win Software for UT-09.....	135
Figure 5.16	The modeled resistivity curves using IPI2Win Software for UT-10.....	136
Figure 5.17	The modeled resistivity curves using IPI2Win Software for UT-11.....	137
Figure 5.18	The modeled resistivity curves using IPI2Win Software for UT-12.....	138
Figure 5.19	The modeled resistivity curves using IPI2Win Software for UT-13.....	139
Figure 5.20	The modeled resistivity curves using IPI2Win Software for UT-14.....	140
Figure 5.21	The modeled resistivity curves using IPI2Win Software for UT-15.....	141
Figure 5.22	The modeled resistivity curves using IPI2Win Software for UT-16.....	142
Figure 5.23	The modeled resistivity curves using IPI2Win Software for UT-17.....	143
Figure 5.24	The modeled resistivity curves using IPI2Win Software for UT-18.....	144

Figure 5.25	The modeled resistivity curves using IPI2Win Software for UT-19. ....	145
Figure 5.26	The modeled resistivity curves using IPI2Win Software for UT-20. ....	146
Figure 5.27	The modeled resistivity curves using IPI2Win Software for UT-21. ....	147
Figure 5.28	The modeled resistivity curves using IPI2Win Software for UT-22. ....	148
Figure 5.29	The modeled resistivity curves using IPI2Win Software for UT-23. ....	149
Figure 5.30	The modeled resistivity curves using IPI2Win Software for UT-24. ....	150
Figure 5.31	The modeled resistivity curves using IPI2Win Software for UT-25. ....	151
Figure 5.32	Iso-resistivity contour map of layer 1 .....	154
Figure 5.33	Iso-resistivity contour map of layer 2.....	155
Figure 5.34	Iso-resistivity contour map of layer 3.....	156
Figure 5.35	Iso-resistivity contour map of layer 4.....	157
Figure 5.36	Iso-resistivity contour map of layer 5.....	158
Figure 5.37	Thickness contour map of Layer 1. The contours are in meters (m) .....	159
Figure 5.38	Thickness contour map of layer 2. The contours are in meters (m) .....	160
Figure 5.39	Thickness contour map of Layer 3. The contours are in meters (m).....	161
Figure 5.40	Thickness contour map of Layer 4. ....	162
Figure 5.41	Thickness contour map of Layer 5. ....	163
Figure 5.42	Contour map of Longitudinal Unit Conductance (S) .....	166
Figure 5.43	Contour map of Transverse Unit Resistance (T).....	167
Figure 5.44	Contour map of Longitudinal Resistivity (RS).....	168
Figure 5.45	Contour map of Transverse Resistivity ( $R_T$ ) .....	169
Figure 5.46	Lithology log for two boreholes Well A and Well B from study area .....	170
Figure 6.1	(a) TDS and the (b) pH distribution in shown is graphical form WHO Standards (WHO, 2017) .....	176
Figure 6.2	Elemental distribution in graphical form is shown (WHO, 2017).....	177
Figure 6.3	Rotated Space Diagram (PCA) shows the genetic affiliation of the major ions in the groundwater of the study area.....	179
Figure 6.4	Trace Element distribution in graphical form is shown, WHO Standard (WHO, 2022). The values are given in $\mu\text{g/l}$ .....	181
Figure 6.5	Resistivity Layers and lithologies from the well logs. ....	187
Figure 6.6	The 3D subsurface model from the geoelectrical layers and bore hole data. Four major lithologies have been identified a. Unconsolidated Surficial material b. Sand and Gravel c. Sand and Clay and d. Sand (water bearing). The blue line shows top of the water bearing layer. ....	190

Figure 6.7 The correlation between two well logs with the lithologies identified from the resistivity data. A fifth layer comprising of Clay can be seen at a few ERS points.....	191
Figure 6.8 Geoelectrical layer 4 and TDS distribution of the study area.....	193
Figure 6.9 Geoelectrical layer 4 and Ca distribution of the study area.....	194
Figure 6.10 Geoelectrical layer 4 and Na distribution of the study area.....	194
Figure 6.11 Geoelectrical layer 4 and HCO <sub>3</sub> distribution of the study area.....	195
Figure 6.12 Geoelectrical layer 4 and K distribution of the study area .....	195
Figure 6.13 Geoelectrical layer 4 and Mg distribution of the study area.....	196
Figure 6.14 Geoelectrical layer 4 and SO <sub>4</sub> distribution of the study area.....	196
Figure 6.15 Geoelectrical layer 4 and Cl distribution of the study area .....	197
Figure 6.16 Geoelectrical layer 4 and the NO <sub>3</sub> distribution of the study area .....	197
Figure 6.17 Geoelectrical layer 5 and TDS distribution of the study area.....	199
Figure 6.18 Geoelectrical layer 5 and Ca distribution of the study area.....	199
Figure 6.19 Geoelectrical layer 5 and HCO <sub>3</sub> distribution of the study area.....	200
Figure 6.20 Geoelectrical layer 5 and K distribution of the study area .....	200
Figure 6.21 Geoelectrical layer 5 and Na distribution of the study area.....	201
Figure 6.22 Geoelectrical layer 5 and Mg distribution of the study area.....	201
Figure 6.23 Geoelectrical layer 5 and SO <sub>4</sub> distribution of the study area.....	202
Figure 6.24 Geoelectrical layer 5 and Cl distribution of the study area .....	202
Figure 6.25 Geoelectrical layer 5 and NO <sub>3</sub> distribution of the study area. ....	203
Figure 6.26 The groundwater zones (a) shows the distribution of TDS (b) resistivity distribution of fourth layer (c) the groundwater zones from the correlation of TDS and resistivity.....	204

## LIST OF TABLES

Table 4.1 Measure of hardness (WHO, 2017) .....	75
Table 4.2 Physical parameters for water samples of study area .....	75
Table 4.3 Major ions for water samples of study area .....	78
Table 4.4 Physical parameters and major cation and anions of the study area (WHO, 2017).....	93
Table 4.5 Trace element analysis of water samples of the study area .....	111
Table 5.1 VES Points with latitudes, longitudes and elevations.....	126
Table 5.2 Depth, thickness and distribution of geoelectrical layers .....	152
Table 5.3 The estimated values of Dar Zarrouk Parameters .....	165
Table 6.1 Correlation Matrix of major elements in groundwater .....	178
Table 6.2 WHO drinking water permissible limits .....	182
Table 6.3 Minimum, Maximum and mean values of the physical parameters and major cations and anion in the water samples of the study area.....	183
Table 6.4 Minimum, Maximum and mean values of the trace elements of the water samples of the study area .....	183
Table 6.5 Summary of the geoelectrical layers of study area .....	186
Table 6.6 Lithologies from the well log data of the study area.....	188
Table 6.7 Reference values for Dar Zarrouk parameters for fresh and saline water.....	189
Table 6.8 Comparison of TDS and Resistivity Values and the Groundwater Zones.....	205

## LIST OF ABBREVIATIONS

Al	Aluminum
As	Arsenic
BDL	Below Detection Limit
Ca	Calcium ion
Cd	Cadmium
Cl	Chloride
Co	Cobalt
Cr	Chromium
Cu	Copper
D.C	Calcium ion Direct Current
DZ	Dar Zarrouk
EC	Electrical conductivity
ERS	Electrical Resistivity Survey
Fe	Iron
GPS	Geographical position System
HCO <sub>3</sub>	Bicarbonates
IP	Induced Potential
K	Potassium
MASL	Mean Average Sea Level
Mg	Magnesium ion

MHT	Maximum Holding Time
Mn	Manganese
Na	Sodium
Ni	Nickle
Pb	Lead
PH	Potential hydrogen
R <sub>S</sub>	Longitudinal resistivity
R <sub>T</sub>	Transverse resistivity
S	Longitudinal conductance
T	Transverse unit resistance
SO <sub>4</sub>	Sulfate
TDS	Total dissolved solids
VES	Vertical Electrical Sounding
WHO	World Health Organization
Zn	Zinc



## LIST OF SYMBOLS

I	Current
K	Geometric factor
$\Omega$	Resistance
$\Delta V$	Potential difference
$\rho$	Apparent resistivity
$\Omega\text{-m}$	Ohm-meter
mg/l	Milligrams per liter
$\mu\text{g/l}$	Micrograms per liter
$\mu\text{S/m}$	Micro Siemens per meter

# CHAPTER 1

## INTRODUCTION

### 1.1 Introduction

Our planet earth is called the blue planet because 71 % of its surface is covered by water. The 97% of water on earth is saline water and present in oceans, and approximately 3% is the freshwater Gupta (2021). The distribution earth's water is given in Figure 1.1. The total freshwater reserves are only approximately 3% and the groundwater constitutes of 30% of this freshwater reserve. Thus the importance of groundwater and its quality is immense.

Life on earth depends on water and its use has increased exponentially over the past several decades due to population expansion. Rains fluctuate due to climate change. Pakistan's surface water resources are not sufficient to meet the increase demand of water. The surface water resources mainly consist of Indus River and its tributaries, with almost 65% of the flow being from Indus, 17% from Jhelum and 19% from Chenab. The water in other two rivers, Ravi and Sutlej is restricted under the Indus Basin Treaty Kahlown and Majeed (2003). Under such circumstances, the use of groundwater in Pakistan is increasing

rapidly (Haq et al., 2021; Khair et al., 2015; Khan et al., 2008; Rahman, 1996). The lack of focus on water recycling in developing countries, especially in Pakistan, has drawn the attention of researchers to the need for more and more research on water. Furthermore, in areas where rainfall is scarce and groundwater use is high, research work to check water quality should be carried out continuously.

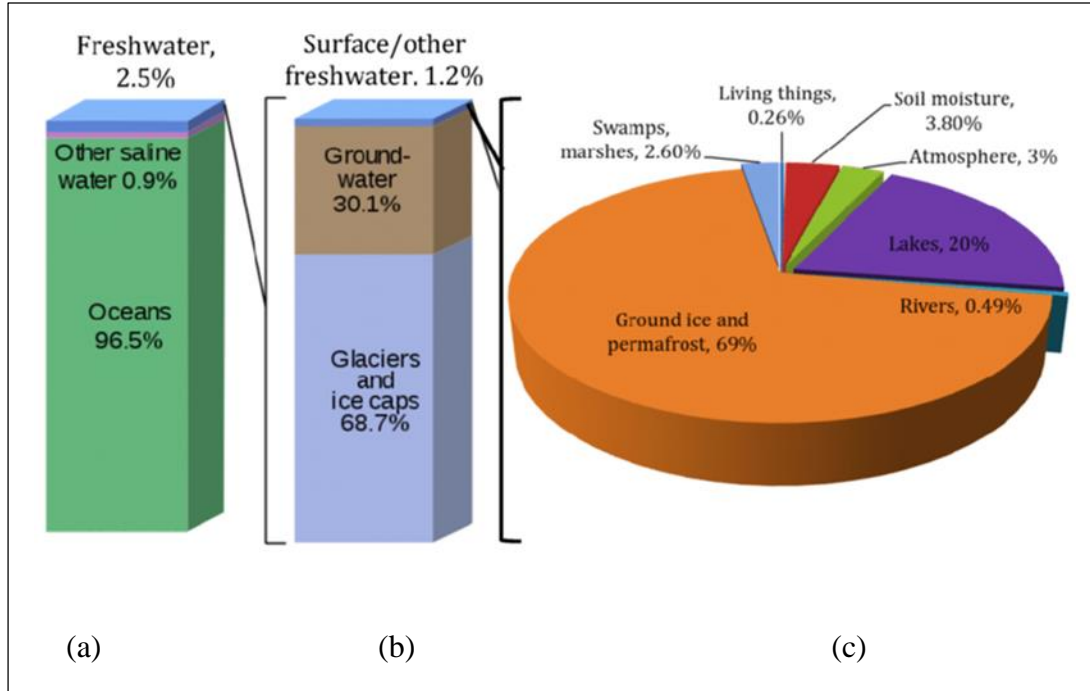


Figure 1.1 (a) The total water on earth and its distribution in saline and fresh water. (b) The total freshwater distribution. (c) Details of the fresh surface water as a pie chart Gupta (2021).

Uthal being a semi-arid area has always suffered water scarcity. According to the census of 2017 (DCR, 2017) there has been a rapid increase in the population, which has worsened the situation. The main sources of water are the groundwater resources and a few ephemeral streams (Hamza, 2011). Therefore, the quality of groundwater is the one of the main issues for the population of Uthal. Furthermore, the groundwater quality integrating ERS and geochemical data, in the surrounding areas of Uthal has been established on the basis of scarce data point, which makes any analysis weak and unreliable. In order to determine whether the water is fit for consumption and in line with the WHO's standards

there is a dire need to establish the integration of ERS and geochemical data.

## **1.2 Spatial Dimensions and groundwater quality**

Water is a prime necessity for life. Human life is simply impossible without drinking water. According to research, water content in the adult human body is 70% of its total body weight (Nakamura et al., 2020). The heart and brain consist of approximately 74% of water. Lungs, skin, bones, muscles, and kidneys contain about 84%, 64%, 32%, and 79% water, respectively (Randhir, 2012). Water, being the abundant chemical in the human body, plays a vital role in the regulation of nutrient transport, cell volume, and removal of wastes (Qadeer, 2004; Sajid et al., 2012).

Water quality depends on its source, which is primarily influenced by natural and human factors. In recent years (Bilotta & Brazier, 2008; Murdoch et al., 2000; Ntengwe, 2006), the main aim of environmental scientists has been to investigate water contamination with heavy metals. Heavy metals can be derived from both natural (weathering and erosion of ores and bedrocks) and anthropogenic (industries, mining, irrigation., wastewater and agriculture) origins (Prasad & Narayana, 2004).

Characteristics of rivers and groundwater are closely related to the rocks around them. Rocks disintegrate to form soil and the elements present in them dissolve in the water to change their chemical properties (Burke et al., 2016; Fulai et al., 2021; Zhang et al., 2021). In the same way, groundwater dissolves rock constituents in close proximity in accordance with their properties. That is why the water that flows on the ground surface and underground has different effects on different aspects due to the rock composition. Water analysis over spatial dimensions makes it easier to identify the difference of water chemistry of one area from that of another (Smith et al., 1997). Natural factors are more relevant than the issues resulting from human activities which cause disruption. One of the factors of water quality variation is that the levels of various trace elements and compounds in available water supplies vary due to differences in geological and geographical factors

(Hamza, 2011). Although trace elements often seem to be very insignificant nevertheless, they do have an essential role in life; therefore, identification and quality assessment of these elements become necessary. Polluted water can be very hazardous for human health. An excess amount of elements may cause harmful effects in the body. Polluted water may be the cause of severe diseases among humans, animals, and plants, sometimes even causing deaths (Kabata-Pendias, 2010). Toxic metals such as Pb, Cr, Cd, and Ni tend to accumulate in certain reservoirs (water, soils, sediments, etc.) from which they may be released by various processes of solubility and remobilization thereby entering into the biological food chain (Soetan et al., 2010).

### **1.3 Previous Work**

In the study area most of the work done is related to the geology of the area and water quality as assessed by the geochemical parameters particularly for irrigation. Very little work has been done by conducting the geophysical surveys for the investigation of spatial dimensions and the groundwater quality. The analysis of water chemistry and the impact of anthropogenic activities have been studied by Yang et al (2021) and Buke et al (2016). Many researchers have done the detailed assessment of the groundwater quality for different areas of Balochistan (Baloch et al., 2015; Bashir et al., 2007; Burke et al., 2016; Farid et al., 2014; Mustafa & Qazi, 2007; Naseem et al., 2010; Naseem et al., 2013; Naseem et al., 2014; Van Steenberg, 1995, 1996; Van Steenberg et al., 2015). The study area and adjoining areas have seen an increase in the agricultural activities over the last few decades. Farid et al., 2014 have studied the soil conditions, particularly the salinity and sodicity of the soil and its effect on the crop yields. In recent studies various spatial aspects of groundwater has been studied by Hasan et al. (2020) and Hamza (2019).

Worldwide the geophysical techniques have extensively been used to study the spatial dimensions and depth of the groundwater. Groundwater level monitoring using the geophysical techniques for different areas of Pakistan have been studied by many scholars

(Ahmed et al., 2019; Ahmed et al., 2021; Khair et al., 2012; Qureshi, 2018; Wada et al., 2010; Watto et al., 2018). Non-invasive geophysical methods for groundwater quality estimation for semi-arid regions have been studied by (Asadi et al., 2019; Fitriani et al., 2020; Islami et al., 2020). The estimation of the extent of contamination of groundwater based on the geophysical surveys has been done by many researchers (Ekwok et al., 2020; Rehman et al., 2021; Shailaja et al., 2019; Stanly et al., 2021; Vasantrao et al., 2017). Various geophysical techniques and equipment have been extensively used for groundwater exploration in various areas of the Punjab Province in Pakistan (Farid et al., 2017; Hasan et al., 2018; Hussain et al., 2017; Sikandar et al., 2010). In Balochistan some work has been done to demarcate the aquifer table of Quetta valley through electrical resistivity and seismic reflection techniques (Alam & Ahmad, 2014). The resistivity distribution through Electrical Resistivity Sounding (ERS) as a function of the physical properties of the subsurface materials has been studied by a few researchers (Akhter & Hasan, 2016; Bahammou et al., 2021; Sharma, 1997; Storz et al., 2000).

The geological framework and the stratigraphy of and Bela Ophiolite of Uthal has been described by Hamza, (2019). It also discussed in detail by many researchers (Kazmi & Jan, 1997; Sarwar, 1992). The Bela Ophiolite and the sedimentary formations in the study area belong to Early Jurassic to Triassic age (Anwar, 1991; DeJong & Subhani, 1979; Fatmi et al., 1990). The major rock types of the study areas have been extensively discussed by Shah, (2009). The Bela Ophiolite, its zones and the structure have been studied by (HSC, 1960; Narejo et al., 2019). The geological mapping of the area has been done by Bashir, (2008) and DeJong & Subhani, (1979).

#### **1.4 Gap Analysis**

The existing studies show that there is a gap in knowledge pertaining to the geochemical analysis and quality of groundwater for Uthal Balochistan. Most of the work done in the study area is related to only the geochemical analysis of water of the

surrounding areas such as Winder Town (Naseem et al., 2010; Naseem et al., 2013; Naseem et al., 2014). The available data focuses mainly on the irrigation water quality (Akbar et al., 2014). The establishment of main parameters defining the quality of groundwater with the geophysical parameters for assessing the groundwater quality are not established for the study area.

The groundwater quality, integrating Electrical Resistivity Sounding (ERS) and geochemical data, in the surrounding areas has been established on the basis of scarce data point, which makes any analysis weak and unreliable. The geophysical analysis for the study area (Uthal) has not been conducted prior to this study.

### **1.5 Problem Statement**

Uthal being a semi-arid area has always suffered water scarcity. According to the census of 2017 (DCR, 2017), there has been a rapid increase in the population, which has worsened the situation. In Uthal the main sources of water are the groundwater resources and in addition to the groundwater there a few ephemeral streams are present in the area (Hamza, 2019). Therefore, the quality of groundwater is the one of the main issues for the population of Uthal. Furthermore, the groundwater quality, integrating ERS and geochemical data, in the surrounding areas has been established on the basis of scarce data point, which makes any analysis weak and unreliable. To have a clear demarcation of the type of subsurface materials and the level of water an integration of various type of data is in need. In addition to this, the integration giving a geological view of the groundwater distribution is also needed. In order to determine whether the water is fit for consumption and in line with the WHO's standards there is a dire need to establish the integration of ERS and geochemical data.

## **1.6 Significance of the Study**

The study is significant as it presents a detailed analysis of the groundwater through geophysical and geochemical analysis, it is a detailed spatial analysis of groundwater in context of chemical variance and its depth spatially. The study aims at establishing a detailed quantitative assessment of the sources that contribute various elements and trace metals in groundwater of the study area and to demarcate the major groundwater producing zones. The study is an effort to create awareness regarding geological impacts on the quality of water along with highlights which may ultimately cause adverse effect on health of the inhabitants of the area.

This study will prove to be helpful in establishing spatial database of Uthal and its peripheral area. The current work will also play a significant role in demarcation of high and low values of trace metals in the groundwater. The study integrates Dar-Zarrouk parameters based on the distribution of the geoelectrical layers with the geochemical parameters. The zones of various groundwater potential based on this integration is for the first time presented for the study area.

It also provides the region's quantitative methodology for analyzing and integrating the geochemical and geophysical parameters in assessing the groundwater resources. The generated model will ensure good water management practices by monitoring groundwater reservoirs, analysis of hydrofacies, and the interpretation of trending data. The results of the study form a legend that can be applied to the other semi-arid to arid regions and water deficit localities.



## **1.7 Objectives of the study**

The current study was to demarcate groundwater boundary and identify areas of saline water if present in the subsurface from the available geophysical technique. In addition to this the analysis of groundwater samples described the geochemistry and its suitability for irrigation and drinking purposes. The role of igneous and sedimentary rocks in contributing to different trace elements has been discussed. The trace element content is compared with WHO drinking water standards and the biological role of each element has been included.

The present study helps to understand the impact of rocks on drinking water quality, thus creating awareness for the inhabitants of the area for better planning and mitigation of environmental problems. In this study GIS (Geographical Information System) was also used to demarcate zones of water quality. This study has also mainly focused on the assessment of groundwater quality regarding the presence of certain major and trace metals in order to identify trends relevant to the deterioration of drinking water quality. For a better understanding of the research, geographical outline of the study area has been discussed herewith. Based on the above discussion the objectives of the study are as follows:

1. To identify the geo-electrical layers and identify the major water producing zones from the apparent resistivity.
2. To analyze the groundwater quality regarding the presence of certain major elements and trace metals to determine the suitability for drinking/ agricultural purposes.
3. To correlate the spatial distribution of geophysical and geochemical parameters for drinking water quality and understand the impact of geology on drinking water quality.

## **1.8 Description of the Study Area**

Uthal is at a distance of 125 km from Karachi and can be accessed through the Regional Corporation Development (RCD) Highway (Figure 1.2). The nearest town to Uthal is Winder, located at distance of 11 km. Uthal, is the district headquarter of Lasbela district, Balochistan. It is in the north of the Lasbela district and is present at a distance of 13 to 26 km landwards from Miani Hor, which is a swampy lagoon towards the south of the study area. Uthal lies in Porali Plain in Balochistan and has an altitude between 20 to 75 m above mean sea level. The present study area extends between 25°48'34.55"N & 66°32'60.00"E and 25°51'36.00"N & 66°32'60.00"E longitudes (Figure 1.2) covering approximately an area of 600 Km<sup>2</sup>. Uthal is situated in the central part of the alluvial plains of Porali River basin; in the east, the mountain ranges of Pab and Mor, in the north Bela Plain while the west is covered by the Haro Range and the south the lower part of the Porali Plain extends towards the Siranda Lake.

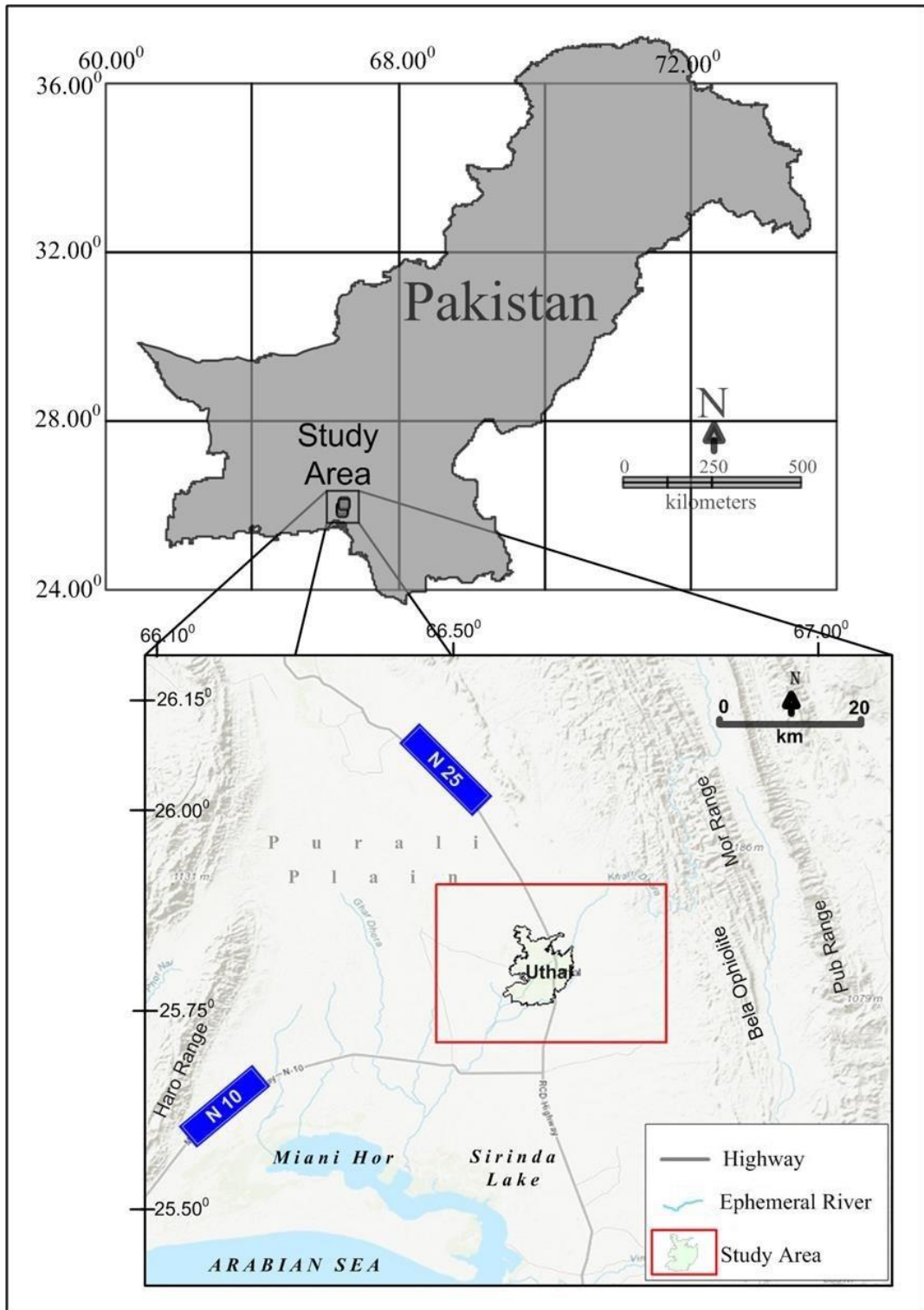


Figure 1.2 Location of the Study Area- District Lasbela, Balochistan.

### **1.8.1 Population**

In terms of revenue system, it is a Tehsil of Lasbela consisting of 72526 populations according to the 2017 census if which the urban part is composed of 29414 persons (DCR, 2017). The economy of the people living here mainly depends on agriculture. In addition, there is a limited source of income from government employment (Huda & Burke, 2012).

### **1.8.2 Climate**

Uthal, Lasbela climatically is an arid area where summers record extreme hot months while winters record moderate cold and dry conditions (Khan, 2019). Due to scanty annual precipitation, the area is a characteristically desert condition (Burke et al., 2005). Summers commence from April and extend until October during which May and June are the hottest months while winter is recorded during November to March. Geographically, according to the Köppen-Geiger climate classification, this type of climate is classified as BWh. In Uthal, the average yearly temperature is 27.2 °C and the yearly rainfall average is 178 mm (Bender, 1995). The northwestern winds, that blow from October to February, become strong as the cold season ends and very cold days are experienced from January to February. The summer season experiences extreme temperature with scorching hot days in April and May. Average yearly temperature for Uthal is shown in the Figure 1.3. The data for this study was acquired during the post monsoon days.

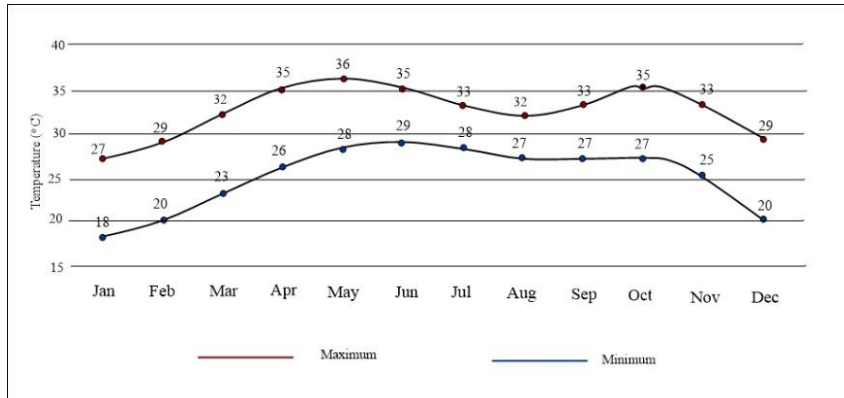


Figure 1.3 Average yearly temperature of Uthal shows high to warm weather

### 1.8.3 Physical Structure

Uthal is a land of contrast, where bare, barren and rugged mountains border from the east and west. Alluvial plains provide bases of agriculture. Physically, Uthal is a widespread plain area sharply divided into rocky and plain areas while the lower part extent towards the coastal region of Lasbela district. In the present study, Uthal is classified into three categories i.e. hills, plains and coastal area (Figure1.2).

### 1.8.4 Hills

Uthal borders the area towards the east laid on widespread foothills of the Pab, while towards the west are the Haro ranges. Eastern foothills vary between 48 to 93 mean average sea level (MASL). The western side of the Haro foothills, however lies on a lower altitude within a range of 20 to 54 MASL (Figure 1.2).

### **1.8.5 Plains**

The study area largely covered by the Porali plain spreads into the mountains. All agricultural activities are practiced on these plain soils (Akbar et al., 2014). The Porali Plain is almost flat, generally similar to the formation of the Kacchi Plain which comprise the central parts of Balochistan (Figure 1.2).

### **1.8.6 Coastal Area**

Uthal is nearly 26 kilometers away from the long Coastal area of Balochistan. The coastal areas, known as the Makran coast consists of the Gwadar and Lasbela districts (Figure 1.2) and extends for 750 km from the Iranian border to the Hub River estuary near Karachi. It constitutes the southern limits of the province (Figure1.2).

## **1.9 Drainage System**

There is no permanent river flow in the Uthal due to absence of any glacier source and scanty rain. After the seasonal rain water disappears in the sandy, pebbly topography, hence drainage is characterized by ephemeral channels (Figure 1.4). The largest ephemeral drain, Khantra Nai (Nai = River) in the study area flows from north to south and Kharrari Nai which starts from the eastern mountains of Mor Range, flowing through the narrow valleys are noticeable rivers. In the central part, Titian Nai is present. Wayaro Dhora (Dhora =small stream) exists in the southern part of the study area. Main tributaries of Khantra Nai are Watto, Rohri, Dhirjo and Duddo streams. Other streams are very small in size. Streams present in the study area have dendritic pattern in the high relief areas and sub-parallel in the plain areas (Ahsanullah, 1971). After heavy rains, rivers become raging torrents due to the topography but gradually become dry due to excessive percolation and

evaporation (DAR, 2000). Groundwater is free from industrial waste because there is no significant industry in the Uthal and its surroundings.

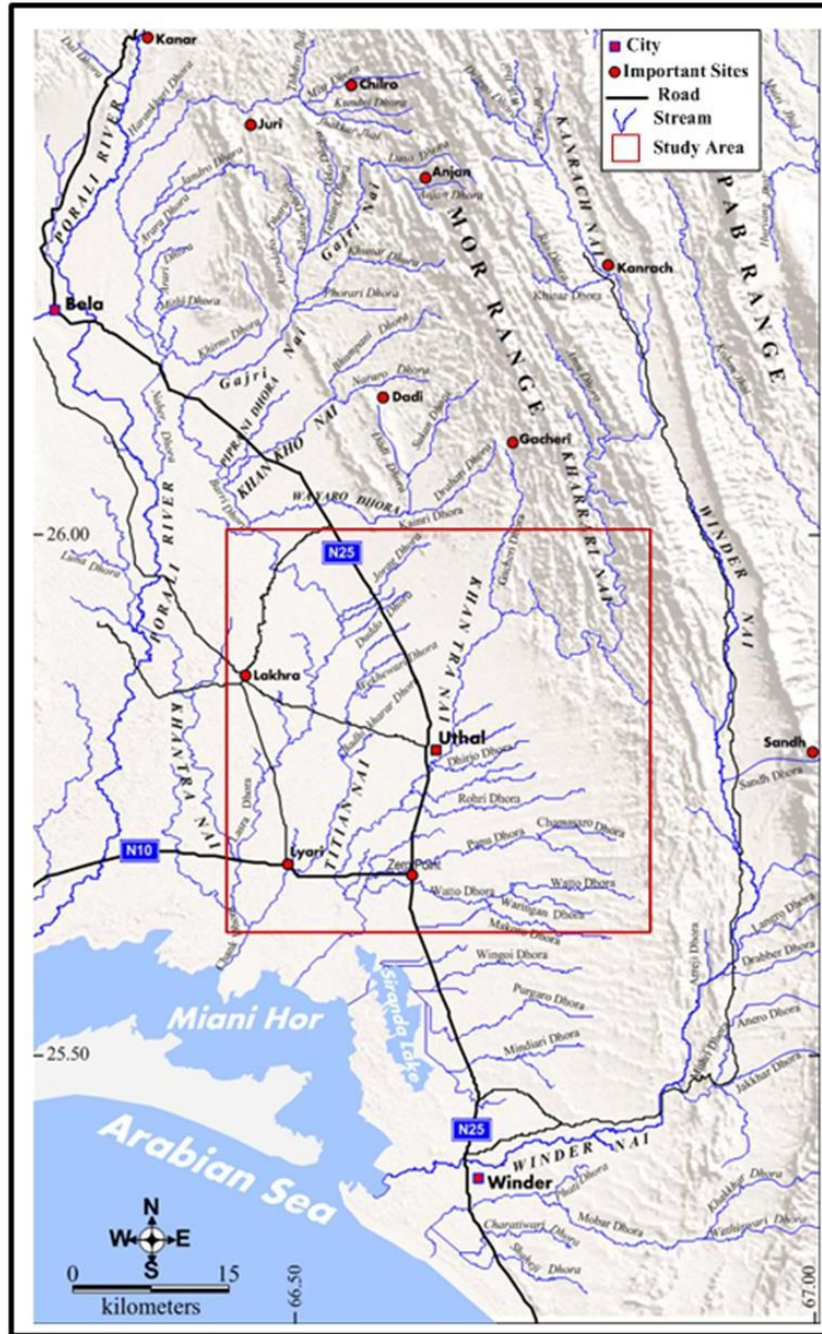


Figure 1.4 Drainage of the Study Area (Hamza, 2019). The important sites include towns and villages.

## **1.10 Geology of the Study Area**

Geologically, Uthal is rich in a variety of complexes of structures, namely Ferozabad Group, Shirinab Formation, Sembar Formation and Bela volcanic group while the plain contains recent sediments (Hamza, 2011).

### **1.10.1 Ferozabad Group**

Ferozabad group was previously named as Shirinab Formation. Shinab is a river that drains the Chapper, Magochar Valleys of central Balochistan where oldest rocks were formed, and the name Sirinab Formation was given by the Hunting Survey Corporation (HSC, 1960). The Ferozabad Group consists of three formations. The type locality of Ferozabad Group is the Ferozabad village, 13 km west of Khuzdar. The name was introduced by Fatmi et al. (1986) and described by Fatmi et al., (1990) and Anwar et al., (1991). The three formations of this group are Kharrari, Malikhore and Anjira, and are discussed in the next chapter.

### **1.10.2 Sembar Formation**

The name Sembar Formation, after its type locality Sembar Pass in Marri Hills, was coined by Williams (1959). The name was given to include the lower part of the “Belemnite Beds” of Oldham (1892) and the “Belemnite Shales” of Vredenburg (Fatmi & Rawson, 1993).



### **1.10.3 Bela Ophiolite**

Bela Ophiolite is 450 kilometers long and 20 kilometers wide, stretching from Ornach in the north to Winder in the south. Volcanic rocks are subordinate in the north and dominant in the south of Ornach. It is made up of a mix of volcanic and sedimentary materials. The Bela Ophiolite consists of pillow lava of marine origin, has planktonic sedimentary rocks, dolerite gabbro sills and has debris horizons (Sarwar, 1992). The age of Bela Ophiolites is Cretaceous (Shah, 2009).

### **1.11 Soil**

The importance of soil can be gauged from the fact that it is a basic component of 27 types of ecosystems, especially forests. Formation of soils of any area depends on rocks particles i.e., sand, silt and clay which originate from existing mountain erosion and weathering (Righi & Meunier, 1995), air and river transportation. Significance of soil depends on holding capacity of varying amounts of moisture and climatic conditions (Piedallu et al., 2011). The soil texture in Uthal is alluvial, being mostly composed of a mixture of light loose clay, and fine sand (Akbar et al., 2014). On the eastern side where hilly area is present, rock fragments proliferate. They are covered by alluvium deposits of Kharrari River.

### **1.12 Agriculture**

Agriculture provides the main source of economic activities for the inhabitants of the Uthal area. Due to climatic conditions agriculture has been divided into two main cropping seasons namely Rabi and Kharif. Wheat, barley, pulse and some kinds of vegetables are sown in winter as Rabi crops while cotton, sorghum, maize, sesame, castor

seed, mung bean, onion, chillies and guar seed and melon are also the major produce of the area (DAR, 2000). Horticulture also plays a significant role in the local economy because Uthal in the Balochistan is a major producer of banana. The land use data (Figure 1.5) show the distribution of banana crop along with other crops, shrubs and grassland of Uthal. In addition, chikoo production also play a valuable role in the local economy.

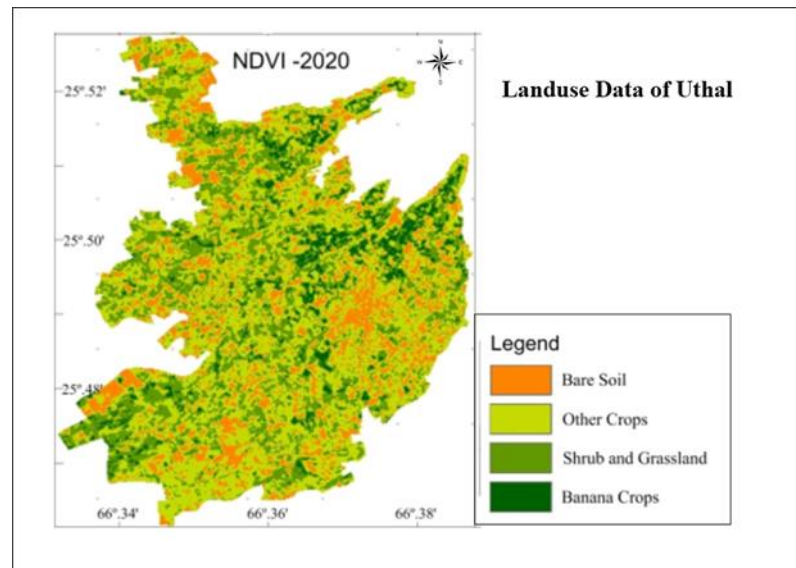


Figure 1.5 Distribution of banana crop, shrubs and grassland, other crops and bare soil in Uthal.

### 1.13 Vegetation and Forest

Due to scanty rain levels, greeneries are very low except in areas of cultivated agriculture. Regarding tree plantations, variety of species of forests and herbs were seen in the study area (Hamza, 2011). Pelu (*Salvadora oleoides*), Kandi (*Prosopis cineraria*), Ber (*Ziziphus nummularia*), Date Palm (*Phoenix dactylifera*), Gaz (*Tamarix spp.*), Kikar (*Acacia jacquemontii*), and Kotor (*Cadaba farinosa*). Major shrubs of the area are Euphorbia Caducifolia, Haloxylon sp., Calligonum Polygonoides, Gugul (*Commiphora mukul*), Merin (*Heliotropium sp.*), Gujo (*Aerva Javanica*), Aak (*Calotropis procera*), Alhagi Camelorum and Mazri (*Nannorrhops ritchiana*).

## **CHAPTER 2**

### **LITERATURE REVIEW**

#### **2.1 Introduction**

The current study is based on the importance of the groundwater quality and its spatial distribution, which is one of the major water resources of the area. Uthal is located on Porali Plain which is covered by the Quaternary Sediments and has hills on the eastern side (Malkani, 2015, 2020). The quality and distribution of groundwater in the study area is affected by the climate (Maqsood et al., 2013) and geology of the area (Malkani, 2020; 2015). The groundwater quality is determined by using the hydrogeochemical and geophysical techniques. In this chapter the existing literature on the groundwater quality is discussed and various geophysical techniques used in assessing the groundwater quality in similar environments are discussed.

## 2.2 Spatial study of groundwater

Availability of groundwater in any type of terrain is largely controlled by the prevalence and dimensions of primary and secondary porosity. Groundwater investigation entails description and mapping of various lithological structures and geo-morphological units. Characteristics of rivers and groundwater is closely related to the rocks around it (Bashir et al., 2007). Excessive usage of groundwater and its impact has been studied in many regions of the world (Mostafa et al., 2017; Zhou et al., 2020). The shallow water aquifers that supply water for a small farm and household are more prone to various contamination (Brindha et al., 2017). Rocks underlie soils and the elements in them dissolve in water to change their chemical properties (Hunt, 2021; Naseem et al., 2012). In the same way, groundwater dissolves the constituents within rocks around them which become part and parcel of the soil properties. Thus, the water that flows on the ground and underground has different effects on different aspects of its geology (Naseem et al., 2014). Water analysis in its spatial dimensions makes it easier to identify why the water chemistry of one area differs from that of another area (Yang et al., 2021). Natural factors are more relevant as also factors resulting from human activities are causing disruption (Burke et al., 2016). The purpose of spatial dimensions of groundwater study is to investigate types of contaminations under with the domain of specific areas. In the present study, the selected area is spanned by northeast mountains, southern parts by the Arabian Sea and the western region connected to the Bela Plain. Due to its status of District Headquarter, urban Uthal is thickly populated and produces some sort of low-level anthropogenic activities. In previous studies groundwater quality was observed in various parts of Balochistan but with reference to Uthal geophysical and chemicals studies are rare/few (Baloch et al., 2015; Bashir et al., 2007; Burke et al., 2016; Mustafa & Qazi, 2007; Naseem et al., 2010; Naseem et al., 2013; Naseem et al., 2014; Van Steenbergen, 1995, 1996; Van Steenbergen et al., 2015). Researchers were mainly focused on water quality estimation in limited fields on one or two parameters. Akbar et al. (2014) in a study on Uthal area focuses on the groundwater quality in terms of the salinity & sodicity and their effect on crop yields. Their

study in the result and discussion sections mentioned that the effect of water quality was affecting the soil of the study area, which in turn was affecting crop production of the area. Groundwater quality is greatly affected by the mineralogical composition of the subsurface lithologies. Various minerals are dissolved in the groundwater and determine the quality. The soil composition at the surface is governed by many factors, the surrounding mountainous areas have great impact on the soil in Uthal.

In this regard, simply saying that the quality of water is polluting soil is against scientific principles. The research conducted by Akbar et al. (2014) is important in describing many aspects of soil quality but lacks integration with the geology of the study area. The aspect of spatial dimensions is strongly studied by Hamza (2019) as an HSE project and the study lends support to the present study as per above mentioned justification.

### **2.3 Geophysical technique and groundwater quality**

Groundwater monitoring reflects the decreasing water level trend in various parts of the world especially huge parts of southern Pakistan (Ahmed et al., 2019; Khair et al., 2012; Peña-Arancibia et al., 2021; Wada et al., 2010). Low rain and absence of water management are the reasons for decline groundwater table. In recent years pumping wells from groundwater resources have exceeded in comparison to natural recharge (Qureshi, 2018; Watto et al., 2018). In the early stages of planning and design of water projects it is important to assess the ground conditions. Most investigations are conducted using traditional geotechnical methods, which are more expensive and provides limited approach because extracted information is only for discrete points. Non-invasive methods include various geophysical surveys for groundwater quality estimation. These survey record parameters using instruments such as resistivity meters. The data thus collected provides the information regarding subsurface lithology and the fluids present in it. Such methods are economical and a good alternative to test boring. The available groundwater resources

can be assessed after using the parameters estimated by these surveys (Asadi et al., 2019; Fitriani et al., 2020; Islami et al., 2020). The data can be later correlated with the lithologs of existing boreholes and can be used for better management of groundwater resources. Such practices can lead to overcome the water shortage for agricultural and domestic purposes. The non-invasive geophysical methods using electrical resistivity techniques have been used for studying the quality of groundwater optimally, in the irrigated semi-arid areas of Punjab Province in Pakistan (Mehmood et al., 2020a).

Several researchers from various regions of the world have published numerous research studies on the presence and contamination of groundwater based only geophysical surveys (Ekwok et al., 2020; Rehman et al., 2021; Shailaja et al., 2019; Stanly et al., 2021; Vasantrao et al., 2017). It can be determined that geophysical survey is important in terms of testing the availability and quality of groundwater. In Pakistan, various scholars applied geophysical techniques and equipment for investigation of groundwater quality and availability especially in various areas of the Punjab Province (Hasan et al., 2018; Hussain et al., 2017; Sikandar et al., 2010). Balochistan is facing serious water shortage due to increase of population and agricultural activities (Alam & Ahmad, 2014).

Balochistan is of significance importance for geological studies as it is located along two major geological plates i.e., Eurasian and Indian. Being a geological garden, experts are continuing their research in several fields of earth sciences at Balochistan areas. The developments of geophysics equipment have facilitated scientific studies of geology. Geophysical based equipment such as earth resistivity meter facilitates identification of groundwater quality and depth at plain areas. These data show major strata of rocks and structural features of shallow earth due to their synoptic coverage and capability (Arsène et al., 2018).

The aquifer table of Quetta valley is rapidly decreasing due to increase in population and agricultural activities. During the geophysical study of groundwater Alam & Ahmed (2014) observed drastic water depletion through electrical resistivity and seismic reflection techniques. The purpose of using the Earth Resistance Meter for current studies

was to facilitate existing research. Researchers around the world use this tool to testing water quality based on its salinity (Ebong et al., 2017; Elbarbary et al., 2021; Juanah et al., 2013).

In geophysical investigation for the detection of water, from in-depth to bedrock, sand, and gravel, etc., the Electrical Resistivity Meter (ERM) and Ground-Penetrating Radar (GPR) technologies, provides fast and economically, details of availability of groundwater based on location, depth and resistance of sub soil geological formations. Visual interpretation of ERM and GPR mapping are obtained in a resourceful and effective way using basic interpretation keys or elements (Cataldo et al., 2014; Tarussov et al., 2013). Several studies were conducted through Earth Resistivity Meter and traced water with quality (Ahmed & Sulaiman, 2001; Ebraheem et al., 1997; Wilson et al., 2006). In addition, integrated hydro-geophysical surveys were used to discriminate water types near the coastal area (Hasan et al., 2020).

The present study is unique and significant regarding Uthal groundwater investigation because no such studies have been previously conducted. Uthal surface configuration in terms of geological features demands such types of studies conducted with the aid of modern equipment and techniques. In the present study, groundwater was studied on the basis of geophysical survey in view of its existing significance.

## **2.4 Geology of the Study Area**

The study area covered several geological groups among which Ferozabad, Kharrari Formation, Malikhore/Shirinab Formation and Anjira Formation were significant (Hamza, 2019). According to several scholars (Fatmi et al., 1990; Anwar et al., 1991; Shah, 2009), these formations belong to Early Jurassic to Triassic age. Rocks types in terms of deposits of these formations are known as sandstone, limestone, calcareous shale and Argillaceous limestone (Shah, 2009).

Main rocks composing this area were argillaceous limestone, sandstone, calcareous shale, limestone and intra-formational mass flow deposits. Bela volcanic group (Bela Ophiolite) was also a significant geological phenomenon with reference to the study area. According to the HSC (1960) basaltic lava, coarse grained agglomerate and bedded tuff were found. Due to lava flows the common structure were shaped pillows and spilitics. These volcanic materials weathered reddish brown and green types were common. In addition, the more massive weathered black deposits also found here difficult to distinguish from intrusions.

The study area also showed that altered and fractured rock structures were filled with carbonate and epidote while augite phenocrysts with chlorite rims were common; amygdules of calcite and microlites of feldspar were also abundant. Similarly, ultrabasic, basic, and intermediate composition rocks of interbedding structures consisted of limestone, marl, shale, conglomerates and radiolarian chert (Narejo et al., 2019). There was no quarry of granitic rocks except conglomerate pebbles in the form of the true granite. The largest deposit of ultrabasic Bela Ophiolite rocks was altered in the form of pyroxenite, serpentinitized peridotite, amorphous and sheared serpentinite, while the diorite and gabbro types with a composition of intermediate structure were reported and in Wad Town 10km south of Porali River a small body of granodiorite was found. Types of concordant and discordant intrusions were also found, while iridescent soapstone had been deposited from Nal area.

#### **2.4.1 Ferozabad Group**

The Ferozabad group was named by Fatmi et al. (1990) derived after Ferozabad village, 13 km west of Khuzdar. This group includes the following formations such as Kharrari Formation, Malikhore Formation and Anjira Formation (Figure. 2.2).



#### **2.4.1.1 Kharrari Formation**

This name was derived from Kharrari Nai Winder area that drains Uthal territory, introduced by Fatmi et al. (1990). It is composed of a mixed clastic carbonate facies, and the formation included limestone, dolomite, sandstone, siltstone, and shale in the type locality. The sandstone is gray, light gray, purplish brown, weathering brownish grey, thin to medium bedded, fine to medium grained, well sorted, quartzose and micaceous. The limestone is gray to brownish grey, weathered brown, covered, thin bedded and unfossiliferous. The area of siltstone is greenish grey to brownish grey and weather brown. The shale is black to greenish grey, weathered brownish grey and sandy. It is micaceous and silty at places.

During his study, Anwar et al. (1991) mapped the formation only in the western fold belt where northwards in the Khuzdar area limestone was present with minor shale intercalations. In addition, a contact relation of base formation was not exposed while its thickness in the type locality was more than 464 m, with nearly 248 m thickness in Ferozabad section and 824 m in Lakh Rud Section. In addition to this, its contact with Malikhore Formation was found to be transitional. According to Anwar et al. (1991) the stratigraphy of Kharrari Formation was explicit as in the main of Early Jurassic but extended into Triassic.

#### **2.4.1.2 Malikhore Formation**

The Stratigraphy Committee of Pakistan approved the name Malikhore Formation which was introduced by Fatmi et al. (1990) to differentiate large to thick bedded middle to carbonate unit of Winder group with reference to Malikhore village i.e., 27 km west-northwest of Khuzdar. The formation was previously the middle member of the Shirinab Formation. The formation consists of dark grey to black colored limestone. The limestone

is crystalline platform type and is hard and compact (Ahsan et al., 2000; Kadri, 1995), and the limestone beds are thin to medium. The shale in Malikhore Formation is very subordinate. It is present in form of thin partings only (Shah, 2009). The various textures like conquinoid, pelletic, oolitic and micritic are present in the formation. The asymmetric cyclic repetition of strata is observed in the formation (Ahsan et al., 2000; JICA, 1987).

The age of this formation is Early Jurassic and it has a transitional contact with the overlying Anjira Formation (Kazmi, 2008; Shah, 2009; Williams, 1959; Woodward, 1959). Drifting of plates during Gondwana are land evident from Mor Range Anjira Formation, Malikhore Formation and Kharrari Formation. Shah (2009) described generalized stratigraphy of the study area (Figure 2.2).

The formation being extremely resistant forms steep slopes. The formation towards the south of Balochistan is 387 m thick within the type locality, 204 m within the Kharrari section and 136 m within the Lukh Rud section. Also, the Early Jurassic age of this contact with the underlying Kharrari Formation and overlying Anjira Formation are transitional (Anwar et al., 1991).

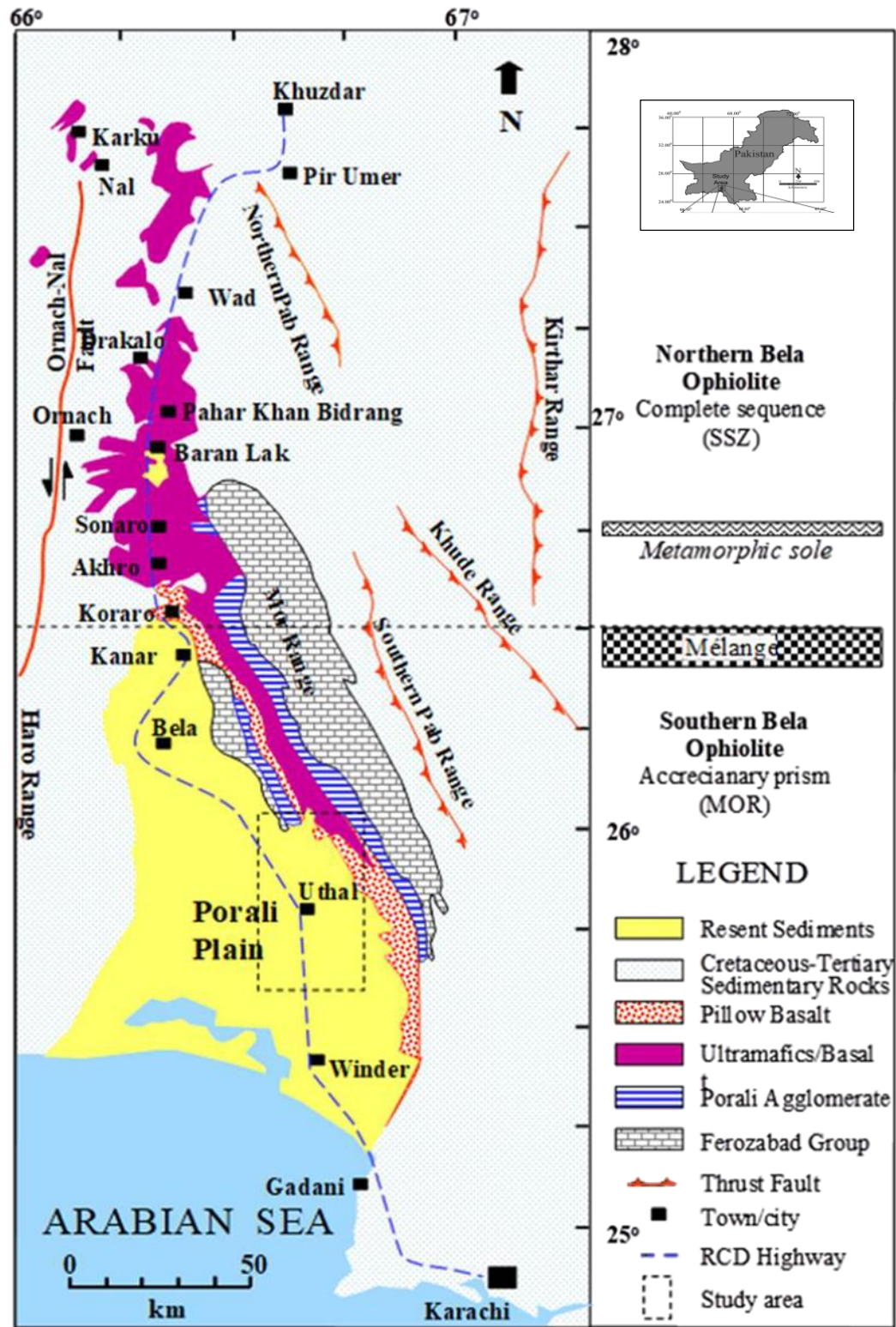


Figure 2.1 Generalized geological map of the study area, simplified after (Bashir et al., 2009; DeJong & Subhani, 1979).




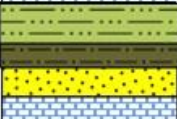
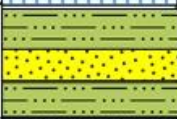
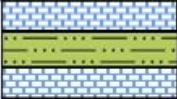

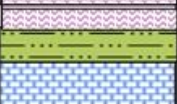
Epoch	Thickness (m)	Formation	Lithology	Description
Quaternary	300	Alluvium		Clay, Sand, Gravel, Sandy Clay
Cretaceous	490 - 600	Pab Sandstone		Fine to coarse grained, medium to thick bedded quartz rich sandstone with minor marks and shales.
	286 - 600	Parh Limestone		White, bluish white, medium light grey, creamy thin bedded, biomicritic, pelagic limestones rich in globotruncana.
	60 - 536	Gom Formation		Pink, light grey, creamy, thin bedded with pink, light grey shales and siltstones.
	133	Sembar Formation		Dark greenish grey, olive green Belemnitic shales with siltstones and nodular limestones
Jurassic	312	Anjira Formation		Argillaceous limestone and calcareous shale, intraformational mass flow deposits, limestone.
	204	Malikhor Formation		Platform facies, micritic limestone with shale interbeds.
	248	Khararri Formation		Sandstone with calcareous beds increasing up section and interbeds of glauconitic sandstone.

Figure 2.2 Generalized stratigraphy of the study area (Shah, 2009).

### **2.4.1.3 Anjira Formation**

Fatmi et al. (1990) introduced as rank of formation, raised recently after earlier acknowledged Anjira Member of Shirinab Formation. According to Fatmi et al. (1990) study, the name Anjira Formation as described here is the uppermost formation of the Ferozabad group because originally this name was introduced by Williams (1959) derived from the Anjira village with the type locality, 12 km east of Anjira (Anwar et al., 1991). The formation is widely distributed within southern Balochistan with 110 m thickness at the type locality, 168m within the Goru section, 312 m within the Ferozabad section, 100 m within the Lukh Rud section and 352 m within the Kharrari section, while the lower contact with the Malikhore Formation is transitional. In the case of the upper contact with the Sembar Formation it is disconformable, with altogether measured sections except within the type locality, overlain disconformably by the Goru Formation.

### **2.4.2 Sembar Formation**

Sembar Pass of Mari hills was the reference of the named Sembar formation introduced by Williams (1959). This formation has covered the lower part of the Belemnite Beds of Oldham and the Belemnite Shales of Vredenburg (Oldham, 1892; Vredenburg, 1909). Goru formation and the Parh limestone is also overlies the Belemnite Beds” of Oldham (Figure 2.2).

According to the survey report of HSC (1960), this formation was considered as a segregate unit but added to the lower part of the Parh Series or Parh Group. The type section of the formation is spread about two kilometers southeast of near Sembar Pass of Marri-Bugti mountain area.

Generally, black silty shale interbedded with black siltstone along with nodular rusty weathering argillaceous limestone beds or concretions is part of the Sembar

formation. Some species gives greenish hue to the weathering color commonly present due to Glauconite. Geographically, the thickness at type locality, Sembar Pass, is 133 m while the formation thickens approximately 262m reported in the Mughal Kot Section of the Sulaiman Range. The subsurface formation is also much thicker (Williams, 1959). The thickness of the formation is reduced to a few meters and the formation is absent in parts of Western Fold Belt and the Kirthar Range where the overlying Goru Formation directly overlies the Jurassic limestone around the neighborhood of Quetta and Ziarat areas.

Sembar's upper contact consists of Jurassic disconformable Mazar Drik formation, Chiltan limestone and Shirinab formation while the lower contact is generally gradational with Goru formation. Stratigraphy being mainly Neocomian extending most likely into the late Jurassic, has been recorded. Sembar formation has a geologically nexus with the Kohat- Potwar Province of the Chichali Formation. The Sembar Formation is considered as a very good source rock for petroleum in the Lower and Middle Indus Basin and is also a good source rock in the Sulaiman- Kirthar (Wandrey et al., 2004).

#### **2.4.3 Bela volcanic group**

Geologically, Bela volcanic group is the known largest Group around Uthal area because it spreads over 450 km length and 20 km width. Geographically, the northern parts extend towards Ornach while the southern part extends towards Winder. In terms of volcanic deposits these volcanic rocks dominate towards the south while the northern parts of Ornach are less significant. The Group consists of intermixed volcanic and sedimentary rock types in which basalt, lava, coarse grained agglomerate and bedded tuff are mainly volcanic.

The Bela Ophiolites are divided into two units, upper and lower units. The distribution is on the basis of the age of the units and the emplacement style of the two units in the mélangé zone (Gnos et al., 1998). The lower Ophiolite unit is of older material

formed by the tectonic accretionary wedge, while the upper units show a true sequence of the ophiolites that can be seen starting from north of Sonaro (Figure 2.3). the upper unit is cut by dykes and sills of doleritic nature (Khan et al., 1999). The ultramafic rocks dominate the northern part of the Bela Ophiolites, and the main units are pillow basalts, gabbros (cumulate and non-cumulate), micro gabbros, diabase, doleritic sheeted dyke complex plagiogranite, diabase (Bashir et al., 2004). The southern part which forms the study area, has pillow basalt with theolitic and with low K- series lava (Khan et al., 1999). In the eastern part, sheared shales, bounding limestone, diabase and gabbro lenses, calcareous slates are exposed. On the western side the Bela Ophiolites are covered by the Quaternary Sediments and do not show many characteristics.

The type of mineralization in the ophiolites is controlled by a number of factors such as, the type of ophiolites, structure and the thickness along with the exposure of these beds. The main mineralization of the Ophiolites is Cr, Ni, Co, Ti, V, Mn and Cu etc. The Cretaceous age Bela volcanic group overlies the Windar group conformably (west of Mor Range), and is overlain (northwest of Bela) unconformably by the Oligocene Nal limestone.

## **2.5 Rocks and Soil Contribution**

The sedimentary rocks and the Bela Ophiolites contribute elements through weathering. The ophiolites are exposed in the northeast of the study area in association with the sedimentary rocks (Bashir et al., 2007; Naseem et al., 2005). These rocks undergo physical and chemical weathering and produce sand and silt by physical and clays, carbonates and iron oxides by chemical weathering. The elemental contribution from the sedimentary and igneous rocks in the study area is given in the schematic diagram given in Figure 2.3.

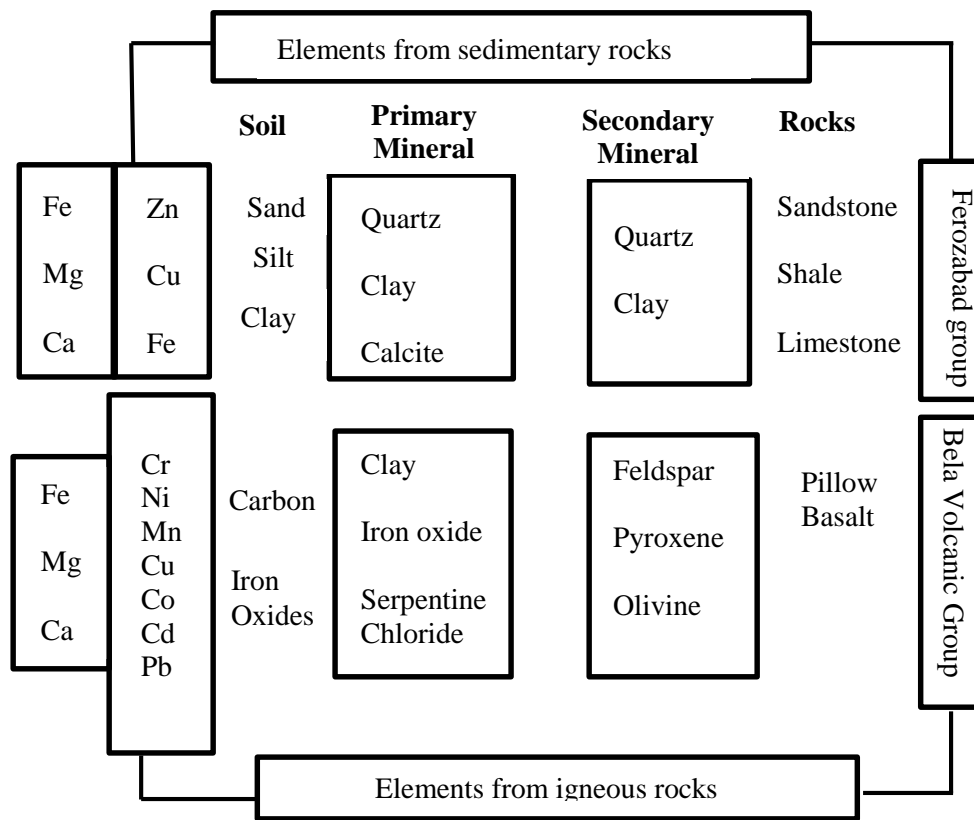


Figure 2.3 A schematic diagram showing the elemental contribution from the geology of the study area (after Hamza, 2011)



## **CHAPTER 3**

### **RESEARCH METHODOLOGY**

#### **3.1 Introduction**

Geophysical methods and surveys are commonly used for exploration with reference to geological phenomena and include surveys like seismic refraction and reflection, electrical resistivity, electromagnetic as well as geophysical well logging (basic exploration geophysics), etc. Geophysical techniques can be classified as invasive and non-invasive techniques. In invasive techniques, the instruments penetrate the earth's surface in boreholes and acquire data from near-surface horizons, and can go to several km deep into the earth. These are expensive techniques and are only used where complex situations are present or where detailed investigations are required. The non-invasive techniques are the most commonly used in geophysical investigations for hydrocarbons, water resources, minerals, and subsurface structure identifications (Garofalo et al., 2016). Based on different laws and principles of physics the techniques are namely: Seismic, Gravity and Magnetic, Electrical, and Radioactive methods. The seismic method is divided into two broad categories: seismic reflection and seismic refraction. Seismic reflection is widely used while exploring hydrocarbons (Cox et al., 2020; Sun et al., 2020). The seismic refraction methods are also used in foundation studies (Fajana, 2021) for high-rise structures, dam

site evaluation, tunnel building, etc. (Akaa et al., 2020). Gravity and Magnetic methods are used in engineering and environmental studies, mineral ore exploration, lithology and studies, geothermal studies, and archeological studies (Bosch & McGaughey, 2001; Essa et al., 2020; Hinze, 1990; Zhang et al., 2020a; Zhang et al., 2020b). Electrical methods, include the resistivity method and are commonly used as noninvasive methods for groundwater exploration. These methods have a unique advantage of delineation of saline and freshwater boundary for domestic and agricultural uses (Mehmood et al., 2020b; Mertzanides et al., 2020; Paul et al., 2020). For water quality assessment, geochemical analysis plays a vital role (Aouiti et al., 2021; Singh et al., 2021; Zhang et al., 2020c).

For scientific research, it is necessary to show data sources and methodologies. In the present chapter research methods, techniques, data sources and analyses employed under the domain of scientific support criteria for the present thesis have been discussed. Evidence is comprised on the following structure: selection of study area, geophysical earth resistivity meter survey, collection of water samples. Analysis includes geochemical and its integration with the geophysical data. Figure 3.1 shows the general workflow for the thesis.

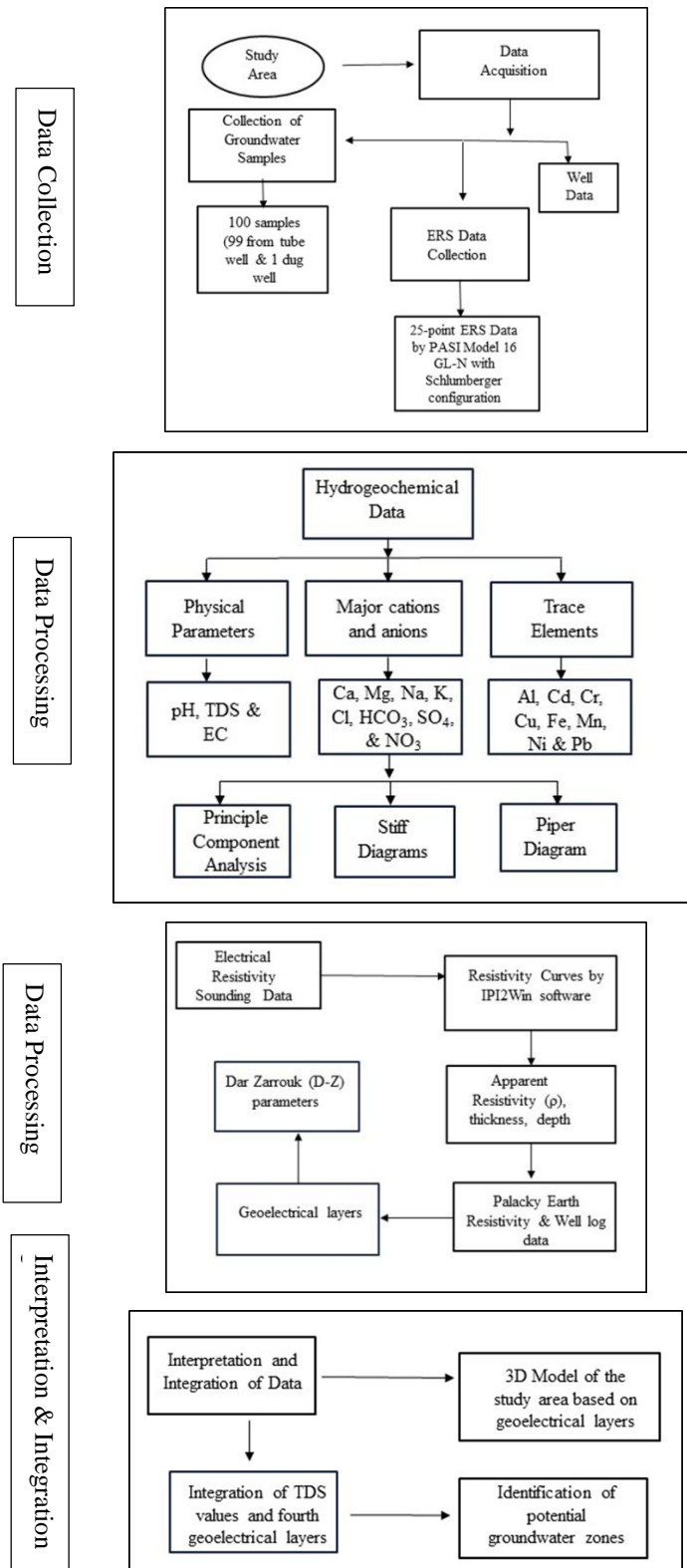


Figure 3.1 Flow chart showing the methodology of the thesis.

### **3.2 Study Area**

The study unit extends from 25.5° N to 26.15° N on latitudes and 66.1° E to 66.75° E longitudes. Area limits were extracted over cultivated agriculture parts. Administratively, Uthal is a District headquarters and small town of Lasbela District. Lasbela has a total population of 576,271 according to the Census 2017 of which the urban population comprised 281,898 (DCR, 2017). Uthal has a population of 72,526 according to the 2017 census (DCR, 2017). The major tribe in Lasbela is 'Lasi' tribe. Besides Lasi, Baloch, Med, Khoja and Hindus have also settled here. The economy of the people living there is dependent on agriculture. In addition, a limited source of income is from government employment (Huda & Burke, 2012). Uthal is a major producer of bananas in Balochistan Province. Besides, vegetables, wheat, and cotton are important agricultural produce. Uthal Tehsil of Lasbela District is located about 30 km off the southern coast of Balochistan Province. Its total area is about 180,000 hectares, while the current study area covers 6130 hectares selected due to the abundance of banana orchards in that area. The only natural sources of water supply are underground reserves that have been in use for centuries. Geographically, this area is located at the convergence of Khantra and Porlai Plain subdivisions of Bela Plain. Porali Plain has an area of 18,260 has an annual rainfall of 150 mm (Mustafa et al., 2013). Due to the presence of mountains in the north, the rain water flowing down is absorbed into the plains through the drains which help to recharge its underground reservoirs. As per geological time scale, Lasbela Plain is of the most Recent era (Naseem et al., 2012).

### **3.3 Electrical Resistivity Survey**

Electrical Resistivity Survey (ERS) is one of a number of geophysical techniques used to measure the bulk resistivity of the ground. This survey or technique was proposed by Archie (1942). An important part of every investigation of aquifer contamination is to

locate and define the extent of the constituents which are responsible for groundwater quality (Jorstad et al., 2004; Mokoena et al., 2021). In general, the quality of groundwater is assessed through the results of its laboratory sample analyses collected from wells drilled, which requires substantial funds and time (Swigart et al., 2021). Nowadays this is conveniently done with the help of the Electrical Resistivity Survey as this method is economical and quick to complete and the results obtained accurately describe the distribution and groundwater quality (Cardoso & Bacellar, 2021). Groundwater since earth resistivity in this method is inversely proportional to the conductivity of the groundwater contamination at a location is quickly detected (Stollar & Roux, 1975).

In order for the resistance mechanism to yield useful results, contradictions of resistance must be present in the concerned areas. For example, if a pollutant does not have significantly more conductivity than natural groundwater, or if groundwater is naturally more conducive to itself, a greater proportion of resistance may not exist and this method may not work (Stollar & Roux, 1975; Wilson et al., 2006). Also, if the water depth is too shallow, the thickness of unsatisfactory sediments can expose any discrepancy between polluted and natural groundwater (Frohlich & Urish, 2002). The geographical environment should be relatively homogeneous to enable the comparison of resistance values and profiles (Schmutz et al., 2014). Such conditions are met on most industrial plant sites and lands. As such, the investigation areas are usually limited to a few hundred acres, where the geology and depth of water are the same (Mondal et al., 2013; Stollar & Roux, 1975) .

The principle behind the electrical resistivity method is Ohm's law, which gives a relationship between the current-voltage drop and the resistance of the circuit. As the current (I) is known and the potential drop (V) is measured, the only unknown variable is the resistance (R) as given in equation 1. In the electrical resistivity method current is induced into the ground and the potential drop is measured with earth being the resistor in this circuit (Figure 3.2).

$$V=I R$$

Eq 3.1

It is the resistor's properties that are studied in the electrical methods, therefore it is important to study this in detail (Robinson, 1988).

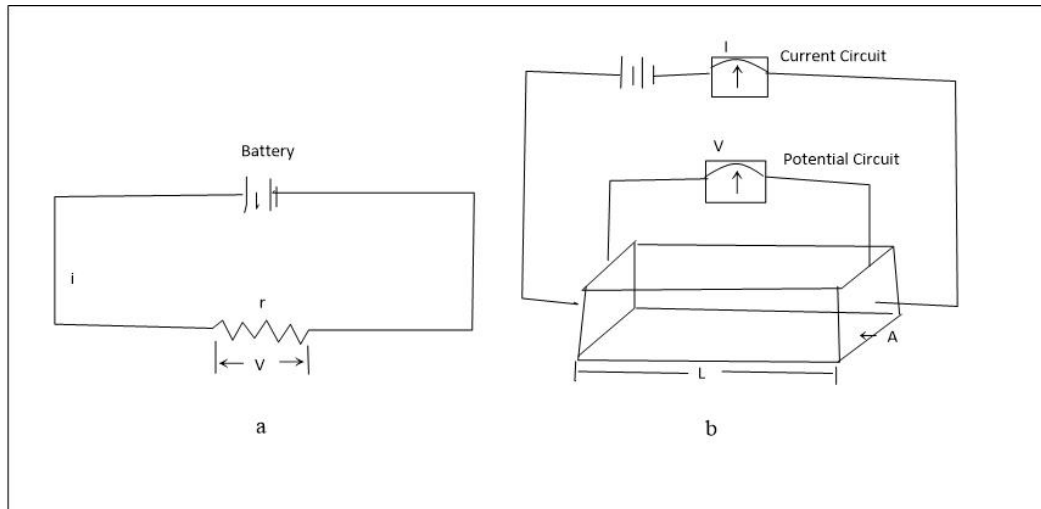


Figure 3.2 (a) An electric circuit with a battery and resistor. (b) An electric resistor depicting earth material having length  $L$ , and area of cross-section  $A$ .

The resistor has resistance ( $r$ ), which depends on its length ( $L$ ) and area of cross-section ( $A$ ) through which the current flows and the resistivity ( $R$ ) the physical property of the material forming the resistor (Eq 3.2).

$$r = RL/A \quad \text{Eq 3.2}$$

Rearranging the above equation, an equation for the resistivity ( $R$ ) can be obtained as given in Eq 3.3

$$R=rA/L \quad \text{Eq 3.3}$$

From the above equation, it can be seen that the resistivity is expressed in resistance  $\times$  length. The commonly used units for resistivity ( $R$ ) are ohm-meter ( $\Omega\text{m}$ ), ohm-centimeter ( $\Omega\text{cm}$ ), and ohm-foot ( $\Omega\text{ft}$ ). In this study units used are ohm-meter ( $\Omega\text{m}$ ).

To measure the resistivity of earth materials, two current electrodes connected to a battery send current into the ground. An ammeter measures the current and a voltmeter is connected to two electrodes to measure the potential drop. The current electrodes A & B and the potential electrodes M & N (Figure 3.3) are all placed mostly in a straight line.

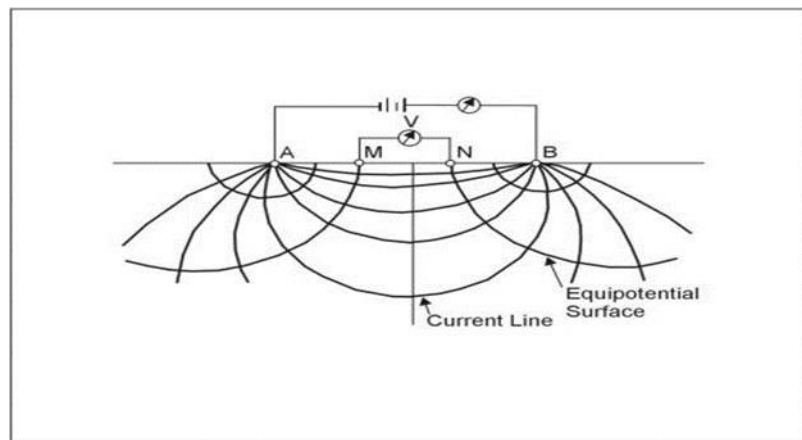


Figure 3.3 Schematic diagram showing the current and equipotential lines in the subsurface (Robinson, 1988).

The resistivity of different subsurface layers is calculated by measuring the potential drop for the input current (Robinson, 1988). As the subsurface is not homogenous therefore the resistivity is termed as apparent resistivity ( $\rho_a$ ). The electrode spacing and alignment are done in a number of ways namely, Pole-Dipole, Dipole-Dipole, Schlumberger, and Wenner configurations (Figure 3.4).

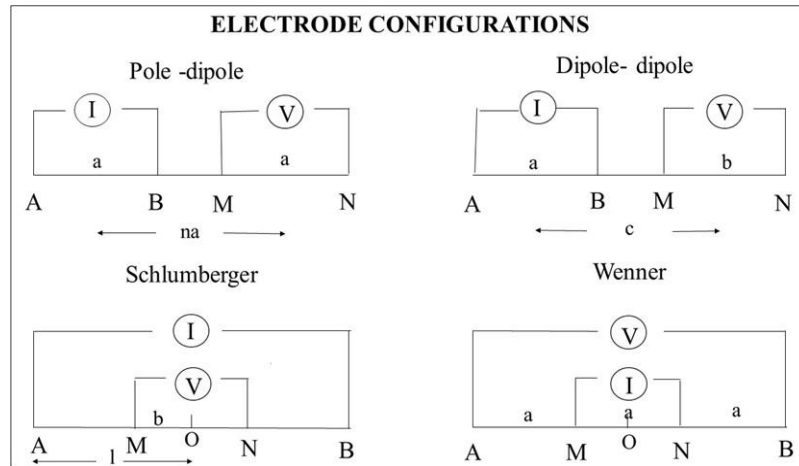


Figure 3.4 Various electrode configurations used for electrical resistivity measurements (Robinson, 1988).

In Pole-Dipole configuration current electrodes are on one side of the profile and potential electrodes on other side (Figure 3.3). Both the current and potential electrodes have the same distance 'a'. The distance from the center of current and potential electrode is 'na'. In Dipole-Dipole configuration one current electrode is kept fixed and the other is moved as the spread increases. The two most commonly used configurations are Schlumberger and Wenner. In Wenner the potential electrodes (M & N) are the inner electrodes and the current electrodes (A & B) are the outer electrodes and the spacing is the same 'a' as given in Figure 3.4. In the Schlumberger configuration also the inner are potential electrodes and outer are the current electrodes. The electrode spacing in the Schlumberger configuration is not the same for all. The electrode spacing is according to the depth of investigation. The depth of investigation is half of the maximum current electrode spacing i.e.  $AB/2$ . Wenner configuration gives good results in resistivity sounding but it is less convenient for field operations. All of the four electrodes are moved for each reading. Schlumberger configuration is therefore, easier to use in the field as the potential electrodes can remain at the same position while the current electrodes are moved apart for deeper penetration (Aizebeokhai, 2010; Robinson, 1988).



For dipole configuration currents, electrodes are fixed and the potential electrodes are moved (Edwards, 1977). Both Wenner and Schlumberger configurations cannot be used for deeper structures. For deep structures dipole configuration is used.

For conducting the electrical survey, we need electrodes for current and potential difference, an ammeter, a battery, and a voltmeter. The electrodes are driven into the ground and are connected with cables to the various components according to the configuration as shown in Figure 3.4. These measurements provide information up to a few hundred meters or feet. Such shallow measurements are important in groundwater investigation, foundation studies, construction industries, etc. All the components are assembled in form of portable equipment. A number of equipment are available in the market; this study is conducted by the Italian make instrument PASI 16LN (Figure 3.5)

For the resistivity survey, a direct current power source supplied by batteries is used. The electrodes are metal rods made of copper, aluminum or steel, and are driven several inches into the ground. In arid to semi-arid areas where the ground is dry, water is used to moisten the ground for better coupling. The survey involved making a profile with the electrode array of the selected configuration. The Figure 3.5 shows the electrode array of the commonly used profiles. Schlumberger configuration gives a good vertical 1D profiling of subsurface and Wenner configuration is for lateral investigation. Both of these are the two most widely used configurations for estimating the apparent resistivity for groundwater and other near surface investigations.



Figure 3.5 Acquiring data using PASI 16GLN.

Resistivity Survey of the area was done with Electrical Resistivity meter, PASI 16GLN, using the Schlumberger Configuration, which is considered as the most reliable method used in investigating water-bearing Lithologies of Quaternary age (Ghani et al., 2022; Mohamaden et al., 2016; Rashid et al., 2019). A total of four electrodes are used in this method comprising of two current and two potential electrodes. The potential electrode difference is much smaller than that of the current electrode. Currents are generated by batteries and sent into the ground by the outer electrodes which are the current electrodes (Rahman & Woobaidullah, 2020). The resulting potential difference  $\Delta V$  as given in Equation 3.4 at the surface is measured by the two inner potential electrodes. Here  $V_M$  is the sum of the potential for A & B at potential electrode M and  $V_N$  which is the sum of the potential for A & B at potential electrode N. The value “I” here stand for the induced current and “ $\rho$ ” is the resistivity at the ground surface which is estimated by the equation Eq 3.4. The resistivity that is measured using the current and potential drop is known as the apparent resistivity ( $\rho$ ) Eq 3.5.

$$\Delta V = V_M - V_N = \rho I / 2\pi \{ (1/AM - 1/BM) - (1/AN - 1/BN) \} \quad \text{Eq 3.4}$$

$$\rho = 2\pi \Delta V / I \{ (1/AM - 1/BM) - (1/AN - 1/BN) \} \quad \text{Eq 3.5}$$

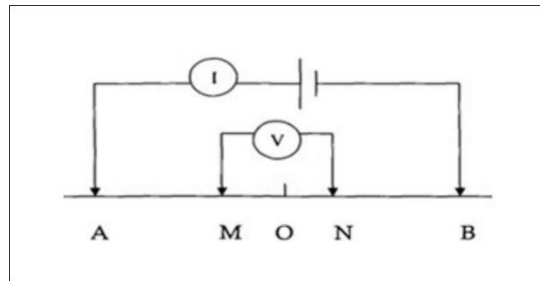


Figure 3.6 Schlumberger electrode configuration used in resistivity measurements (Anomohanran, 2013).

In Schlumberger array configuration four electrodes are placed in a straight line. The electrodes are driven into the ground in such a manner that they make a very good contact with the ground (Figure 3.6). The vertical depth of penetration of current is enhanced by increasing the spacing of the current electrode. A maximum spacing of 300 meters gives penetration of 150 meters. The potential electrode spacing is not changed until the distance between the current electrode spacing becomes quite large. Then the potential electrode spacing is also increased. The ratio of the spacing between the potential electrodes and current electrodes must not be too small otherwise it may affect the accuracy of the data recorded.

The data is collected & processed using IPI2 win software and plotted to get the picture of the subsurface. Based on the set of curves software matches the apparent resistivity calculated from the field data and converts these into the true resistivity of the sub surface Lithology. The subsurface lithology matched with the existing well log data for validation. For basic information 1D models are generated using the established resistivity values as given in the Figure 3.7 (Palacky, 1987).

Subsurface resistivity curves are identified and named on the basis of shapes they exhibit. The curves are interpreted as 2 - layer case where the resistivity generally increases or decreases, 3 - layer case is more complicated and typically described as H, A, K and Q types. A combination of these is used for subsurface comprising of 4 - layers or more (HK Type or KH Type) as shown in Figure 3.8

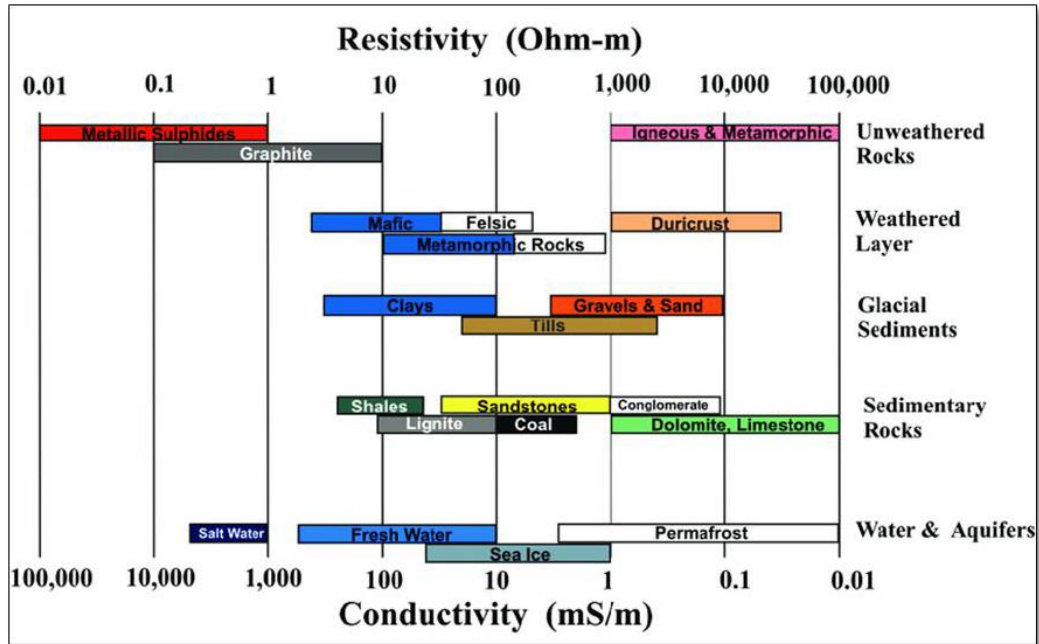


Figure 3.7 Earth Resistivity and the conductivity values for different subsurface materials. (Palacky, 1987).

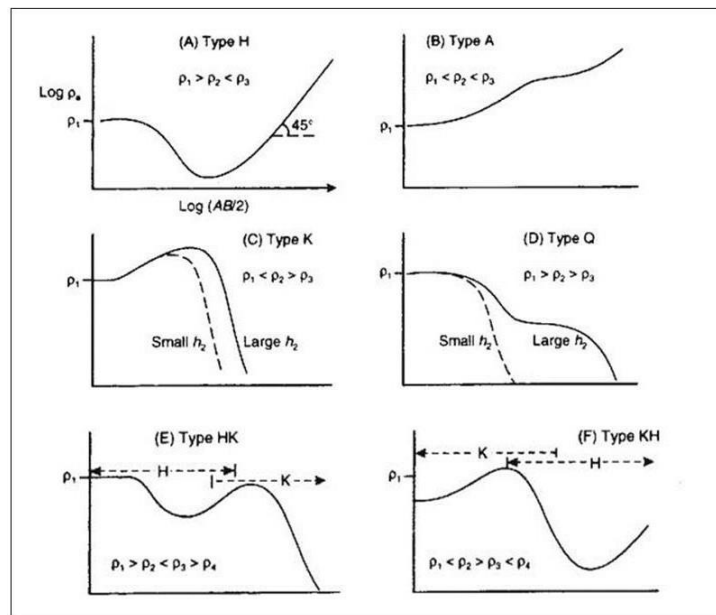


Figure 3.8 Resistivity Curves of various types are shown in the figure from A to F: These types represent the number of the subsurface resistivity layers and their behavior in subsurface. (Sharma & Baranwal, 2005)

### **3.4 Water Sampling Guidelines**

In addition to surveys, laboratory analysis is essential in ground-based studies because in order to introduce a theory into research, it is necessary to gather evidence from every angle in order to substantiate it. One-sided evidence often does not yield conclusions that can be called satisfactory. In addition, the process of gathering multidimensional evidence leads to the formation of more new theories as one theory confirms the other.

The World Health Organization (WHO) a major institution (WHO, 2017) has set guidelines on how to get water samples from remote, especially rural and suburban areas. In this regard, standards have also been set under the ISO-certified system.

The first and most important task for obtaining a sample is to determine the location. The purpose of monitoring water quality in all areas where human populations and activities are taking place is to try to protect people and agriculture from any catastrophe. For water samples, it is important that researchers, as well as the government, agencies to ensure quality as well as on-the-spot testing (Madrid & Zayas, 2007). Strategies to address any significant differences between the two will benefit the people of the area and agriculture. Samples should be taken from locations such as boreholes or wells, treatment plants, storage facilities, distribution networks, and taps supplying water to consumers. It is of great significance to have cognizance of the basic information of each area, individually with reference to the selection of sampling locations. The following general standards are generally applied under the World Health Program (WHO, 2017).

In order to obtain a water sample, locations should be selected from where the regular water supply system has been delivered to the consumers so that the sample can be known as representative of that area. In general, firstly, sites should be selected for sampling where the risk of contamination is high, such as wells or boreholes for groundwater that are close to rocks in which the presence of metals is certain. Subsequently, from built-up areas or parts of land where polluted water from factories is

being absorbed into the ground, as well as places where water supply systems become highly invasive; especially places of potential contamination such as unprotected sources, loop, reservoirs, low pressure areas, system ends, etc (Zhang, 2007).

Sampling sites should be distributed in a sequential manner, taking into account the distribution of cultivation areas and population in the case of the city, in such a way as to be proportional to the number of links or branches through the groundwater zones and piped into the city. The locations selected for growth typically represent the entire and key component system of the region (Barcelona, 1985). The results of physical and chemical analyses lose their relevance when the samples are not stored and tested under the prescribed system. Once the samples have been obtained, it is important to keep them in order in the laboratory, recognizing their importance, following the approved procedures for analysis, and preserving them in an authoritative manner. In general, the interval between the acquisition of the sample and its analysis should be kept to a minimum (Nielsen & Nielsen, 2006; Zhang, 2007) . Water samples in polyethylene or glass bottles should be kept at low temperatures, away from direct sunlight and prepared for laboratory experiments. Care should be taken to ensure that the bottles used for the samples are free from all kinds of dirt and odors. The values of pH, TDS should be detected as soon as possible when sampling so that the use of time during transfer and preservation greatly increases the likelihood of their pH retention.

In the present study, water samples from various wells and boreholes were collected according to the scientifically established principles; determining the boundaries of the study area to test the water quality along with the geological survey. In this regard, several visits were made to the study area. People were also enquired about their views on water quality and its use.

The procedure of obtaining water samples was arranged in such ways that in the first phase a maximum number of samples were collected. Subsequently, samples were selected for analysis on the basis of distance in the study area location. Following which, various mathematical principles are used to compare the selected sample with the results

obtained after the laboratory analysis and the results obtained from the geological survey which facilitates in understanding such studies.

### **3.5 Preparation of collected samples for geochemical analyses**

Water samples are either collected from surface water bodies (rivers, lakes & ponds, etc.) or from aquifers in the subsurface. Groundwater collected from aquifers is done through wells penetrating the aquifer. Collection of groundwater samples requires more time and equipment. In addition to these water is to be collected from numerous wells, must be labeled properly and stored in many containers. This requires good sample planning techniques in the office which in turn greatly reduce field time and increase efficiency (Zhang, 2007). Such preparations include separate containers for surface water and groundwater, labels, coolers & freeze packs if required, pH & conductivity meters, sampling tools (pump and water level indicator), ropes, bags, sample collection documentation forms, etc.

### **3.6 Geochemical analysis of water samples**

Geochemical research in developing countries is in dire need of developing and disseminating scientific laboratories for chemical analyses because there is an urgent need of conducting new experiments to test collected samples from different angles. Water changes its chemical composition very quickly, therefore it is important to take samples to the laboratory as soon as possible for conducting the initial processing steps. Samples cannot be kept for an extended period of time, even with adequate preservation, without the analyte degrading significantly. The maximum holding times (MHTs) are the periods of time a sample can be kept without adversely altering the analytical outcomes after collection and before analysis (or pretreatment). MHTs begin at the time of sampling and stop when the analytical procedure begins. To protect the integrity of the data, samples that



have surpassed their MHTs should be discarded (Zhang, 2007). In addition, lightweight or manual devices should be kept along with the researchers during sample collection and preliminary testing. For the current study, the chemical analysis of the water samples was done for measuring the alkalinity/acidity (pH), total dissolved salts (TDS), & electric conductivity (EC) values, evaluating the concentration of Ca, Mg, Na, K, Nitrate, Bicarbonates, & Sulfates ions. In addition to this trace element analysis was also done for the collected water sample for Al, Cd, Cr, Fe, Mn, Pb & Zn. There are different techniques used for each elemental analysis. Ca and Mg are determined by titration, Na and K by flame photometry, Chloride by titration with silver nitrate, Bicarbonates with turbidometric methods, and Nitrates with gravimetry. The trace element analysis is done by ICP MS. Description of these is given below:

### **3.6.1 Alkalinity/acidity**

Alkalinity is the total number of hydrogen ion ( $H^+$ ) ions in the water. For determining the suitability for water for drinking, domestic, irrigation or industrial purposes, pH is considered as one of the most important and basic parameter. For drinking water normal range of pH is 6.5 to 8.4 as set by World Health Organization (WHO, 2017). Estimation of pH values plays an important role in evaluating the concentration of various ions (Fe, Mn, Zn, Cu, etc.) for healthy growth of plants and human bodies (Atta et al., 2023).

### **3.6.2 Titrimetry**

Generally, Ca and Mg in water are analyzed by the titration method. There are numerous other methods that involve high-tech equipment like auto-titrators atomic absorption spectrophotometric and ion chromatographs and inductively coupled plasma methods.



Figure 3.9 Titration for Ca and Mg

To find the total Ca and Mg a method called complexometric titration, is used to for drinking water, seawater, and various solid materials. This method is also used for determining the hardness of freshwater samples after properly diluting them. The water hardness is a measure of the total amount of Ca and Mg present in the sample. In complexometric titration methods a reagent called EDTA is used. EDTA is a very large molecule and it forms a complex with Ca and Mg ions. The full form of EDTA is ethylenediaminetetraacetic acid. As the indicator, Eriochrome Black T (ErioT) which is a blue dye is used, whereas for estimating Ca alone Patton and Reader is used as an indicator. As the blue dye forms a complex with the Ca and Mg ions, the color of the solution changes color from blue to pink. The ion complex formed by the dye and metal is less stable than the ion complex formed by the EDTA and metal. In the titration process, the solution containing the Ca and Mg ions reacts with an excess of EDTA. An indicator is added to the solution and it remains blue as all the Ca and Mg ions complex with EDTA. Then, with a solution of magnesium chloride, back titration is carried out. This procedure for forming complexes with the excess EDTA molecules till the end-point is reached. At this point, all the excess EDTA has been complexed. After this, the remaining Mg ions in the magnesium chloride solution complex with ErioT indicator (Pal et al., 2018). This is indicated by an immediate change of color from blue to pink. The Equipment needed for titration are burette, 20 mL pipette, 250 mL conical flasks, 100 mL volumetric cylinder.

Solutions that are used for total Ca and Mg ion determination are, EDTA (Ethylene diamine tetra acetic acid) 0.05 M solution, a buffer with pH 10, 7.0 g of ammonium chloride was dissolved in 57 ml of concentrated ammonium chloride dissolved in 100 ml distilled water to dilute it in a volumetric flask. 0.024 mol L<sup>-1</sup> solution of MgC<sub>12</sub>.6H<sub>2</sub>O formed with 2.54 g of magnesium chloride hexahydrate diluted with 500 ml of distilled water in a volumetric flask. For Mg indicator 15 ml of Eriochrome Black T in 15 ml of concentrated ammonia and 5 mL absolute ethanol was used (Gupta et al., 2007).

Freshwater samples, groundwater and other samples already in solution don't require further preparation. EDTA Solution is standardized as given below:

In a conical flask a 10 mL of EDTA solution was pipetted out. Then a 10 mL of ammonia buffer solution was added and 1 mL of Eriochrome Black T indicator solution was also added. The EDTA solution was titrated with magnesium chloride solution until a permanent change of color from blue to pink was reached. The average titrate of magnesium chloride solution was determined, and the number of moles was then determined by the average titrate. The concentration of EDTA solution was calculated using the given the Mg<sup>2+</sup> and the EDTA ratio 1:1 of the solution.

The following titration method for water samples was used: In a 250 mL conical flask, 100 mL of the sample solution was added. By dilution the 0.05 mol L<sup>-1</sup> EDTA solution by a ratio of 1/10, a 0.005 mol L<sup>-1</sup> EDTA solution was created. 20mL of this diluted EDTA was added to the sample mixture. Added 1 mL of the Eriochrome Black T indicator solution and 10 mL of the ammonia buffer. By dilution the 0.025 mol L<sup>-1</sup> magnesium chloride solution by a factor of 1/10, a 0.0025 mol L<sup>-1</sup> magnesium chloride solution was created. This 0.0025 mol L<sup>-1</sup> magnesium chloride solution was used to titrate the sample solution until a persistent pink hue emerged. Until concordant findings (titres agreeing within 0-1 ml) were achieved, the titration was repeated with additional samples (Pal et al., 2018).

The following calculations are done on the results:

- Calculate the total moles of EDTA added to the sample solution.
- Calculate the moles of the magnesium chloride solution used in the back titration from your concordant results. From the equation of the titration below, the moles of  $Mg^{2+}$  will be equivalent to the moles of excess EDTA.
- Given the ratio of  $(Ca^{2+} + Mg^{2+}) : EDTA = 1 : 1$ , calculate the moles of  $Ca^{2+}$  and  $Mg^{2+}$  that must have been complexed with EDTA by subtracting the excess EDTA from the total moles of EDTA added to the sample. This result is the moles of  $Ca^{2+}$  and  $Mg^{2+}$  in the sample solution.

When titrating chloride ions with a silver nitrate standard solution, the Mohr method uses chromate ions as an indication (Best & Ross, 1977). The sample is first treated with a few drops of potassium chromate indicator before being titrated with silver nitrate solution. According to Clesceri et al. (1988), the titration is carried out until the solution's color shifts from opaque orange-red to yellow. The apparatuses needed for this approach include a burette, a graduated cylinder measuring 100 mL, a transfer pipette measuring 25 mL, a pipette pump, Erlenmeyer flasks measuring 250 mL, desiccator volumetric flask measuring 500 mL, an Amber bottle, and wash bottles (Clesceri et al., 1988).

For, bicarbonates a separate method was used. A potentiometric method is used for the determination of carbonates and bicarbonates in the sample. It is determined by titration of the water sample with a strong acid solution. The estimation of  $CO_3^{2-} - HCO_3^-$  was done with 0.1N HCl solution with phenolphthalein ( $C_{20}H_{14}O_4$ ) and bromocresol ( $C_{21}H_{14}Br_4O_5S$ ) green as indicators. The amount is calculated by the difference method (Clesceri et al., 1988).

### 3.6.3 Flame photometry

Flame photometry is used for the detection of sodium ( $Na^+$ ) and potassium ( $K^+$ ), it has a high resolution for the detection of these alkali metal ions. In a flame photometry, a

solution sample is atomized into a flame the characteristic spectra of an element are separated and the emission is measured. A flame-based device provides low excitation ranging from temperature 1000° C to 3000° C. This method works very well for alkali metals i.e. sodium, potassium and also, calcium and barium etc. This method has advantage over other techniques like ICP-AES and AAS, which are very expensive than the flame photometry (Banerjee & Prasad, 2020).

For the metal ion detection, ICP-AES is more suitable than flame photometry, but in detection of elements such as sodium and potassium its efficiency is much lower, therefore flame photometry is the most suitable method.

When these alkali and alkaline earth metals are added to the flame they are dissociated in different atoms. This excites the atoms to a higher state where they are unstable. When these atoms return back to their stable ground state, they emit the energy in form of a wavelength in the visible spectrum. The alkali and alkaline earth metal has their own characteristic wavelength and can be identified from this wavelength. The presence of sodium in water and other food is essential within a given normal range. However, its higher levels can become harmful for diseases like high blood pressure and kidney disease.

In such cases, food with low sodium is advised. Potassium alongside sodium helps regulate the body's functions. It is an electrolyte and it withstands sodium's gate pressure and it also withstands the pressure generated due to water circulation inside a human body.

Inside the human body cell, sodium and potassium are inseparable (Smith, 1988). It helps in muscle contractions and plays an important role in proper brain functioning. Maintaining a proper potassium level is essential for cardiac function, fluctuations of its levels in the human body can cause cardiac arrest (Byrne et al., 2022).

### 3.6.4 ICP-MS

ICP-MS, an Inductively coupled plasma mass spectrometry is considered as powerful in analyzing various types of elements in mineral and water samples (Chen et al., 2011). An analytical technique called mass spectrometry (MS) ionizes chemical species and sorts the ions according to their mass-to-charge ratios. Using non-interfered low-background isotopes and inductively coupled plasma mass spectrometry (ICP-MS), metals and a number of non-metals can be found at concentrations as low as parts per billion. ICP-MS has an advantage over other methods as it can do elemental analysis with wide elemental coverage, has an extremely low detection limit in ppt/ppm or ng/L to mg/L, has fast analysis times and all elements analysis can be done all at once. It also has some very simple spectra which are high throughput & productivity and can also provide isotopic information. Figure 3.10 Shows the elements analyzed by ICP-MS. The color coding describes the grouping of the elements.

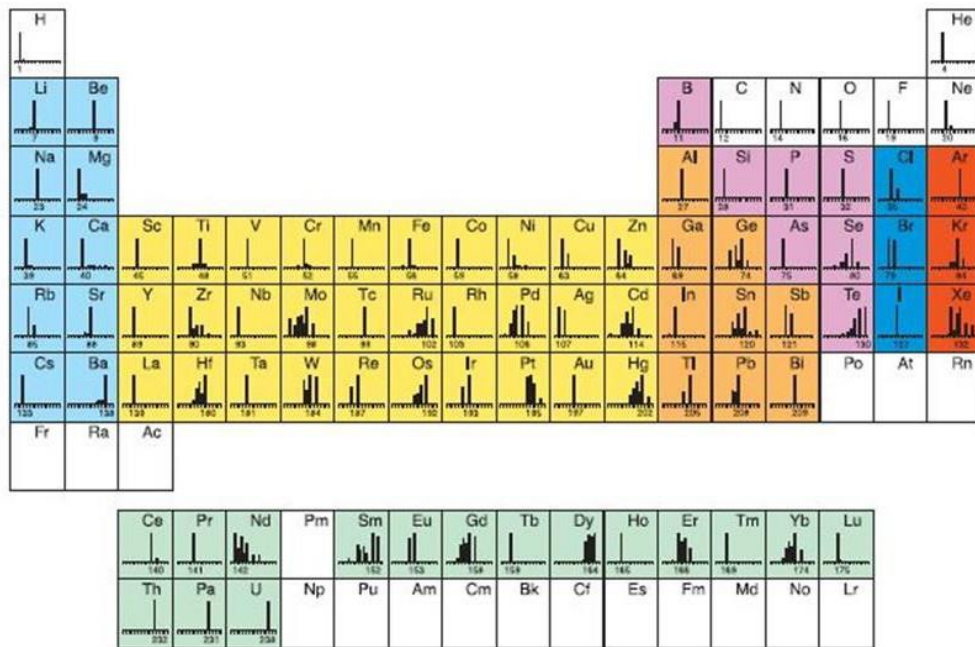


Figure 3.10 ICP-MS color analysis of elements. Groupings of elements that are typically identified by ICP-MS are color-coded. Alkali earth and alkaline earth are light blue; transition metals are yellow; other metals are orange; metalloids are magenta; halogens are dark blue; noble gases are red; and rare earth elements from the Lanthanide and Actinide families are pale green. (Calvete et al., 2017).

ICP-MS is also a semi-quantitative instrument, an unknown sample can be analyzed for 80 elements in only three minutes and this is used for isotopic analysis routinely. In an ICP-MS, the samples are introduced as aerosol droplets into an argon plasma.

A single charged electron is formed in this process. The aerosol is dried by the plasma and it dissociated the molecules after which the electrons are removed. This process forms singly charged ions that are directed into the mass spectrometer for mass filtering. In most of the ICP-MS, a quadrupole mass spectrometer is used which can rapidly scan the mass range. One mass to charge ratio is allowed to pass through the mass spectrometer at any given time. For example, if the charge to mass ratio of 23/1 is set for the quadrupole to pass, only sodium (Na) ions would be allowed to pass and the rest would not pass. When the ions exit the mass spectrometer, they strike the dynode of an electron multiplier. This serves as a detector for the ions. As the ion strikes the detector, a cascade of electrons is released, these are amplified to a point where they can be in form of a pulse that can be easily measured. The concentration of the element is determined by comparing the pulse with standard calibrated curves used as standard, for the given element with the help of software (Calvete et al., 2017).

Typically, only a single isotope of an element is measured, since the ratio of that isotope is fixed in nature as given in Figure 3.10, the figure shows a simple bar graph for each element. The bar graph shows the relative abundance of the isotope for that element in nature. This is termed an isotopic fingerprint for that element. Not all elements follow the rule of natural abundance, like lead (Pb), which has two distinct origins in nature, first was the Pb placed here when the earth was born, second is by the decay of the radioactive minerals in the earth (Zhang, 2007).. Thus, the Pb isotope ratio may vary with the source of Pb. For detection of Pb, it is necessary to sum several Pb isotopes available, for accuracy. Following are the components of an ICP-MS:

- **Sample Introduction System:** This is composed of a spray chamber and nebulizer. The samples are introduced in the instrument through this chamber.

- **ICP torch and RF coil:** The ion source which is the argon plasma is generated through this part of an ICP- MS system.
- **Interface:** The interface is a link that connects the atmospheric pressure ICP ion source to the high vacuum mass spectrometer.
- **Vacuum System:** This provides a high vacuum for the quadrupole, ion optics, and detector
- **Collision/reaction cell:** Before the ions move into the mass spectrometer any interference if present is removed here. This is done to avoid any factor that can degrade the detection limit of the instrument. A universal cell is used that can be used as a collision cell and as a reaction cell.
- **Ion optics:** It guides the particular ions into the quadrupole and discards the photons and the neutral species from the ion beam.
- **Mass Spectrometer:** This is the main component that filters out each ion according to its mass to charge ratio.
- **Detector:** It counts individual ions that are coming out of the quadrupole.
- **Data Handling and System Controller:** This component records and saves the data and obtains the final result of ion concentration (Zhang, 2007).

### 3.6.5 Gravimetry

All analytical methods based on signals originating from the measurements pertaining to change in mass are termed Gravimetry. It is one of the classical methods still



widely used for estimating water chemistry. The soluble ions in an aqueous solution are precipitated with a precipitating agent. The insoluble particles form colloids which coagulate to form a precipitate. The precipitates are then collected and weighed. This method is used for sulfates. Hydrochloric acid (1 ml) is added to the slightly warm water sample in a beaker. Barium Chloride ( $\text{BaCl}_2$ ) is added to water and it reacts with the sulfates to form Barium Sulfate ( $\text{BaSO}_4$ ).  $\text{BaCl}_2$  is soluble in water and  $\text{BaSO}_4$  is insoluble. The precipitated ions are filtered on an ash less filter paper #41 and the filter paper was dried and burned in a pre- weighed crucible. The difference in the weight of the crucible gives the concentration of the sulfates ions in the water sample (Gupta et al., 2007).

### **3.7 Precision and accuracy**

Analytical methods are designed using multiple techniques in which samples are estimated and results accrued. The accuracy of any analysis ensures that the analytical goal achieved has moved through the research steps in the right direction. Better accuracy of samples is measured by the numerical deviation between the components obtained. A standard analytical technique balances the data obtained to clarify and satisfy the necessity of any research. The reason why a standard analytical technique is chosen is based on the presence of equipment and tools in the laboratory. It is important to make sure that the laboratory is free from contaminants before starting research work, in view of the sensitivity of the samples. At the same time, it is essential to keep in mind tools and the working procedures to ensure minimization of mistakes (Zhang, 2007). During chemical analysis, correct estimation of the elements is essential. From sample collection to acquisition of data, the following steps were taken to maintain the accuracy and precision.

#### **3.7.1 Water Sample Preparation**

To maintain accuracy of analytical results it is essential that water samples collected from rivers and bores of the study areas were filtered through 45 membranes and then

stored in two different special plastic bottles. Acidify one bottle with 01% nitric acid to facilitate diagnosis of metal components was ensured. The sample bottles were thoroughly washed thrice with sample water so that no other ingredients would remain. In order to ensure that the water did not oxidize, it was important to fill the bottles completely. After closing the bottle tightly, it was placed e.g. in a dark place protected from the sun, a refrigerator where temperature was maintained at 4° C (Gupta et al., 2007). The sample collected in the second bottle was used for estimating the major constitution.

During water samples analyses, to reduce contamination from containers throughout the experiment, A-grade borosilicate glassware (Pyrex) was utilized (Kozmutza & Picó, 2009). Since all studies used Analar grade Merck/BDH/Fluka chemicals, this was necessary for high-quality chemical analysis. High quality double deionized water with a conductivity of 0.5 S was used to prepare and analyze the samples. In order to ensure the accuracy and reproducibility of the analytical data, blank and repeated samples were added to each batch of the analysis. Each instrument's working conditions were established in accordance with the manufacturer's specifications. A built-in multireading mechanism is available on the Atomic Absorption Spectrophotometer (Perkin Elmer, Model Analyst 700). It automatically calculates the precise value by taking the mean and standard deviations into account.

By introducing a standard sample of basalt, sample# BIR-1 from the USGS was used in each batch of analysis to monitor the working conditions and standards set for the analyses. Ionic Balance Error (IBE) was used to examine the analytical accuracy for the measurements of water ions (Das & Nag, 2015). The value of IBE for majority of the water samples was observed to be within a limit of  $\pm 5\%$ .

### **3.7.2 Presentation of Results**

The results are displayed most commonly in tabular form and the analysis of the water chemistry is reported in standard units. The units used are in milligrams per liter (mg/l), milliequivalents per liter (meq/l) and micrograms per liter ( $\mu\text{g/l}$ ). The data is also

displayed graphically for developing a clear understanding of the spatial distribution in the study area.

### 3.7.2.1 Piper diagram

In most of the natural aquatic environments, the most common ionic species are Sodium ( $\text{Na}^+$ ), Potassium ( $\text{K}^+$ ), Calcium ( $\text{Ca}^{2+}$ ), Magnesium ( $\text{Mg}^{2+}$ ), Chloride ( $\text{Cl}^-$ ), Carbonate ( $\text{CO}_3^{2-}$ ), Bicarbonates ( $\text{HCO}_3^-$ ), and Sulphates ( $\text{SO}_4^{2-}$ ). The percentage composition of three ions can be displayed in terms of a trilinear diagram. By grouping the two ions, sodium, and potassium ( $\text{Na}^+$  &  $\text{K}^-$ ), the major cations can be displayed on one trilinear diagram. Similarly, the carbonates and bicarbonates ( $\text{CO}_3^{2-}$  &  $\text{HCO}_3^-$ ) are grouped, and there are three major groups displaying the major anions. Figure 3.11 shows a Piper diagram that is commonly used to display water chemistry (Piper, 1944). The analysis is shown in the percent of each anion and cation.

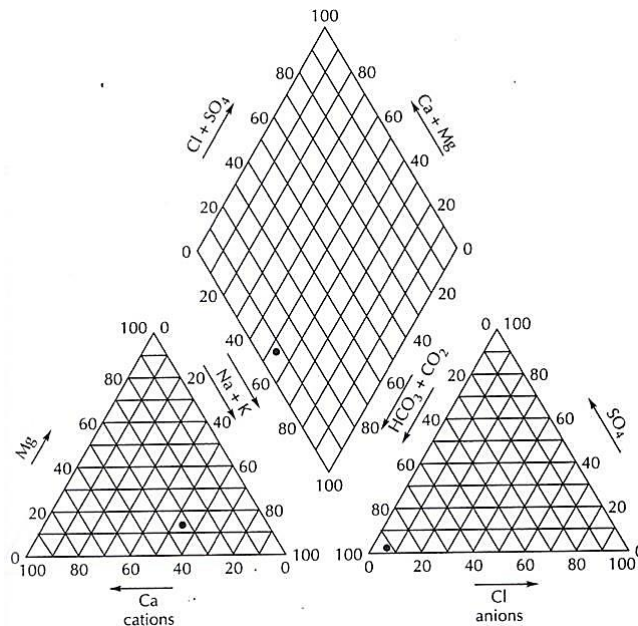


Figure 3.11 The piper diagram used to represent the chemistry of water samples (Fetter, 2001)

The apex of each triangle represents 100% concentration for one of the constituents. In the case of two constituents being present in a sample, then the point representing the percentage of each group would be plotted on the line between the apex the apexes for these two. In the case of all three groups, the analysis is plotted in the interior of the field. A diamond-shaped diagram is generated placed in the middle of the two triangles representing the chemistry of the water. It represents both cations and anions in water samples.

The cation points are projected onto the diamond-shaped field parallel to the side of the triangle labeled Mg, and the anions on the side of the triangle labeled  $\text{SO}_4^{-2}$ . The intersection of the two points is plotted as a point on the diamond-shaped field. As the water flows within an aquifer its composition acquires certain chemical characteristics based on the interaction between the water and the subsurface lithology. The bodies of groundwater in subsurface aquifers have different chemical composition and the term hydrochemical facies is used to describe these bodies. Hydrochemical facies can be classified on the basis of the dominant ion types by piper diagram (Fetter, 2001) as shown in Figure 3.12.

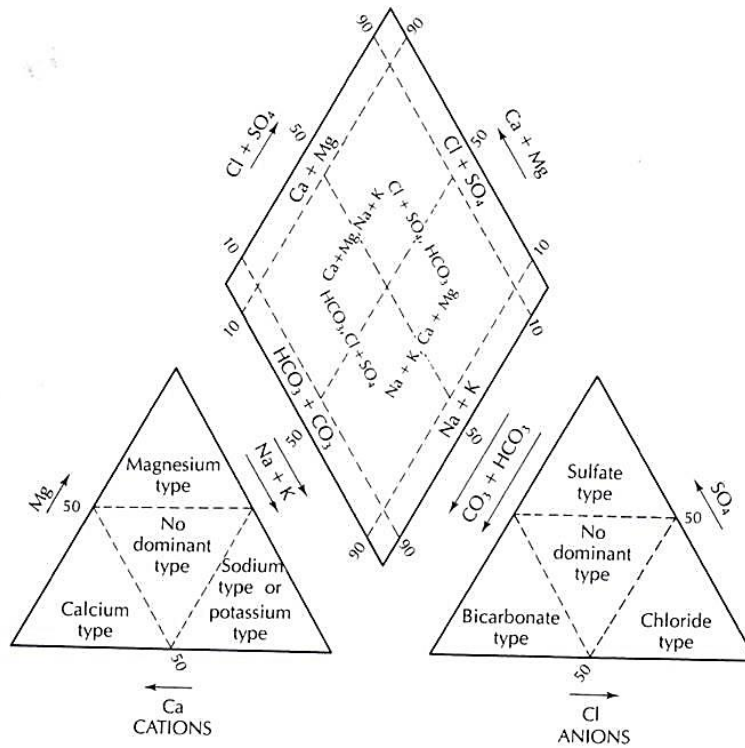


Figure 3.12 Hydrochemical classification for natural water using the Piper diagram(Fetter, 2001)

### 3.7.2.2 Stiff Pattern

Another way of graphical representation of the chemical analysis is the Stiff Pattern as shown in Figure 3.13 (Stiff, 1951). A polygonal shape is formed extending on both sides of the zero axis. Four parallel horizontal axes are used to form the polygonal shape. Cations and anions are plotted on the left and right of the zero axis, respectively, as shown in Figure 3.13. The stiff pattern effectively displays the concentration of various ions in the water samples for domestic use for the study area. The area of the polygon indicates the concentration of the ions in water. The smaller area under polygon shows low concentration and the larger area shows a high concentration of various ions.

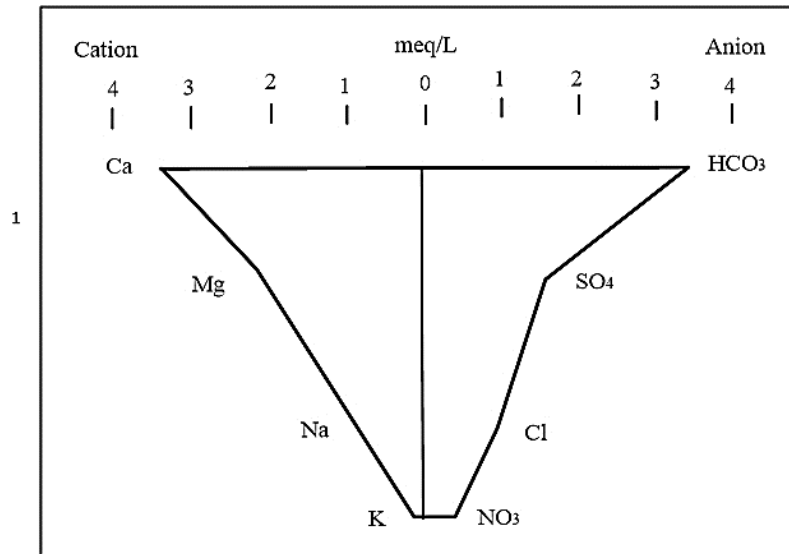


Figure 3.13 Stiff pattern showing cation and anion distribution across the zero axis line (Stiff, 1951)

### 3.8 Supporting software

In scientific research, there is a patient process of collecting data and drawing conclusions through various estimates, which have been made very easy by the software. This software helps in all forms of data analysis, its graphical presentation and pictorial analysis.

#### 3.8.1 Microsoft Excel

In the present study, data collected from the sample has been made readable with the help of Microsoft Excel. During this time, rules were formulated to check the data with the help of various formulae to keep it error-free while converting it for digital technology. Microsoft Excel is an excellent data handling software used by a large number of researchers (Kachholz & Tränckner, 2021; Kliengchuay et al., 2021).

### **3.8.2 Google Earth Engine**

Google Earth technology has revolutionized the field of ground studies for researchers (Tooth, 2015; Viles, 2016). Satellite imagery has made it easier to locate the sample area and study its surroundings with the help of GPS. It also helps to describe the situation in different regions at different times. Google Earth Engine provides a platform for geospatial data processing and analysis (Boothroyd et al., 2021; Dronova et al., 2021). Satellite images from the Google Earth engine have been used in the present research.

### **3.8.3 IPI 2 Win**

The main software used for the electrical resistivity data for the current study is IP2 Win, which is one of the most used software for calculating and interpreting geoelectrical data. With various electrode configurations like Schlumberger, Wenner, pole-dipole, dipole-dipole, etc. The software is designed to analyze and then interpret the data separately. The same can be done by making the curves and matching them manually, which is a very tedious and time-consuming process. The same can be done with the help of software like IPI 2 Win and saves a lot of time and effort. Manual work has a greater chance of error, whereas computer-assisted work has a very small possibility of making mistakes in calculations etc.

IP2Win is a user-friendly software that can analyze the geoelectrical data for vertical electrical sounding (VES) points (Bobachev, 2002). The 1D data acquired by any of the standard electrode configurations mentioned earlier is analyzed and interpreted by the software. Following are the main steps in using IPI2Win.

### **3.8.3.1 Data Input and Output**

The data input and output files are in ASCII text and the input data is saved in a file with the .mt file extension. The interpreted results in the software are saved as files with the mod file extension. The input data can be done from the field data. The field data consists of sounding data such as AB/2 which is the current electrode spacing, 'V' which is the voltage, 'I' current, and the geometric factor 'K' which is calculated from the field data using the equations (Bobachev, 2002) for each of the electrodes configurations. Data input can also be done from the field data directly by inputting AB/2 and pa values.

### **3.8.3.2 Data Error correction**

Sometimes data corrections are required in the phase and amplitude curves displayed in the curve window. After editing the curves the new phase value and apparent resistivity is stored in the data file and the old values are stored in a file with an extension BAK and will be overwritten when the data file is opened next time (Bobachev, 2002).

### **3.8.3.3 Viewing Data**

The electrical resistivity sounding curve of a point is displayed in the curve window with the title as the sounding point number or name. Only one curve window can be displayed at a time (Figure 3.14). The apparent resistivity values from the field data are given by circles. The curve is drawn in black line and plotted with logarithmic scales for both apparent resistivity pa values (y-axis) and the AB/2 (x-axis).



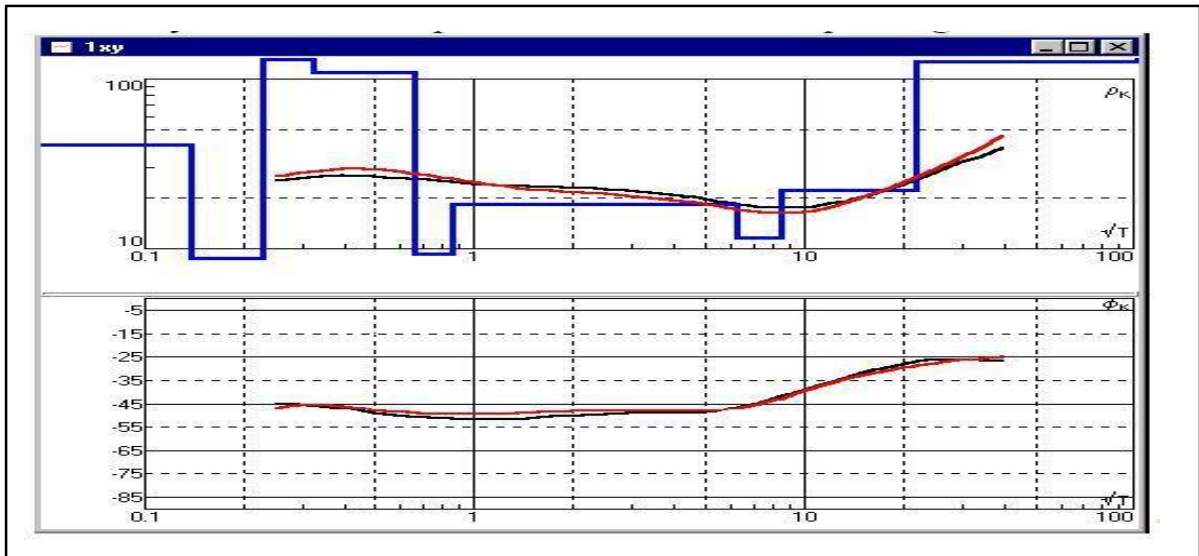


Figure 3.14 IPI2WIN Software curve window

### 3.8.3.4 Viewing cross-section

The pseudo cross-sections and the resistivity values can be viewed in the pseudo cross-section and the resistivity cross-section window. The name of the sounding is displayed in the top horizontal ruler and the sounding coordinates at the bottom horizontal ruler (Figure 3.15).

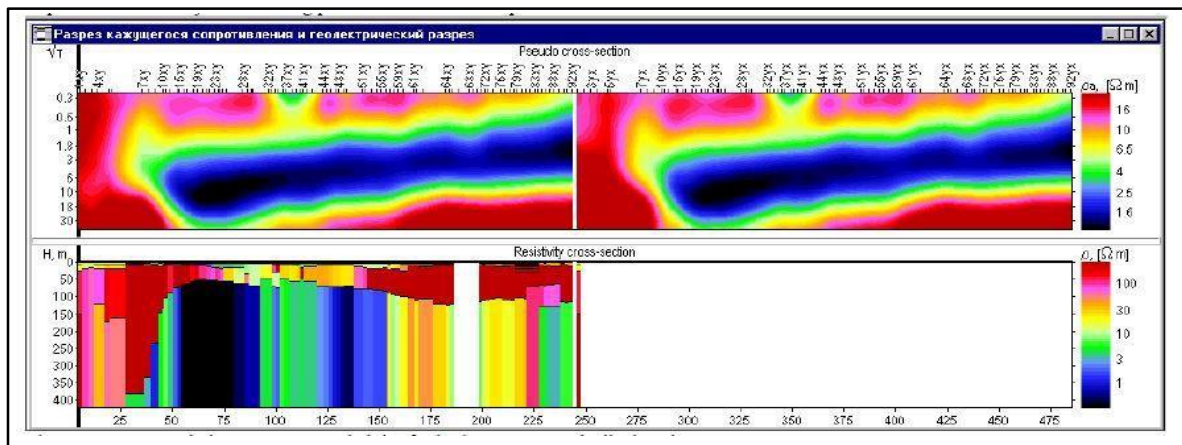


Figure 3.15 IPI2WIN Software cross-section window

### **3.8.4 Global Mapper**

Global Mapper is a powerful and easy-to-use GIS data processing application which provides the right level of GIS functionality to satisfy both experienced GIS professionals and mapping aspirants (Baby, 2012). Global Mapper is a great application for those looking for an affordable solution to meet the needs of enterprise-wide GIS applications or their mapping with unparalleled access to datasets of local and data rendering capabilities. Global Mapper is essentially a desktop application for anyone looking for maps or local data. In the present study, Global Mapper 18 was used for online downloading of Digital Elevation Model (DEM) of the study area. In addition, Image Analysis regarding banana cultivation was executed through Global Mapper application.

### **3.8.5 ArcGIS**

Geographic Information System (GIS) is great significance in our time because it is a comprehensive information system that is still evolving in line with the latest technology (Liu et al., 2017; Mitasova et al., 2004). The present age can be termed as the information age, when the whole world is experiencing and interacting with a new revolution that changes our traditional way of looking at things in a completely different manner. Research activities related to agriculture, industry, business, society and education, all emphasize on technology and its use. Advances in technology have changed our approach to the world and our need for complete reliance on technology and data (Patel et al., 2012). The importance of information is becoming of overriding importance for development. GIS package itself is an important module of the spatial information system (Anselin & Getis, 1992; Bajjali, 2018). The ideology of all industrialized countries and many other nations around the world relies heavily on services regarding research and development. This means that the current economy is increasingly dependent on computers, networking, accurate information and data (Castells, 1999; Kleine & Unwin, 2009). This change demands on increasing number of skilled workers able to handle

technology and data processing.

GIS technology is no exception when it comes to its use in water resources, geology, and environmentally relevant parameters (Almasri, 2008; Mouratidis et al., 2010). It is a powerful tool for evolving solutions for many applications, from creating color coded geological maps to managing dissemination of groundwater quality, as also monitoring and controlling water resources on local, regional scale or international scales (Singha et al., 2019).

Water is the most valuable resource for socio-economic growth and environmental sustainability. ArcGIS provides on easiest way for development of all natural resources database and its analysis with the help of statistical and visual data (Zhao et al., 2021). Geogenic contamination in groundwater sources is associated with types of rock deposits. Hence, toxic minerals creating health hazard remains a global challenge to safe groundwater supplying authorities. Therefore, necessary to develop big data strata and ArcGIS is the leading software which supports it is investigation such types of typical phenomena (Addison et al., 2020; Bhattacharya & Bundschuh, 2015; Naseem et al., 2014).

GIS has also been very helpful in the study of well water-related formations in order to facilitate supply more fresh water to the growing groundwater supply and irrigation supply in different regions (Jha et al., 2020; Valley, 2009) . GIS can be used to capture data for all components of aquatic resources to generate hydrological datasets, understand the hydrology of any region, its sources of pollution, to produce maps of water quality and water rock interaction, as well as to delineate water areas and much more (Ghoraba, 2015; Oh et al., 2011). In the present dissertation, development of GIS database for spatial analysis and displaying results through maps were computed on ArcGIS 10.5 software. The kriging method, one of the most common and widely used geostatistical interpolation method is applied for generating the maps (Béjar-Pizarro et al., 2016). Kriging generates maps by an inbuilt variogram model or appropriate variogram model can be specified. This method effectively incorporates the anisotropy and generates the underlying trends efficiently for the given data.

### **3.8.6 Grapher**

Without quality data, scientific research is considered incomplete (Kmet et al., 2004; Van Calster et al., 2021; Wesch et al., 2017). As such, the use of large quantities of data in research articles is facilitated with the help of various mathematical principles and expressions (Friedman, 2004). Results obtained are henceforth summarized and presented through easy-to-understand, tables and figures.

Data should however, in no way differ from the material on which the hypothesis is based. There are many ways to present tables and statistics the choice of which are based on the results obtained. In addition, some rules have been set forward by scholars in the APA and MLA research papers, both requiring tables and data, but having different rules. Tables and figures often extend results in the simplest terms in research. Software facilitates in creating a variety of tables and shapes to enhance the presentation of results are beautiful. In the present study, data for water analysis charts have been employed through Grapher Version 14.3. Grapher's extensive analysis charts and statistical features have been utilized to identify trends, find new insights, and locate opportunities. Grapher provides a holistic view of data.

### **3.9 Statistical Analysis**

Basic statistical analysis provides a clearer picture and description of the spatial distribution of water quality parameter for water samples of any area. The groundwater quality distribution for the study area has been studied by applying various statistical parameters. The description of these parameters are as follows.

### 3.9.1 Measure of Central Tendency and Dispersion

There are two basic descriptive statistics that can characterize the data from groundwater samples (Zhang, 2007), namely the central tendency and the dispersion of the data. For measurement of central tendency, three parameters are determined; mean, median and mode. The sample mean, also known as the arithmetic mean, is simply calculated by add all the samples and dividing it by the total numbers of samples. The median is determined by arranging the sample values in ascending or descending order and then finding out the central value. For odd numbers of samples the median is the exact central value of the data and for the even numbers of the sample the samples the median is calculated by taking the average of the two central sample values (Zhang, 2007). The value that is most repeated in the sample data is the modal value or simply the mode.

Dispersion of a data is represented by three statistical parameters: range, variance and standard deviation. The range of the data is described by the difference between the maximum sample value and the minimum sample value. The range is influenced by very low or very high sample values and its use in describing the dispersion is not much. The variance of samples is defined as Eq 3.6 (Zhang, 2007).

$$\sigma^2 = \frac{\sum(x - \bar{x})^2}{N} \dots\dots\dots \text{Eq 3.6}$$

The standard deviation is the under root of the variance as given in the Eq 3.7.

$$\sigma = \sqrt{\frac{\sum(x - \bar{x})^2}{N}} \dots\dots\dots \text{Eq 3.7}$$

N is the total number of samples and the term  $(x - \bar{x})$  is the difference between each value from the sample mean.

### 3.9.2 Principal Component Analysis

The most important step in improving any river basin's water quality and ecosystem is to evaluate it. Finding the factors that influence water quality and assessing it throughout a whole river basin is a very difficult and complicated procedure (Canobbio et al., 2013). To provide a holistic vision of all the variables involved in the system, PCA was used on the groundwater sample data for the study area (Gorgoglione et al., 2018; Gorgoglione et al., 2019).

The PCA method is composed of five main operation steps, as follows: (1) The original data matrix is listed in Eq 3.8.

$$X = (x_{ij})_{n \times p} = \begin{bmatrix} x_{11} & \cdots & x_{1p} \\ \vdots & \vdots & \vdots \\ x_{n1} & \cdots & x_{np} \end{bmatrix} \quad \text{Eq 3.8}$$

The originally measured data in the matrix is given by  $x_{ij}$ , the stations monitored re designated as  $n$ , and the water quality parameters are represented as  $p$ . To eliminate the impact of dimension, the original data is standard with Z-score standardization by the formula given below (Equation 3.9)

$$x_{ij}^* = (x_{ij} - \bar{x}_j) / s_j, \quad \text{Eq 3.9}$$

where  $x_{ij}^*$  is the standard variable,  $\bar{x}_j$  is the average value for  $j$ th indicator, and  $s_j$  is the standard deviation for  $j$ th indicator. The correlation coefficient matrix  $R$  is calculated with standardized data and the correlation between the indicators is determined.

$$R = (r_{ij})_{p \times p} = \frac{1}{n-1} \sum_{t=1}^n x_{ti}^* \cdot x_{tj}^* \quad (i, j = 1, 2, \dots, p) \quad \text{Eq 3.10}$$

The eigenvalues and the eigenvectors for the correlation coefficient matrix R is calculated and it is used to determine the principal components. The eigenvalues of the correlation coefficient matrix, R, are represented by  $\lambda_i$  ( $i = 1, 2, \dots, n$ ) and their eigenvectors are  $u_i$  ( $u_i = u_{i1}, u_{i2}, \dots, u_{in}$ ) ( $i = 1, 2, \dots, n$ ). The  $\lambda$  value corresponds to the variance of the principal component. And the value of variance is positively correlated with the contribution rate of the principal components. Further, the cumulated contribution rate of the first m principal components should be more than 80%, which means:  $\sum_{j=1}^m \lambda_j / \sum_{j=1}^n \lambda_j \geq 0.80$ . The principal component is represented by Equation 3.11

$$F_i = u_{i1}x_1^* + u_{i2}x_2^* + \dots + u_{in}x_n^* \quad (i = 1, 2, \dots, n) \quad \text{Eq 3.11}$$

where  $x_i^*$  is the standardized indicator variable.  $x_i^* = (x_i - \bar{x}_i) / s_i$ . The equation 3.12 is used to calculate comprehensive evaluation function is obtained by weighted sum of the calculated principal component.

$$F = \frac{\lambda_1}{\lambda_1 + \lambda_2 + \dots + \lambda_n} F_1 + \frac{\lambda_2}{\lambda_1 + \lambda_2 + \dots + \lambda_n} F_2 + \dots + \frac{\lambda_n}{\lambda_1 + \lambda_2 + \dots + \lambda_n} F_n \quad \text{Eq 3.12}$$

## **CHAPTER 4**

### **HYDROGEOCHEMISTRY**

#### **4.1 Introduction**

The assessment of the chemical and physical properties of groundwater is as important as the determination of groundwater distribution and available quantity (Haghnazar et al., 2022). Waters occurring in the natural environment are never pure, and many factors control their quality (Haiyan et al., 2021; Zhang et al., 2019). The groundwater resources are affected by the processes occurring at the surface as well as the nature and geological composition of the aquifer in which it occurs (Davraz & Batur, 2021).

Groundwater's use for any specific purpose depends on its quality. One reason for the degradation of groundwater quality is the presence of elements like arsenic and fluoride. By proper illustration of the chemical parameters by various diagrams such as Stiff and Piper, groundwater quality distribution can easily be understood. In addition to



this rise in groundwater, salinity is also another major problem. The increase in salinity may be caused by various reasons including proximity to the coastal areas, residual seawater, high rates of evapotranspiration etc.

Due to these, the total useable storage of groundwater for domestic and agricultural purposes gets restricted greatly for the semi-arid to arid areas (Edmunds, 2012; Mathivanan et al., 2022). Uthal in Balochistan is an arid region present near the coast, therefore the effective management of water resources has always been a challenge.

There is limited data on groundwater quality and also the knowledge at the national scale. This hinders the development of groundwater resources and also the management of scarce water resources. For sustainable groundwater monitoring related to its quality and occurrence, this study was conducted in Uthal, Balochistan (Figure 4.1), at 100 sites water samples were collected and analyzed Except for one sample, all water samples were collected from tube wells, and one sample was collected from a dug well. The groundwater level was 60 to 70 meters in the center plain area and 80 to 85 meters on the NE side towards the hills at the time of water collection.

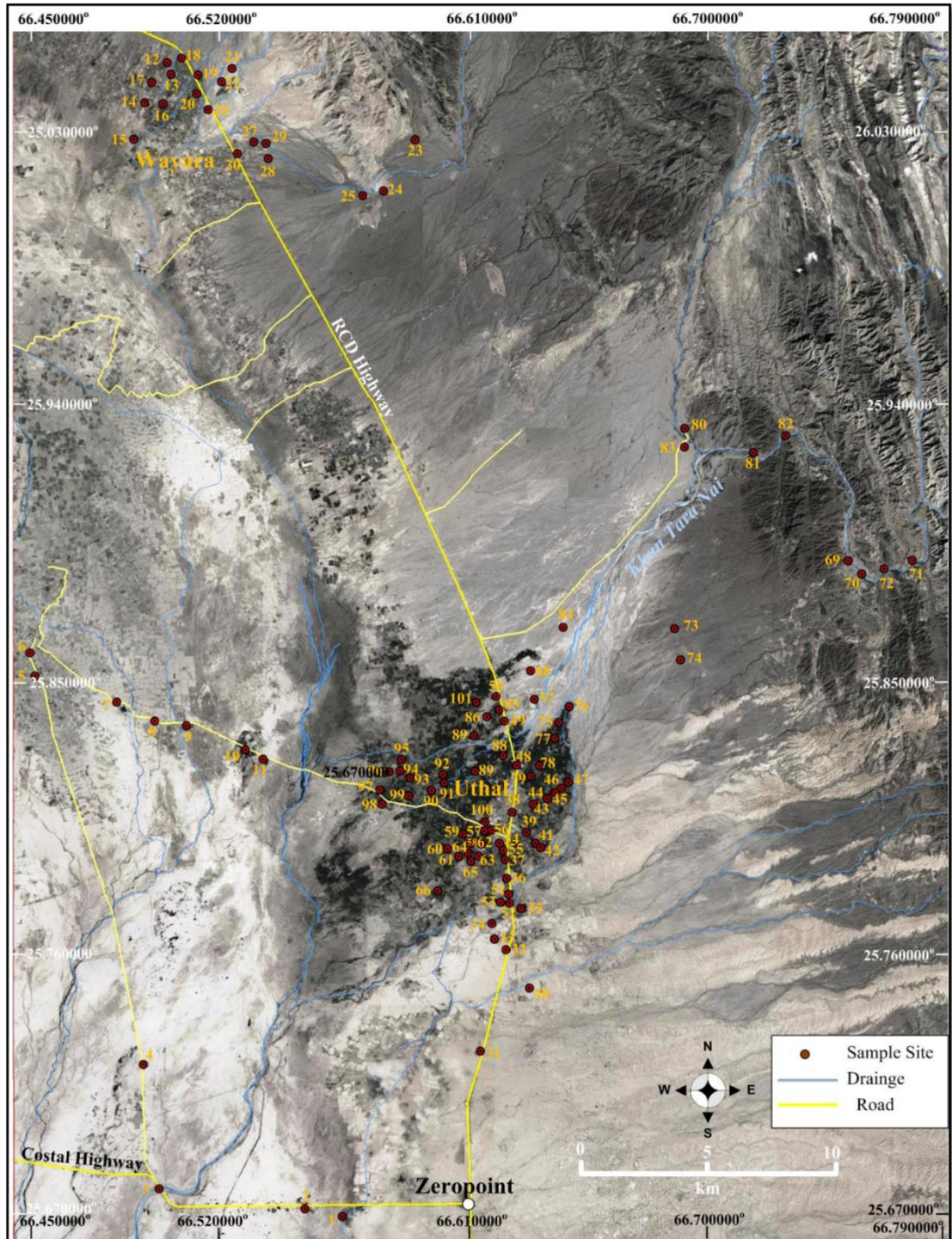


Figure 4.1 Location of water samples.

## 4.2 Geochemistry

Geochemical studies give us an insight through various parameters linking the geology and the water affected by the elements present in these rocks (Xiao et al., 2022). Geochemistry is the study of water quality based on the rock-water interaction. Rock is an aggregate of minerals, and these minerals are composed of elements. Many of these elements through various processes enter the surface and groundwater. The composition of rocks determines the elements entering groundwater and in the study area, various sedimentary rocks and Ophiolite are present. The biophile elements' physiological role is also of great importance for the health-related issues as well as the crops are grown in the study area (Naseem et al., 2010). The source of ions as mentioned earlier are the sedimentary rocks of the formations of the Ferozabad Group, and from Bela Volcanics intermixed with sedimentary sequences. Their interaction with water and the relative mobility of ions are studied for Uthal Balochistan. Hydrofacies analysis has been done from the Piper diagram, which effectively shows the type of water and its source.

Various diagrams have been plotted to show their effectiveness with respect to the water quality data analysis (Kut et al., 2019). The soil of all types is enriched with trace elements and thus study of the trace elements forms an important part of the study for assessing the drinking water quality. An excessive amount of trace elements in water may eventually produce toxicity in the drinking water and water for agricultural usage (Mthembu et al., 2021; Tiwari et al., 2021).

Water quality is also determined as the softness or hardness of the water. The water hardness is measured by the capacity of how it reacts with soap. More soap is required to produce lather in hard water. Hard water also produces greater deposits in the pipes and pans containing the water. The hardness is caused by the wide number of metallic ions like calcium(Ca) & magnesium(Mg) cations and other cations like aluminum (Al), iron (Fe), barium (Br), strontium (Sr), manganese (Mn) , and zinc (Zn), etc, dissolved in water (Jiang et al., 2022; Zhang et al., 2021). The hardness of the water sample is expressed in units of milligrams (mg) of calcium carbonate per liter. Table 4.1 shows the ranges of hard and soft

waters.

Table 4.1 Measure of hardness (WHO, 2017)

<b>Water Type</b>	<b>CaCO<sub>3</sub> (mg/l)</b>
Soft	< 60
Moderately hard	60-120
Hard	120-180
Very hard	>180

The physical parameters for 100 water samples from the study area are given in Table 4.2 and the cations and anions of major elements are given in the Table 4.3.

Table 4.2 Physical parameters for water samples of study area

<b>Latitude</b>	<b>Longitude</b>	<b>pH</b>	<b>TDS</b>	<b>EC</b>
25.6726	66.5642	6.6	9000	18
25.6751	66.5505	7.3	1807	3.614
25.6817	66.497	6.7	3860	7.72
25.7228	66.4912	7.7	3040	6.08
25.8514	66.4513	7.8	1070	2.14
25.859	66.4495	6.1	6860	13.72
25.8427	66.4814	7.9	1559	3.118
25.8364	66.4954	7.7	1410	2.82
25.8349	66.507	7.9	1572	3.144
25.827	66.5287	8	1638	3.276
25.8239	66.5352	7.8	1704	3.408
26.0538	66.5	8.1	536	1.072
26.0500	66.5015	7.5	588	1.176
26.0407	66.4918	8.1	909	1.818
26.0286	66.4877	8.1	1060	2.12
26.0402	66.4986	7.8	824	1.648
26.0474	66.4944	7.8	682	1.364
26.0553	66.5054	7.3	265	0.53
26.0498	66.5114	8	644	1.288

<b>Latitude</b>	<b>Longitude</b>	<b>pH</b>	<b>TDS</b>	<b>EC</b>
26.0519	66.524	8.1	511	1.022
26.0281	66.5914	1.1	1128	2.256
26.0115	66.5796	7.6	282	0.564
26.0100	66.572	7.1	280	0.56
26.0383	66.5152	6.8	725	1.45
26.0275	66.532	7.5	774	1.548
26.0221	66.5373	7.4	950	1.9
26.0271	66.5365	7.8	747	1.494
26.0237	66.526	8.2	1058	2.116
25.7273	66.615	7.7	3340	6.68
25.7609	66.6244	7.6	3820	7.64
25.7643	66.6202	7.5	1890	3.78
25.7696	66.6193	7.7	1940	3.88
25.7745	66.6299	7.4	3340	6.68
25.7845	66.6247	7.9	1337	2.674
25.7906	66.6241	7.6	1258	2.516
25.8063	66.6267	7.6	1463	2.926
25.7997	66.632	7.7	1232	2.464
25.7482	66.633	7.1	867	1.734
25.7961	66.6353	7.8	930	1.86
25.7947	66.6372	7.7	1554	3.108
25.809	66.6344	7.6	904	1.808
25.8108	66.6396	8	1406	2.812
25.8129	66.6425	7.6	1565	3.13
25.8143	66.6448	7.2	1280	2.56
25.8162	66.6474	7.3	1418	2.836
25.8219	66.6283	7.4	886	1.772
25.8365	66.6238	7.4	828	1.656
25.8446	66.6208	7.5	1235	2.47
25.7792	66.6254	7.5	1688	3.376
25.7763	66.6257	7.7	1263	2.526
25.7766	66.6225	7.6	2000	4
25.7961	66.622	7.5	1650	3.3
25.7938	66.6234	7.5	1110	2.22
25.8004	66.6192	7.5	1086	2.172
25.8002	66.6165	7.5	910	1.82
25.796	66.6116	7.5	4480	8.96
25.7991	66.6087	6.8	1612	3.224
25.7942	66.6029	7.3	1381	2.762
25.7917	66.607	7.7	2820	5.64

<b>Latitude</b>	<b>Longitude</b>	<b>pH</b>	<b>TDS</b>	<b>EC</b>
25.7958	66.6153	7	3020	6.04
25.7919	66.6142	7.5	1294	2.588
25.7928	66.6105	7.8	1390	2.78
25.7901	66.6116	7.9	2440	4.88
25.7803	66.5993	7.6	800	1.6
25.8437	66.6348	7.7	543	1.086
25.853	66.6335	7.5	609	1.218
25.8892	66.75	7.5	748	1.496
25.8849	66.755	7.6	717	1.434
25.8893	66.7734	7.9	733	1.466
25.8866	66.7631	8	740	1.48
25.8669	66.6864	7	1580	3.16
25.8566	66.6886	7.6	1466	2.932
25.836	66.6439	7.9	744	1.488
25.8411	66.6476	7.6	613	1.226
25.8308	66.6424	7.4	1130	2.26
25.8218	66.6367	7.1	1245	2.49
25.8182	66.6336	7.4	786	1.572
25.933	66.6901	7.4	718	1.436
25.9249	66.7153	7.1	745	1.49
25.9306	66.7271	7.2	735	1.47
25.9269	66.6901	7	740	1.48
25.8674	66.6455	7.5	607	1.214
25.8402	66.622	7.6	928	1.856
25.8379	66.6174	7.3	1139	2.278
25.8316	66.6127	7.7	783	1.566
25.825	66.6235	7	890	1.78
25.8198	66.6131	7.5	876	1.752
25.8135	66.5971	7.3	1685	3.37
25.816	66.6018	7.3	1120	2.24
25.8187	66.6013	7	1194	2.388
25.8177	66.5892	7.3	1357	2.714
25.82	66.5856	7.5	1582	3.164
25.8238	66.586	7.7	1720	3.44
25.8197	66.5815	7.5	1097	2.194
25.8137	66.5781	7.3	1668	3.336
25.8089	66.579	7.1	911	1.822
25.8117	66.5887	7.8	1648	3.296
25.8032	66.6167	7.3	1030	2.06
25.8426	66.6135	7.6	1290	2.58

Table 4.3 Major ions for water samples of study area

Latitude	Longitude	Ca	Cl	HCO <sub>3</sub>	K	Mg	Na	NO <sub>3</sub>	SO <sub>4</sub>
25.672584	66.564194	93	620	107	18	160	832	85	993
25.675113	66.550497	102	325	187	10	41	494	68	769
25.681667	66.496956	163	120	123	22	62	1157	53	793
25.722845	66.49115	216	144	71	8	73	865	61	310
25.851379	66.451348	95	200	410	6	95	233	55	318
25.858975	66.449503	857	803	235	34	193	1534	61	4411
25.842726	66.481372	69	330	103	2	45	415	51	276
25.83644	66.495357	77	610	134	3	47	356	59	156
25.834933	66.507009	72	701	142	3	56	475	53	256
25.826959	66.52874	103	710	140	3	62	421	62	189
25.823902	66.535192	102	750	174	4	70	446	53	242
26.053804	66.500045	43	80	230	2	48	95	62	95
26.049994	66.5015	64	110	253	3	55	116	55	123
26.040689	66.491833	89	230	191	3	87	147	59	281
26.02862	66.48774	73	350	221	1	77	208	69	181
26.04021	66.49857	73	130	246	2	71	135	63	190
26.04735	66.49438	61	180	242	2	53	112	72	130
26.05532	66.50539	57	100	284	2	56	104	51	101
26.049777	66.51141	61	100	284	2	47	117	51	119
26.04353	66.51099	58	120	248	2	47	114	59	117
26.05186	66.52403	53	100	205	2	31	107	59	153
26.02811	66.59137	99	430	295	3	46	280	58	169
26.01147	66.57961	50	64	136	4	9	53	48	44
26.01	66.57195	45	7	58	4	6	51	58	61
26.03829	66.51521	52	180	270	2	52	159	54	117
26.02753	66.53203	55	250	231	2	42	156	57	80
26.022053	66.53734	65	350	262	2	61	188	62	110
26.02706	66.53654	62	180	228	2	48	142	65	74
26.02368	66.52601	89	330	221	2	62	214	76	173
25.727334	66.614964	158	2060	116	5	96	1063	63	166
25.760872	66.624403	73	2150	406	5	109	1540	95	648
25.76434	66.6202	116	880	132	5	56	563	67	181
25.76955	66.61926	150	850	161	5	80	515	73	279
25.77448	66.629941	50	1270	448	4	52	1033	100	432
25.78445	66.6247	97	590	133	4	45	328	70	182
25.79064	66.62406	123	590	138	5	56	287	62	104
25.8063	66.62674	199	500	131	5	113	261	111	284
25.79965	66.632	144	380	273	5	75	295	82	257
25.748191	66.633	79	320	170	4	38	220	67	158

Latitude	Longitude	Ca	Cl	HCO <sub>3</sub>	K	Mg	Na	NO <sub>3</sub>	SO <sub>4</sub>
25.79612	66.63526	65	260	182	3	23	209	68	136
25.79468	66.63715	34	300	188	2	12	233	63	107
25.809	66.63444	122	450	384	4	66	340	81	227
25.81083	66.6396	108	410	355	3	63	309	78	219
25.81286	66.64254	133	620	346	4	72	326	80	252
25.81428	66.64484	138	380	291	4	75	282	85	243
25.816163	66.64744	147	610	301	4	81	243	67	105
25.82185	66.628345	110	190	276	4	54	155	78	185
25.836469	66.623796	99	300	230	6	46	149	71	167
25.844564	66.620796	42	420	327	8	70	319	61	249
25.77917	66.62543	38	420	437	3	44	609	84	275
25.77629	66.62571	34	320	362	2	35	432	77	195
25.77655	66.62245	117	820	229	4	74	608	75	374
25.79607	66.62199	205	560	242	5	112	283	82	420
25.79377	66.62336	101	550	169	4	48	234	67	152
25.800449	66.619231	138	370	183	5	65	184	82	235
25.800171	66.616463	92	260	143	5	43	199	63	218
25.79603	66.6116	562	1460	211	10	281	546	69	1206
25.79912	66.6087	196	380	201	6	92	266	83	472
25.79424	66.60293	171	570	145	6	75	243	67	297
25.79174	66.60703	449	1260	169	8	205	379	72	848
25.79579	66.61534	242	800	287	6	155	633	94	999
25.79188	66.61421	134	490	155	5	62	226	72	264
25.79277	66.61052	134	540	156	4	63	253	79	290
25.7901	66.61156	306	890	197	7	135	327	86	519
25.78032	66.59934	62	280	154	3	28	159	65	148
25.84365	66.63483	73	122	196	5	28	79	71	102
25.85304	66.63354	75	148	202	5	30	92	66	120
25.889234	66.750017	98	170	204	7	33	141	60	211
25.884913	66.754956	79	206	201	6	31	144	57	221
25.889324	66.773434	89	192	244	6	31	150	60	228
25.886556	66.763139	86	196	211	6	32	152	92	226
25.86694	66.68636	19	560	470	1	6	574	67	46
25.85661	66.68856	43	320	860	2	9	565	57	72
25.83603	66.64388	81	160	317	4	39	144	78	163
25.84114	66.64761	70	150	251	4	32	123	72	140
25.83075	66.64238	117	300	391	4	58	239	64	259
25.82177	66.63668	147	412	264	5	72	212	94	317
25.81823	66.63364	99	232	291	4	43	143	68	179
25.93297	66.69014	114	174	366	4	35	150	77	118



Latitude	Longitude	Ca	Cl	HCO <sub>3</sub>	K	Mg	Na	NO <sub>3</sub>	SO <sub>4</sub>
25.92492	66.71526	95	216	236	6	34	152	57	216
25.93056	66.72712	90	204	233	6	35	143	62	219
25.926867	66.690067	98	176	362	4	35	146	67	110
25.86742	66.64548	86	164	209	5	29	99	72	148
25.84023	66.62195	108	283	293	6	53	187	77	200
25.83788	66.6174	128	368	298	6	67	242	71	295
25.83163	66.61268	83	240	199	5	42	167	62	207
25.82501	66.62346	131	254	291	5	60	167	73	214
25.8198	66.61311	115	282	221	5	56	150	74	204
25.81352	66.59708	196	640	306	6	115	307	83	527
25.81598	66.60184	124	450	221	5	61	228	58	289
25.81872	66.6013	160	440	219	6	76	209	854	333
25.81765	66.5892	176	560	202	5	84	225	70	297
25.81997	66.58558	223	670	161	4	114	228	78	374
25.82378	66.58598	184	630	303	6	146	326	73	433
25.81972	66.5815	117	420	206	4	65	210	69	218
25.81369	66.57811	155	920	141	6	74	414	66	259
25.80894	66.57895	83	360	157	4	41	195	60	180
25.81168	66.58865	178	810	185	5	92	274	67	245
25.80321	66.61671	124	290	196	4	61	175	77	266
25.84264	66.61352	106	310	396	4	60	269	71	263

#### 4.2.1 pH and Alkalinity of groundwater

For any given water sample pH value refers to H<sup>+</sup> molecule concentration in the solution. suitability and usage of water is determined by the pH value. pH values of water range from 0 to 14. Freshwater pH values depend on weather conditions, human activities, surface and subsurface geology, and natural processes. Water having a pH value of 7 is neutral, less than 7 is termed as acidic and the water has more free H<sup>+</sup> concentration. Water is termed basic if it has greater than 7 pH indicating a higher concentration of hydroxyl ions. According to WHO standards safe drinking water range and for daily domestic use is 6.2 to 8.8 (WHO, 2017). The water may contain different concentration of elements dissolved, which is determined by the pH value. It also indicated the concentration of heavy metal that is dissolved in it and the nutrients it may contain (WHO, 2017). The water

samples having a lower value indicate that a higher amount of elements are dissolved in it.

The higher concentrations of  $\text{CO}_3$  and  $\text{HCO}_3$  ions cause the groundwater to become alkaline. The minimum pH value obtained for the water samples of the study area is 6 and the maximum 8.2 (Table 4-1). The standard deviation and the average difference between all water samples are 0.4 and 7.5 respectively. Many different kinds of micronutrients like Fe, Mn, Zn & Cu, etc, essential for the healthy growth of crops are also indicated by the pH values (Bailey & Bilderback, 1997).

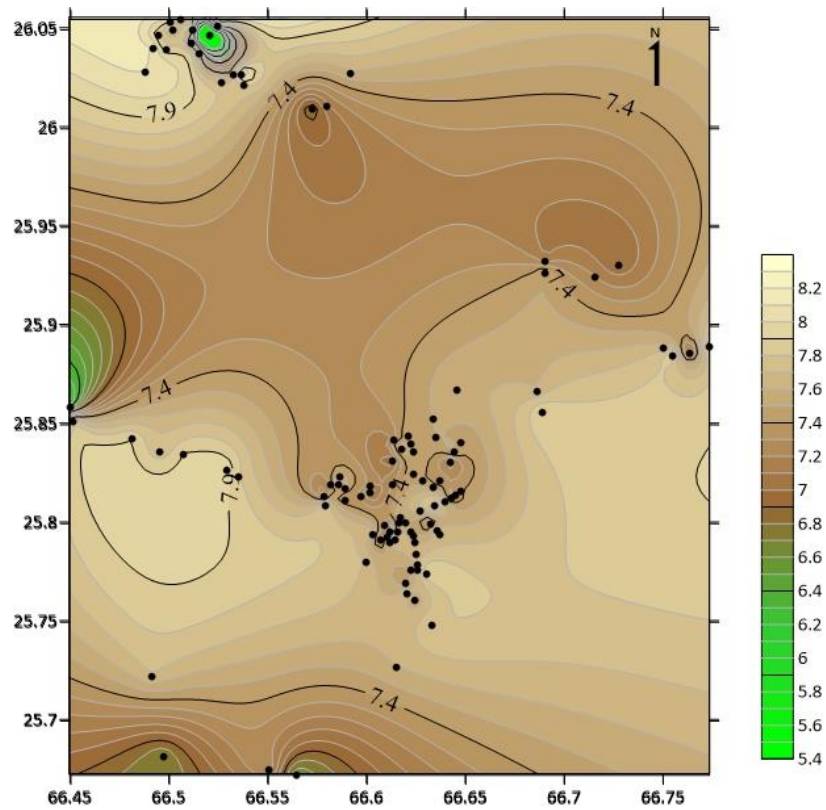


Figure 4.2 pH distribution for the study area

#### **4.2.2 Electrical Conductivity (EC) and Total Dissolved Solids (TDS)**

The measure of the ability of water to conduct current is termed as Electrical conductivity (EC). TDS is the number of salts in water. Both EC and TDS, provide a measure of the number of dissolved salts and the inorganic material in the water sample. The electric current in water flows due to the presence of ions. Due to the breaking of salt into positive and negative ions, the water becomes electrically conductive. Therefore, the amount of dissolved salts determines the Electric Conductivity in water (Rusydi, 2018). Higher EC values indicate the presence of higher amounts of chemicals or salts dissolved in water. Siemens (S) or mS are the units for measuring EC of the water sample and it is reciprocal to the resistance of water (ohms/meter) at 25 ° C. for drinking purposes high saline water gives a bad taste, whereas for agricultural productivity the salinity of the water has more far-reaching effects on yield and quality (Safdar et al., 2019). High salinity of the water is considered a hazard for agricultural purposes and thus forms the main parameter while assessing agricultural productivity based on the water quality (Bouaroudj et al., 2019).

Total dissolved salts (TDS) for the study area is in the range of 265 mg/l to 9000 mg/l (Figure 4.3), with a mean value of 1437 mg/l. Water samples from the study area are mostly all in the range of hard water according to the WHO standard (WHO, 2017) of water for daily use. Most of the water samples from the study area are within the extremely hard water ranges, four samples in hard water range and only one sample in soft water range. Thus, the water of study is categorized as extremely hard and not very well suited for domestic use. This can cause taste issues in the population of the study.

Samples from the study area indicate that EC is in the range of 0.53 to 18, with a mean value of 2.8 (Figure 4.4). The high EC of water reduces the ability of plants to obtain water, which in turn absorbs other essential ions in the soil solution.

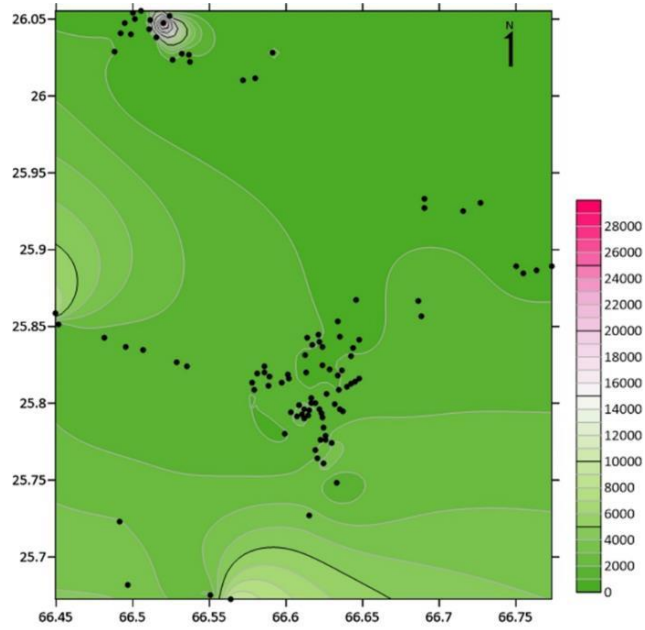


Figure 4.3 Spatial distribution of Total Dissolved Salts TDS

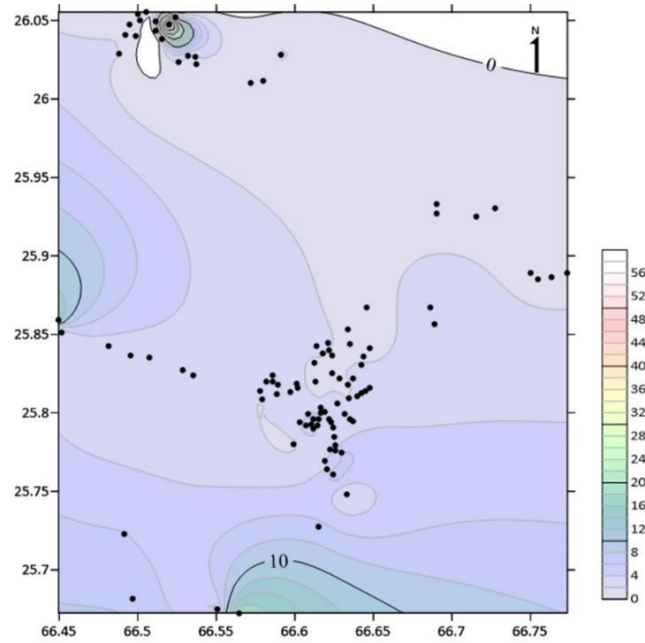


Figure 4.4 Spatial distribution of electrical conductivity ( $\mu\text{s}/\text{cm}$ )

### **4.2.3 Sodium (Na) and Potassium (K)**

#### **Sodium (Na)**

The groundwater samples from the study area had sodium distribution in range of 50.7 – 1858 mg/l (Figure 4.5). The permissible sodium limit by WHO is 200 mg/l. The total sodium content of the study area is much higher than the permissible limit. High Na content in water can cause hypertension, heart disease, calcium retention & bone density, and kidney disease (Zhang et al., 2020c). Na is important as it regulates the electrolytic balance in human bodies. Most of the Na, (approximately 98%) is absorbed in the intestines. Some Na loss occurs through sweating while most of the remaining sodium is excreted by the kidneys. For a healthy adult, the sodium is balanced in the body by the excretion of sodium being equal to the intake under normal conditions (Doyle, 2008). Sodium distribution (Figure 4.5) indicated low Na values in the north, northeast, and northwest of the study area. Higher sodium values are observed in the south and southwest of the study area, which is a plain land towards the coastal areas of Miani Hor. The Uthal agricultural lands show low sodium concentration.

#### **Potassium (K)**

Potassium concentration in groundwater samples from the study area is between 01 mg/l to 34 mg/l, and has an average value of 4.9 mg/l (Figure 4.6). The concentration of Potassium in the study area is within the safe limits (Table 4.2) as given by WHO (2017). Potassium is the third most abundant element in the human body, acts as an electrolyte along with sodium. Potassium helps in regulating body functions, it regulates the heart, kidney, brain, muscle tissues, and other important organs and keeps them in good health.

A high intake of potassium in the human lower the excretion of calcium from the urinary track, its adequate quantities in the human body is essential for the management of hypercalciuria and kidney stones. Its increased intake, thus lowers the risks of osteoporosis, especially in females. With lower K serum, the body may become glucose intolerant and may develop diabetes. With adequate K intake development of diabetes can be prevented (He & MacGregor, 2008).The Figure 4.6 shows the Potassium (K) concentration for the collected water samples of the study area. High levels of K were found same sample sites of Na while whole upper and central samples contained low level of K. Mostly Uthal agricultural land showed low K zone in the study area.

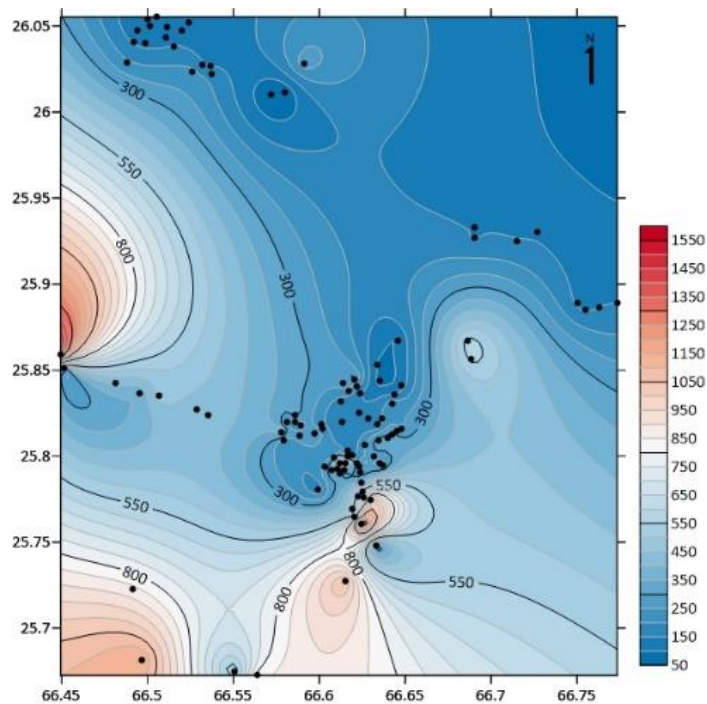


Figure 4.5 Spatial Distribution of Sodium (mg/l)

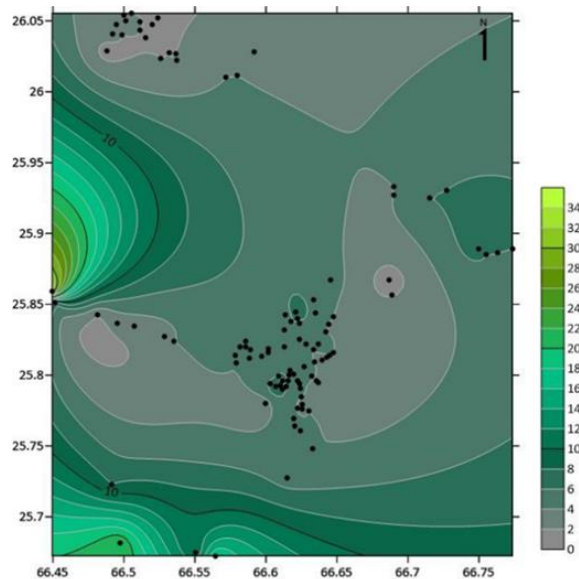


Figure 4.6 Spatial distribution of Potassium (mg/l)

#### 4.2.4 Calcium (Ca) and Magnesium (Mg)

##### Calcium (Ca)

Calcium variation in water samples of study area is from 19 mg/l to 857 mg/l and shows an average of 124.5 mg/l (Table 4.3). According to WHO, (2017) the permissible limit for Ca in drinking water is 200 mg/l. It is within the permissible drinking water limit for most of the groundwater samples from the study area as recommended by WHO, except for a few samples (Figure 4.7). Calcium is one of the most important and abundant metals in the human body. It is a mineral included in the daily diet and 1.2 kg of calcium is present in the human body. It has key metabolic functions, besides being the main constituent of bones and teeth. It also helps the functions of nerves and muscles. Lack of calcium is of the main cause of osteoporosis. Osteoporosis is a disease in which bones are extremely porous and subject to fracture. Muscle tissue and blood also contain Calcium. Calcium is essential for the development of the cell membrane, it is also one of the components responsible for the contraction of muscles, and also important in blood clotting (Lenntech, 2013). For an adult, a daily intake of 1000 mg of Ca is recommended for the proper working of body functions.

## Magnesium (Mg)

The lowest value of Mg content in the water samples is 5.77 mg/l and the highest concentration in the water samples 281 mg/l (Figure 4.8) with a mean value of 65 mg/l. According to WHO 2017, standard for drinking water, Mg from 30 mg/l is ideal and the Mg concentration levels up to 150 mg/l is considered safe. Higher concentrations of Mg, particularly above 700 mg/l, may have laxative effects on the human body. However, with a continuous high intake of magnesium, the body adapt to the laxative effect. Magnesium is responsible for maintaining muscles and nerve function and also activation of enzymes, in the human body. Low magnesium in the human body causes fatigue, nausea, loss of appetite, weakness, and vomiting. All these are early signs of Mg deficiency in the human body (Faryadi, 2012). With severe magnesium deficiency, numbness, cramps, tingling and muscle contractions may occur. In the case of severe Magnesium deficiency, can cause very low levels in low levels of Ca and K in the blood (Rude, 1998). Disease like cholesterol level hypertension, cardiovascular disease, type2 diabetes can be control by taking high Magnesium (Ross et al., 2013)

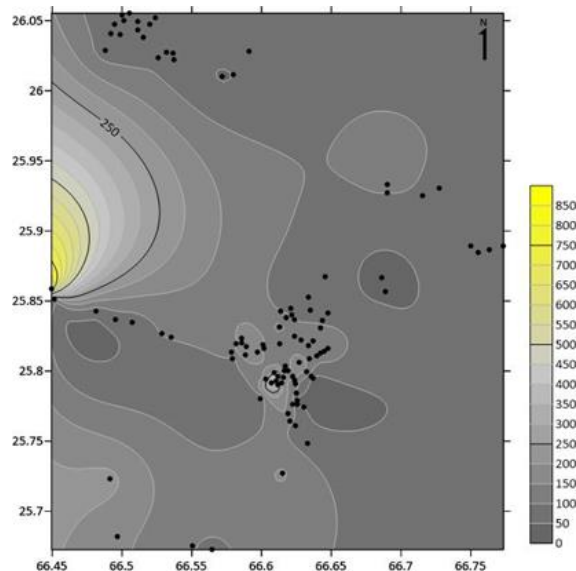


Figure 4.7 Spatial distribution of Calcium (mg/l)



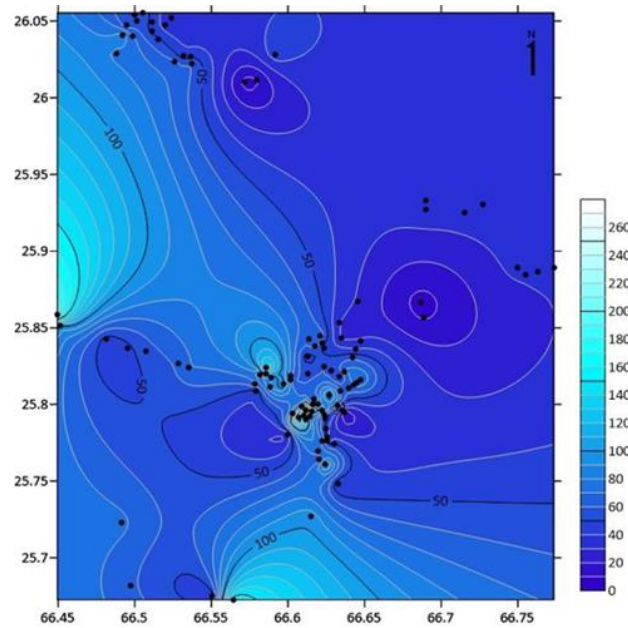


Figure 4.8 Spatial distribution of Magnesium (mg/l)

#### 4.2.5 Sulphate (SO<sub>4</sub>) & Chloride (Cl)

##### Sulphate (SO<sub>4</sub>)

SO<sub>4</sub> is the third most abundant ion in Uthal, with the concentration next to Cl and HCO<sub>3</sub>. SO<sub>4</sub> values are in the range of 44 to 4411 and have an average concentration of 295.7 mg/l (Figure 4.9). According to WHO (2017) the permissible limit for drinking water is 200 and 600 mg/l. The average concentration of SO<sub>4</sub> in groundwater samples is approximately 295.7 mg/l which is well within the permissible limits, only four water samples have higher concentrations. Excess of SO<sub>4</sub> can cause diarrhea and dehydration in those who are not accustomed to the high consumption of SO<sub>4</sub> ions. Kids in particular are more sensitive to SO<sub>4</sub> than adults. SO<sub>4</sub> concentration is one of the most essential parameters in determining the water quality as its high concentration can cause laxative effects in humans (WHO,

2017), therefore it is considered as one of the main parameters while assessing the quality of groundwater. The groundwater samples show that the concentration of  $\text{SO}_4$  is low in the study area, only a slightly higher concentration is observed from the water sample on the southwestern side of the study area.

### **Chloride (Cl)**

The most abundant anion of the study area is chloride. The concentration of  $\text{Cl}^-$  in the groundwater samples is in the range of 7-2150 mg/l. This amount is much higher than the desirable limit of 250 mg/l and is also higher than the maximum permissible limits for drinking water (Figure 4.10). Chloride contributes to the osmotic activity in human body fluids and 88% of it is extracellular. Chloride is an important constituent of our body and along with potassium and sodium, it performs very important functions in regulatory bodily tasks. Along with sodium and potassium, chloride forms channels in the specific channels in the membranes of our cells which help to carry out different vital tasks.

Chloride is an important constituent of our body and along with potassium and sodium, it performs very important functions in regulatory bodily tasks. Along with sodium and potassium, chloride forms channels in the specific channels in the membranes of our cells which help to carry out different vital tasks. Chlorides are vital in keeping the electrolytic balance in our bodies and regulate the movement of water and other nutrients in the body cells of the human body. Thus, it plays a vital role in regulating blood pressure and the pH value in the human body. It is also important for muscles, heart function, and for nerve cells. It also helps in the digestion of food. Chloride toxicity is not common in humans and can only be seen in impaired NaCl metabolism caused by congestive heart failure. In humans, fluid loss normally is about 1.5-2 liter/day and the chloride with it is 4 g/day. Most of the chloride is excreted in the urine, with a minor amount of chloride loss in feces and sweat (Bashir et al., 2012). Not much is known about the high intake of chloride in diet (WHO, 2017).

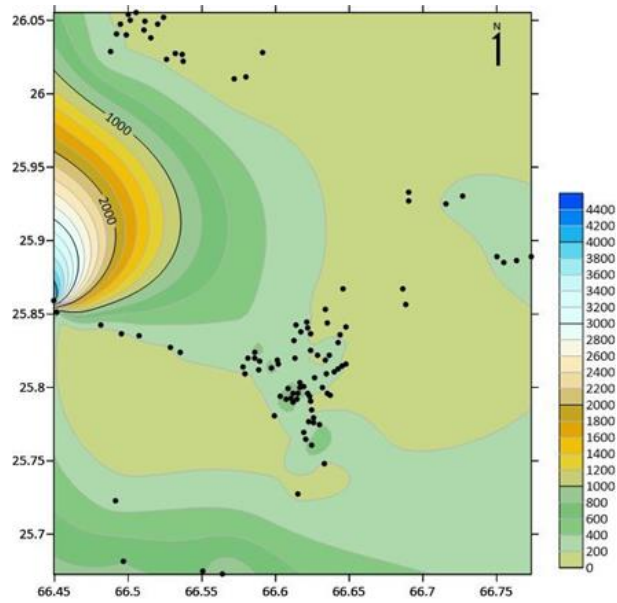


Figure 4.9 Spatial distribution of SO<sub>4</sub> (mg/l)

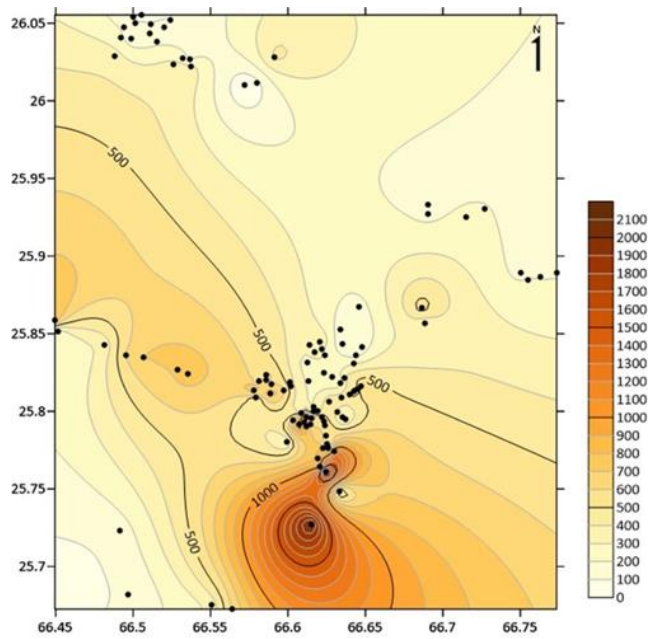


Figure 4.10 Spatial distribution of Chlorides (mg/l)

#### 4.2.6 Bicarbonate

The bicarbonates in water samples from the study area are in the range of 58 mg/l to 860 mg/l, with a mean value of 238.5 mg/l. This is less than the minimum desired limit of 300 mg/l. The maximum permissible limit is 600 mg/l. Figure 4.11 shows the distribution of bicarbonates in the water samples. Bicarbonates is important in pH control in the cardiac cell of the body. It also plays an important role in digestion as it is secreted by the stomach. It is also one of the major elements in our body. It helps in reducing the acidity due to the diet. It maintains the acid-base balance in the human body and balances the pH of the blood. Water having adequate quantities of  $\text{HCO}_3$  are helpful in the prevention of uric acid renal stones and reoccurrence of calcium oxalate (Frassetto et al., 1997). Bicarbonate also works with Na & K to help regulate the electrolytic balance. Figure 4.11 explained distribution of  $\text{HCO}_3$  concentration based on collected water samples. IDW interpolation located high  $\text{HCO}_3$  groundwater sites and its impacts on neighborhood. Highest concentration extracted from the samples sites which found foothills of eastern mountains.

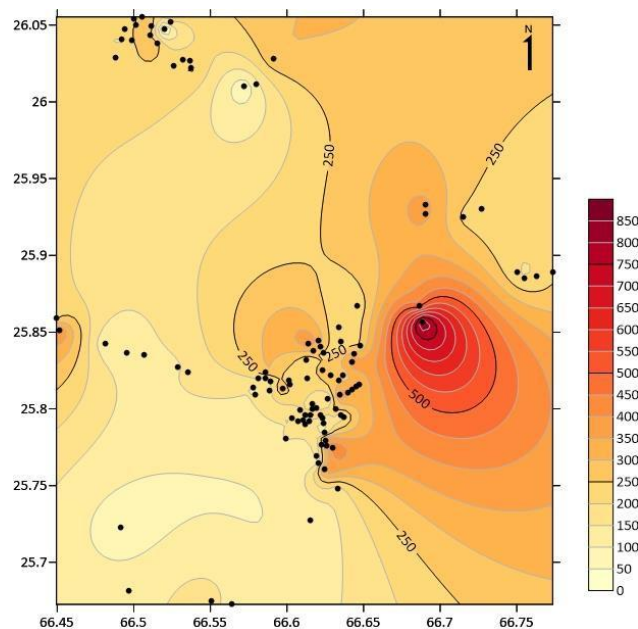


Figure 4.11 Spatial concentration of Bicarbonates (mg/l)

#### 4.2.7 Nitrate

The  $\text{NO}_3$  was ranged from 48 to 854 mg/l with an average of 76.69 mg/l in the study area, which was too much higher than the limit. The permissible limit of  $\text{NO}_3$  is 50 mg/l (WHO, 2017). Figure 4.12 shows the highest concentration of nitrate in the agriculture areas. The result showed that the artificial fertilizer used for cultivation may leach and affects groundwater quality. The Distribution of  $\text{NO}_3$  clearly depicted that cultivated area affected due to uses of artificial fertilizer that has been utilized for soil fertility. Only very small area recorded highest value of  $\text{NO}_3$  in the groundwater. Interpolation demarcated some significant value only on core cultivated zone in the study area. Although nitrate is an essential nutrient for the plant and animal, but in humans, the higher intake may cause diarrhea, dehydration and changes of hemoglobin in blood because high nitrate hinders to transport oxygen to other part of the body.

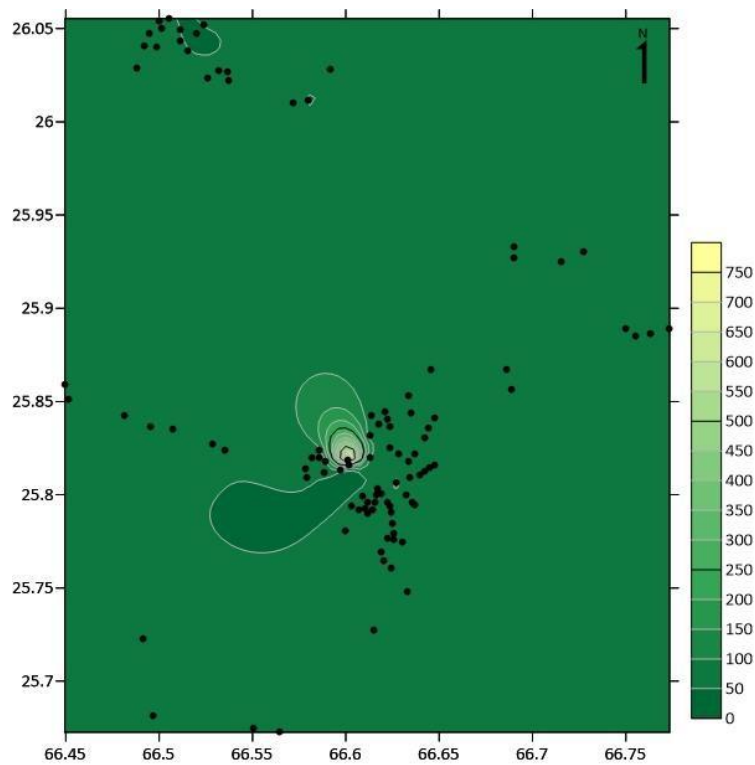


Figure 4.12 Spatial concentration of  $\text{NO}_3$  (mg/l)

The physicochemical properties of the groundwater samples were statistically calculated, and the findings, comprising of minimum, maximum, average, and standard deviation values, are shown in Table 4.4.

Table 4.4 Physical parameters and major cation and anions of the study area (WHO, 2017)

<b>Parameters</b>	<b>Min</b>	<b>Max</b>	<b>Average</b>	<b>SD</b>	<b>WHO Standards</b>
pH	6.1	8.2	7.5	0.4	6.2-8.8
TDS (mg/l)	265	9000	1437	1222	1000
EC ( $\mu$ s/cm)	0.50	18	2.82	1.216	--
Na (mg/l)	50.7	1858	324	311	200
K (mg/l)	1	34	4.9	4.07	4.5
Ca (mg/l)	19	857	124.5	107.7	200
Mg (mg/l)	5.77	281	65	42	150
SO <sub>4</sub> (mg/l)	44	4411	295.7	459	600
Cl (mg/l)	7	2150	432	372	250
HCO <sub>3</sub> (mg/l)	58	860	238.5	106	600
NO <sub>3</sub> (mg/l)	48	854	76.7	79.4	-

### 4.3 Ionic Composition

The ion balance error (IBE) of positive and negative ions of groundwater from the study area was estimated. The water samples always have a balance of positive and negative ions, in accordance with the principle of electromagnetism (Riveros-Perez & Riveros, 2018). To establish the validity of the analytical work, an Ion Balance Error (%) is estimated by the equation given below:

$$\text{Ion Balance Error (\%)} = [\sum\text{Cations} - \sum\text{Anions}] / [\sum\text{Cations} + \sum\text{Anions}] \times 100$$

The maximum ion balance error (%), according to Moiseenko et al., (2018) should not be more than 5% between the total cations and anions. For the groundwater analysis of Uthal, a maximum value of IBE was 3%, that is within the acceptable range. It reflects a high degree of precision and accuracy of the analytical work.

### 4.4 Hydrofacies

To represent the ionic structure of water, a piper diagram is generated. In a piper diagram, two straight triangles on the right are for cations and the two triangles on the left are for the anions. The cations and anions are collectively shown in the center of the diagram in the central diamond shaped area as a single point (Ray & Mukherjee, 2008). The genetic association of water is represented by the hydro facies. With a piper diagram, a clear concentration of cations and anions can be observed separately. The ionic structure of a large number of samples can easily be shown on a piper diagram. Thus, two water samples from different sources can easily be imaged with a piper diagram (Arslan et al., 2012).

Figure 4.13 shows the distribution of the cations and anions for the groundwater samples of the study area. More than 80% of the groundwater samples are indicating mixed cation and anion distribution, and approximately 20% of the samples are Na-K-type. In the main event, 61% of the samples are prepared in the mixed type and 39% fall into the Cl

type. From the hydrofacies analysis of the water samples, it was indicated that the water originates from the geological environments of the study area. The type of water is indicated as MgCaCl, as most of the cations and anions have been plotted in the upper middle part of the diamond shaped section (Figure 4.13).

The variation of cation observed is a reflection of water–rock interaction. Groundwater interface with basaltic or sedimentary rocks results in a particularly large ion ratio. Na, based on Mg and Ca, Tweed et al. (2005) marked flow of these two distinct climate systems. Samples from the study area show greater proximity to the basaltic rock than sedimentary rocks (Figure 4.13).

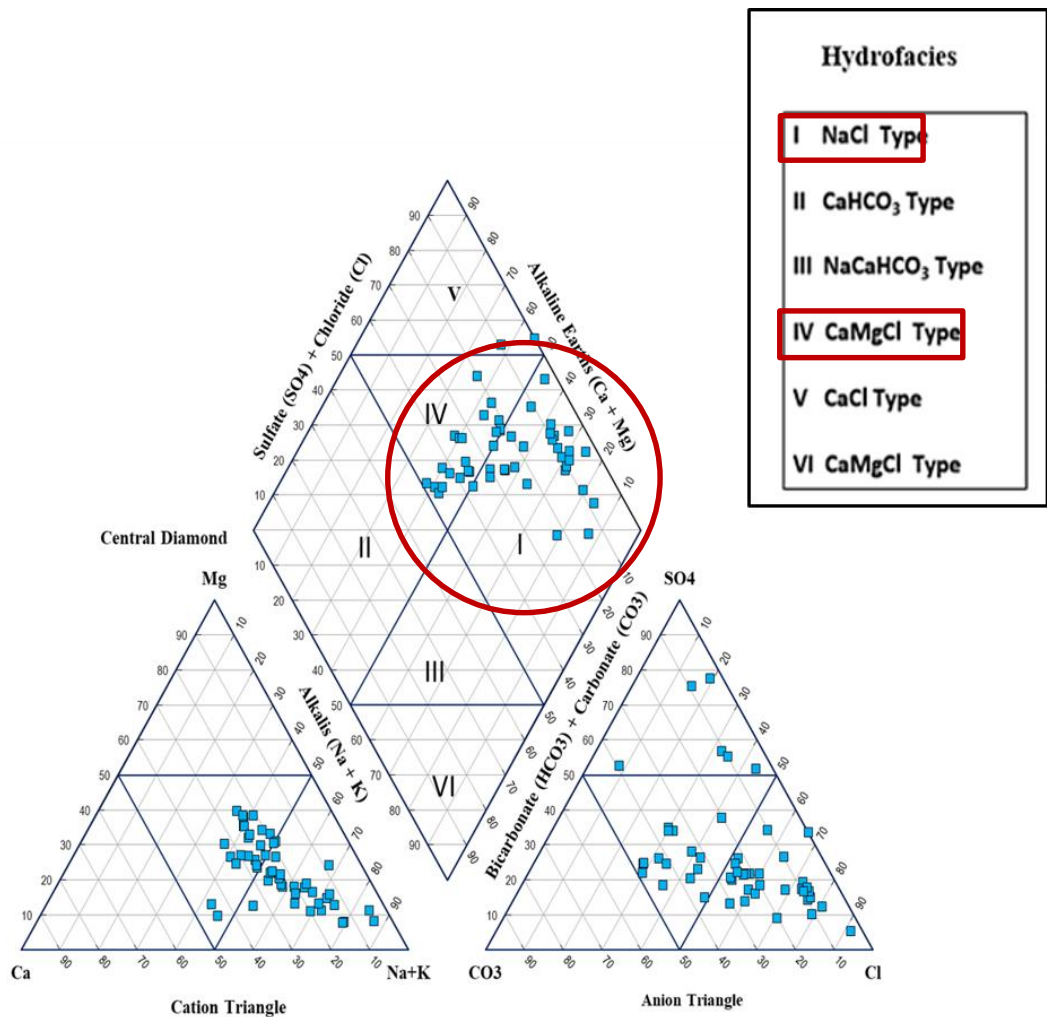


Figure 4.13 Piper diagram of groundwater chemistry in the Uthul.



#### 4.5 Analysis of Stiff pattern

For the construction of a Stiff pattern, multiple polygraphs have been formed from three parallel horizontal axes using meq/l cations and anions. Figure 4.14 to 4.23 show the plot of cations and anions on the stiff pattern for individual samples. Anions are plotted on the right and the cations are on the left of the vertical line of the zero axis. The stiff pattern of individual samples is generated for a graphical comparison of anions and cations. The analysis of the relative concentration of cations and anions in the stiff pattern for the water samples is as follows:

For samples 1 to 10 the analysis is given in the Figure 4.13. The figures show that in sample 1, Na, Mg, Cl & SO<sub>4</sub> have an almost balanced concentration. Whereas, Ca and HCO<sub>3</sub> have lower concentrations. In sample 2,3& 4, Na is on higher side where as Ca and SO<sub>4</sub> re moderately high. Whereas, Cl, Ca, Mg & HCO<sub>3</sub> are have low concentrations. For sample 5, concentration of Na, Cl, HCO<sub>3</sub>, SO<sub>4</sub> & Mg is high, whereas Ca has low concentration. Sample 6 shows high concentration of Na, and a very high concentration of SO<sub>4</sub>. While Ca & Mg are moderate and very low for HCO<sub>3</sub>. In samples 7,8,9 &10, an almost similar distribution is observed with high to moderate Na & Cl and low Ca, HCO<sub>3</sub>, Mg and SO<sub>4</sub>.

For samples 11 to 20 the analysis is given in Figure 4.15. Sample 11 has high concentration of Na & Cl, moderate concentration of Ca, Mg, HCO<sub>3</sub> and SO<sub>4</sub>. Sample 12 has high concentration of N, Mg and HCO<sub>3</sub>, moderate concentration of Ca, Cl & SO<sub>4</sub>. Sample 13 shows high concentrations of Na, HCO<sub>3</sub>, Mg, SO<sub>4</sub> and moderate concentrations of Cl and Ca. Sample 14, shows high concentration of Na, Cl, Mg & SO<sub>4</sub>, whereas Ca & HCO<sub>3</sub> show a moderate concentration. Sample 15 shows a high concentration of Na & Cl, a moderate concentration of Ca, HCO<sub>3</sub> and SO<sub>4</sub>. Sample 16, has a high concentration of Na, Cl, Mg, HCO<sub>3</sub> and SO<sub>4</sub> and a moderate concentration of Ca. Sample 17, has high concentration of Na & Cl, moderate Ca, Mg, HCO<sub>3</sub> and SO<sub>4</sub>. Samples 18, 19, & 20 show similar patterns having high values of Mg, Na, Cl and HCO<sub>3</sub>. Whereas, Ca & SO<sub>4</sub> is

moderates.

For samples 21 to 30 the analysis is given in Figure 4.16. Sample 21 shows high relative concentration of Na & HCO<sub>3</sub> and, moderate Cl, Ca, Mg and SO<sub>4</sub> concentrations. Sample 22 has high Na, Cl & SO<sub>4</sub> concentration whereas moderate concentration of Mg, Ca and low HCO<sub>3</sub>. Sample 23 shows high concentration of Na & Cl, a moderate concentration of Ca, HCO<sub>3</sub>, Mg and SO<sub>4</sub> ions. Sample 24 has a high concentration of Na, Cl, Ca, & HCO<sub>3</sub> and a low concentration of and low Mg & SO<sub>4</sub> concentration. Sample 25 has high Na, Ca, & SO<sub>4</sub> and a moderate concentration of Cl & HCO<sub>3</sub> and low Mg. Sample 26 has high Na, & Cl and a moderate concentration of Mg & HCO<sub>3</sub> and Low Ca & SO<sub>4</sub> concentration. Samples 27 & 28 has very high Na, & Cl and a moderate concentration of Ca, HCO<sub>3</sub> & Mg, and low SO<sub>4</sub>. Sample 29 has a high concentration of Na & Cl, moderate Ca, HCO<sub>3</sub> & Mg and low SO<sub>4</sub>. Sample 30 shows high concentration of Na & Cl, moderate Ca, HCO<sub>3</sub>, Mg & SO<sub>4</sub>.

For samples 31 to 40 the analysis is given in Figure 4.17. Sample 31 has a high concentration of Na, & Cl, a low concentration of Ca & Mg and very low values of HCO<sub>3</sub>. Sample 32 has high Na & Cl and low Mg & SO<sub>4</sub> and a very low Ca, HCO<sub>3</sub>. Sample 33 & 34 show a similar stiff pattern and has a high value of Na & Cl, and low Ca, HCO<sub>3</sub>, Mg & SO<sub>4</sub>. Sample 35 & 36 has high Na, & Cl, low HCO<sub>3</sub> & Ca and moderate Mg & SO<sub>4</sub>. Samples 37 has very high concentration of Na & Cl, a moderate concentration of Ca, & Mg and low concentrations of HCO<sub>3</sub> and SO<sub>4</sub>. Sample 38 has a high concentration of Na, Cl, Ca, & Mg and a moderate concentration of SO<sub>4</sub> and low concentration of HCO<sub>3</sub>. Sample 39 has a high concentration of Na, Cl, SO<sub>4</sub> & Mg, and a moderate concentration of Ca, & HCO<sub>3</sub>. Sample 40 shows high concentration of Na & Cl, Moderate Ca, HCO<sub>3</sub>, Mg & SO<sub>4</sub>.

For samples 41 to 50 the analysis is given in Figure 4.18. samples 41 & 42 show a similar pattern and has high Na & Cl, moderate Ca, HCO<sub>3</sub>, Mg & SO<sub>4</sub>. Samples 43 & 44 show a high concentration of Na & Cl, a moderate values of Ca, HCO<sub>3</sub>, Mg & SO<sub>4</sub>. Samples 45 & 46 have high concentrations of Na & Cl and moderate concentrations of Ca, Mg, HCO<sub>3</sub> & SO<sub>4</sub>. Sample 47 shows a high concentration of Na & Cl, and moderate Ca,

Mg, HCO<sub>3</sub> & SO<sub>4</sub>. Sample 48 has high equally distributed concentration of all cations and anions. Sample 49 shows a high concentration of Na, Cl, Ca, & Mg, and a moderate concentration of HCO<sub>3</sub> & SO<sub>4</sub>. Sample 50 shows a moderate concentration of Na & Cl and low Ca, HCO<sub>3</sub>, Mg & SO<sub>4</sub>.

For samples 51 to 60 the analysis is given in Figure 4.19. Samples 51 & 52 show a similar pattern with high concentration of Na, and moderate values of Cl, HCO<sub>3</sub> & SO<sub>4</sub> and a low concentration of Ca, & Mg. Sample 53 has a high concentration of Na, & Cl, moderate values of Ca, Mg and a low concentration of HCO<sub>3</sub> & SO<sub>4</sub>. Sample 54 has high Na, Cl, Ca, Mg and moderate HCO<sub>3</sub> & SO<sub>4</sub> concentrations. Sample 55 shows high Na, & Cl, medium Ca, & Mg and low concentrations of HCO<sub>3</sub> & SO<sub>4</sub>. Sample 56 shows an evenly distributed high Na, Cl, Mg & Ca ions and a moderate concentration of HCO<sub>3</sub> & SO<sub>4</sub>. Sample 57 shows high Na & Cl, and a moderate distribution of Ca, Mg, HCO<sub>3</sub> & SO<sub>4</sub>. Samples 58, 59 & 60 show an almost similar pattern of ion distribution with Na, Cl, Mg, Ca & SO<sub>4</sub> having high concentrations and HCO<sub>3</sub> moderate concentration.

For samples 61 to 70 the analysis is given in Figure 4.20. Sample 61 has a high concentration of Ca & Cl, a moderate concentration of Na, Mg & SO<sub>4</sub> and a low concentration of HCO<sub>3</sub>. Sample 62 shows a high concentration of Na, Cl & SO<sub>4</sub> ions whereas a moderate concentration of Ca, Mg & HCO<sub>3</sub>. Samples 63 & 64 shows similar ion distribution with high Na & Cl, and moderate Ca, Mg, HCO<sub>3</sub> & SO<sub>4</sub>. Samples 67 & 68 show a similar trend with evenly distributed ions of Na, Cl, Ca, Mg, HCO<sub>3</sub> & SO<sub>4</sub>. Samples 69 & 70 show a similar trend of ion distribution for Na, Cl, Ca, Mg, HCO<sub>3</sub> & SO<sub>4</sub>.

For samples 71 to 80 the analysis is given in Figure 4.21. Samples 71 & 72 show similar patterns with evenly distributed Na, Cl, Ca, Mg, HCO<sub>3</sub> & SO<sub>4</sub> ions. Samples 73 & 74 show a similar distribution of ions with high Na, moderate Ca and HCO<sub>3</sub>, and Low Ca, Mg & SO<sub>4</sub>. Samples 75 & 76 show a similar pattern for ion concentration, with Na, Cl, & HCO<sub>3</sub> having higher concentrations and Ca, Mg & SO<sub>4</sub> moderate concentrations. Sample 77 shows a high concentration of Na, Cl & HCO<sub>3</sub>, and moderate concentrations of Ca, Mg & SO<sub>4</sub>. Sample 78 shows a high concentration of Na, Cl, Ca, Mg, & SO<sub>4</sub> and a moderate

concentration of  $\text{HCO}_3$ . Sample 79 show a high concentration of Na, & Cl, and a moderate concentration of Ca, Mg,  $\text{HCO}_3$  &  $\text{SO}_4$ . Sample 80 show high concentrations of Na, Cl, Ca,  $\text{HCO}_3$  and moderate concentrations of Mg &  $\text{SO}_4$ .

For samples from 81 to 90, the analysis is given in Figure 4.22. Samples 81 & 82 show a similar pattern of ion distribution with high Na, Cl &  $\text{SO}_4$  and moderate Ca, Mg &  $\text{HCO}_3$ . Sample 83 shows a high concentration of Na, Cl, &  $\text{HCO}_3$  and a moderate concentration of Ca, Mg, &  $\text{SO}_4$ . Sample 84 has high concentrations of Na, Cl Ca, &  $\text{SO}_4$  and moderate concentrations of Mg &  $\text{HCO}_3$ . Samples 85 & 86 show a similar distribution of ions with high Na & Cl and moderate distribution of Ca, Mg,  $\text{HCO}_3$  &  $\text{SO}_4$ . Sample 87 has a high Na & Cl and moderate Ca, Mg,  $\text{HCO}_3$  &  $\text{SO}_4$ . Samples 88 & 89 show a similar pattern and have high Na, Cl, & Ca, and moderate Mg,  $\text{HCO}_3$  &  $\text{SO}_4$ . Sample 90 has high Na, Cl &  $\text{SO}_4$  and moderate Ca, Mg &  $\text{HCO}_3$ .

For samples from 91 to 100 the analysis is given in Figure 4.23. Samples 91 has high Na & Cl concentration, moderate Ca, Mg, &  $\text{SO}_4$  and low  $\text{HCO}_3$ . Sample 92, 93 & 94 show a similar pattern with high Na, & Cl, moderate Ca, Mg &  $\text{SO}_4$  and low  $\text{HCO}_3$ . Sample 95 & 96 have a similar pattern of ion distribution with high Na, & Cl and moderate Ca, Mg,  $\text{HCO}_3$  &  $\text{SO}_4$ . Samples 97 & 98 show high Na, & Cl concentrations, moderate Ca, Mg, &  $\text{SO}_4$  and low  $\text{HCO}_3$ . Samples 99 & 100 have high Na, & Cl, moderate Ca, Mg &  $\text{SO}_4$  and low  $\text{HCO}_3$  concentrations.

The stiff patterns from the study area indicate that the geochemistry of water is indicating its origin from the composition of the study area. The stiff pattern for seawater intrusion was not observed at any location. Slightly higher values of Na and Cl ions with low to moderate Ca, Mg,  $\text{SO}_4$  and  $\text{HCO}_3$  are observed near the South and Southwestern part of the study area which may indicate higher evaporation rates.

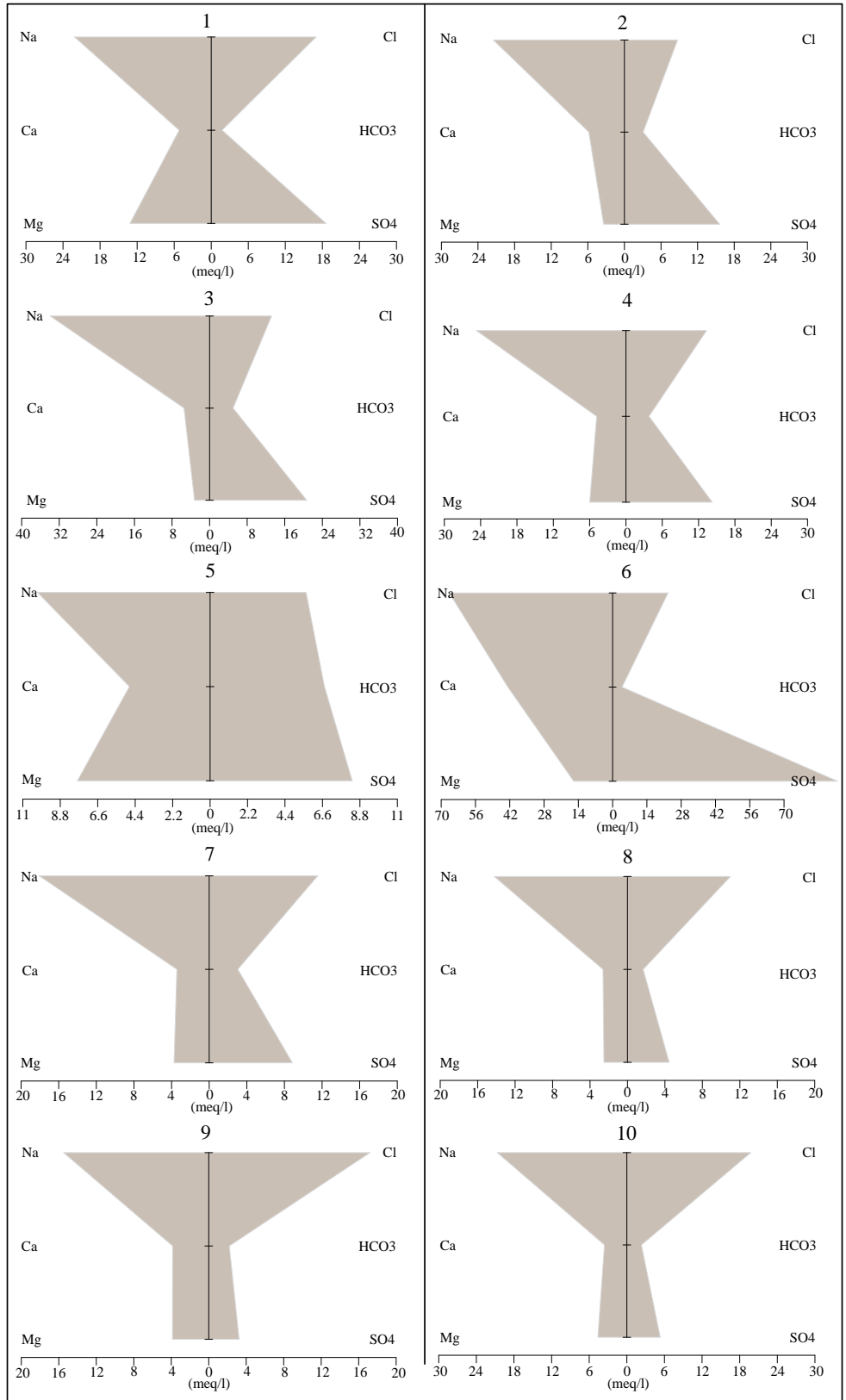


Figure 4.14 Stiff pattern of groundwater samples from the Uthal (samples 1 to10)

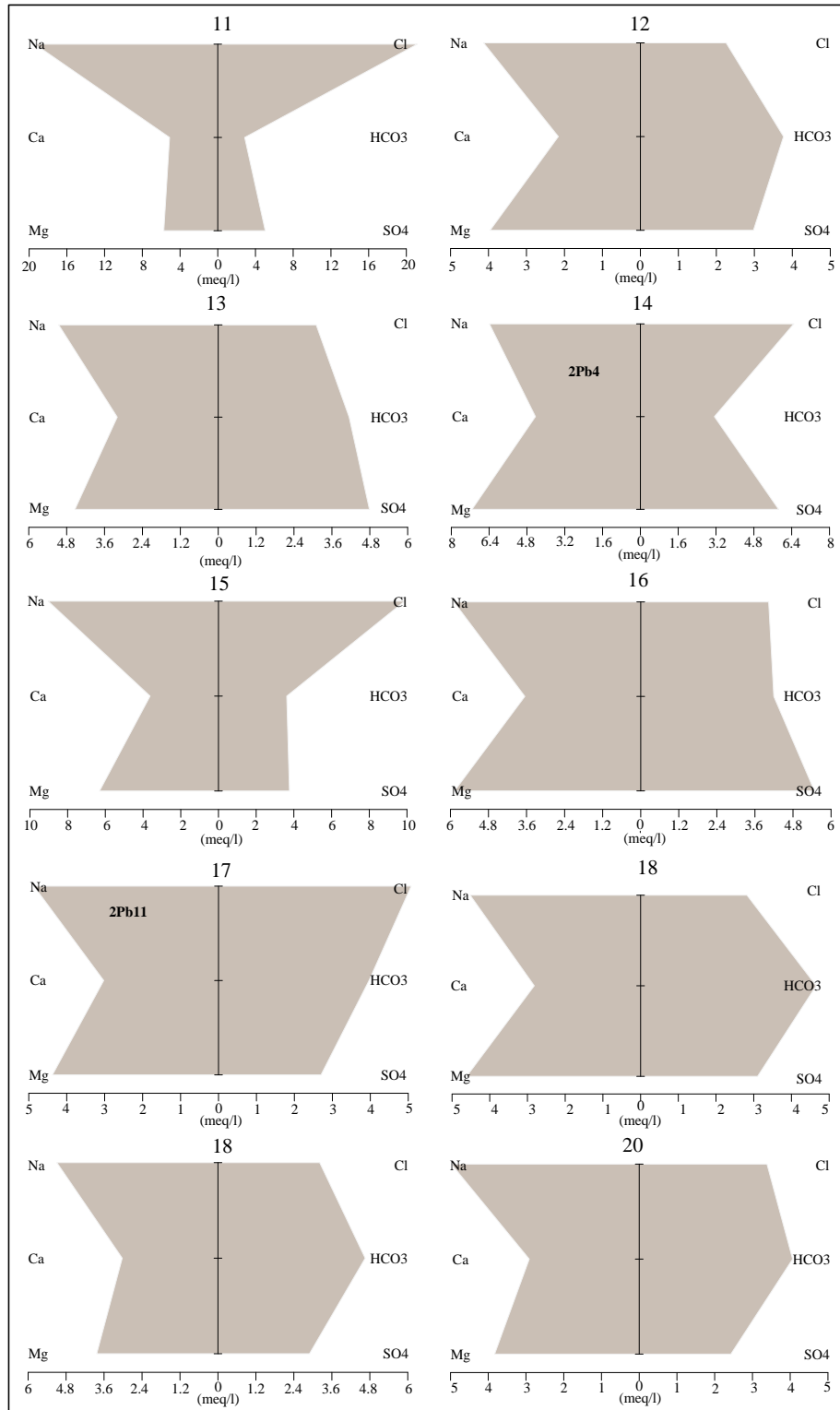


Figure 4.15 Stiff pattern of groundwater samples from the Uthal (samples 11 to 20)

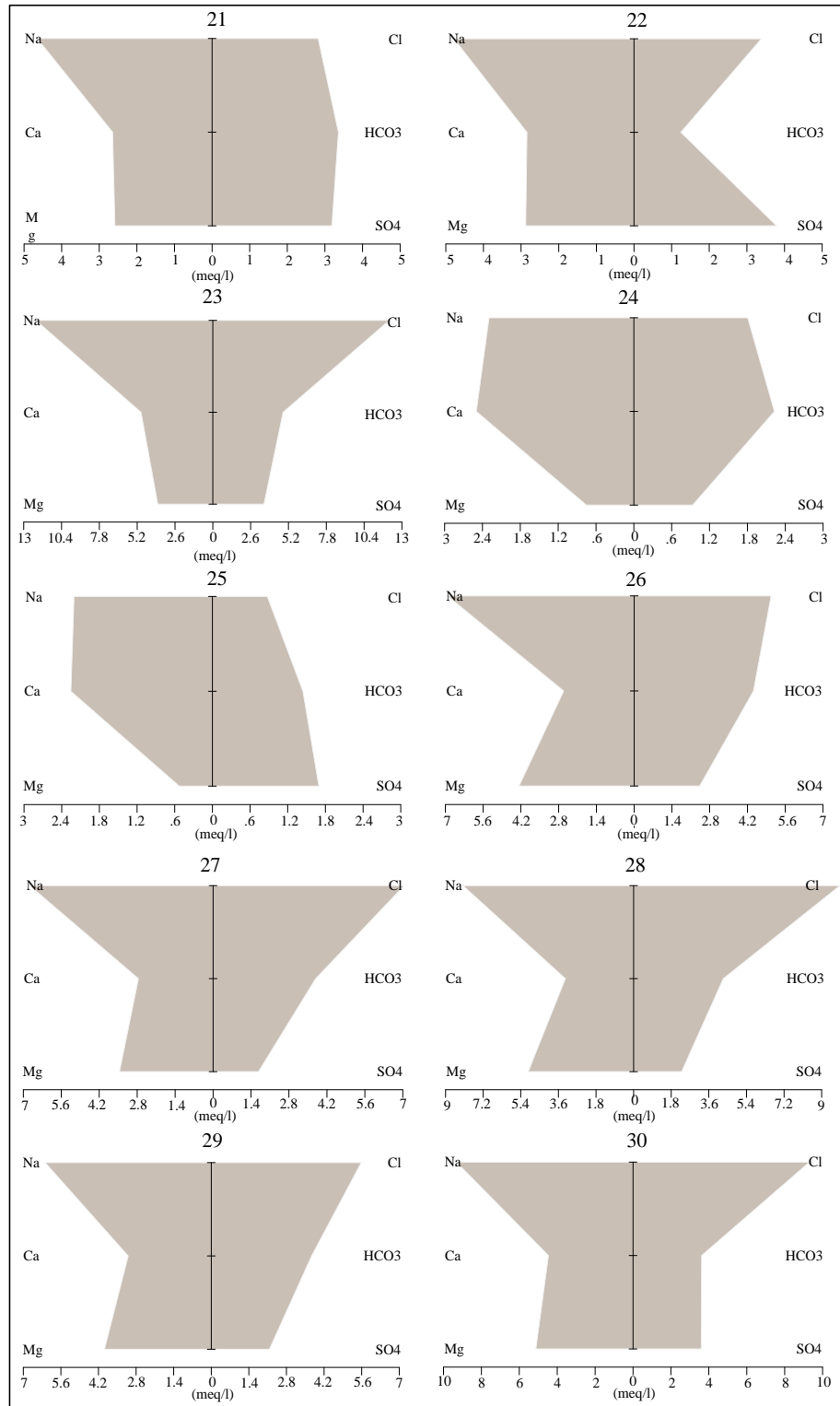


Figure 4.16 Stiff pattern of groundwater samples from the Uthal (samples 21 to 30)

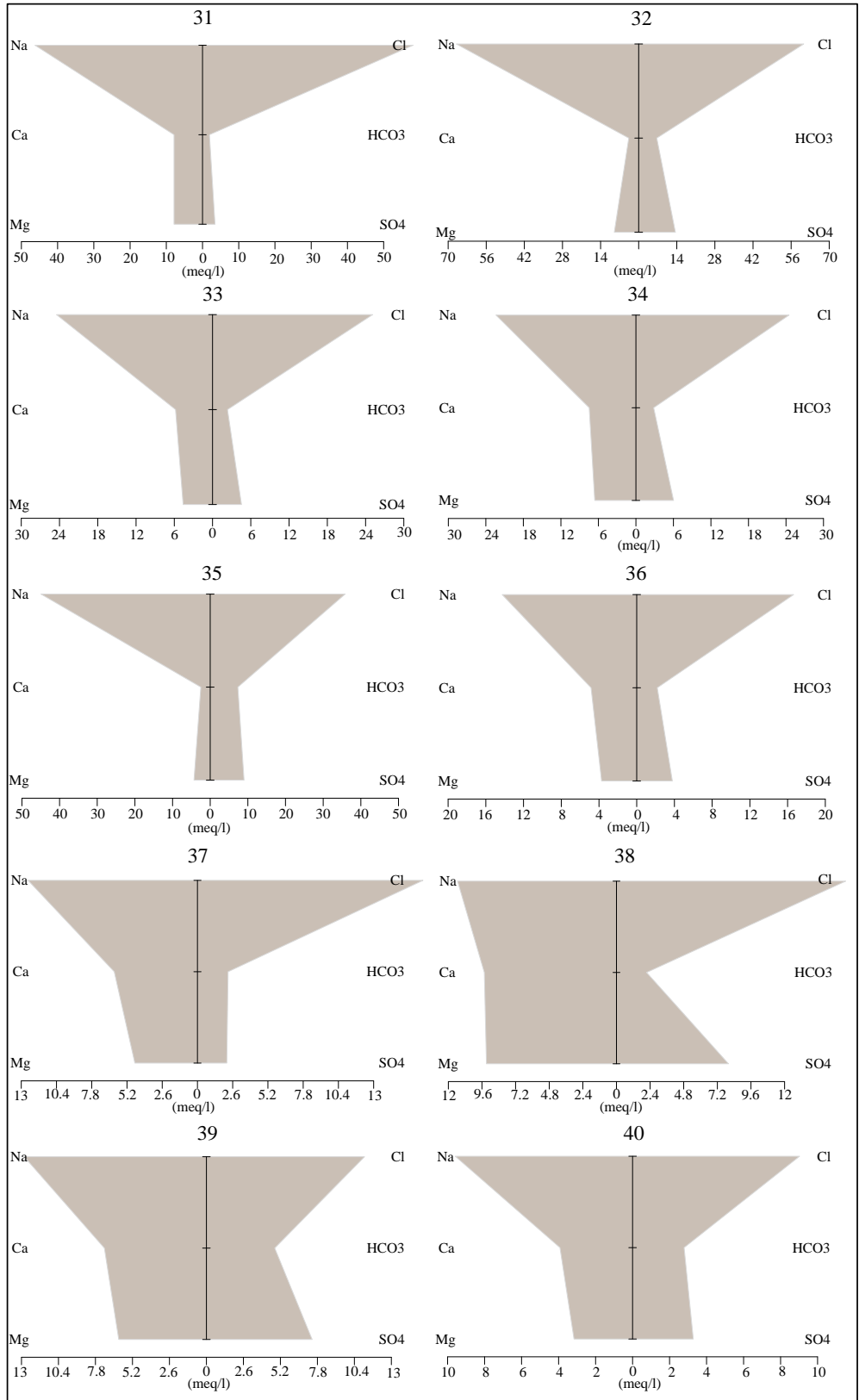


Figure 4.17 Stiff pattern of groundwater samples from the Uthal (samples 31 to 40)



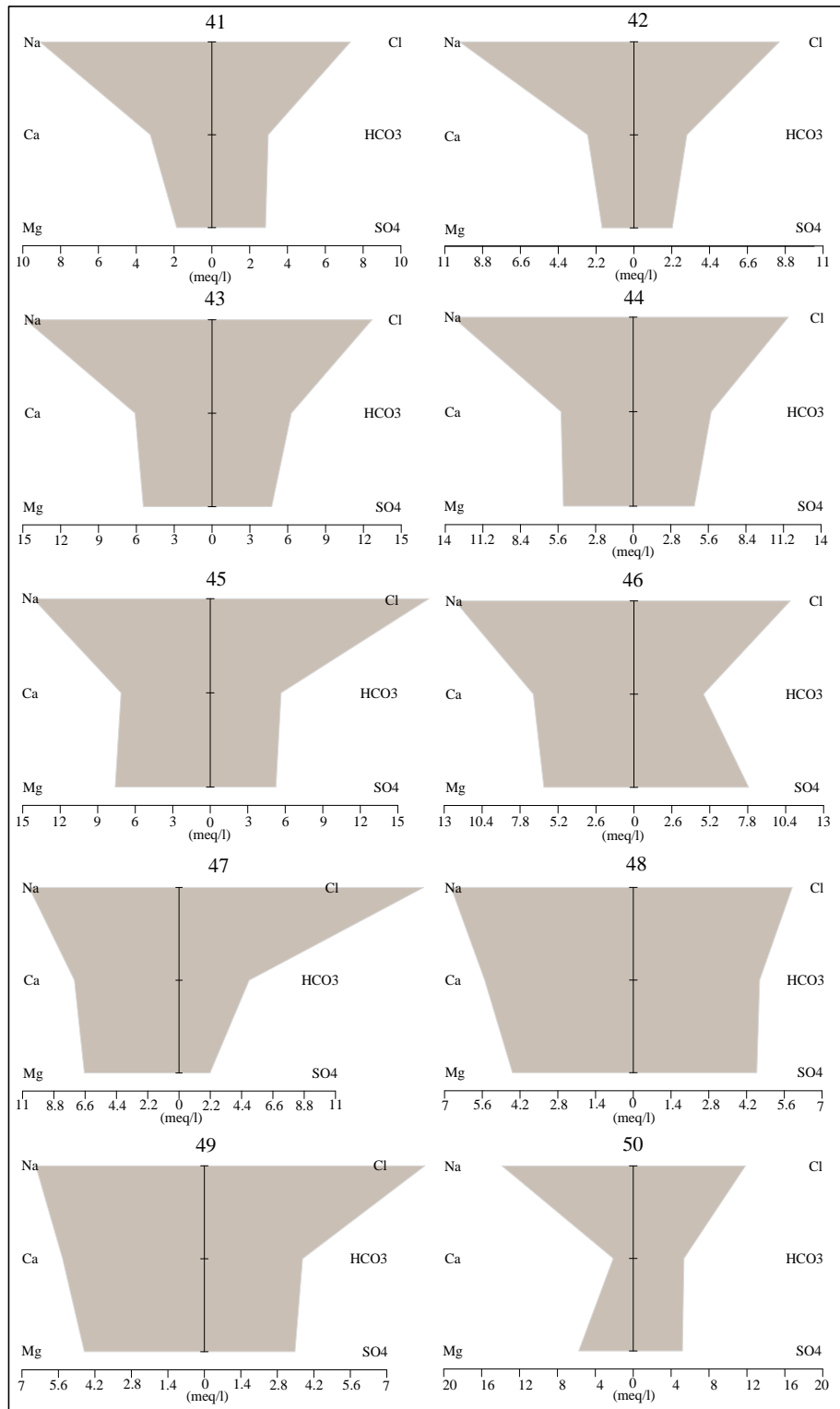


Figure 4.18 Stiff pattern from groundwater samples from Uthal (41 to 50)

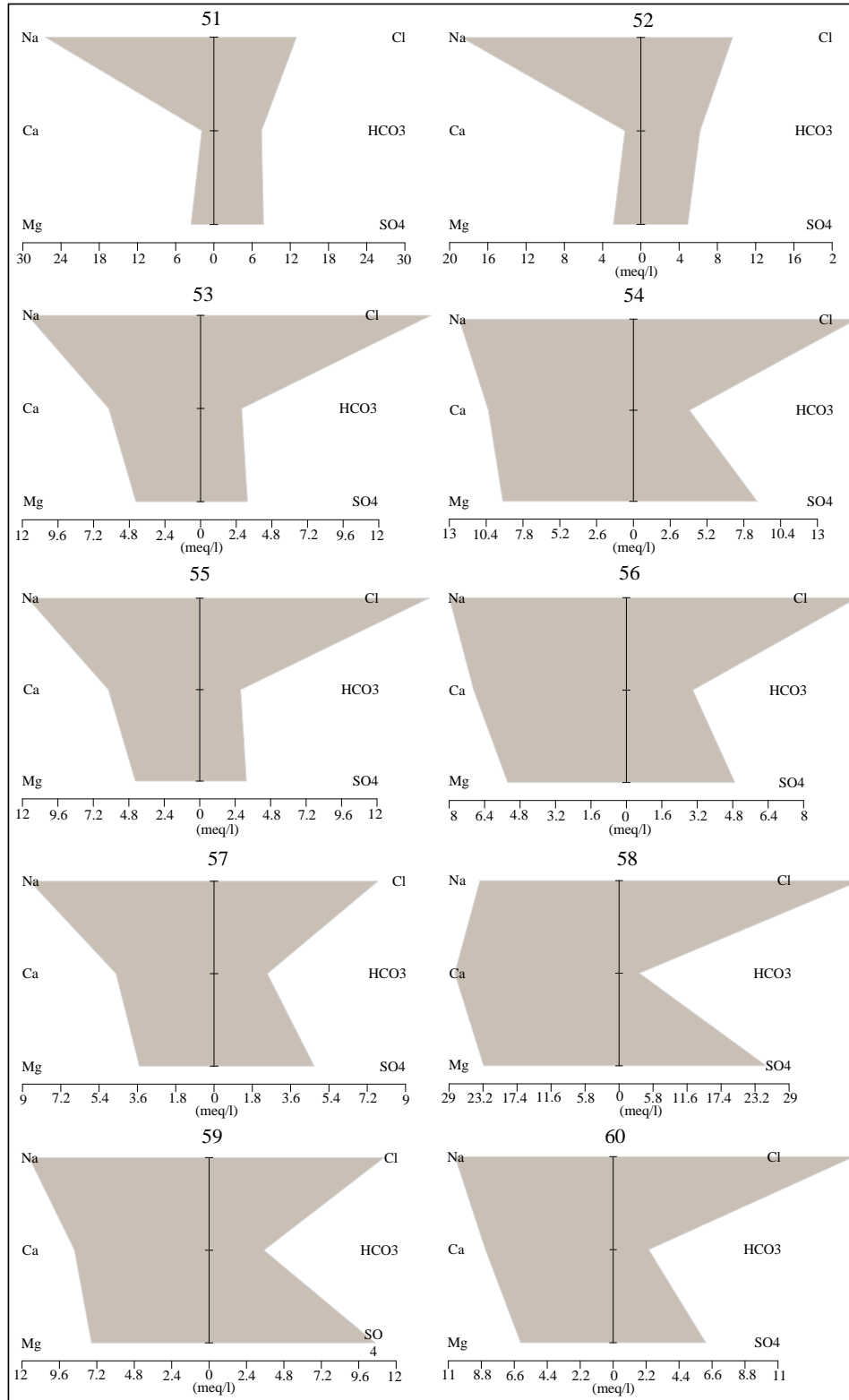


Figure 4.19 Stiff pattern for groundwater samples of Uthal (51 to 60)

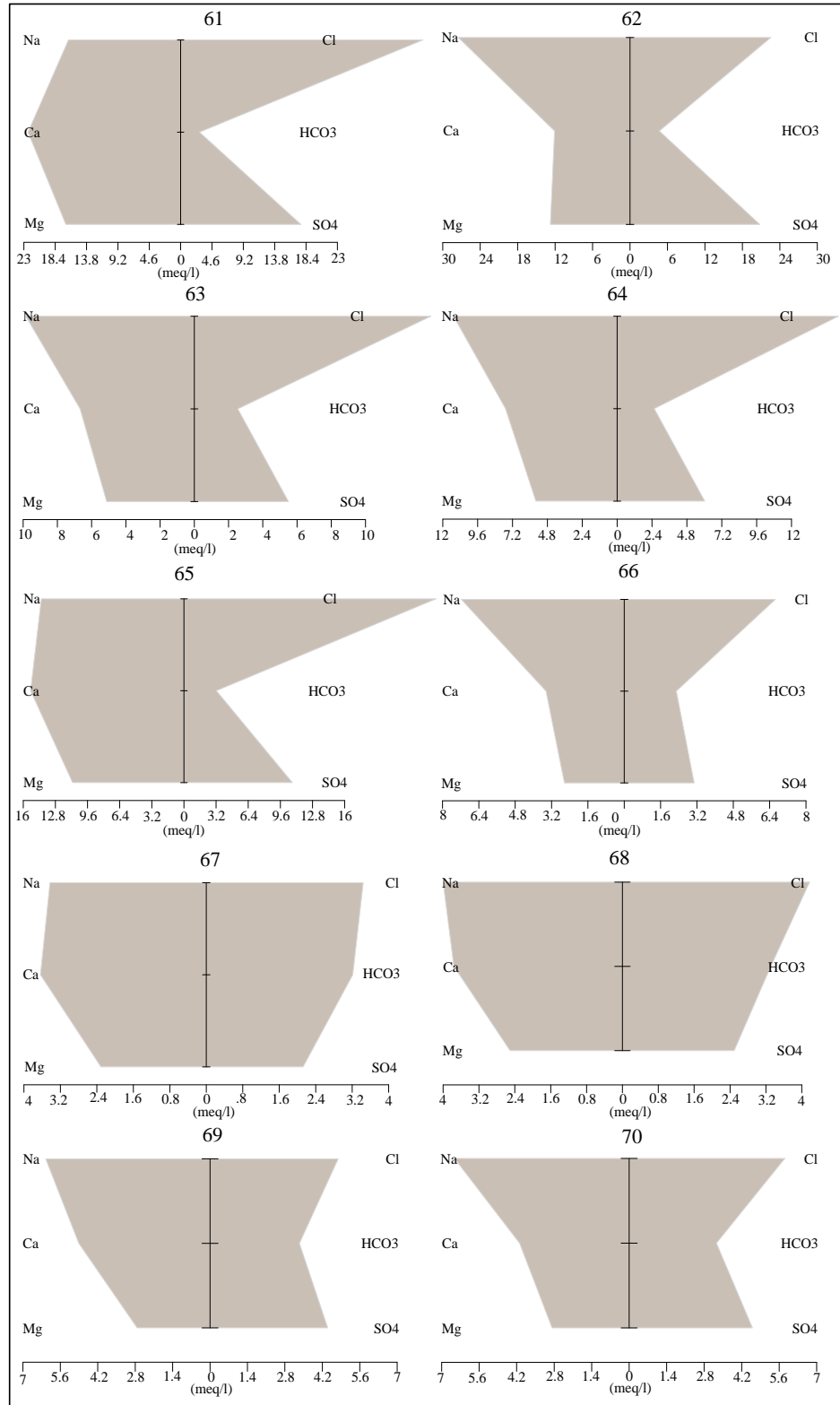


Figure 4.20 Stiff pattern from groundwater samples for Uthal (61 to 70)

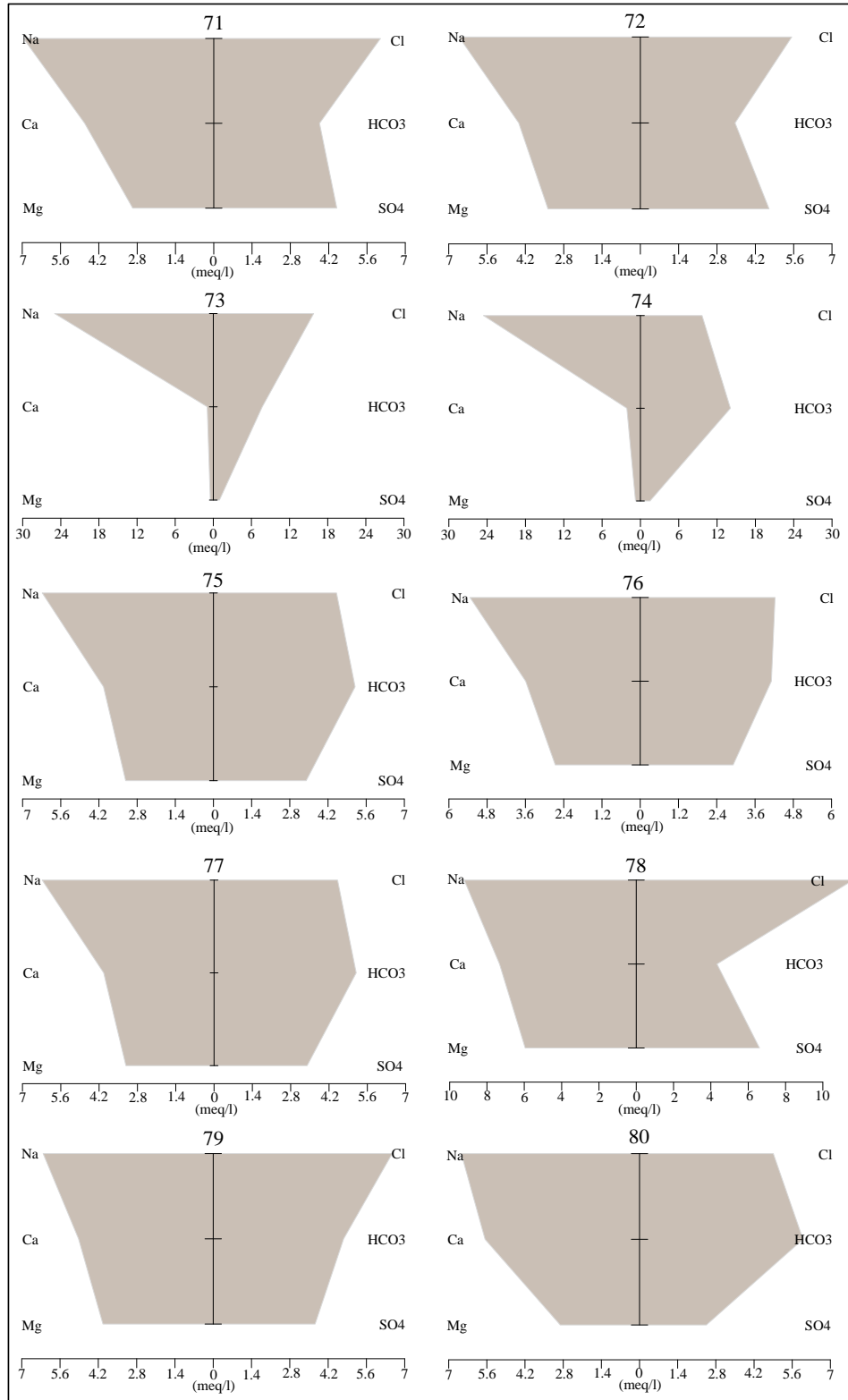


Figure 4.21 Stiff pattern for groundwater samples of Uthal (71 to 80)

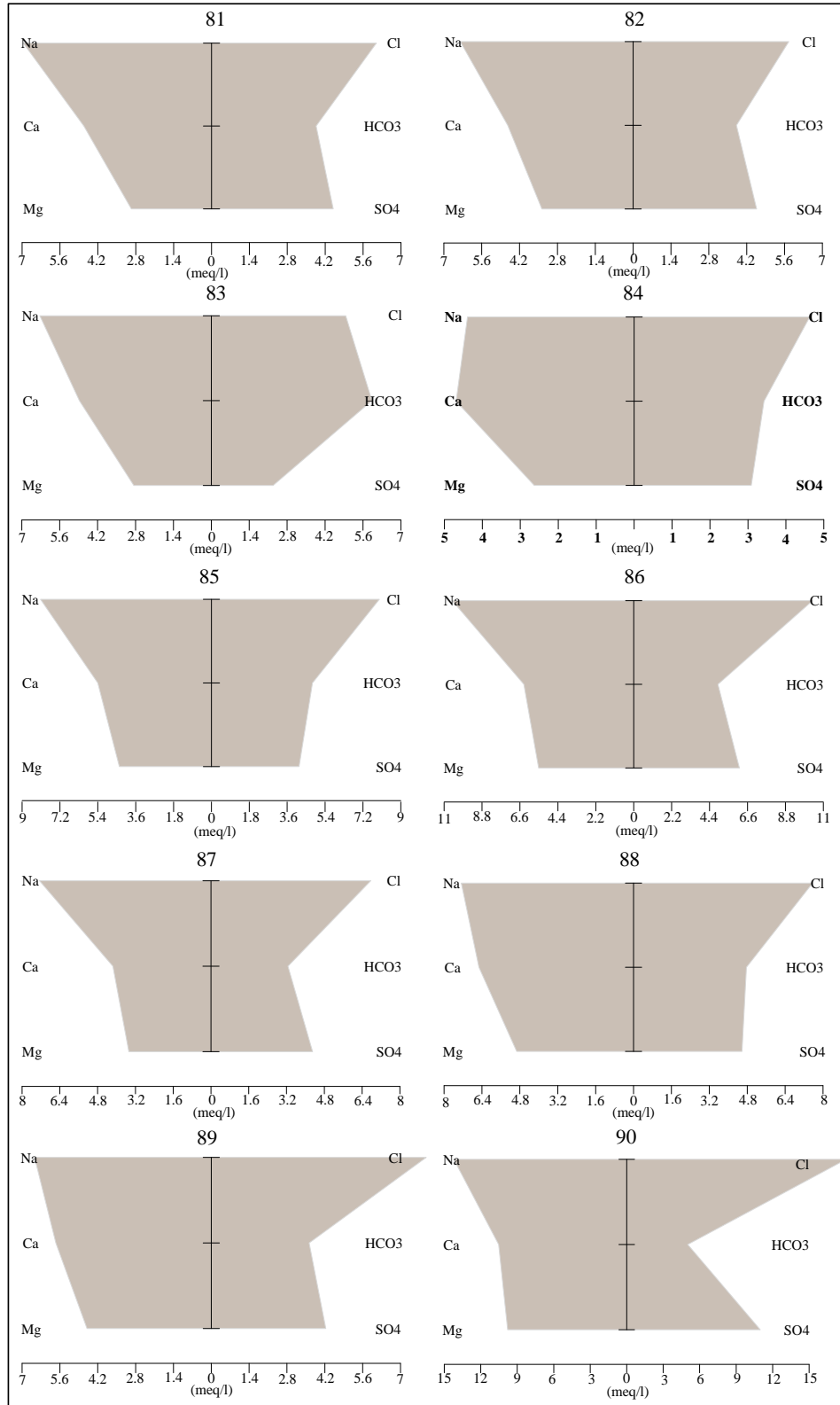


Figure 4.22 Stiff pattern for groundwater samples for Uthal (81 to 90)

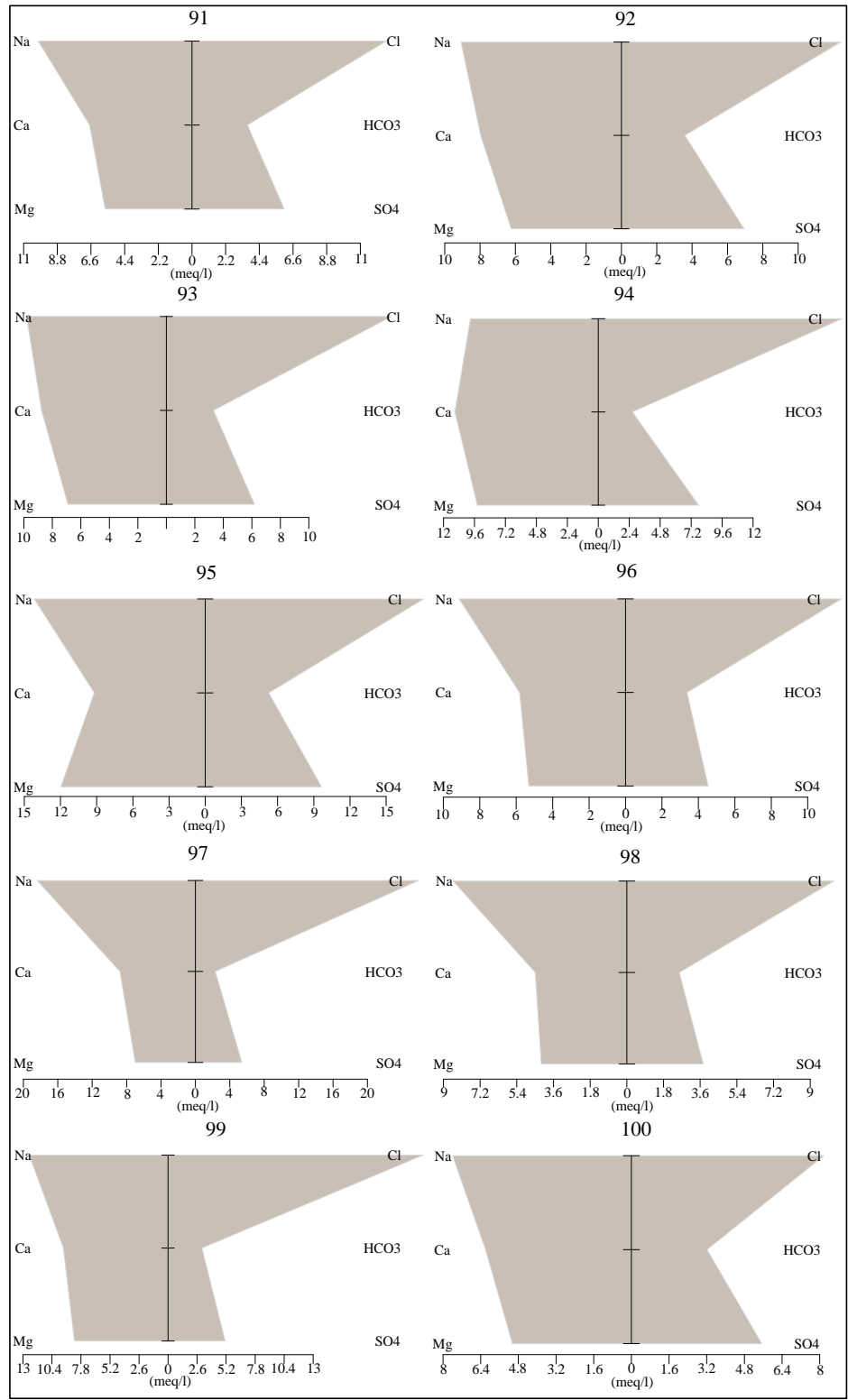


Figure 4.23 Stiff pattern for groundwater samples for Uthal (91 to 100)

## **4.6 Trace Elements**

There are many elements present in very small concentrations in water, these are termed as trace elements. The presence of a few of these elements is important for human growth and other body functions and the presence of a few of these is harmful (Dokmen, 2004). The trace elements commonly found in groundwater are; Aluminum (Al), Arsenic (As), Cadmium (Cd), Chromium (Cr), Cobalt (Ca), Copper (Cu), Iron (Fe), Lead (Pb), Manganese (Mn), Nickel (Ni), Titanium (Ti), and Zinc (Zn). The concentration of these elements in the groundwater is very important for human health (WHO, 2022). The concentration of Arsenic (As), Cobalt (Co), and Titanium (Ti) were below the detection limit (BDL) for the groundwater samples of the study area. Whereas, a significant concentration of trace elements, Aluminum (Al), Cadmium (Cd), Chromium (Cr), Copper (Cu), Iron (Fe), Manganese (Mn), Nickel (Ni), Lead (Pb), and Zinc (Zn), was found in the groundwater samples. The concentration of these elements is given in the Table 4.5.

### **4.6.1 Cadmium**

The abundance of Cadmium abundance in the Earth's crust is approximately 100µg/kg. The two common elements associated with Cd in the natural environment are Zn and sulfides minerals. The common sulfide minerals with Cd are CdS (greenockite and CdSe cadmium selenide. The source of cadmium in groundwater for Uthal is assumed to be the sulfide segment of the Bel ophiolite. As there are no industries in Uthal, therefore no contribution from anthropogenic sources is assumed.

Table 4.5 Trace element analysis of water samples of the study area

	<b>Minimum</b>	<b>Maximum</b>	<b>Average</b>	<b>SD</b>	<b>Median</b>	<b>WHO*1</b>	<b>PAK*2</b>
<b>Al</b>	5	756	63.4	115	18	200	-
<b>As</b>	BDL	BDL	BDL	-	-	05	50
<b>Cd</b>	0	24	2.8	6.17	0.03	03	10
<b>Co</b>	BDL	BDL	BDL	-	-	100	-
<b>Cr</b>	0.5	114	32.19	29.5	19.5	50	50
<b>Cu</b>	0.05	354	64.65	73	45	2000	2000
<b>Fe</b>	19	2116	328	393	216	300	-
<b>Mn</b>	2	657	95	113	63.5	500	500
<b>Ni</b>	0	412	46	66	25	70	20
<b>Pb</b>	1.5	79	17.75	21.4	8.6	10	50
<b>Ti</b>	BDL	BDL	BDL	-	-	100	-
<b>Zn</b>	5	801	62.65	130	24	3000	5000

Note: All values are in µg/l (ppb).

Cadmium enters the groundwater due to the weathering of the cadmium-bearing rocks of the Bela Ophiolite and Cadmium is highly mobile and water-soluble (Naseem et al., 2014). The concentration of Cadmium in the groundwater is mainly controlled by the pH of the water (Kubier et al., 2019). In Uthal, Cadmium in the groundwater sample was in the range of 0 – 24 µg/l (Table 4.5). The average value of Cadmium is within the permissible limits (WHO, 2022). The samples collected from the mountainous areas have a higher concentration of Cd, showing their proximity to the source. Cadmium bears no



positive influence on human health. The lower levels can lead to nausea, vomiting, and diarrhea. Fragile bones can be the effect of long exposure to cadmium in humans. It can also cause cancer, high blood pressure, heart disease, and kidney failure (Naseem et al., 2014).

#### **4.6.2 Chromium**

The Chromium (Cr) abundance, on average, in groundwater is 1 µg/l, approximately. The groundwater samples from the study area have Cr from 0.5 – 114 µg/l, with an average value of 32.4 µg.l. The samples show higher than the permissible limit of Cr in drinking water. The reason for higher values is the presence of ophiolitic rocks. The ultramafic rocks generally have a higher concentration of Cr. The groundwater is affected by the presence of the Ophiolite in the areas as indicated by the Cr concentration. Existence of oxygen with neutral-to-alkaline pH favors the persistence of CrVI and supports its mobility (Dong et al., 2009). The presence of Chromium is harmful to humans as it is categorized as a carcinogenic element. The distribution of Cr is shown in Figure 14.4 C.

#### **4.6.3 Copper**

In water, Cu III & IV, are unstable and are capable to form complexes in the +1 - +4 valence states. Cu II, however, is highly insoluble in water under the reducing conditions. The main soluble complex in water is Cupric (CuII) (Dong et al., 2009). The concentration of Cu in samples of the study area is between 0.05 – 35 µg/l and the average value is 64.1 µg/l (Figure 14.4 D). The maximum concentration recommended by WHO (2017) in drinking water is 200 µg/l. The groundwater samples are within the safe limits

#### **4.6.4 Iron**

The groundwater samples of the study area have Fe variation from 0.05 – 2116 µg/l, with an average value of 328 µg/l. This Fe value for the samples on average shows the value near to the permissible limit in drinking water by WHO standards which is 300 µg/l. Fe is one of the most abundant element in the earth's crust is found in ophiolite segments in the study area. It is also found in sulfides in MVT or Sedex. The groundwater samples locations near the exposed rocks show a higher concentration of Fe (Figure 4.15).

#### **4.6.5 Manganese**

The Manganese concentration in groundwater for the study area is between 02 – 657 µg/l, and the average value is 95.08 µg/l. The Mn concentration is higher in the study area as Mn mineralization is widespread in Uthal and its adjoin areas and also in the northern areas (Naseem, 1996). Manganese has been noted in groundwater at concentrations ranged between 02 and 657µg/l, and average is 95.08 µg/l. According to figure 19 Mn was slightly higher than the standard and it is significant to note that Mn mineralization is widespread in the neighborhood of Uthal area but also in the northern areas (Naseem, 1996).

#### **4.6.6 Nickel**

The groundwater samples from Uthal have Nickle variability from 0 – 412 µg/l (Figure 4.24). In a few samples, Ni was not detected. The reason for the absence of Ni in these samples is their proximity to the coast. The higher concentration of Ni is observed towards the hilly areas in the northeast and the lower concentration is observed in the southwest. This is in concurrence with the geology of the area. the Ophiolite are present in the northeast and Ni is associated with massive volcanic sulfides (MVS), podiform chromite, and in different segments of ophiolite (Vine & Kearey, 1990). Nickle

concentrations above 70 µg/l were observed in samples closely collected from areas near the mountains. Ni concentration in groundwater is higher in groundwater samples for the study area than the permissible limits by WHO, 2017 for drinking purposes. A higher concentration of Nickel in the human body has many negative effects. Higher values of Ni may damage the kidney and stomach. It may suppress the immune system and modify certain enzymes in case of extremely high Ni concentration.

#### **4.6.7 Lead**

Lead (Pb) is a chalcophile element and sulfide deposits are enriched in Pb. Lead (Pb) in groundwater of Uthal is from 1.5 – 79 µg/l. The Pb have low mobility (Reedman, 2012), due to this reason the lead concentration in the study area is higher for the sample sites near the outcrops in the eastern part of Uthal. The highest permissible limit of Pb in drinking water is 10 µg/l, whereas the highest value of lead in groundwater samples is 79 µg/l.

#### **4.6.8 Zinc**

Zinc (Zn) is an important element in human body and it is essential in various enzyme systems. It is also important for healthy skin, energy production and growth regulation of a human body (Marschner, 1995). 20mg/kg, is approximately required in its for healthy growth. The samples from the study area show concentration of Zinc from 50 – 801 µg/l and an average value of 62.6 µg/l. These values are much lower than the required Zn concentration for maintaining a healthy body.

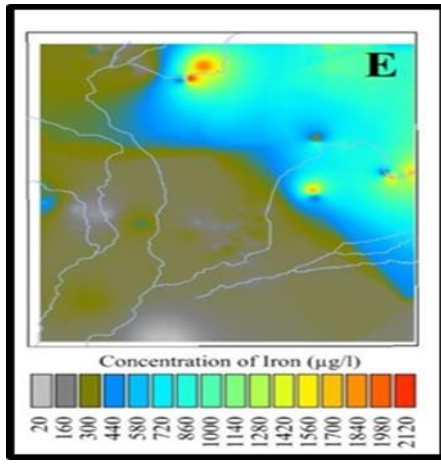
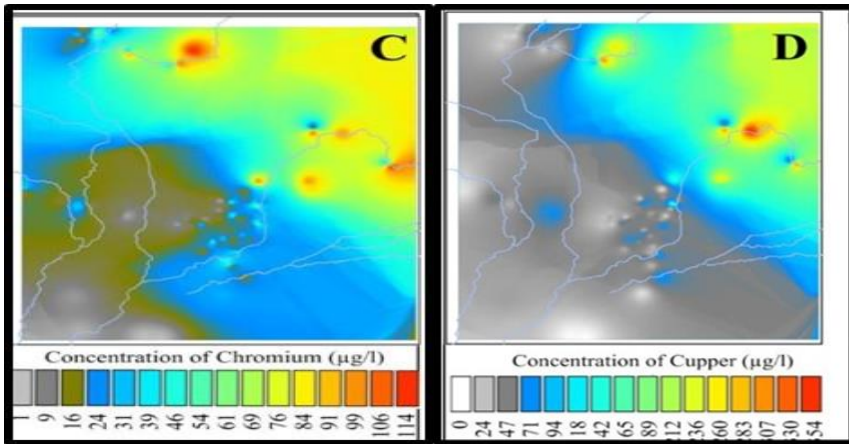
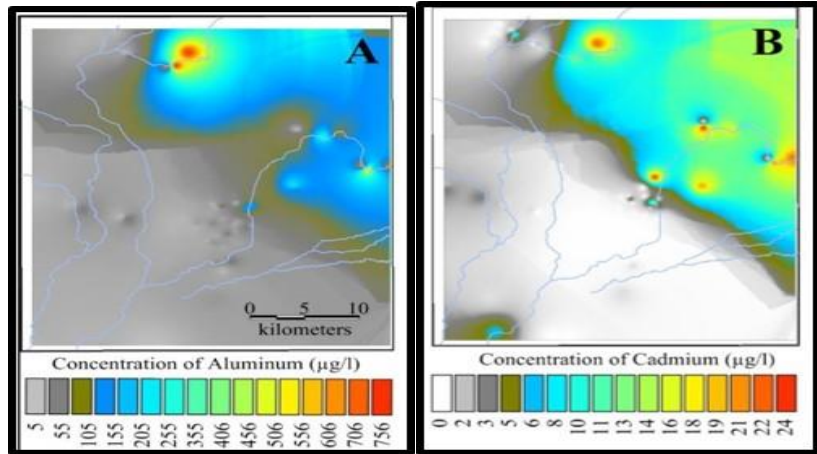


Figure 4.24 Concentration of trace elements in the study area ( $\mu\text{g/l}$ )

Cont...

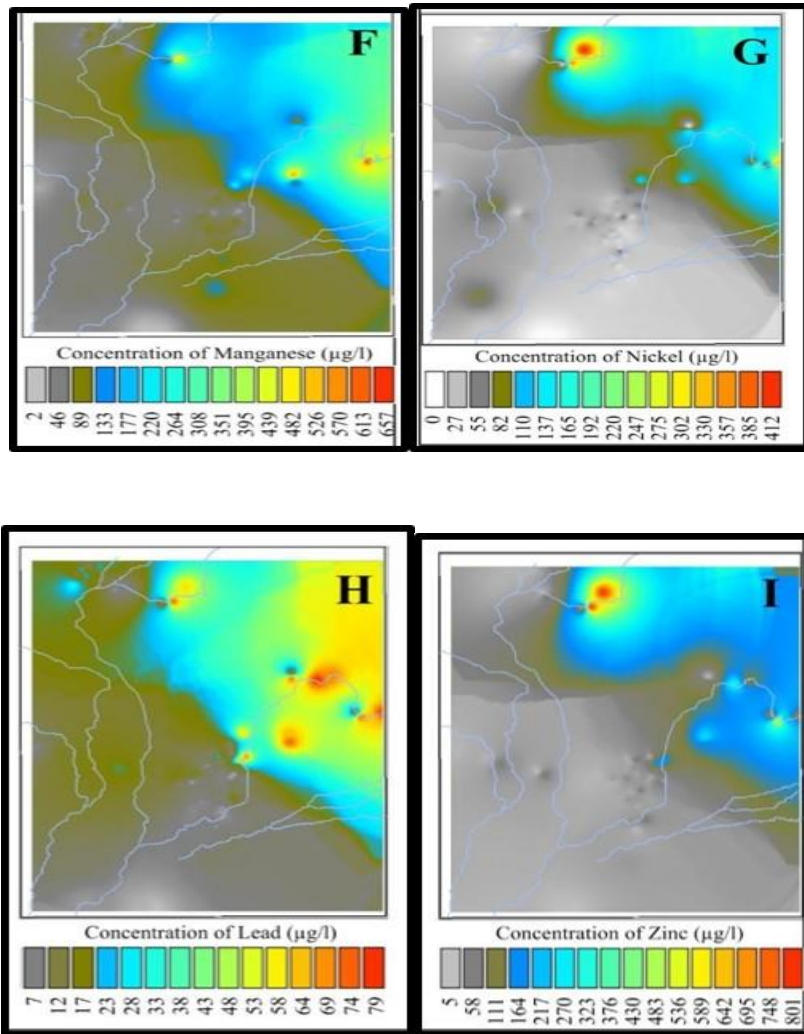


Figure 4.25 Concentration of trace elements in the study area ( $\mu\text{g/l}$ )

## **CHAPTER 5**

### **ELECTRICAL RESISTIVITY SOUNDING**

#### **5.1 Introduction**

In the current age, interest in mapping and exploring groundwater resources has increased rapidly. This rapid increase has led to greater research in underground aquifer studies in terms of aquifer properties and their spatial distribution. Overall degradation of water resources due to natural and anthropogenic activities has enhanced the use of various geophysical techniques for exploring underground water resources. This technique is also used in exploring mineral resources (Bauman, 2005; Legault, 2015) and some archeological studies (Griffiths & Barker, 1994; Tsokas et al., 2008)

Geophysical techniques are considered as the most suitable method in exploring groundwater, its distribution and, quality assessment, for geophysical, geotechnical, and environmental studies (Muchingami et al., 2012). The most commonly used geophysical technique is based on electrical resistivity measurements for subsurface lithologies which is not only a simple method but also less expensive. Electrical Resistivity Soundings as it

is generally known is one of the simplest and an effective methods based on surface measurements and is used as a tool for preliminary groundwater investigations and effectively generates 1D models that can be latter converted to 3D models (Loke et al., 2013). It is widely employed for measuring depth and thickness of the subsurface lithologies, aquifer delineation and studying the environment of the aquifers. With additional support from the well data it gives reliable information about the groundwater location, thicknesses and depth in the subsurface.

## 5.2 Basic Principle

An Electrical Resistivity Survey (ERS) is conducted for measuring and mapping the resistivity values subsurface lithologies (Samouëlian et al., 2005). This survey is carried out to get an image of the subsurface geology based on the measurement of the electrical properties of the subsurface materials (Jayeoba & Oladunjoye, 2015). An electrical current is sent into the ground at many locations along with a profile or a grid and the resulting drop in the voltage is measured. Electrical Resistivity Sounding (ERS) data generated indicates the response of the earth's materials to the flow of electrical current, where the Earth is behaving as the resistance to the flow of current.

Measurements made in ERS method are based on Ohm's Law (Eq.5.1) the and resistivity of the Earth's materials.

$$V=IR$$

Eq 5.1

The empirical relation in the equation above shows the relationship between voltage drop (V) across a resistance(R) and current (I). Resistivity measurement are conducted by inducing. An electric current is induced into the ground by two current electrodes (C1 and C2), and two potential electrodes (P1 and P2) measure the resultant voltage drop. The (pa)

which is the apparent resistivity can be calculated from the voltage (V) and current (I).

$$\rho_a = kV/I$$

Eq 5.2

The geometric factor (K), depends on the alignment of current and potential electrodes. Depth of imaging in the electrical resistivity sounding (ERS) method depends on the spacing between the current electrodes. As the electrode spacing is increased the depth of imaging is also increased. The total depth of imaging is also effected by the total length of the electrode array. In addition to these, the depth of penetration also depends on subsurface resistivities. The depth of imaging decreases with high resistive layers. The groundwater resistivity values are in the range of 10 to 100  $\Omega$ -m (Keller & Frischknecht,1996), The groundwater values also depend on the amount of dissolved salts that are present in it, as given in Figure 5.5 (Palacky, 1987). However, an overlap can be seen in the values of resistivity of different types of waters, which depends on numerous factors such as, degree of water saturation, porosity, permeability and amount of salts dissolved.

### **5.2.1 Vertical Electrical Sounding (VES)**

The method of Vertical Electrical Sounding (VES), is used for determination of the subsurface variations in the resistivity values. VES is applied for areas where the subsurface layers are generally horizontal and have small lateral variation. This is because the VES curves are interpreted by using a horizontal layered subsurface (1D) model. For measuring the apparent resistivities, a resistivity meter is used. By this the resistivity value is given in terms of resistance value.



$$R=V/I$$

Eq 5.3

Therefore, in practice, for calculating apparent resistivities Eq 5.4 is used:

$$\rho_a=kR$$

Eq 5.4

The resistivity value thus calculated does not give true resistivity of the lithologies in the subsurface, rather they give an “apparent” value which depicts resistivities for a homogeneous subsurface model that will generate the similar resistance value if the electrode alignments are same. A complex relationship exists between the apparent and the true resistivities of the subsurface. For determining the true values of the subsurface resistivity, an inversion is done by specialized resistivity softwares. On a log-log paper, the values of measured apparent resistivity are plotted. The data generated by 1D VES survey is interpreted, assuming that the subsurface lithologies are nearly horizontal. The same assumptions are applied for the study area of Uthal. Balochistan.

### **5.2.2 Electrode Configurations**

The 1D sounding method has various electrode arrangements which are termed as arrays or configurations. The four common configurations based on these arrangements of electrode in 1D sounding are; Schlumberger, Wenner, pole-pole, dipole-dipole.

### 5.2.2.1 Wenner Configuration

This Wenner configuration was developed in 1916. In Wenner configuration, A and B, the outer electrodes send direct current into the ground and the two electrodes M and N, measure the potential difference. The Common midpoint (O), between current and the potential electrodes images the depth of the investigation. In the Wenner configuration the electrode distance is kept same, i.e.  $AM = MN = NB = a$ .

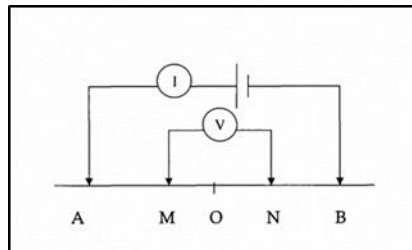


Figure 5.1 Wenner Electrode Configuration

### 5.2.2.2 Schlumberger Configuration

The Schlumberger technique was developed in 1916. In the Schlumberger configuration the distance between potential electrodes (MN) is less than the distance between the two current electrodes (AB). L is designated as the distance between two current electrodes and N is designated as the distance between two potential electrodes. Thus,  $AB = L$  is the separation between current, and  $MN = a$ , is the separation between potential electrodes.

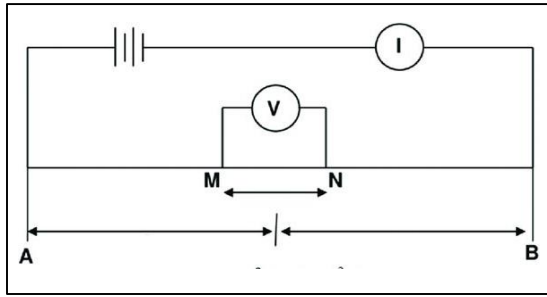


Figure 5.2 Schlumberger Electrode Configuration

### 5.2.2.3 Dipole –Dipole Configuration

The electrode spacing in this configuration for the current electrodes (C1-C2) is ‘a’ and it is equal to the distance (P1-P2) between the two potential electrodes. There is another factor “n” in this array and it is the ratio of the distance between the C1 and P1 electrodes to the C2-C1 (or P1-P2) dipole length “a”.

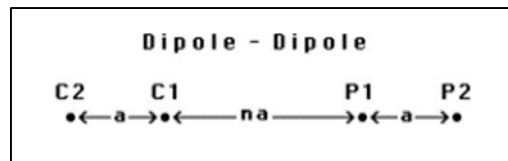


Figure 5.3 Dipole- Dipole Electrode Configuration

### 5.2.2.4 Pole – Pole Configuration

In Pole-Pole configuration, the current electrode or the potential electrode is kept at some infinite distance and the other electrodes remain in their positions as in the symmetrical configuration. In geoelectrical profiling, this arrangement of three electrodes is moved and the apparent resistivity values are obtained (Telford et al., 1990).

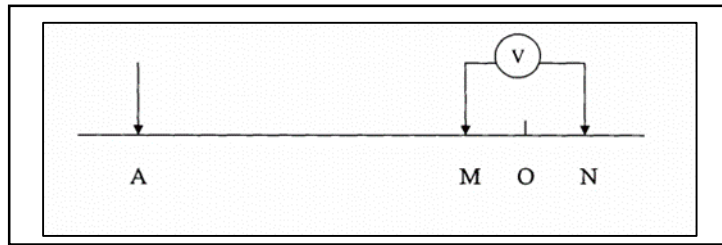


Figure 5.4 Pole-Pole Electrode Configuration

From the resistivity surveys the image of the subsurface distribution of resistivity is generated by one of these configurations (Batayneh, 2006). The resistivities are converted into a meaningful subsurface geological picture. This is done with typical resistivity values already existing (Palacky, 1987) for the subsurface materials and is integrated with the geology of the study area. Resistivity values for different geologic materials are given in Figure 5.6 and these are taken as the reference values and integrated with the geology of the area for subsurface interpretation.

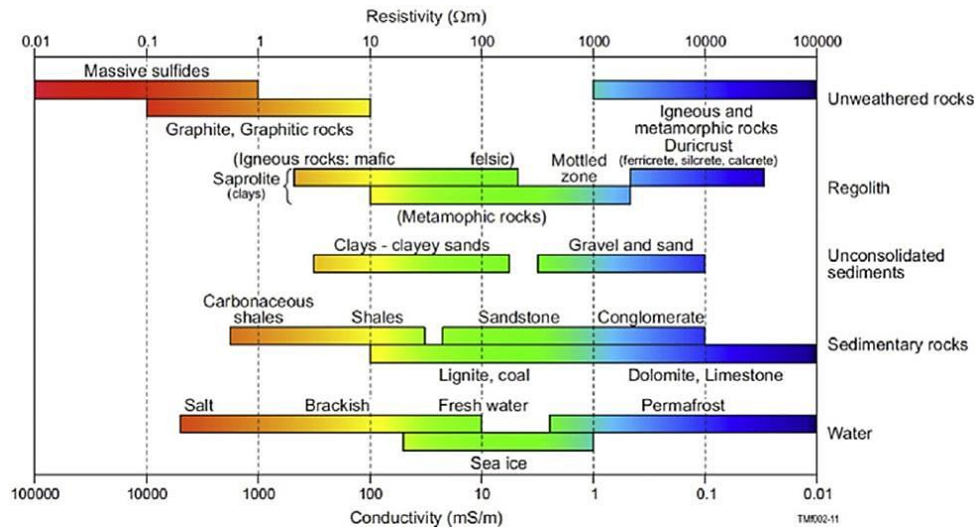


Figure 5.5 Electrical Resistivity Ranges in ohm-m and conductivity in mS/m for various Earth materials (Palacky, 1987)

The interpretation of methodology for 1D ERS curves involves two steps. In the first step, the data is plotted to generate an approximated interpretation by doing the curve-matching, and then the interpretation is done on the basis of automated interpretation through softwares (Zohdy, 1989). Finally, in the next step the resistivity values for each layer and the layer thicknesses are then obtained. From these values i.e. of resistivities and the thicknesses, spatial distribution is determined with the help of contour maps. The high and low resistivity areas and the thickness of the aquifers can then be determined and delineated (Maillet et al., 2005).

### **5.3 Electrical Resistivity of study area**

ERS survey using Schlumberger electrode configuration was carried out using Italian made PASI Electrical Resistivity Imaging System for the study area in Uthal, Balochistan. The electrode spacing was kept at 5.00 meter and the total spread of electrodes was 300 meters. The geoelectrical parameters that were measured were analyzed by IPI win software. The VES data for 25 points were obtained for the survey area in Uthal (Figure 5.6). The data was obtained with the Schlumberger arrangement (M-AB-N). For each data point the resistivity profile, the distance between the potential electrode (MN) was increased gradually from 0.5 to 20 m and the resultant potential drop across the electrodes was measured. The current electrode distance (AB/2) was gradually increased from 1.5 to 150 m. The maximum depth of penetration was directly proportional to the spacing of electrode and inversely proportional to the conductivity of the subsurface lithologies (Mussett & Khan, 2000).

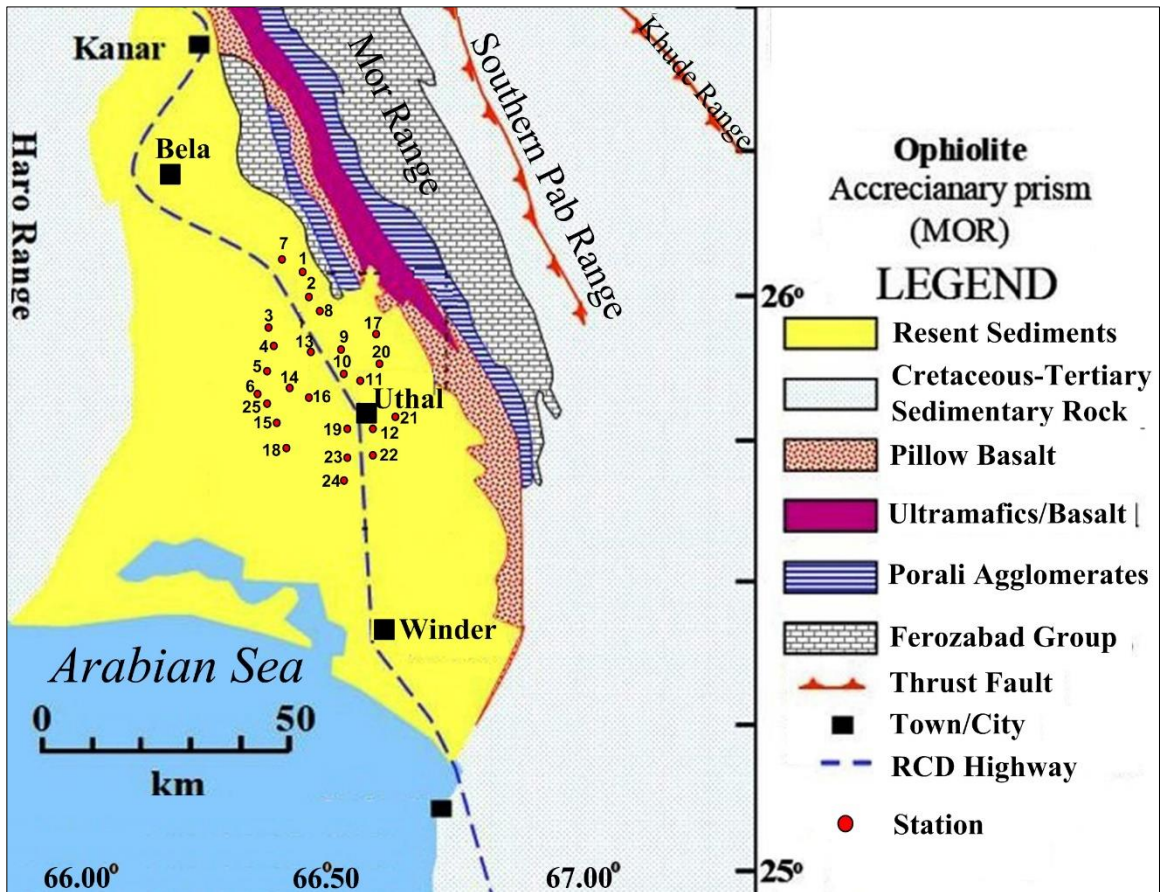


Figure 5.6 Location of Electrical Resistivity Data points shown on the geologic map of the area. Well locations are also marked (Bashir et al., 2009).

Table 5.1 VES Points with latitudes, longitudes and elevations

<b>S.No</b>	<b>ERS Points</b>	<b>Latitude</b>	<b>Longitude</b>	<b>Elevation (m)</b>
1	UT 01	26.043420	66.518678	69
2	UT-02	26.002169	66.529687	67
3	UT-03	25.947617	66.45730	41
4	UT-04	25.915978	66.468695	36
5	UT-05	25.871843	66.457689	32
6	UT-06	25.829204	66.440905	25
7	UT-07	26.064262	66.481560	74
8	UT-08	25.978939	66.555524	79
9	UT-09	25.913493	66.597312	60
10	UT-10	25.871106	66.600277	48
11	UT-11	25.862008	66.628356	64
12	UT-12	25.774807	66.657028	47
13	UT-13	25.903570	66.564901	39
14	UT-14	25.840506	66.497341	26
15	UT-15	25.782984	66.478211	19
16	UT-16	25.825566	66.534304	24
17	UT-17	25.915664	66.661229	114
18	UT-18	25.736070	66.494177	16
19	UT-19	25.776971	66.629317	32
20	UT-20	25.903843	66.670091	110
21	UT-21	25.799547	66.702965	93
22	UT-22	25.730145	66.657078	49
23	UT-23	25.726747	66.613830	28
24	UT-24	25.685617	66.606683	23
25	UT-25	25.817761	66.460540	25

## 5.4 Interpretation of VES Points

### UT-01

For UT-01, first electrode is at 0.5 meters and last electrode at 150 meters. The total spread length is 300 meters and at UT-01 the range of resistivity values is from 42.4 to 2060  $\Omega$  m. From the interpretation of the curves (Figure 5.7), five layers have been identified. The first layer from surface till the depth of 2.22m is present and this layer comprises of unconsolidated sand and has a resistivity of 2060  $\Omega$  m. Beneath this layer unconsolidated gravely sand is present, from 2.22 till 4.77 m, with a resistivity values of 1331  $\Omega$  m. This is followed by a thin layer of sand with saline water, from 4.77 till 5.94 m, and has a resistivity values of 42.4  $\Omega$ m. Underneath this is another layer of unconsolidated sediments (gravely sand) from 5.94 to 91.9 m with a resistivity of 1144  $\Omega$ m. Beneath this layer is a fresh water aquifer in sand and it is present at a depth of 91.9 to 147 m and revealing a resistivity of 81.1  $\Omega$ m. The lithologies and depth have been calibrated with the borehole data from the study area. The resistivity model under this point is  $\rho_1 > \rho_2 < \rho_3 < \rho_4 > \rho_5$ .

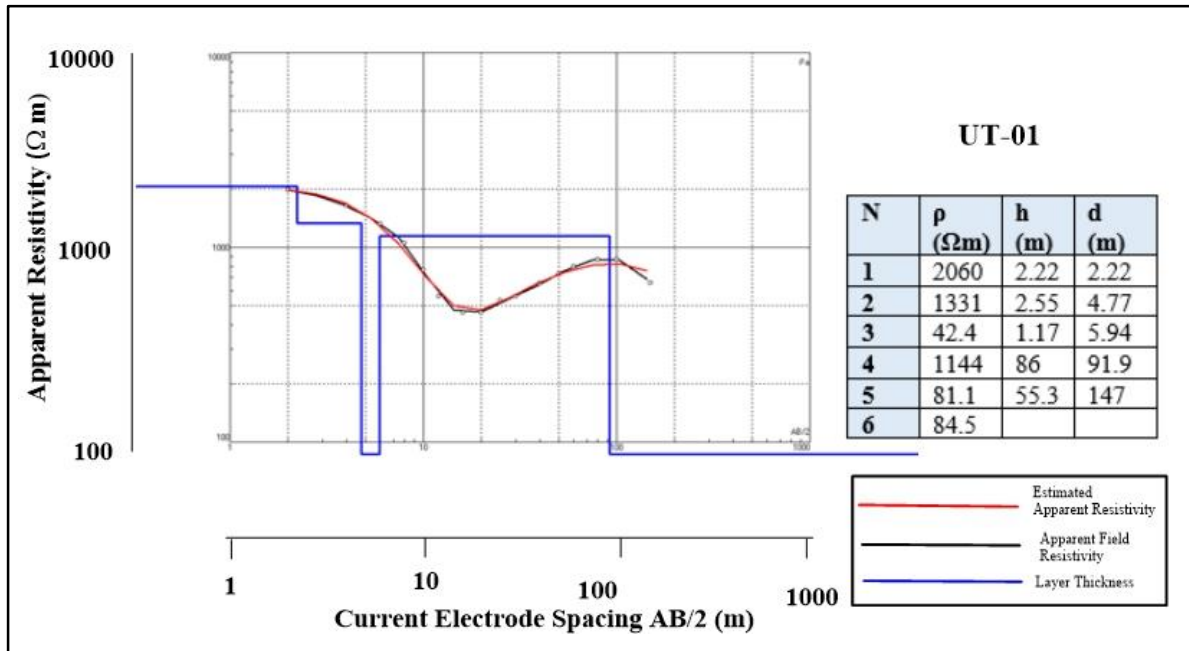


Figure 5.7 The modeled resistivity curves using IPI2Win Software for UT-01.



## UT-02

For UT-02 first electrode is at 0.5 meters and last electrode at 150 meters. The total spread length is 300 meters. For UT-02 the resistivity values range from 75.8 to 3869  $\Omega$  m. Five layers have been identified from the interpreted curves (Figure 5.8), with first layer from surface till a depth of 4.35 m is of sand and has a resistivity of 646  $\Omega$ m. Under the top, from 4.35 till 12.9 m, unconsolidated sand is present and showing resistivity of 3869  $\Omega$ m. From 1, the depth of 2.9 till 33.8 m, unconsolidated sand and gravel is present with resistivity values of 1144  $\Omega$ m. This layer is followed by a freshwater aquifer in sand from 33.8 to 141 m with a resistivity of 75.8  $\Omega$ m. Resistivity values at UT-02, show the presence of a thick fresh water aquifer in sand at a depth of 33.8 m from the surface which goes down to a depth of 141 meters. The lithologies and depth have been calibrated with the borehole data from the study area. The resistivity model under this point shows  $\rho_1 > \rho_2 < \rho_3 > \rho_4 < \rho_5$ .

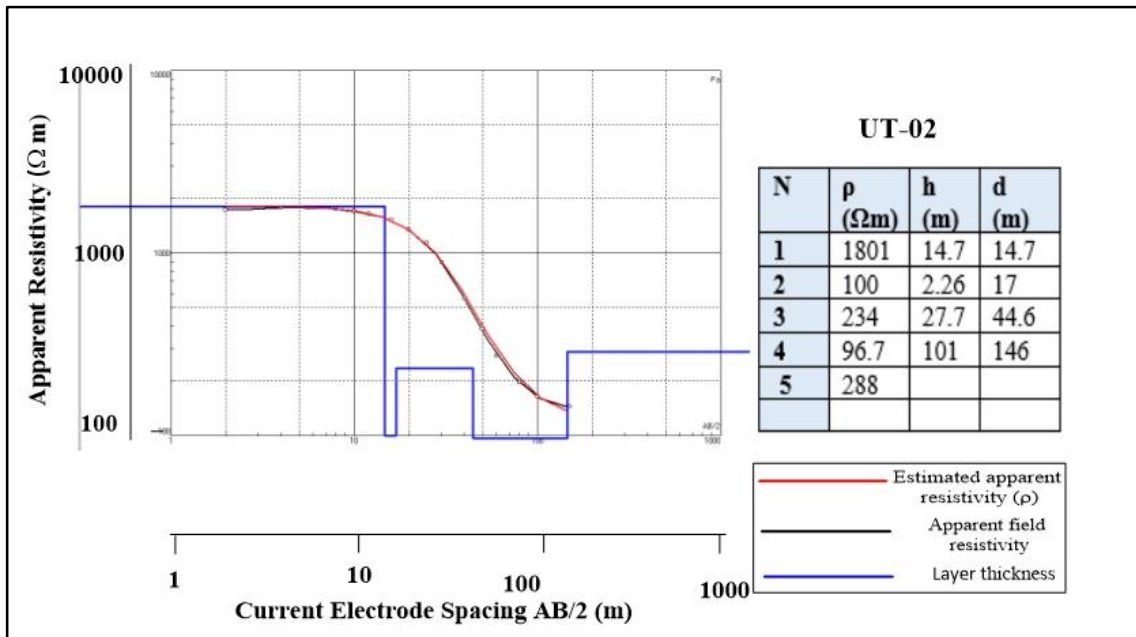


Figure 5.8 The modeled resistivity curves using IPI2Win Software for UT-02

### UT-03

For UT-03 first electrode is at 0.5 meters and last electrode is at 150 meters. The total spread length is 300 meters. The resistivity values here range from 93.5 to 4316  $\Omega\text{m}$ . At UT-03 four layers are identified from the interpreted curves (Figure 5.9). The top most layer from surface to a depth of 1.79 consists of unconsolidated gravelly sand and shows the resistivity value of 1309  $\Omega\text{m}$ . Beneath this, from 1.79 to 10.6 m, a layer of unconsolidated sand is present with a resistivity of 4316  $\Omega\text{m}$ . From 10.6 to 39.7 m, compact sand is present with a resistivity values of 959  $\Omega\text{m}$ . This is followed by a zone of fresh water aquifer having a resistivity of 93.5  $\Omega\text{m}$ . from 39.7 till 152 m. The lithologies and depth have been calibrated with the borehole data from the study area. The resistivity model under this point shows  $\rho_1 > \rho_2 > \rho_3 < \rho_4 < \rho_5$ .

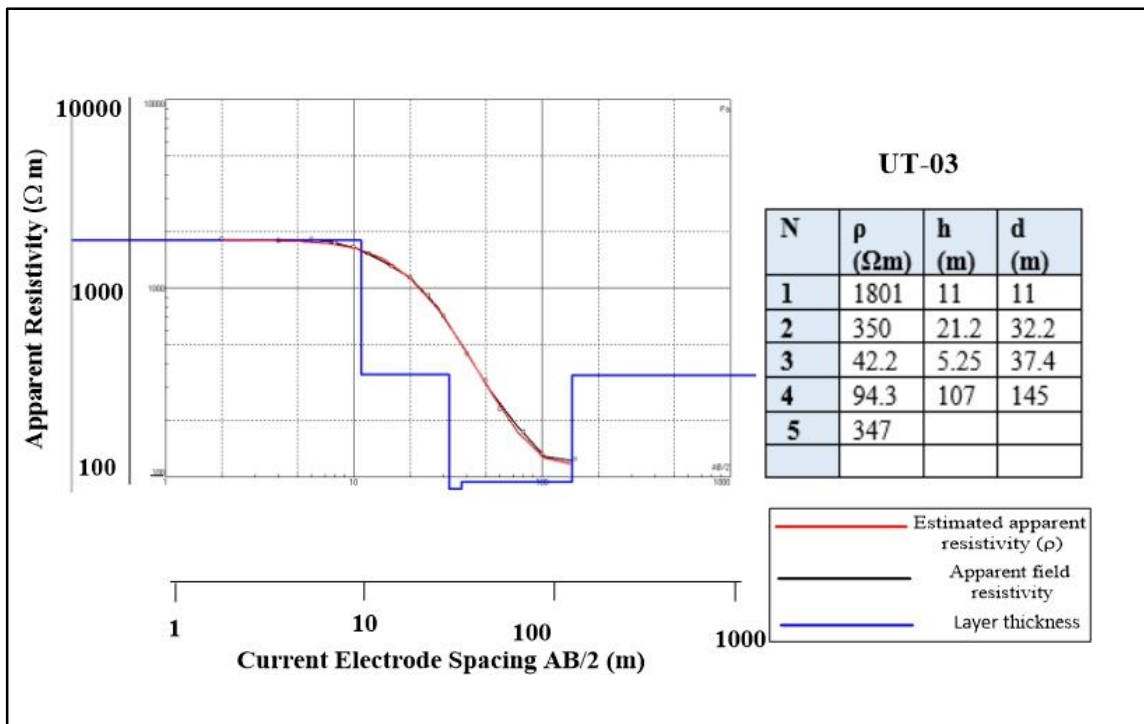


Figure 5.9 The modeled resistivity curves using IPI2Win Software for UT-03.

## UT-04

For UT-04 first electrode is at 0.5 meters and last at 150 meters. The total spread length is 300 meters. The resistivity value here ranges from 75.8 to 2975  $\Omega$  m. At UT-04, four layers have been identified, with the first from surface up to a depth of 2.26 m with a true resistivity of 777  $\Omega$  m. Beneath this unconsolidated Sand is present from 2.26 to 10.3 m, having a resistivity of 2975  $\Omega$  m. From 10.3 to 35.6 m the resistivity values show the presence of Clay with 201  $\Omega$  m. Underneath there is a fresh water aquifer with a resistivity of 75.8  $\Omega$  m from 35.6 to 146 m. Below this is a layer of dry sand with resistivity of 630  $\Omega$  m. At UT-04, the resistivity values show the presence of fresh water aquifer at a depth of 35.6 m from the surface and extend down till 146 meters. The lithologies and depth have been calibrated with the borehole data from the study area. The resistivity model under this point shows that  $\rho_1 > \rho_2 > \rho_3 > \rho_4 < \rho_5$ .

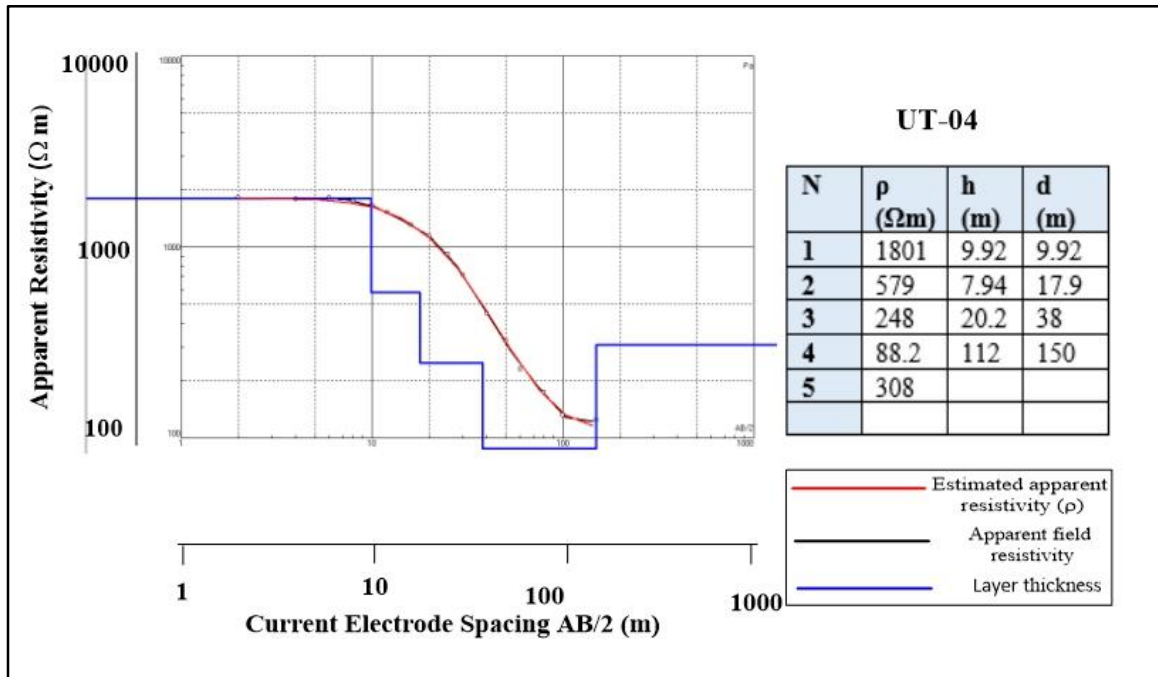


Figure 5.10 The modeled resistivity curves using IPI2Win Software for UT-04..

## UT-05

For UT-05, first electrode is at 0.5 meters and last at 150 meters. The total spread length is 300 meters. Here the resistivity values for the subsurface lithologies range from 88.2 m to 6851  $\Omega$  m. At UT-05, five layers are identified from curves (Figure 5.11), with the first layer sand from surface to a depth of 2.91 and has a resistivity of 594  $\Omega$  m. Underneath this is a layer of unconsolidated sediments up to 5.65 m. This is a high resistivity layer of 6851  $\Omega$  m. From 5.65 to a depth of 12.1 m compact sand is present with a resistivity of 674  $\Omega$  m. Underneath this, from 12.1 m up to 50.2 m clay with a resistivity of 256  $\Omega$  m is present. From a depth of 50.2 m to 152 m, fresh water aquifer in sand is present. The lithologies and depth have been calibrated with the borehole data from the study area. The resistivity model under this point indicates that  $\rho_1 > \rho_2 > \rho_3 < \rho_4 < \rho_5$ .

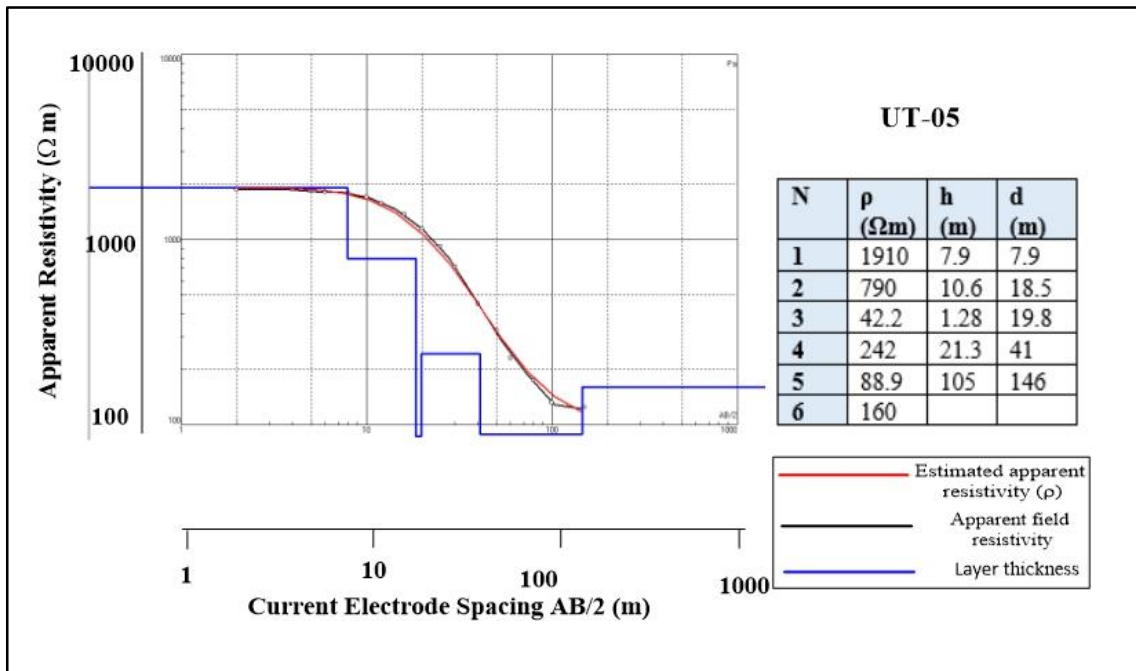


Figure 5.11 The modeled resistivity curves using IPI2Win Software for UT-05.

## UT-06

For UT-06, first electrode is at 0.5 meters while last at 150 meters. The total spread length is 300 meters. The resistivity values here are in range of 42.4 to 3869  $\Omega$  m. From the curve matching by software (Figure 5.12), five resistivity layers are identified. From surface to a depth of 2.65 m, unconsolidated gravelly sand, with the true resistivity of 1223  $\Omega$  m is present. Beneath this layer, from 2.65 m up to a depth of 6.19 m, an unconsolidated sand layer is having a resistivity value of 3869  $\Omega$  m is present. Underneath this unconsolidated sand layer, is a thin layer of saline water, from 6.19 to 7.64 m, in sand and has a resistivity value of 42.4  $\Omega$  m. From 7.64 to 49 m, there another unconsolidated sand layer from 7.64 till 49 m. It shows a resistivity value of 1309  $\Omega$  m. Below this is a present freshwater aquifer in sand, from the depth 49 from the surface and going down to 148 m. It shows a resistivity value of 81.1  $\Omega$  m. At UT-06, the resistivity values show a thick fresh water aquifer. The lithologies and depth have been calibrated with the borehole data from the study area. The resistivity model under this point indicated that  $\rho_1 > \rho_2 < \rho_3 < \rho_4 < \rho_5$ .

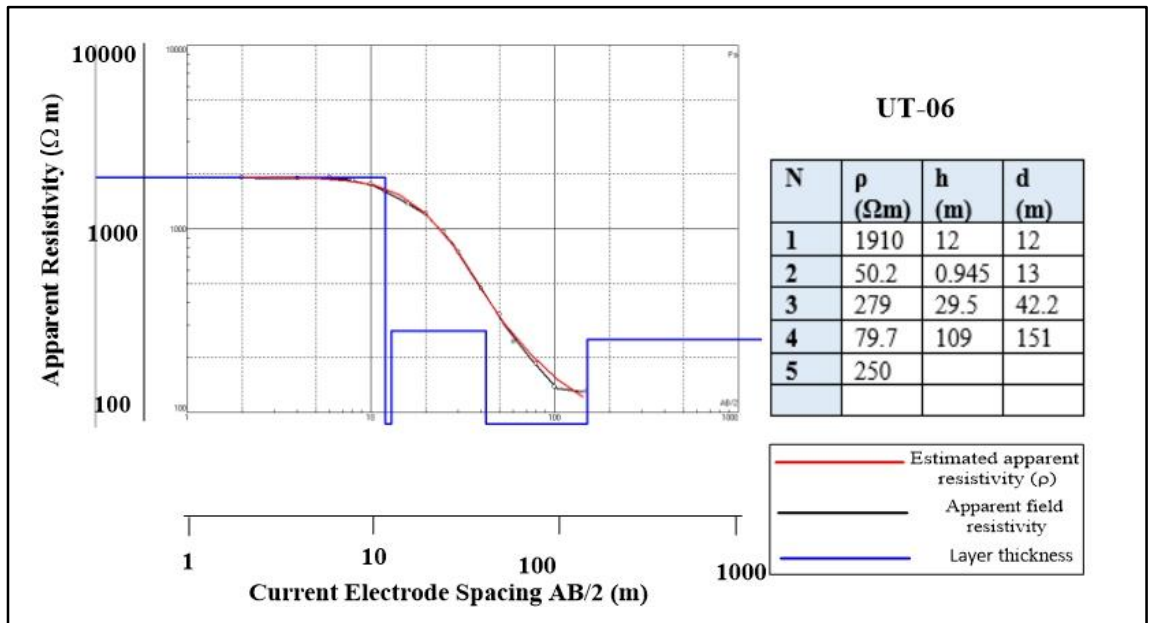


Figure 5.12 The modeled resistivity curves using IPI2Win Software for UT-06.

## UT-07

For UT-07, the first electrode is at 0.5 meters and the last electrode is at 150 meters. The total spread length is 300 meters. At this point the resistivity values are in the range from 79.7 to 11249  $\Omega$  m by the curve matching (Figure 5.13), four layers are identified. From surface till a depth of 7.03 m is unconsolidated gravely Sand with the true resistivity of 1298  $\Omega$  m. Under this layer from 7.03 up to 17.7 is a high resistivity layer of igneous rock with a resistivity of 11249  $\Omega$  m. Under this is a compact sand layer from 76.4 m having a resistivity of 511  $\Omega$  m. From 76.4 m till 147 m freshwater aquifer is present showing resistivity values of 81.1  $\Omega$  m. The lithologies and depth have been calibrated with the borehole data from the study area. The resistivity model under this point shows that  $\rho_1 < \rho_2 > \rho_3 > \rho_4 > \rho_5$ .

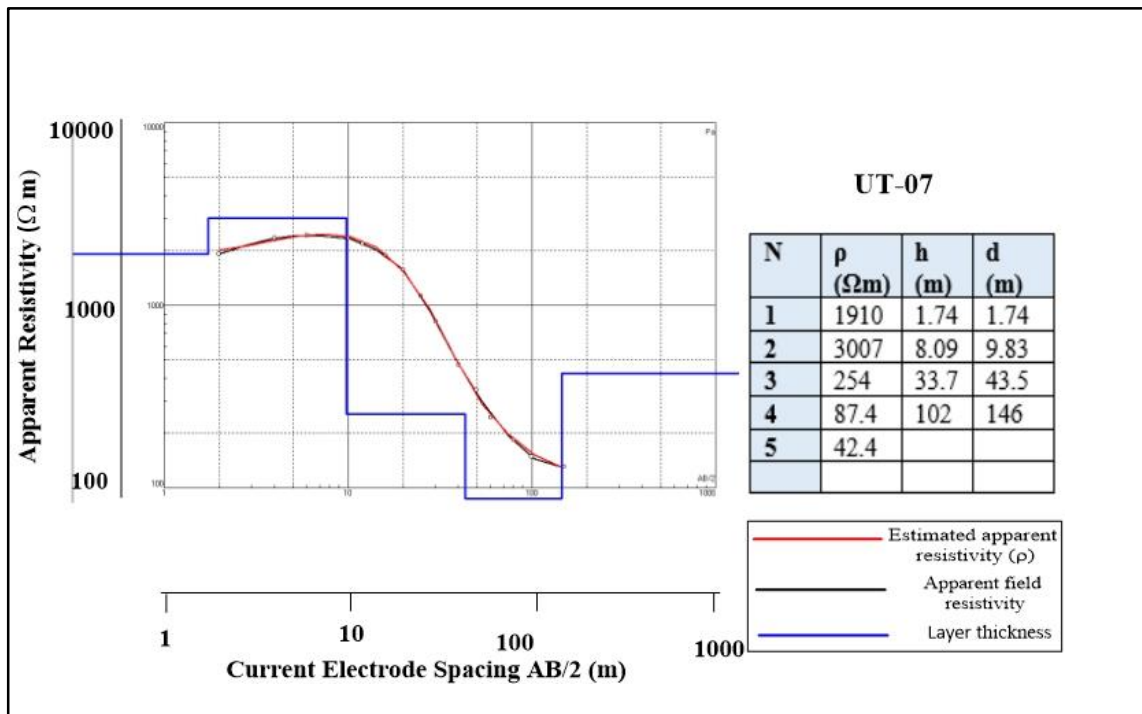


Figure 5.13 The modeled resistivity curves using IPI2Win Software for UT-07.

## UT-08

For UT-08, first electrode is at 0.5 meters while last is at 150 meters. The total spread length is 300 meters. Here the resistivity values are from 76.4 to 4069  $\Omega\text{m}$ . From the curve matching (Figure 5.14), four layers were identified. From surface until a depth of 5.19 m, a high resistivity layer of 1309  $\Omega\text{ m}$  comprising of unconsolidated gravely sand is present. Under this layer, from 5.19 till 16.68 m, another layer of unconsolidated material showing a higher resistivity value of 4069  $\Omega\text{ m}$  is present. This is followed by a fresh water zone in Sand, from 16.8 till 55.1 m with a resistivity value of 76.4  $\Omega\text{ m}$ . Under this from 55.1 to 142 m, a layer of clay having a resistivity of 117  $\Omega\text{ m}$  is present. It is again followed by a low resistivity layer having 79.7  $\Omega\text{ m}$ . Resistivity values show the presence of fresh water aquifer at a depth 55.1 m to 142 m from the surface. The lithologies and depth have been calibrated with the borehole data from the study area. The resistivity model under this point indicates that  $\rho_1 < \rho_2 > \rho_3 < \rho_4 > \rho_5$ .

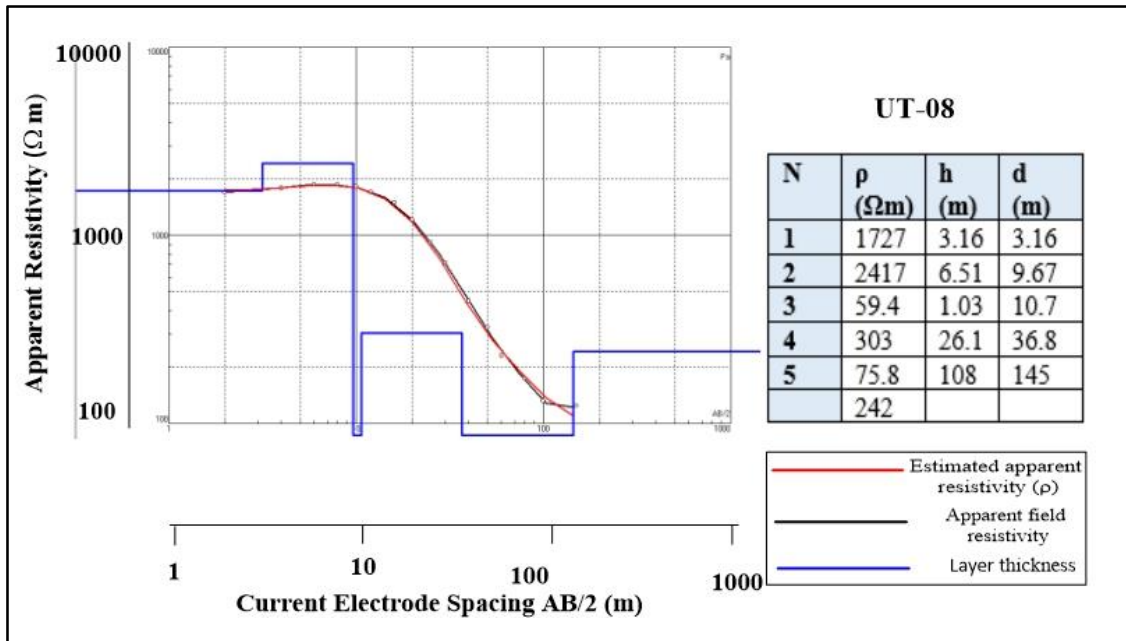


Figure 5.14 The modeled resistivity curves using IPI2Win Software for UT-08.

## UT-09

For UT-09, first electrode is at 0.5 meters while last at 150 meters. The total spread length is 300 meters. Here the resistivity values range from 97.5 to 6299  $\Omega$  m and four layers are identified by curve matching (Figure 5.15). The first layer from surface up to a depth of 1.36 m consists of unconsolidated gravelly sand and has a resistivity of 2113  $\Omega$  m. Underneath this, from 1.36 to a depth of 6.19 m unconsolidated sand is present showing with a resistivity value of 6299  $\Omega$  m. Below this, from 6.19 till 37.4 m a layer of clay with a resistivity values of 230  $\Omega$  m is present. This is followed by a fresh water aquifer with a resistivity of 97.5  $\Omega$ , from a depth of 37.4 to 146 m. Resistivity values indicate the presence of fresh water aquifer from a depth of 37.4 m to 146 m from the surface. The lithologies and depth have been calibrated with the borehole data from the study area. The resistivity model under this point is  $\rho_1 < \rho_2 > \rho_3 > \rho_4 < \rho_5$ .

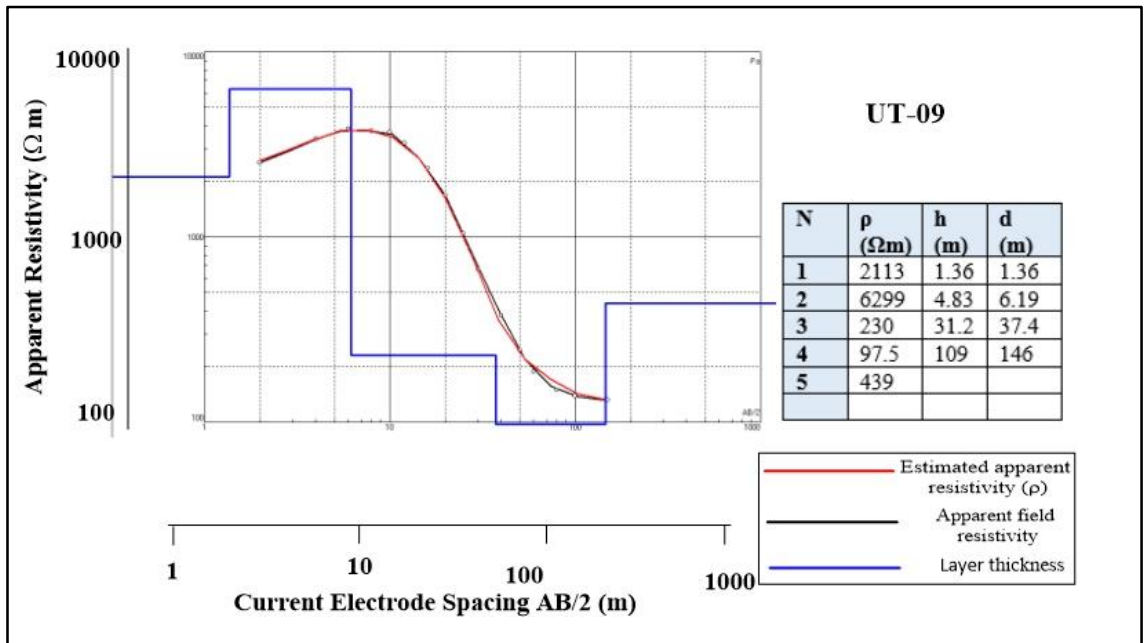


Figure 5.15 The modeled resistivity curves using IPI2Win Software for UT-09.



## UT-10

For UT-10, first electrode is at 0.5 meters while last at 150 meters. The total spread length is 300 meters. The resistivity values at UT-19 range from 87.4 to 1910  $\Omega$  m. From curve matching (Figure 5.16), four layers are identified, with first layer from surface up to a depth of 1.74 m a thin unconsolidated gravelly sand layer with a resistivity of 1910  $\Omega$  m. This layer is followed by another high resistivity layer of 3007  $\Omega$  m consisting of unconsolidated sand, from 1.74 to 9.83 m. under this, from 9.83 to a depth of 43.5 clay is present with a resistivity value of 254  $\Omega$  m. From 43.5 till 146 m a fresh water aquifer is present showing a resistivity values of 87.4  $\Omega$  m followed by a clay layer of 424  $\Omega$  m. The lithologies and depth have been calibrated with the borehole data from the study area. The resistivity model under this pint indicates that  $\rho_1 > \rho_2 > \rho_3 > \rho_4 < \rho_5$ .

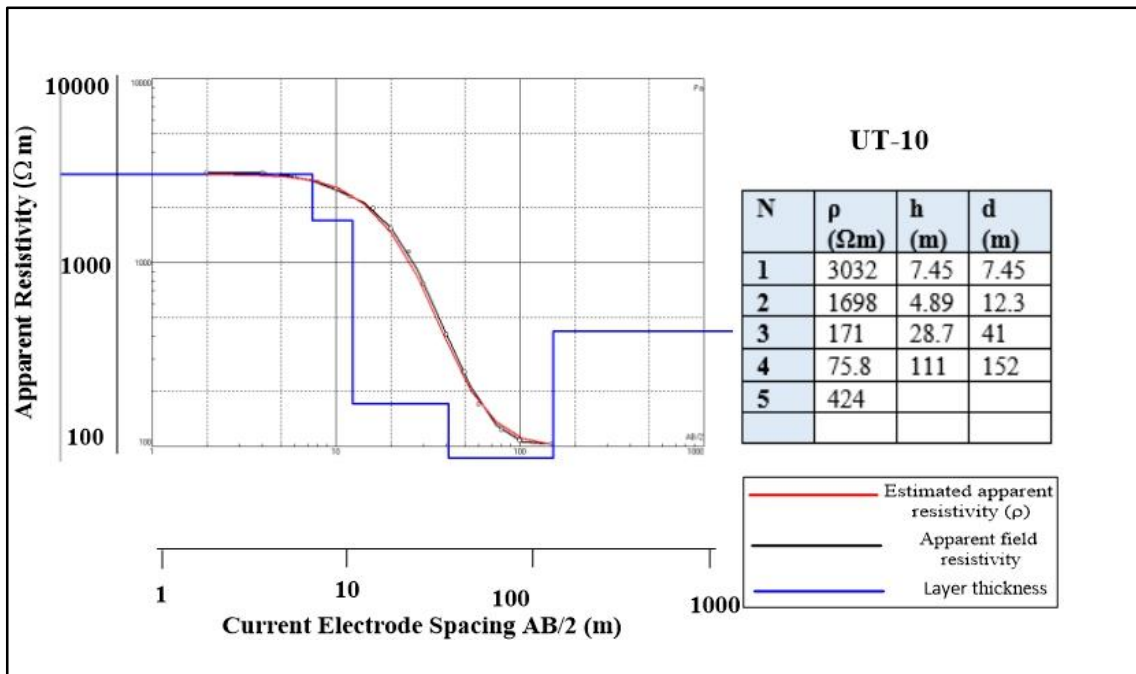


Figure 5.16 The modeled resistivity curves using IPI2Win Software for UT-10.

## UT-11

For UT-11, first electrode is at 0.5 meters while last is at 150 meters. The total spread length is 300 meters. At UT-11 the resistivity values are in range of 96.7 to 1801  $\Omega$  m. From the curve matching (Figure 5.17), four layers are identified. The first layer from surface to a depth of 14.7 m shows a resistivity of 1801  $\Omega$  m and comprises of gravelly sand. Under this from 14.7 to 17 m a thin layer of sand with fresh water is present with a resistivity value of 100  $\Omega$  m. From 17 m up to 44.6 m a compact clay showing a resistivity value of 234  $\Omega$  m is present. Below this is the main fresh water aquifer in sand from a depth of 44.6 to 146 m is present, having a resistivity value of 96.7  $\Omega$  m. The lithologies and depth have been calibrated with the borehole data from the study area. The resistivity model under this point indicates that  $\rho_1 < \rho_2 > \rho_3 > \rho_4 < \rho_5$ .

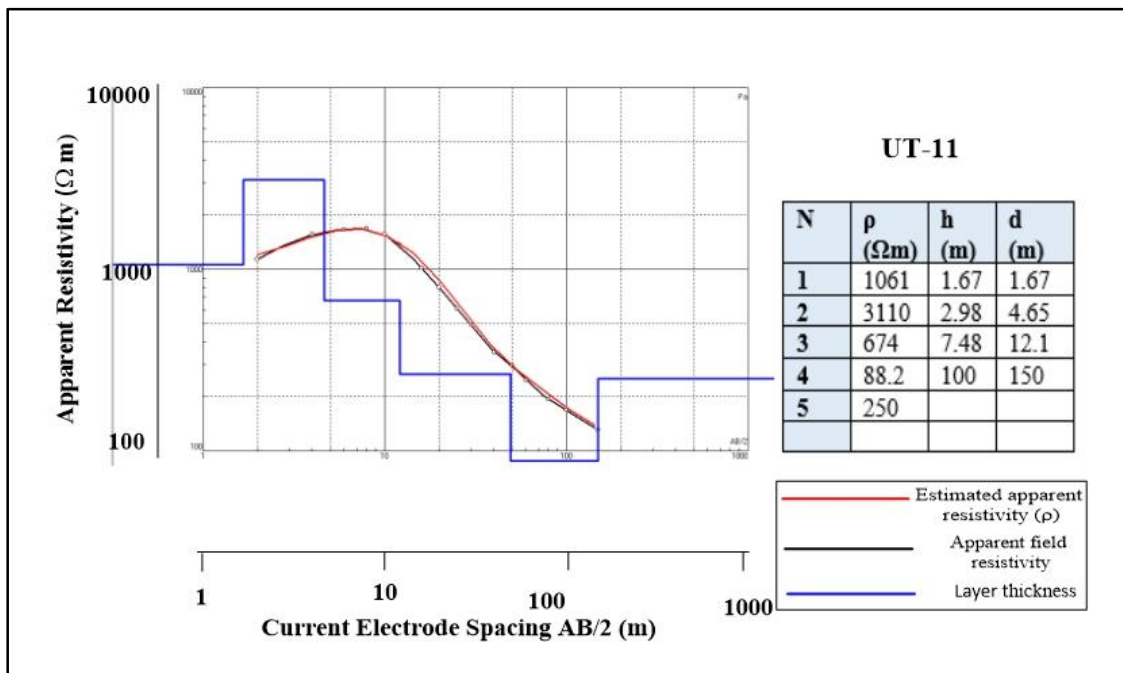


Figure 5.17 The modeled resistivity curves using IPI2Win Software for UT-11.

## UT-12

For UT-12, first electrode is at 0.5 meters while last is at 150 meters. The total spread length is 300 meters. At this point the resistivity values range from 42.4 to 1801  $\Omega$  m, and by the curve matching four layers are identified (Figure 5.18). The first layer from surface to a depth of 11 m comprising of unconsolidated gravelly sand has a resistivity of 1801  $\Omega$  m. Under this layer, from 11 to 32.2 m clay is present with a resistivity value of 350  $\Omega$  m. Under this from 32.2 up to 37.4 m saline water having a resistivity value of 42.4  $\Omega$  m. Underneath this layer from 37.4 to 145 m a fresh water unconfined aquifer is present having a resistivity of 94.3  $\Omega$  m followed by a clay layer showing a resistivity of 347  $\Omega$ . Resistivity values show the presence of fresh water aquifer at a depth of 37.4 m to 145 m from the surface. The lithologies and depth have been calibrated with the borehole data from the study area. The resistivity model under this point shows that  $\rho_1 < \rho_2 > \rho_3 > \rho_4 > \rho_5 < \rho_6$ .

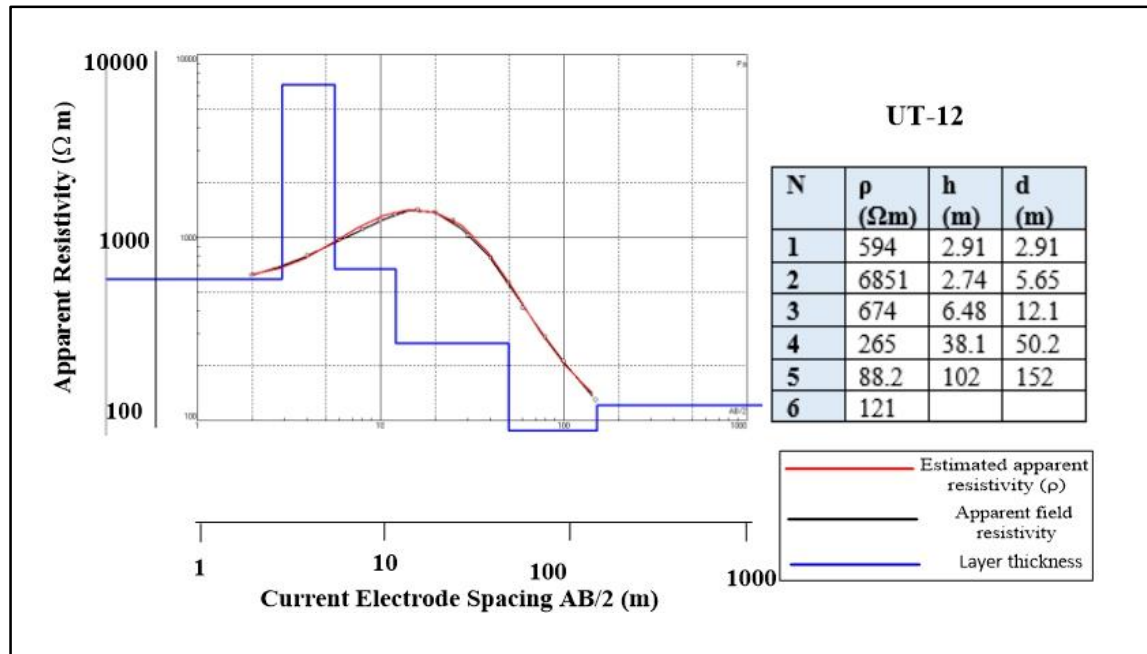


Figure 5.18 The modeled resistivity curves using IPI2Win Software for UT-12.

## UT-13

For UT-13, first electrode is at 0.5 meters while last is at 150 meters. The total spread length is 300 meters. At UT-13, the resistivity values range from 59.4 to 1727  $\Omega$  m and by curve matching five layers are identified (Figure 5.19). The first layer from surface to a depth of 3.16 m is of unconsolidated gravelly sand for UT-13, first electrode is at 0.5 meters while last is at 150 meters. The total spread length is 300 meters. At UT-13, the resistivity values range from 59.4 to 1727  $\Omega$  m and by curve matching five layers are identified (Figure 5.20). The first layer from surface to a depth of 3.16 m is of unconsolidated gravelly sand with a resistivity of 1727  $\Omega$  m. Then from 3.16 till 9.76 m another layer of unconsolidated sand is present having a resistivity value of 2417  $\Omega$  m. Underneath this from 9.76 till 10.7 m a thin layer of saline water is present showing a resistivity values of 59.4  $\Omega$  m. Below this is a clay layer with a resistivity of 303  $\Omega$  m from 10.7 to 36.8 m and from 36.8 m to 146 m fresh water aquifer is present is present having a resistivity of 75.8  $\Omega$  m underlain by Clay. Resistivity values show the presence of fresh water aquifer at a depth of 36.8 m to 145 m from the surface. The lithologies and depth have been calibrated with the borehole data from the study area. The resistivity model under this point indicates that  $\rho_1 < \rho_2 > \rho_3 > \rho_4 < \rho_5$ .

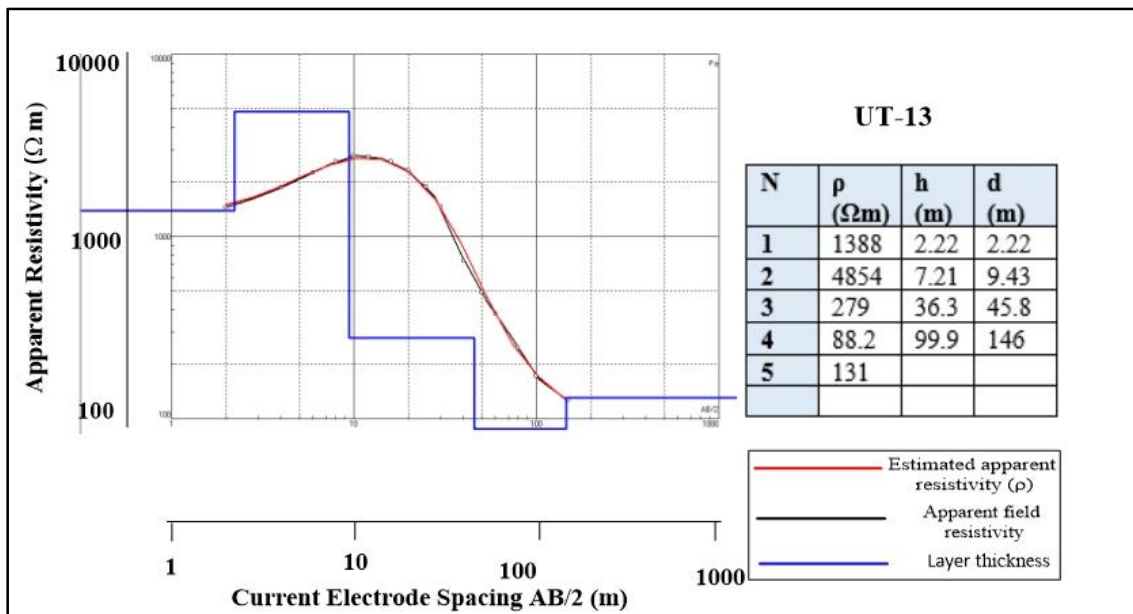


Figure 5.19 The modeled resistivity curves using IPI2Win Software for UT-13.

## UT-14

For UT-14, first electrode is at 0.5 meters while last is at 150 meters. The total spread length is 300 meters. Here the resistivity values are from to 88.2 to 3110  $\Omega\text{m}$ . Five geoelectrical layers have been identified from the curve matching (Figure 5.20). The first layer is from surface to a depth of 1.67. It comprises of unconsolidated gravelly sand and has a resistivity of 1061  $\Omega\text{m}$ . Under this layer is unconsolidated sand, from 1.67 m till 4.65 m, with a resistivity of 3110  $\Omega\text{m}$ . From 4.65 m till 12.1 m compact sand is with a resistivity value of 674  $\Omega\text{m}$ . Under this layer clay with a resistivity value of 265  $\Omega\text{m}$ . From 37.2 m till 150 m fresh water aquifer is present showing a resistivity value of 88.2  $\Omega\text{m}$ . The lithologies and depth have been calibrated with the borehole data from the study area. The resistivity model under this point indicates that  $\rho_1 > \rho_2 < \rho_3 > \rho_4 < \rho_5$ .

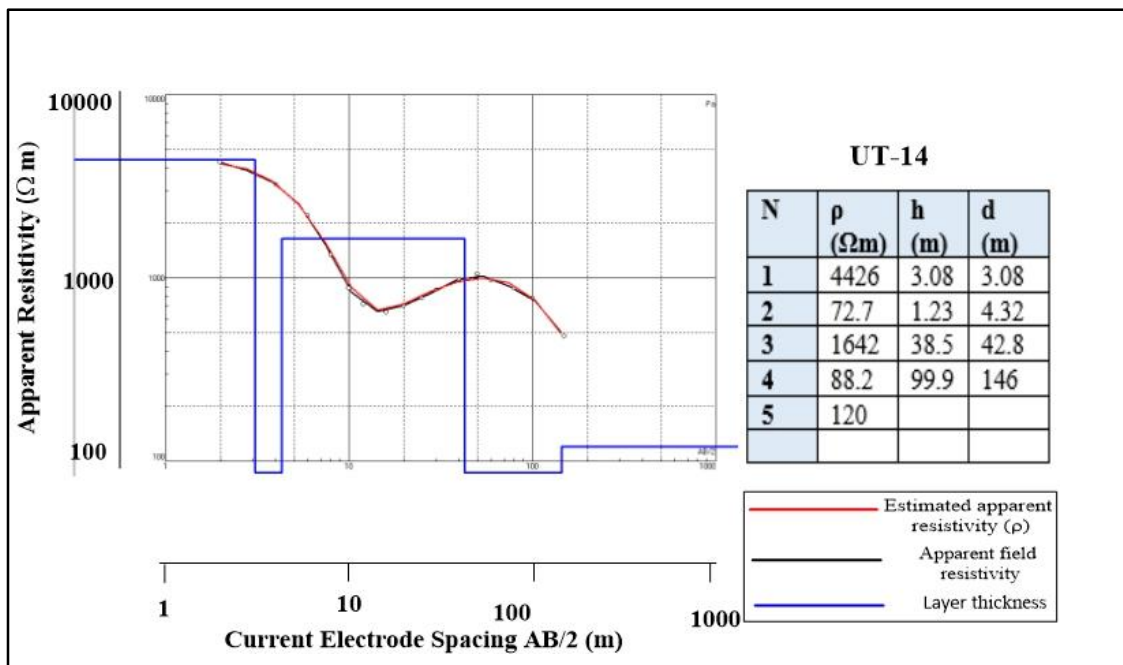


Figure 5.20 The modeled resistivity curves using IPI2Win Software for UT-14.

## UT-15

For UT-15, first electrode is at 0.5 meters while last is at 150 meters. The total spread length is 300 meters. At this point the resistivity values range from 56.5 to 3710  $\Omega\text{m}$ . Five geoelectrical layers are identified by curve matching (Figure 5.21), the first layer from surface up to a depth of 5.51 m is of unconsolidated sand with a resistivity value of 3710  $\Omega\text{m}$ . Underneath this, from 5.51 to 6.79 m, is a thin layer of sand with saline water. It has a resistivity of 56.5  $\Omega\text{m}$ . From 6.79 till 26.3 m another layer of unconsolidated sand is present showing resistivity value of 1097  $\Omega\text{m}$ . Below this, from 26.3 till 49 m, an unconsolidated sand is present with resistivity of 1614  $\Omega\text{m}$ . A fresh water aquifer is from 49 m to 144 m from the surface with a resistivity of 72.1  $\Omega\text{m}$ . Resistivity values show the presence a sand layer with of fresh water at a depth of 49 m to 144 m from the surface. The lithologies and depth have been calibrated with the borehole data from the study area. The resistivity model under this point indicates that  $\rho_1 > \rho_2 < \rho_3 > \rho_4 < \rho_5$ .

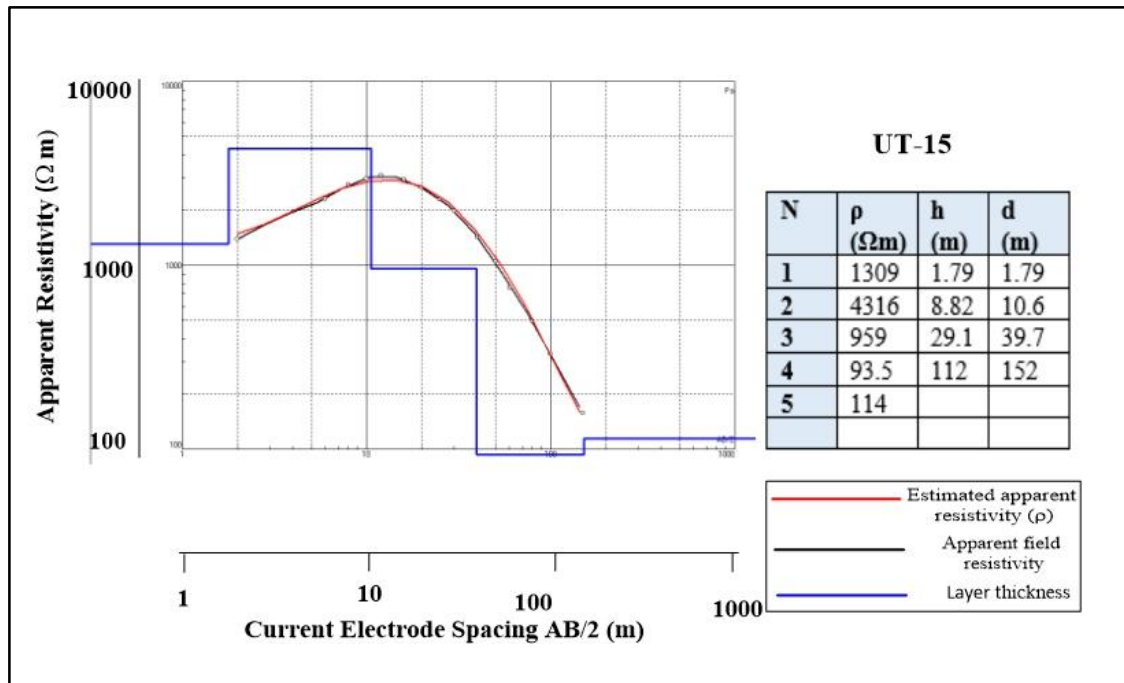


Figure 5.21 The modeled resistivity curves using IPI2Win Software for UT-15.

## UT-16

For UT-16, first electrode is at 0.5 meters while last is at 150 meters. The total spread length is 300 meters. At this point the resistivity values range from 81.1 to 3498  $\Omega$  m. Five layers (Figure 5.22) are identified, with first from surface till a depth of 2.65 m comprising of unconsolidated gravelly sand and a resistivity of 1435  $\Omega$ m. From 2.65 m till 6.19m unconsolidated sand is present showing resistivity values of 3498  $\Omega$  m. Underneath this is compact sand up to 14.4 m with resistivity of 751  $\Omega$ m. From 14.4 to 48.9 m clay is present showing resistivity value of 276  $\Omega$  m. Under this layer sands with fresh water is present and has a resistivity of 81.1  $\Omega$  m. The lithologies and depth have been calibrated with the borehole data from the study area. The resistivity model under this point indicates that  $\rho_1 < \rho_2 > \rho_3 < \rho_4 > \rho_5 < \rho_6$ .

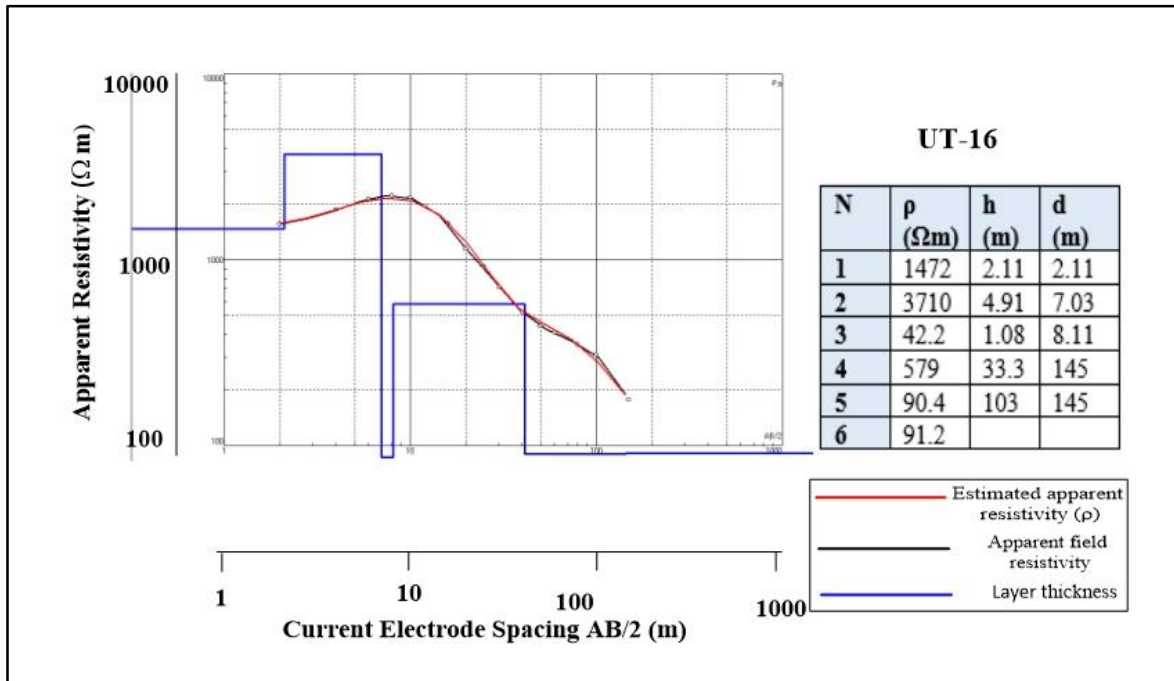


Figure 5.22 The modeled resistivity curves using IPI2Win Software for UT-16.

## UT-17

For UT-17, first electrode is at 0.5 meters while last is at 150 meters. The total spread length is 300 meters. At this point the resistivity values range from 75.8 to 3032  $\Omega$  m. Four layers are identified (Figure 5.23), from surface to a depth of 7.45 a layer comprising of unconsolidated gravelly sand and has resistivity of 3032  $\Omega$  m. Underneath this is another high resistivity, 1698  $\Omega$  m, layer of unconsolidated sand from 7.45 to 12.3 m. From 7.45 till 41 m clay is present showing a resistivity values of 171  $\Omega$  m. Below this, from 41 to a depth of 152 m sand with fresh water is present with a resistivity value of 75.8  $\Omega$  m. Resistivity values show the presence of fresh water aquifer at a depth of 41 m to 152 m from the surface. The lithologies and depth have been calibrated with the borehole data from the study area. The resistivity model under this point indicated that  $\rho_1 < \rho_2 > \rho_3 > \rho_4 < \rho_5$ .

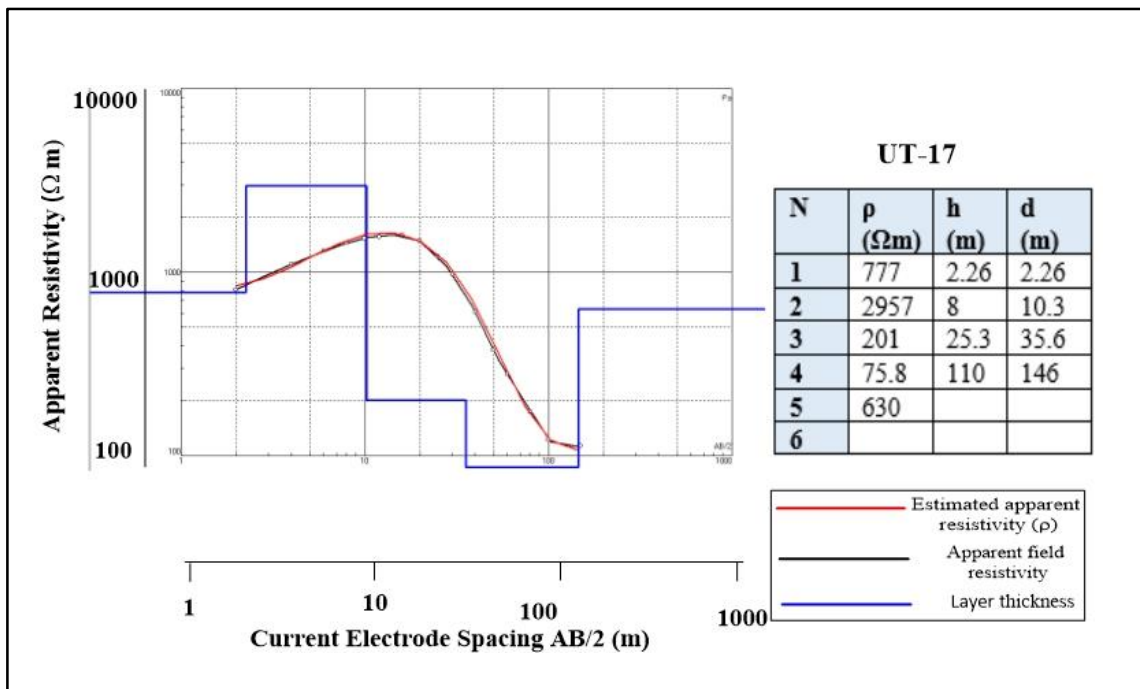


Figure 5.23 The modeled resistivity curves using IPI2Win Software for UT-17.



## UT-18

For UT-18, first electrode is at 0.5 meters while last at 150 meters. The total spread length is 300 meters. Here at UT-18, resistivity values are in range of 88.2 to 4854  $\Omega$  m. From the curve matching (Figure 5.25), four layers are identified. First layer from surface up to a depth of 2.22 m comprises of unconsolidated gravelly sand and has a resistivity of 1388 $\Omega$ m. Below this is another high resistivity layer of unconsolidated material from 2.22 to 9.43 m, showing a value of 4854  $\Omega$  m underneath this, from 9.43 till 45.8 m Sand is present with a resistivity values of 279  $\Omega$  m. From 45.8 till 146 m, sand with fresh water is present having a resistivity values of 88.2  $\Omega$  m. It is followed by a clay layer of 131  $\Omega$  m. Resistivity values show the presence of fresh water aquifer at a depth of 45.8 m to 146 m from the surface. The lithologies and depth have been calibrated with the borehole data from the study area. The resistivity model under this point indicates that  $\rho_1 > \rho_2 < \rho_3 < \rho_4 > \rho_5 < \rho_6$ .

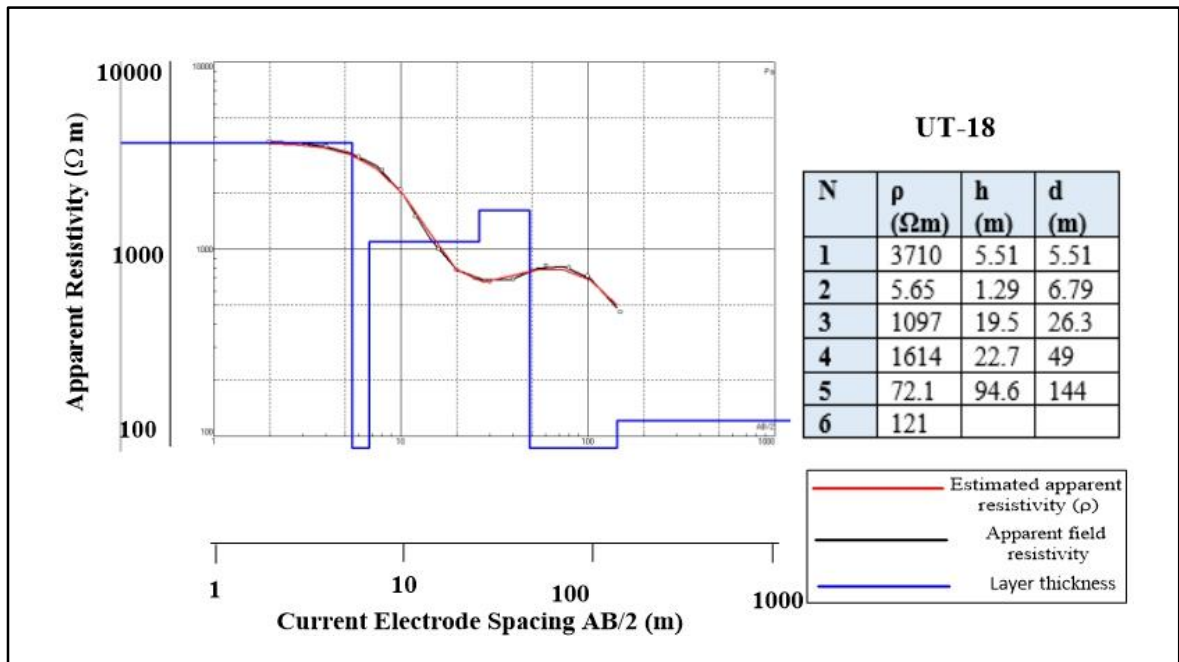


Figure 5.24 The modeled resistivity curves using IPI2Win Software for UT-18.

## UT -19

For UT-19, first electrode is at 0.5 meters while last at 150 meters. The total spread length is 300 meters. At UT-19, the resistivity values range from 95.1 to 1801  $\Omega\text{m}$  and four layers are identified from curve matching (Figure 5.25). From surface till a depth of 10.3 m unsaturated zone composed of gravelly sand with the true resistivity of 1801  $\Omega\text{ m}$ . Below this layer from 10.3 till 20.3 m dry sand is present with a resistivity values of 473  $\Omega\text{ m}$ . Underneath this, from 20.3 till 33.5 m clay is present with a resistivity value of 276  $\Omega\text{ m}$  This is followed by a sand layer with fresh water having a resistivity of 95.1  $\Omega\text{ m}$ , from a depth of 150 meters. It is followed by a clay layer with resistivity of 246  $\Omega\text{ m}$  of unknown depth. Resistivity values show the presence of fresh water from a depth of 33.5 m to 150 m from the surface. The lithologies and depth have been calibrated with the borehole data from the study area. The resistivity model under this point indicates that  $\rho_1 < \rho_2 > \rho_3 < \rho_4 > \rho_5$ .

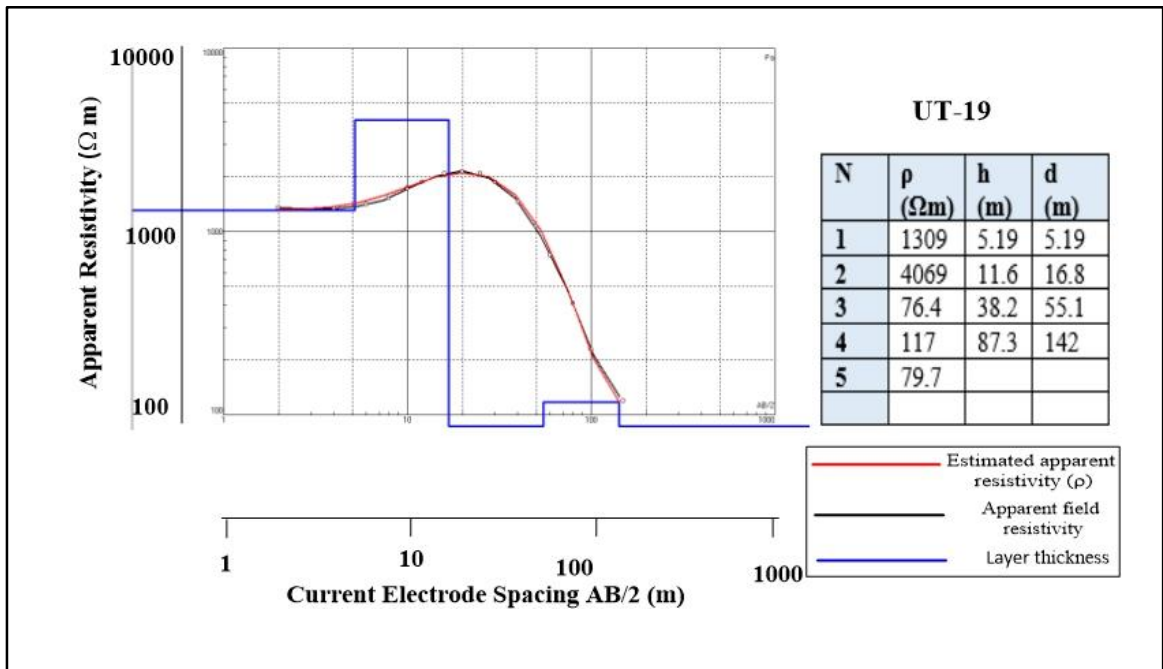


Figure 5.25 The modeled resistivity curves using IPI2Win Software for UT-19.

## UT-20

For UT-20, first electrode is at 0.5 meters while last at 150 meters. The total spread length is 300 meters. At UT-20, the resistivity values range from 79.7 to 1910  $\Omega$  m. Five layers are identified (Figure 5.26) From surface till a depth of 12 m unconsolidated gravely Sand is present with a resistivity of 1910  $\Omega$  m. Below this, from 12 m till 13 m a v thin layer of sand with saline water is present. It has a resistivity of 50.2  $\Omega$  m. From 13 m till 42.2 m Clay is present showing a resistivity value of 279  $\Omega$  m and it is followed by a layer of Sand with fresh water having a resistivity of 79.7  $\Omega$  m from 42.4 to 151 m. Resistivity values show the presence of fresh water aquifer at a depth of 42.2 to 151 m from the surface. The lithologies and depth have been calibrated with the borehole data from the study area. The resistivity model under this point shows that  $\rho_1 < \rho_2 > \rho_3 < \rho_4 > \rho_5 < \rho_6$ .

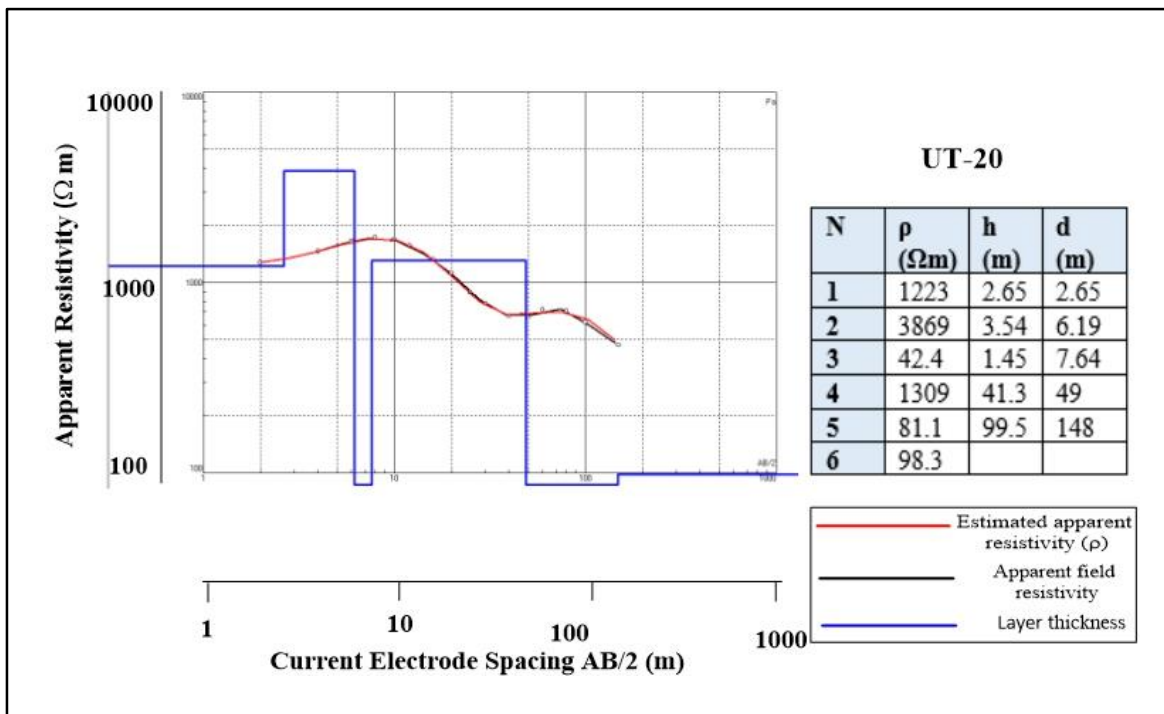


Figure 5.26 The modeled resistivity curves using IPI2Win Software for UT-20.

## UT-21

For UT-20, first electrode is at 0.5 meters while last at 150 meters. The total spread length is 300 meters. At UT-21, the resistivity values range from 1801 to 88.2  $\Omega$  m. Four layers (Figure 5.27) are identified, with first layer from surface to a depth of 9.92 m is of unconsolidated gravelly sand having a resistivity values of 1801  $\Omega$  m. From 9.92 till 17.9 m sand is present having a resistivity of 579  $\Omega$  m. Below, this layer up to a depth of 38 m is a clay is present having a resistivity of 248  $\Omega$  m. From 38 to a depth of 150 m is a sand layer with fresh water having a resistivity of 88.2  $\Omega$  m. The lithologies and depth have been calibrated with the borehole data from the study area. The resistivity model under this point shows that  $\rho_1 < \rho_2 > \rho_3 > \rho_4 > \rho_5 < \rho_6$ ,

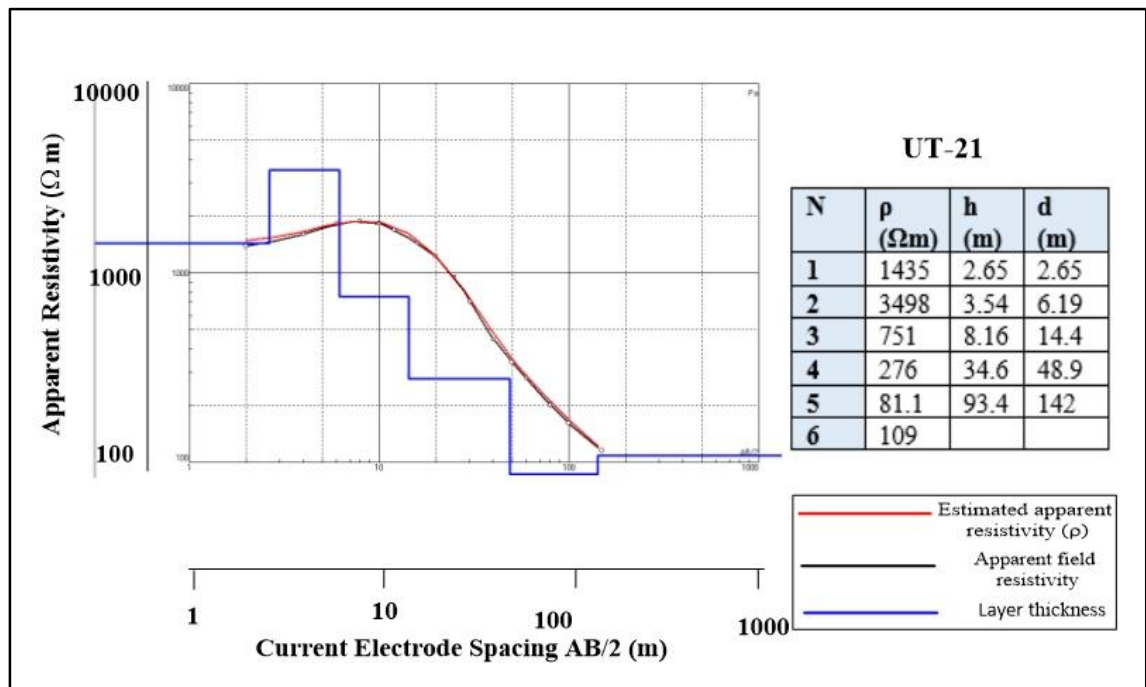


Figure 5.27 The modeled resistivity curves using IPI2Win Software for UT-21.

## UT-22

For UT-22, first electrode is at 0.5 meters while last at 150 meters. The total spread length is 300 meters. At UT-22, the resistivity values range from 72.7 to 4426  $\Omega$  m. From the curves (Figure 5.28) four layers are identified. From surface till a depth of 3.08 m a layer comprising of unconsolidated Sand with the true resistivity of 4426  $\Omega$  m is present. Under this from 3.08 till 4.32 m a thin layer of sand with fresh water is present showing resistivity values of 72.7  $\Omega$  m. Underneath this layer, from 4.32 to 42.8 m, is a high resistivity layer of 1642  $\Omega$  m which may comprise of unconsolidated gravelly sand. From till 42.8 till 145 m a sand layer with fresh water is present showing resistivity values of 83.8  $\Omega$  m. Resistivity values show the presence of fresh water aquifer at a depth of 42.8 m from the surface and extend down to 145 meters. The lithologies and depth have been calibrated with the borehole data from the study area. The resistivity model under this point shows that  $\rho_1 < \rho_2 > \rho_3 > \rho_4 > \rho_5$ .

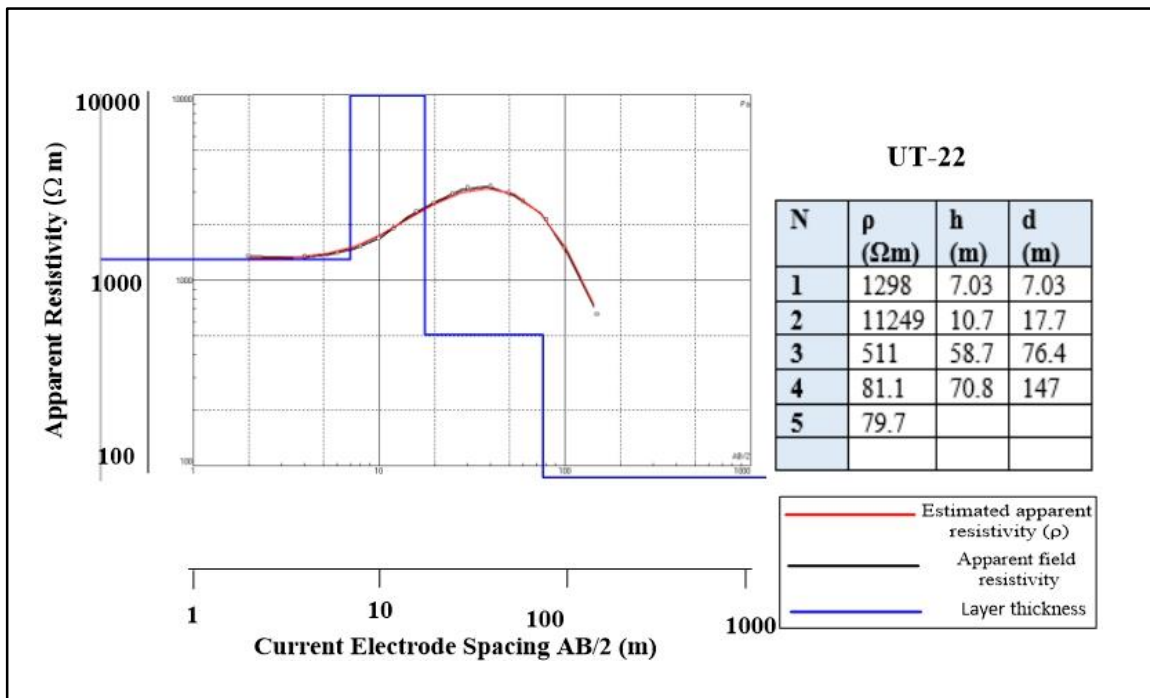


Figure 5.28 The modeled resistivity curves using IPI2Win Software for UT-22.

## UT- 23

For UT-23, first electrode is at 0.5 meters while last at 150 meters. The total spread length is 300 meters. At this point the resistivity values range from 48.1 to 4774  $\Omega$  m. Five layers are identified from the curve matching (Figure 5.29). From surface to a depth of 1.93 m is unconsolidated sand with a resistivity of 1213  $\Omega$  m. Under this from 1.93 m till 11.6 m is another layer of unconsolidated sand with a higher resistivity value of 4774  $\Omega$  m. From 11.6 m till 33.8 m another low resistivity unconsolidated layer of sand is present showing resistivity values of 1265  $\Omega$  m. Underneath this layer is compact sand from 33.8 to 107 m with a resistivity of 594  $\Omega$  m. This is followed by layer of sand with saline water from 107 m to 147 m and has a resistivity of 48.1  $\Omega$ m. The lithologies and depth have been calibrated with the borehole data from the study area. The resistivity model under this point shows that  $\rho_1 > \rho_2 > \rho_3 < \rho_4 > \rho_5 < \rho_6$ .

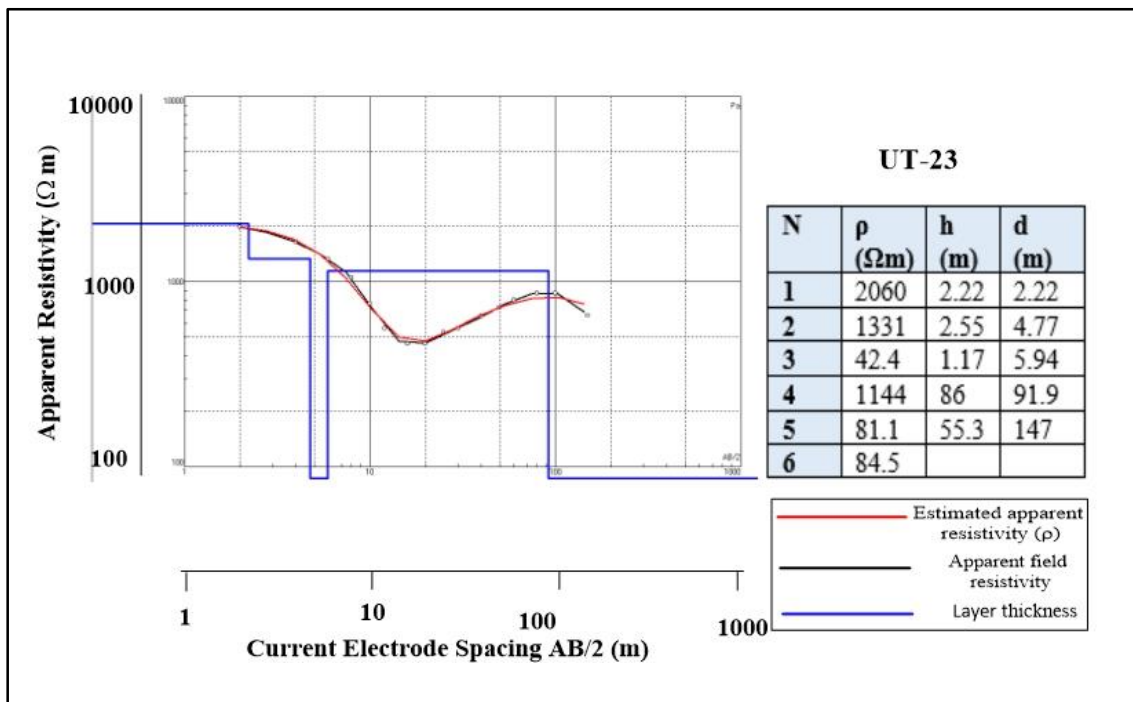


Figure 5.29 The modeled resistivity curves using IPI2Win Software for UT-23.

## UT-24

For UT-24, first electrode is at 0.5 meters while last at 150 meters. The total spread length is 300 meters. At this point the resistivity values range from 42.4 to 1910  $\Omega$  m. Five layers are identified from curve matching (Figure 5.30). From surface till a depth of 7.9 m is an unconsolidated gravelly sand with a resistivity of 1910  $\Omega$  m. Under this layer from 7.9 to 18.5 m compact sand is present showing a resistivity value of 790  $\Omega$  m. Below this is a thin layer which comprised of sand with saline water and has a resistivity of 42.4  $\Omega$  m. Beneath this is clay layer with a resistivity of 242  $\Omega$  m extending down to a depth of 41 m. From 41 m to a depth 146 m a layer of sand with fresh water is present has a resistivity of 88.9  $\Omega$  m. Resistivity values show the presence of fresh water aquifer at a depth of 41 m to 146 m from the surface. The lithologies and depth have been calibrated with the borehole data from the study area. The resistivity model under this point shows that  $\rho_1 < \rho_2 > \rho_3 > \rho_4 < \rho_5$ .

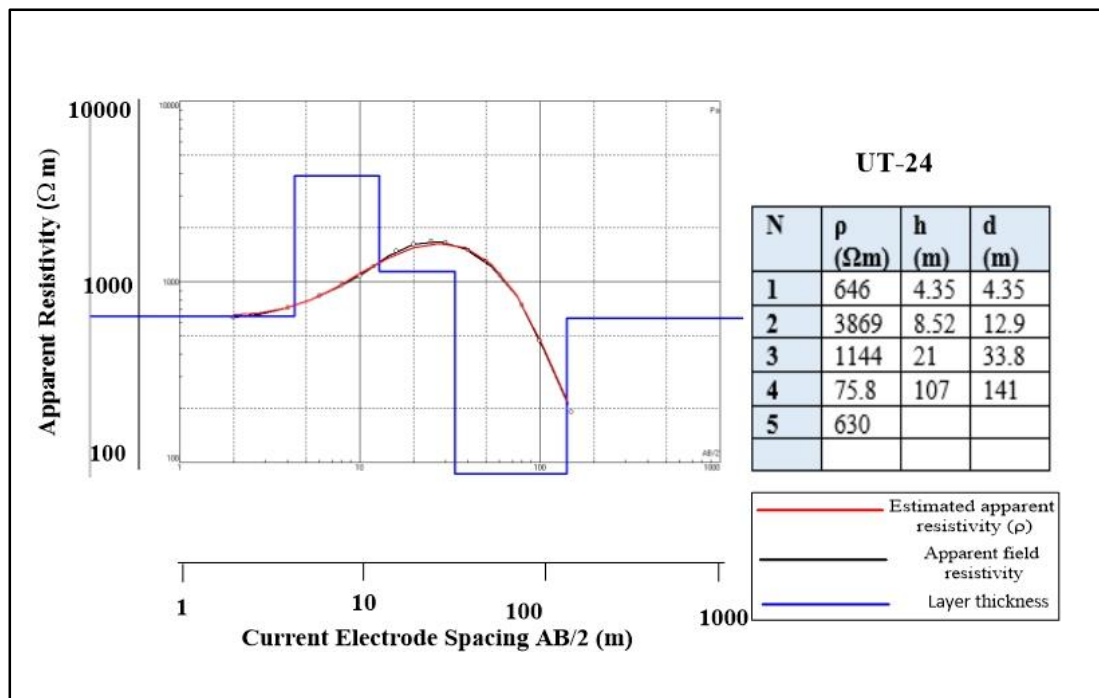


Figure 5.30 The modeled resistivity curves using IPI2Win Software for UT-24.



## UT-25

For UT-25, first electrode is at 0.5 meters while last at 150 meters. The total spread length is 300 meters. At this point the resistivity values range from 42.4 to 3710  $\Omega$  m. Five layers are identified from curve matching (Figure 5.32). From surface till a depth of 2.11 m unconsolidated gravelly sand having a resistivity of 1472 is present  $\Omega$  m. From 2.11 till 7.03 m unconsolidated sand is present showing resistivity value of 3710  $\Omega$  m. This is followed a thin layer of sand with saline water, from 7.03 to a depth of 8.11 m with a resistivity values of 42.4  $\Omega$  m. Underneath this is compact sand from 8.11 to 41.4 m with a resistivity of 579  $\Omega$  m. This is followed by another sand layer with fresh water from 41.4 m to 145 m with a resistivity of 90.4  $\Omega$ m. Resistivity values show the presence of freshwater aquifer at a depth of 41.4 m to 145 m from the surface. The lithologies and depth have been calibrated with the borehole data from the study area. The resistivity model under this point indicates that  $\rho_1 < \rho_2 > \rho_3 > \rho_4 > \rho_5 < \rho_6$ .

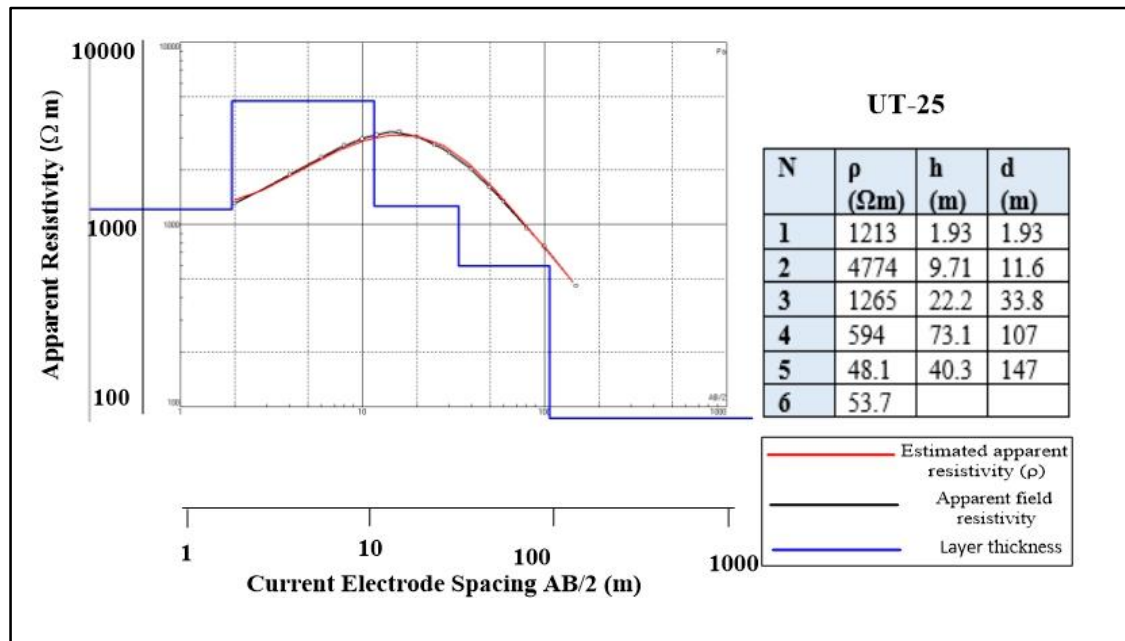


Figure 5.31 The modeled resistivity curves using IPI2Win Software for UT-25.



## 5.5 Spatial Distribution of geoelectrical layers, thickness and depth

Resistivity of the five geoelectrical layers, their depth in the subsurface and the thicknesses of each layer at the VES points are given in the table below. These are generated from the values calculated by the IPI2Win software for each of the resistivity station (UT-01 to UT-25). The geoelectrical layers are labeled from Layer 1 to layer 5 ( $\rho_1$  to  $\rho_5$ ). The geoelectrical properties of each layer is described and plotted from Figure 5.32 to Figure 5.36 and the thickness of each layer is plotted and shown in Figure 5.37 to 5.41.

Table 5.2 Depth, thickness and distribution of geoelectrical layers

ER S	Apparent Resistivity $\Omega\text{m}$					Depth m					Thickness m				
	$\rho_1$	$\rho_2$	$\rho_3$	$\rho_4$	$\rho_5$	d1	d2	d3	d4	d5	h1	h2	h3	h4	h5
UT-01	2060	1331	42.4	1144	81.1	2.22	4.77	5.94	91.9	147	2.22	2.25	1.17	86	55.3
UT-02	646	3869	1144	75.8		4.35	12.9	33.8	141		4.35	8.52	21	107	
UT-03	1309	4316	959	93.5		1.79	10.6	39.7	152		1.79	8.82	29.1	112	
UT-04	777	2957	201	75.8		2.26	10.3	35.6	146		2.26	8	25.3	110	
UT-05	594	6851	674	265	88.2	2.91	5.65	12.1	50.2	152	2.91	2.74	6.48	38.1	102
UT-06	1223	3869	42.2	1309	81.1	2.65	6.19	7.64	49	148	2.65	3.54	1.45	41.3	99.5
UT-07	1298	11249	511	81.1		7.03	17.7	76.4	147		7.03	10.7	58.7	70.2	
UT-08	1309	4096	76.4	117	79.7	5.19	16.8	55.1	142		5.19	11.6	38.2	87.3	
UT-09	2113	6299	230	97.5		1.36	6.19	37.4	146		1.36	4.83	31.2	109	
UT-10	1910	3001	254	87.4		1.74	9.83	43.5	146		1.74	8.09	33.7	102	
UT-11	1801	100	234	96.7		14.7	17	44.6	146		14.7	2.26	27.2	101	

ER S	Apparent Resistivity $\Omega\text{m}$					Depth m					Thickness m				
UT-12	1801	350	42.4	94.3		11	32.2	37.4	145		11	21.2	5.25	107	
UT-13	1727	2417	59.4	303	75.8	3.16	9.67	10.7	36.8	145	3.16	6.51	1.03	26.1	108
UT-14	1061	3110	674	256	88.2	1.67	4.65	12.1	49.4	150	1.67	2.98	7.48	37.2	100
UT-15	3710	56.5	1097	1614	72.1	5.51	6.79	26.3	49	144	5.51	1.29	19.25	22.7	94.6
UT-16	1435	3498	751	276	81.1	2.65	6.19	14.4	48.9	142	2.65	3.53	8.16	34.6	93.4
UT-17	3032	1698	171	75.8		7.45	12.3	41	152		7.45	4.89	28.7	111	
UT-18	1388	4854	279	88.2		2.22	9.43	45.8	146		2.22	7.21	36.3	99.9	
UT-19	1801	473	276	95.1		10.3	20.3	33.5	150		10.3	10	13.3	116	
UT-20	1910	50.2	279	79.7		12	13	42.4	151		12	0.945	29.5	109	
UT-21	1801	579	248	88.2		9.92	17.9	38	150		9.92	7.94	20.2	112	
UT-22	4426	72.7	1642	83.8		3.08	4.32	42.8	145		3.08	1.23	38.5	102	
UT-23	1213	4774	1265	594	48.1	1.93	11.6	33.8	107	147	1.93	9.71	22.2	73.1	40.3
UT-24	1910	790	42.4	242	88.9	7.9	18.5	19.8	41	146	7.9	10.6	1.28	21.3	105
UT-25	1472	3710	42.4	579	90.4	2.11	7.03	8.11	41.4	145	2.11	4.92	1.08	33.29	103.0

Layer 1: The first layer shows an overall uniform distribution of resistivity values from 600 to 2600  $\Omega\text{m}$  in the study area. Lower resistivity values are towards the NW and high values are observed in the lower SE. Pockets of very high resistivity value are observed showing weathered layers' dry surface conditions. This layer is characterized by the presence of unconsolidated material, mostly sand and gravel. Smooth isolines are observed due to scarce data points in the NE where hills are present.

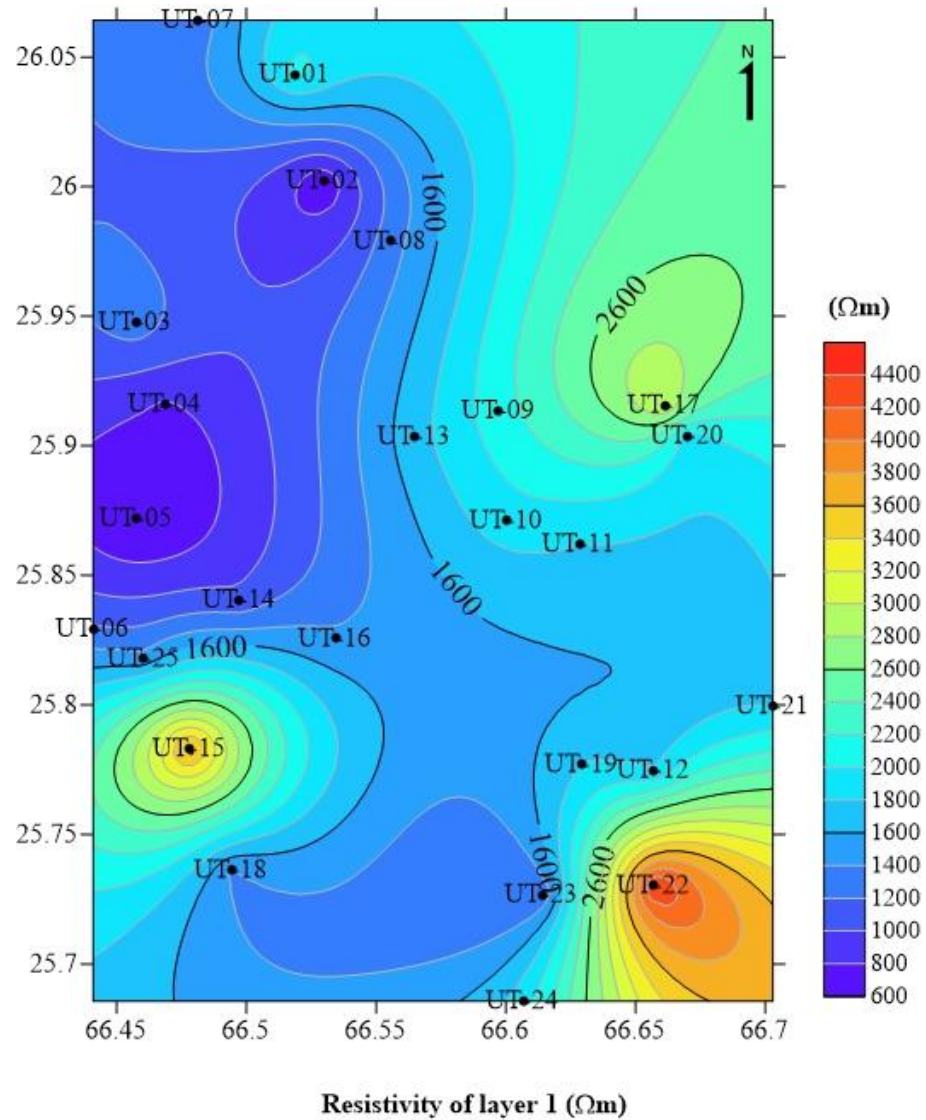


Figure 5.32 Iso-resistivity contour map of layer 1

Layer 2: The resistivity values range from 0 to 11500  $\Omega\text{m}$  with a very high resistivity at the far NW of the study area, indicating dry conditions over there. Lower values are observed toward SE of the study area/ the central part is characterized by uniformly distributed resistivity values. Smooth isolines are observed due to sparse data points in the NE where hills are present.

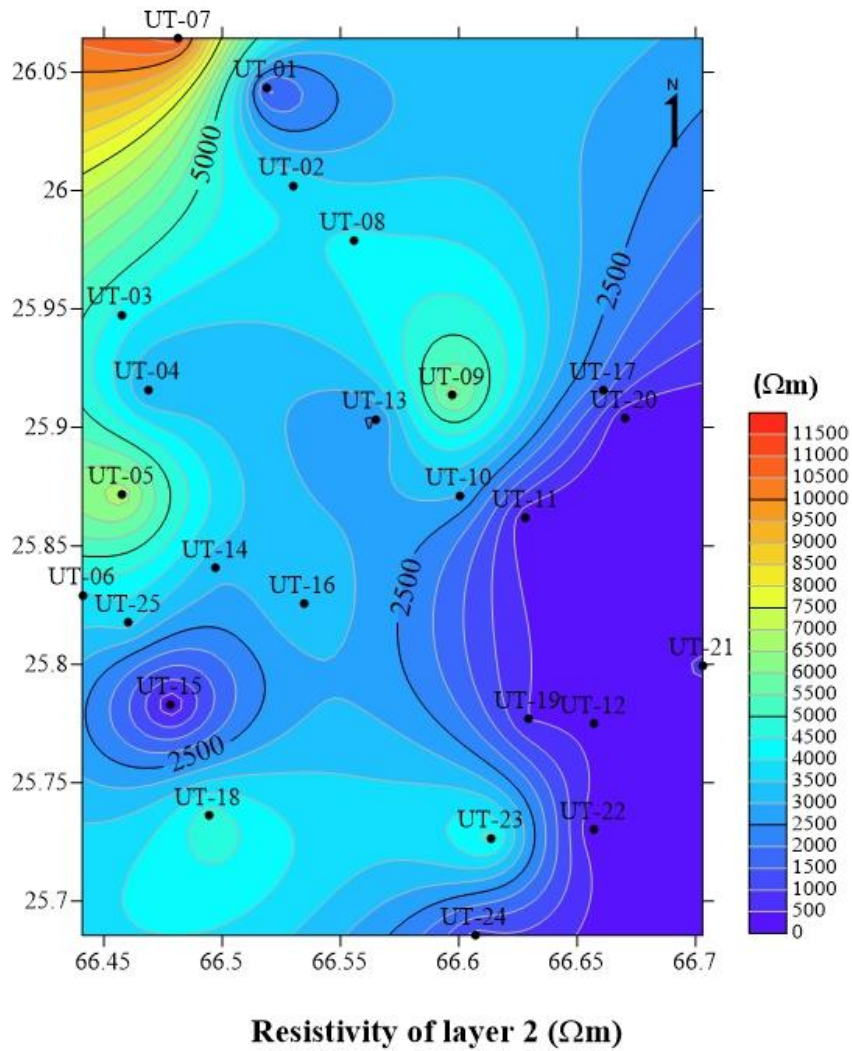


Figure 5.33 Iso-resistivity contour map of layer 2

Layer 3: This layer represents an evenly distributed resistivity with ranges in two zones between 0 to 200 and 600 to 800  $\Omega\text{m}$ . Pockets of high resistivity values are present between 600 to 800  $\Omega\text{m}$  zone and a very high resistivity is present towards SE. Smooth isolines are observed due to sparse data points in the NE where hills are present.

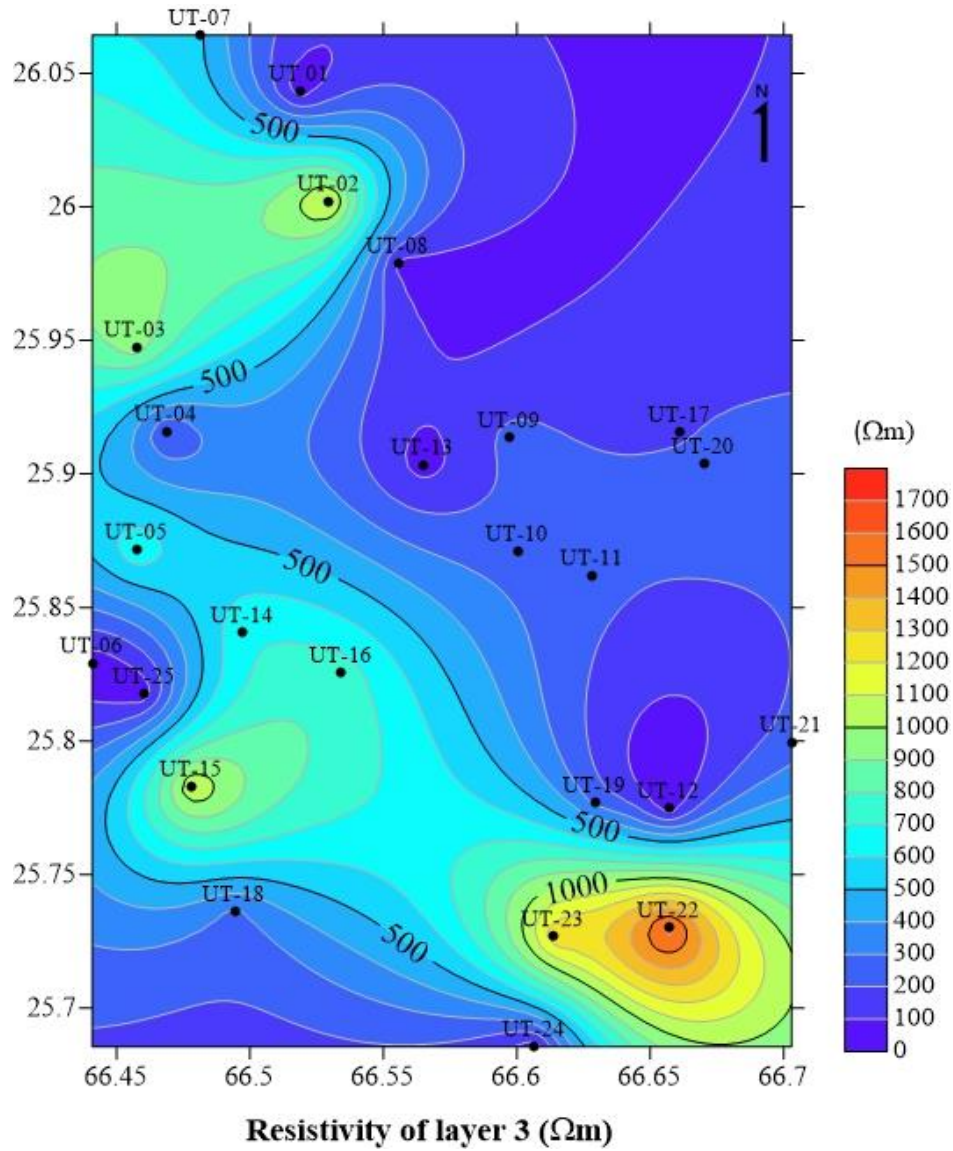


Figure 5.34 Iso-resistivity contour map of layer 3

Layer 4: This layer represents an evenly distributed resistivity with most of the area having resistivity between 0 -100  $\Omega\text{m}$ , indicating fresh water aquifer. Pockets of high resistivity values are present towards NW and N. Smooth isolines are observed due to sparse data points in the NE where hills are present.

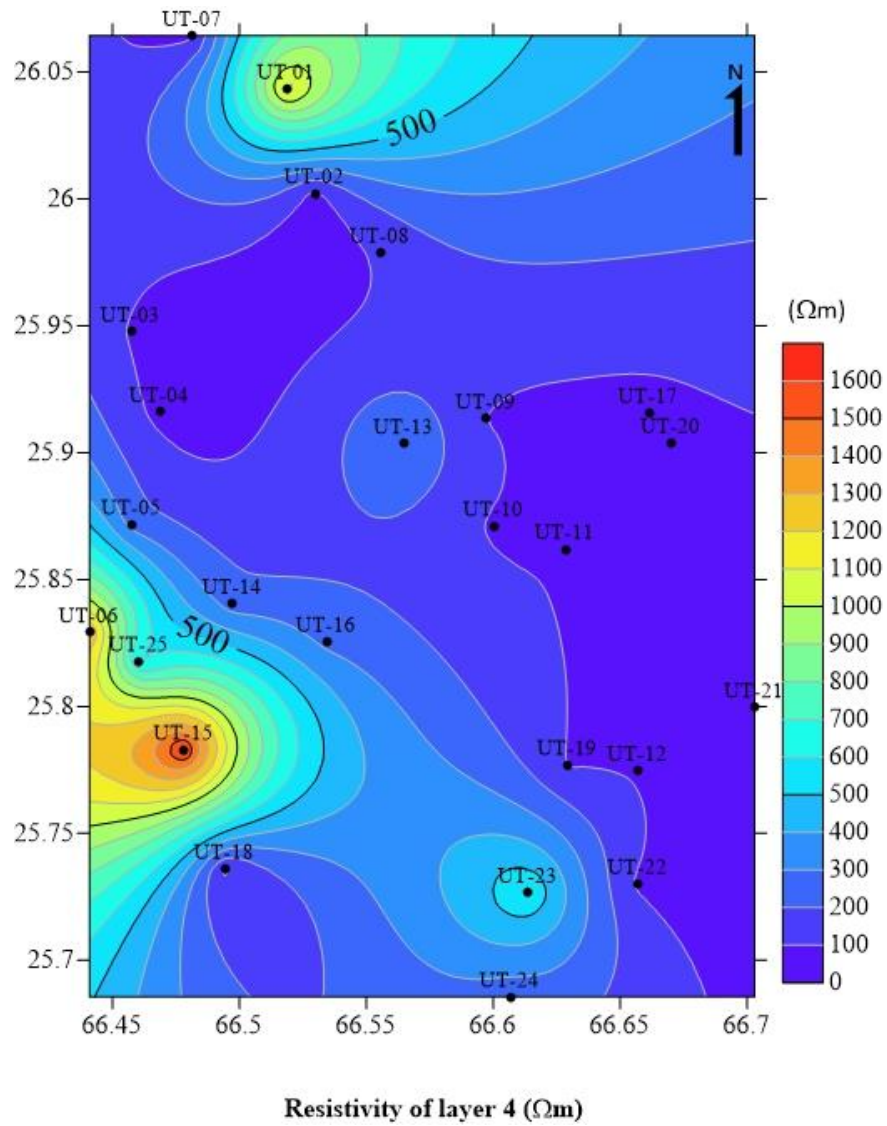


Figure 5.35 Iso-resistivity contour map of layer 4



Layer 5: Smooth isolines are observed due to sparse data points in the NE where hills are present.

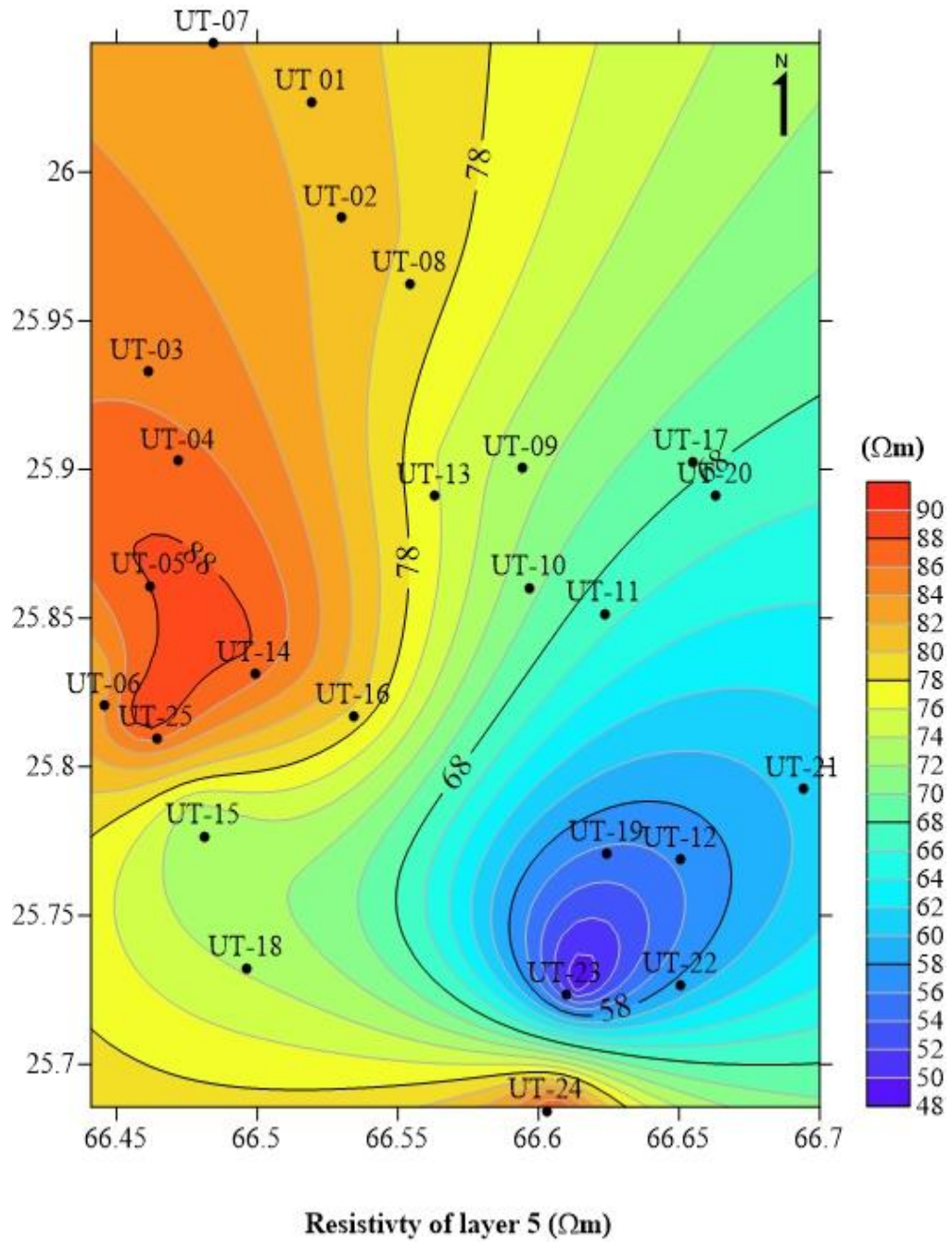


Figure 5.36 Iso-resistivity contour map of layer 5

Layer 1 thickness: The layer thickness is estimated from the resistivity data and the resistivity values are correlated with the resistivity ranges given by Palacky (1987). A thin top layer of unconsolidated material composed of sand and gravel is present in the study area. Towards south east thickness of this layer increases to 15 meters.

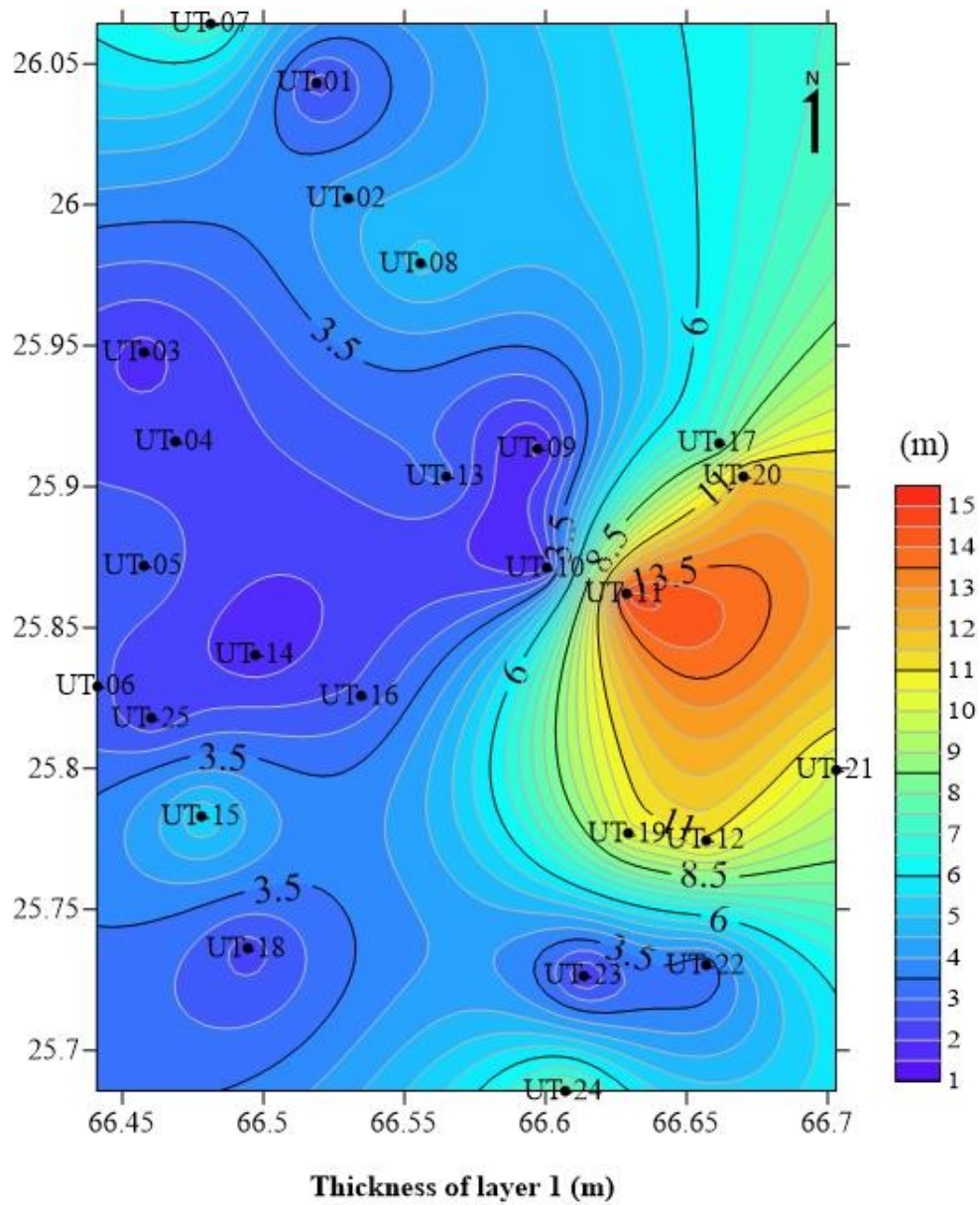


Figure 5.37 Thickness contour map of Layer 1. The contours are in meters (m)



Layer 2 thickness: The layer thickness is estimated from the resistivity data and the resistivity values are correlated with the resistivity ranges given by Palacky (1987). Thickness of layer 2 ranges from 1 meters to 21 meters. Thickness of this layer increases towards SE.

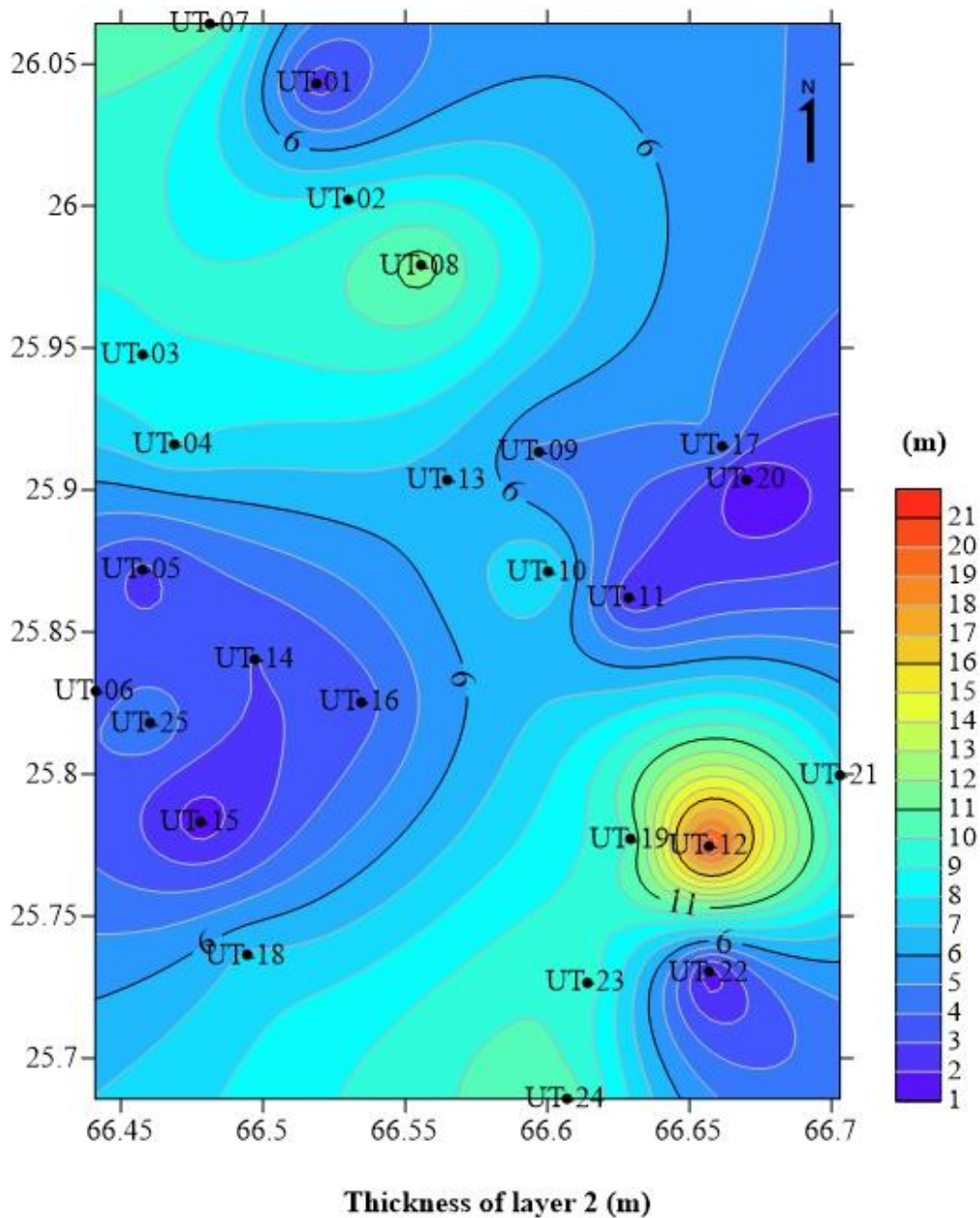


Figure 5.38 Thickness contour map of layer 2. The contours are in meters (m)

Layer 3 thickness: The layer thickness is estimated from the resistivity data and the resistivity values are correlated with the resistivity ranges given by Palacky (1987). This layer shows a uniform thickness with higher values of thickness on the top NW.

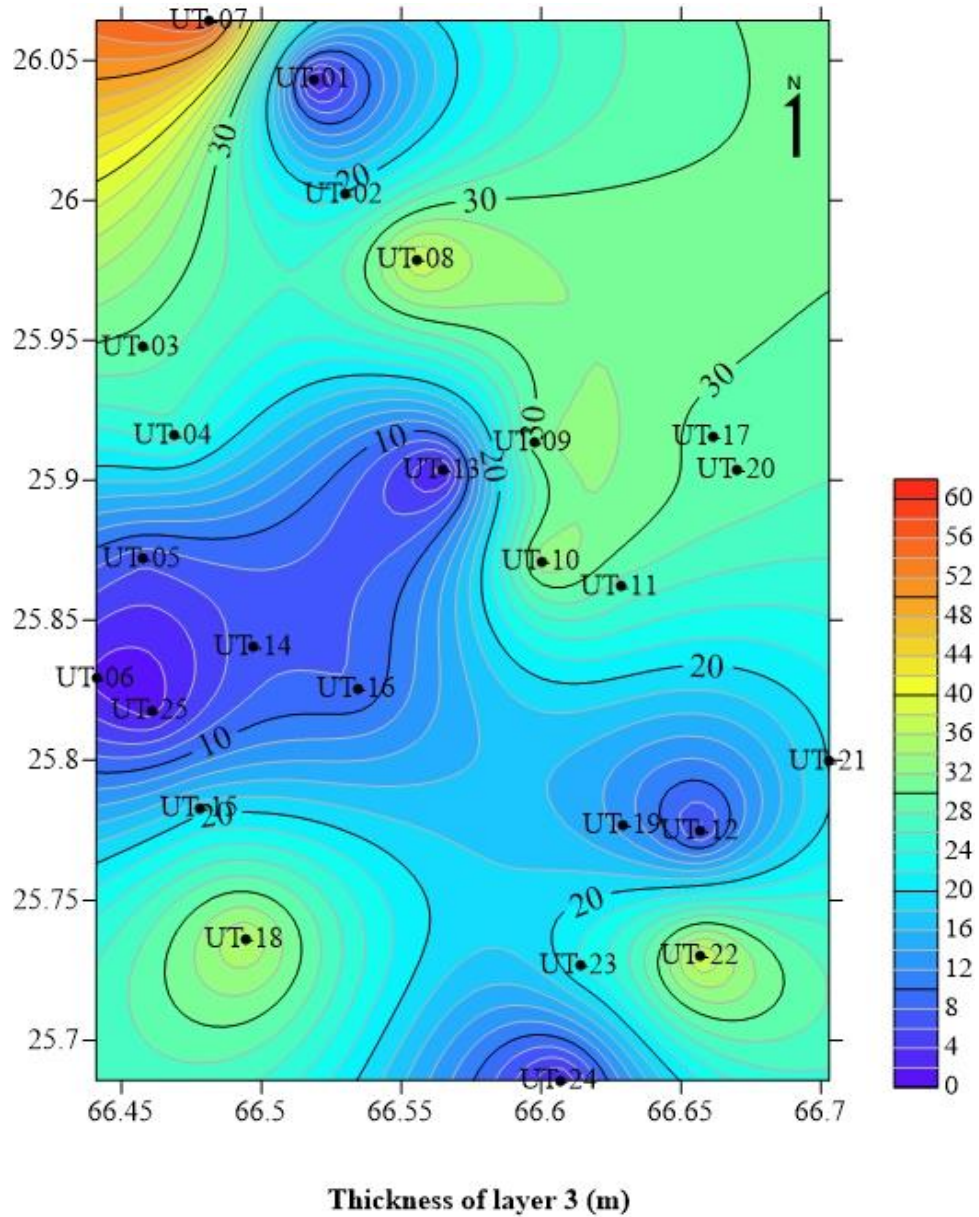


Figure 5.39 Thickness contour map of Layer 3. The contours are in meters (m)

Layer 4 thickness: The layer thickness is estimated from the resistivity data and the resistivity values are correlated with the resistivity ranges given by Palacky (1987). This shows overall very thick layer with thickness going to 120 meters towards NE.

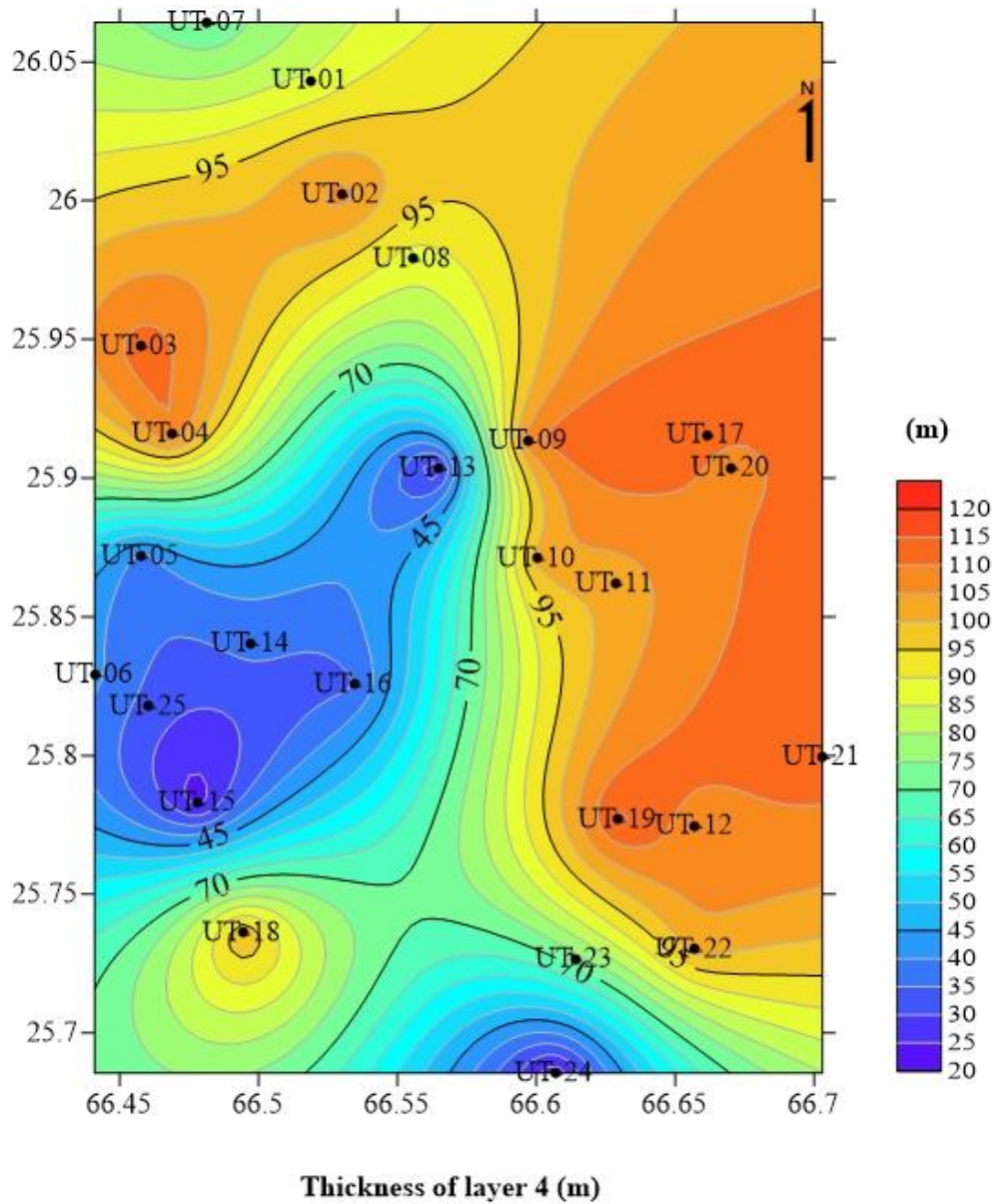


Figure 5.40 Thickness contour map of Layer 4.

Layer 5 thickness: The layer thickness is estimated from the resistivity data and the resistivity values are correlated with the resistivity ranges given by Palacky (1987). The layer thickness varies from 40 m to 110 meters.

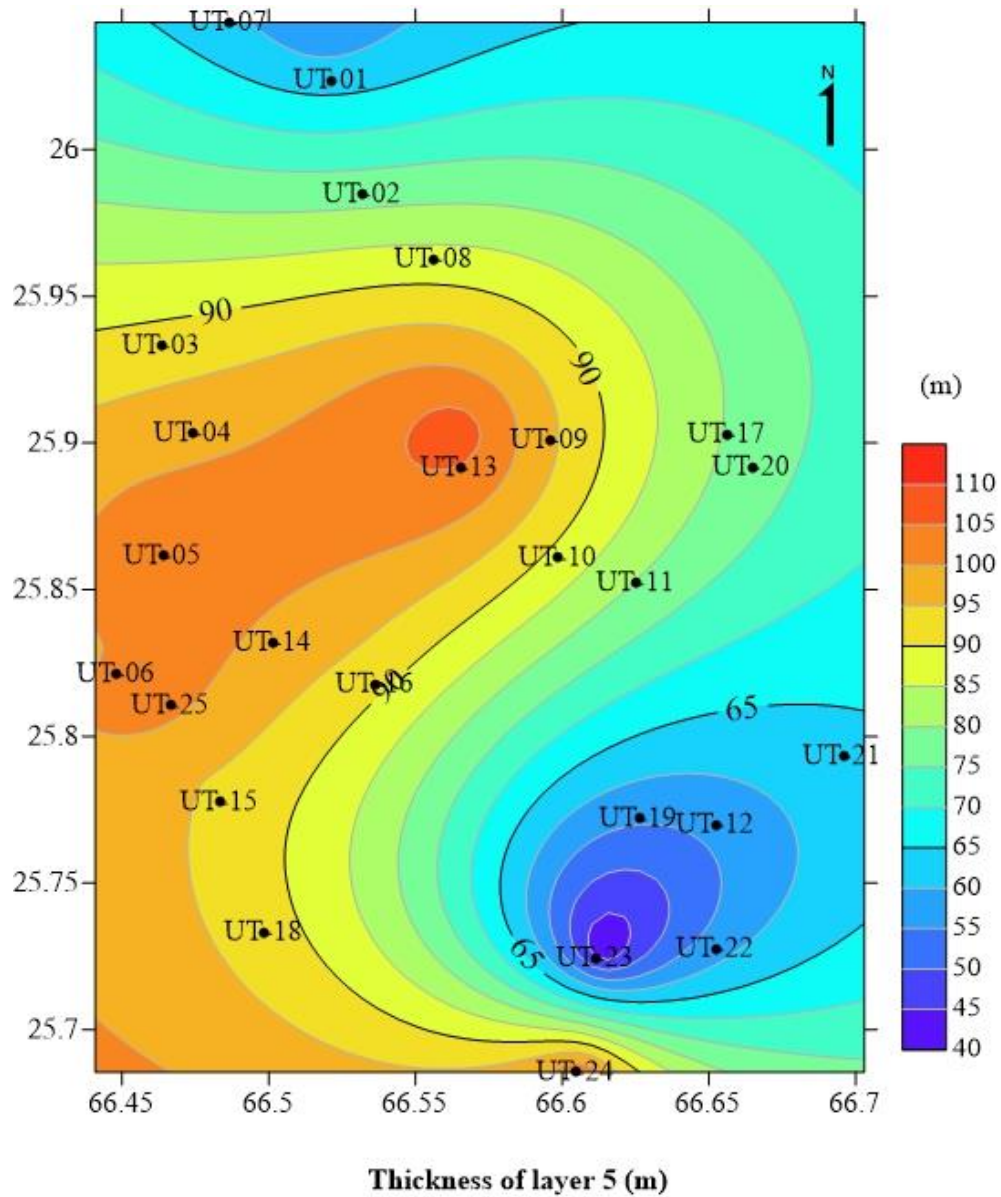


Figure 5.41 Thickness contour map of Layer 5.



## 5.6 Estimation of (D-Z) Dar Zarrouk Parameters from the Electrical Resistivity data

Dar Zarrouk parameters are derived from the surface geoelectrical resistivity sounding data (Maillet, 1947; Zohdy, 1989). This term Dar Zarrouk was coined by Maillet in 1947. Maillet used this to describe a relationship between S the Longitudinal Unit Conductance and T, the Transverse Unit Resistance. The two parameters are calculated by the equation given below:

$$S = \frac{\rho_1}{h_1} + \frac{\rho_2}{h_2} + \dots + \frac{\rho_n}{h_n} + \sum_{i=1}^n \frac{\rho_i}{h_i} \quad \text{Eq 5.5}$$

$$T = \rho_1 h_1 + \rho_2 h_2 + \dots + \sum_{i=1}^n \rho_i h_i \quad \text{Eq 5.6}$$

These parameters are effective in understanding the aquifer properties where clay and sand is present with fresh and saline water (Batayneh, 2013). The other two parameters calculated from the resistivity data are the Longitudinal Resistivity ( $R_S$ ) and Transverse Resistivity ( $R_T$ ). These parameters are measured in units of  $\Omega\text{-m}$  as given in the equations below:

$$R_S = \frac{H}{S} \quad \text{Eq 5.7}$$

$$R_T = \frac{T}{S} \quad \text{Eq 5.8}$$

The Dar Zarrouk parameters have been estimated for the 25-point data of the study area. The estimated values of D-Z parameters are given in Table 5.3.

Table 5.3 The estimated values of Dar Zarrouk Parameters

S.no	VES Points	Latitude	Longitude	Longitudinal Unit Conductance S (mho)	Transverse Unit Resistance T ( $\Omega m^2$ )	Longitudinal Resistivity RS ( $\Omega m$ )	Transverse Resistivity RT ( $\Omega m$ )
1	UT 01	26.043420	66.518678	0.105537	106001.558	1392.8767	721.099
2	UT-02	26.002169	66.529687	1.4389	67908.58	97.99	481.6211
3	UT-03	25.947617	66.45730	1.23161	78789.13	123.4156917	518.35
4	UT-04	25.915978	66.468695	1.582672049	38835.32	92.24965443	265.995
5	UT-05	25.871843	66.457689	1.354743565	33864.2	112.2019	22.79
6	UT-06	25.829204	66.440905	1.28722	79129.55	114.9764	534.6591216
7	UT-07	26.064262	66.481560	0.986832	165178.16	148.9606	1123.660952
8	UT-08	25.978939	66.555524	1.252951	67439.89	113.3324	474.9288
9	UT-09	25.913493	66.597312	1.25501	51101.35	116.33	350.009
10	UT-10	25.871106	66.600277	1.30333	45076.09	112.0207	308.7403
11	UT-11	25.862008	66.628356	1.19146	33066.54447	76.2561	226.48318
12	UT-12	25.774807	66.657028	1.325176	37543.7	109.4194	258.922069
13	UT-13	25.903570	66.564901	1.5328	37347.872	94.598121	257.571531
14	UT-14	25.840506	66.497341	1.2927	34424.39	116.0362	229.495933
15	UT-15	25.782984	66.478211	1.367995	85090.695	105.2635	590.9076
16	UT-16	25.825566	66.534304	1.29076	39427.67	110.0127	277.65964
17	UT-17	25.915664	66.661229	1.6375	44213.12	92.8244	290.8757
18	UT-18	25.736070	66.494177	1.26584	57017.58	115.338	390.5313699
19	UT-19	25.776971	66.629317	1.29481	37982.7	115.8471127	253.218
20	UT-20	25.903843	66.670091	1.50710	39885.239	100.192	264.14065
21	UT-21	25.799547	66.702965	1.37051	37351.18	109.4483	249.00786
22	UT-22	25.730145	66.657078	1.25824	85486.101	115.2403357	589.5593172
23	UT-23	25.726747	66.613830	0.982076	122139.46	149.6829	830.8806
24	UT-24	25.685617	66.606683	1.316861	38006.116	110.8697	260.315863
25	UT-25	25.817761	66.460540	1.22512	49959.712	119.17199	342.1898082

The D-Z parameters are contoured and given in Figure 5.43 to 5.46. The S values are in range of 0.1 to 1.65 ohm, T above 25000 to 165000  $\Omega\text{-m}^2$ , indicated the presence of fresh water in the area. The saline water has not intruded the study area. The values of RS and RT are from 50 to 1350  $\Omega\text{-m}$ . and 0 -1150  $\Omega\text{-m}$  respectively.

### Longitudinal Unit Conductance (S)

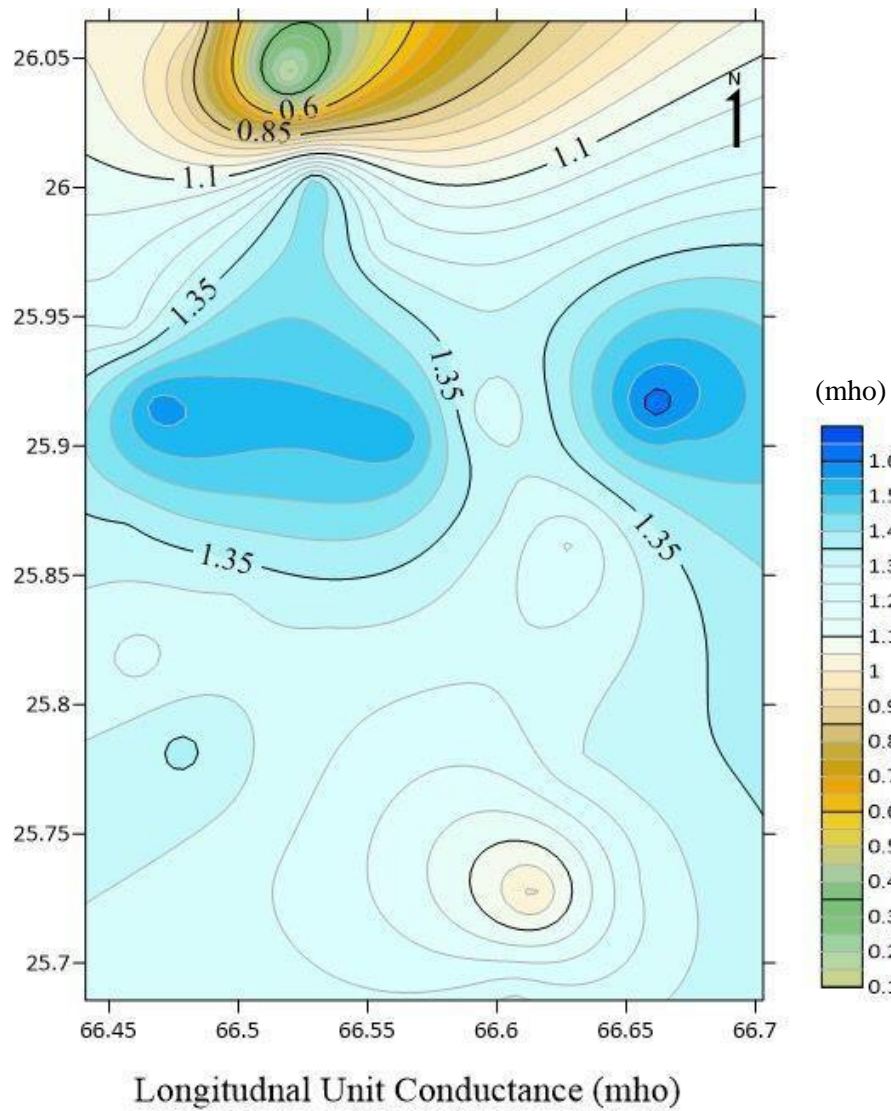


Figure 5.42 Contour map of Longitudinal Unit Conductance (S)

## Transverse Unit Resistance T

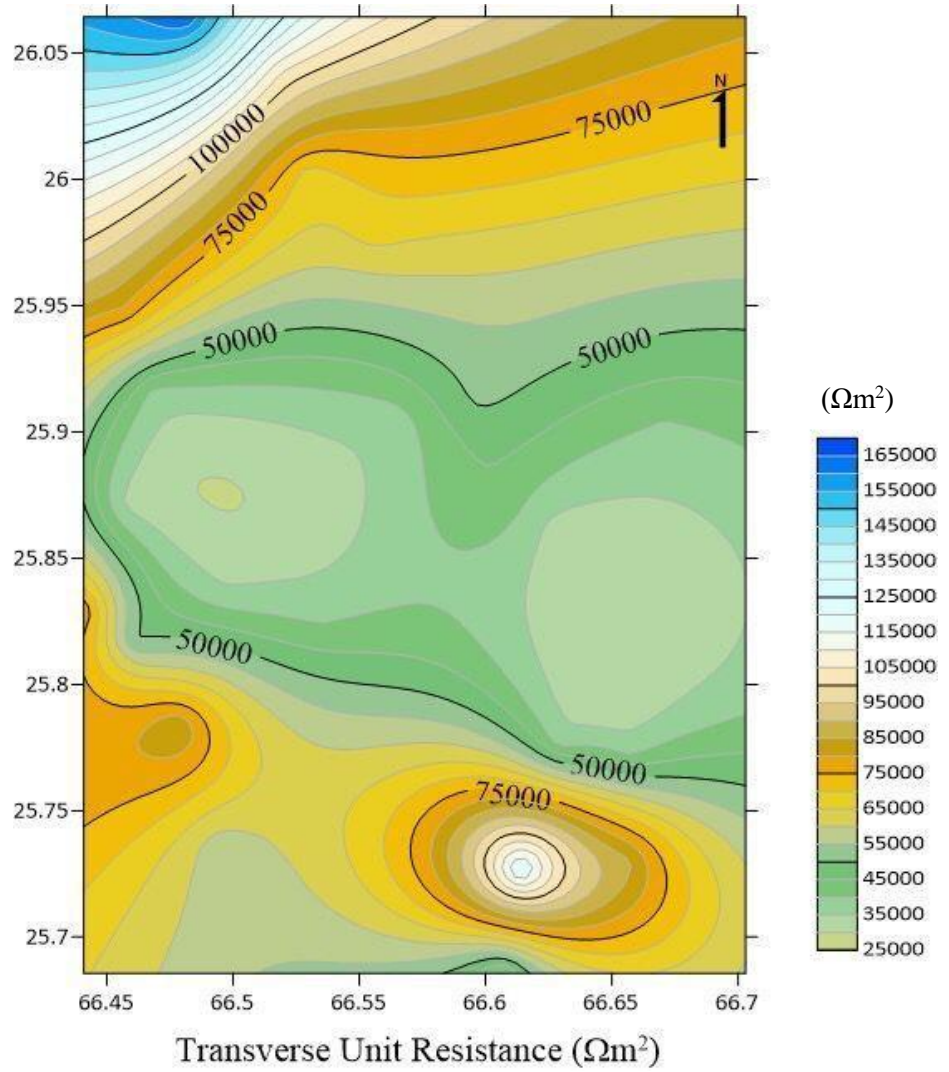


Figure 5.43 Contour map of Transverse Unit Resistance (T)



## Longitudinal Resistivity Rs

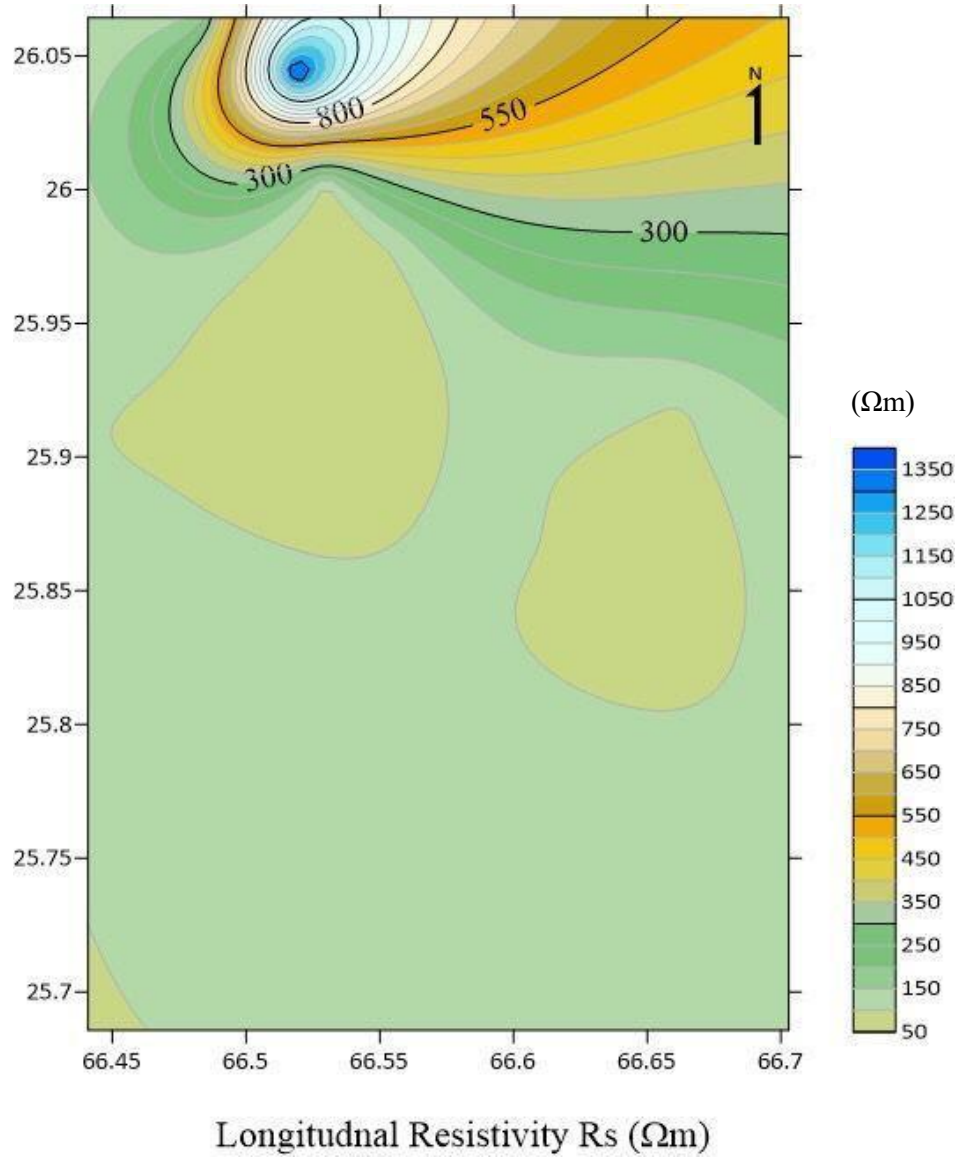


Figure 5.44 Contour map of Longitudinal Resistivity ( $R_s$ )

**Transverse Resistivity  $R_T$**

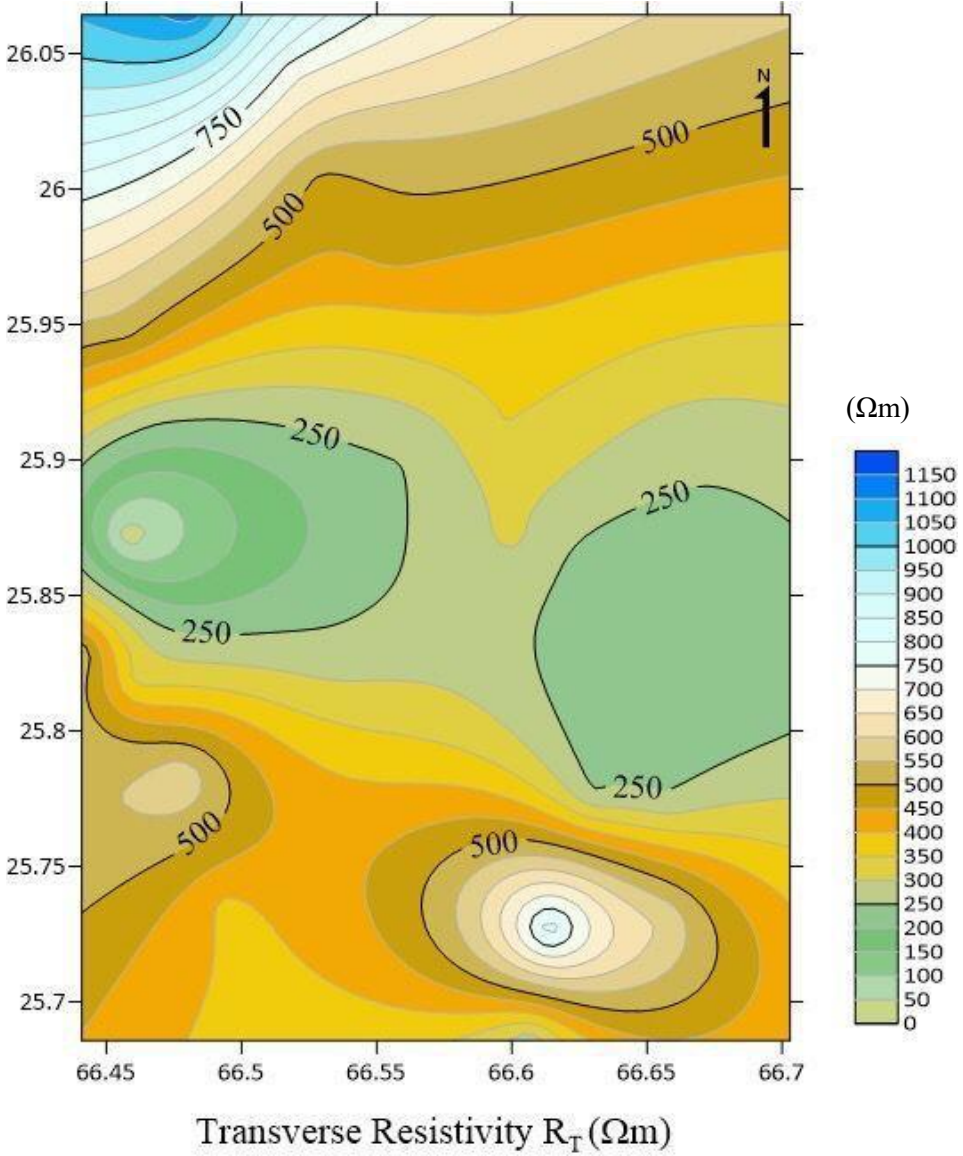


Figure 5.45 Contour map of Transverse Resistivity ( $R_T$ )

## 5.7 Well log Data

"The lithology data was collected from the local tube well owners and plotted on the Log plot. The boring was done before the collection of the resistivity data. The lithologs from Well A located at 25° 41' 18" N & 66° 36' 11" E and Well B located at 25°55'54.00"N & 66°27'31.00"E are shown in the Figure 5.46 The lithologies estimated from the ERS curves from the apparent resistivity ( $\rho_a$ ) were matched with the lithologs for the nearby points. ERS curve with lithologies is shown in Figures 5.8 to 5.32.

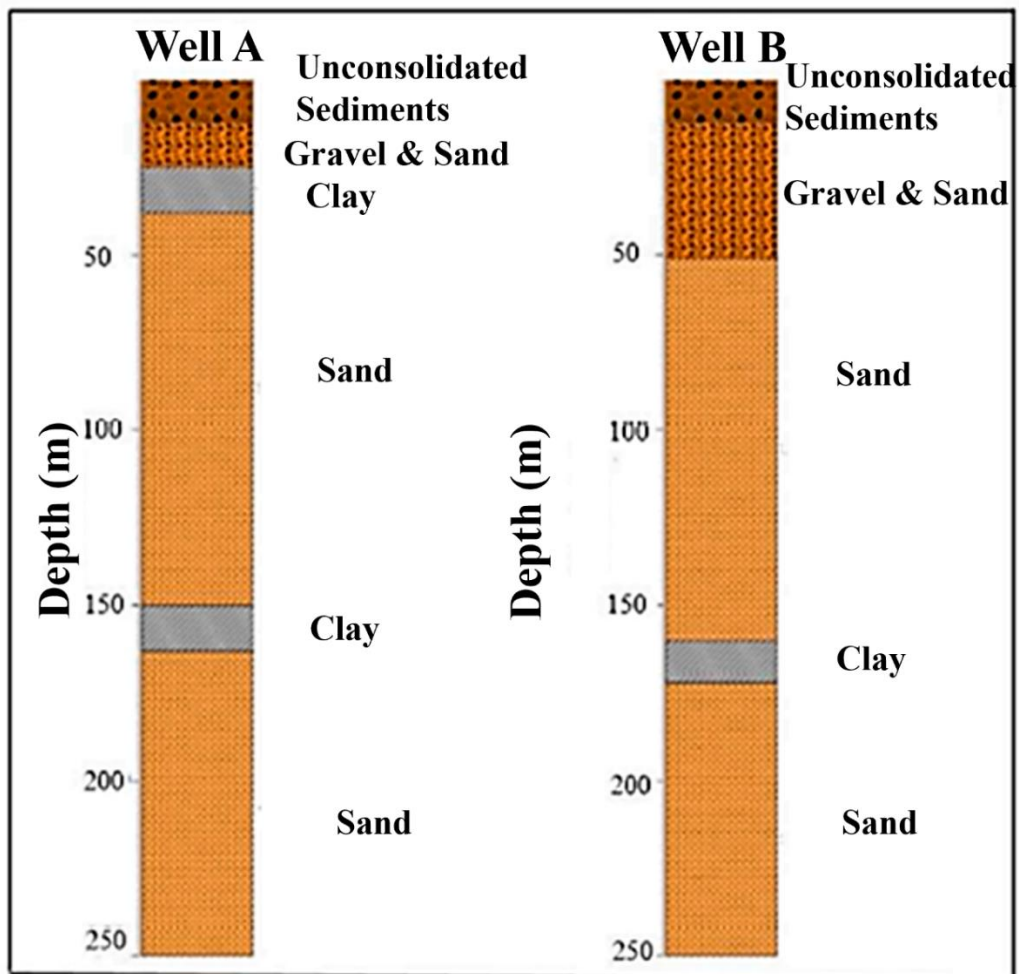


Figure 5.46 Lithology log for two boreholes Well A and Well B from study area

## **CHAPTER 6**

### **RESULT AND DISCUSSION**

#### **6.1 Introduction**

The study area, Uthal, is located in the south of Balochistan, Pakistan, and is present at a distance of 13 to 26 km landwards from Miani Hor. It is a swampy lagoon along the coast of the Lasbela district, Balochistan, Pakistan. Uthal lies in Porali plain in Balochistan, with its altitude between 20 to 75 m above mean sea level. It is a semi-arid area and has seen rapid growth in population in the last few decades. This has led to an increase in water consumption, with groundwater being the primary source. Due to the close proximity of the study area to the coast, the continuous extraction of groundwater may cause seawater to intrude deeper into the land. As the surface water is already scanty in this area and the

continuous threat of seawater intrusion also exists, it is essential to assess groundwater quality. In this study, ERS data of 25 points are acquired, and subsurface resistivity values are estimated. The D- Z parameters are also calculated to demarcate saline and freshwater zones.

The coastal areas worldwide are fast becoming hubs of social & economic activities. This has led to an increase in the population of these areas, and hence the demand for freshwater for domestic use, agriculture, industrial & other activities has also increased (Cardona et al., 2004; Gopalakrishnan et al., 2020). The availability of surface and groundwater is greatly affected by climatological conditions of the arid to semi-arid coastal areas (Hasan et al., 2020). Various natural and anthropogenic activities have also degraded the already scarce surface water resources (Bilotta & Brazier, 2008; Murdoch et al., 2000; Ntengwe, 2006). This has increased groundwater extraction in coastal areas worldwide (Pla et al., 2014).

In semi-arid to arid coastal areas, surface water flow to the sea is in small quantities, leading to the inland flow of saline seawater (Bear et al., 1999). Seawater intrusion is one of the significant problems that influence the sustainable management of groundwater resources (Leghouchi et al., 2009). In the coastal areas, fresh groundwater resources are present landwards and the saline groundwater towards the coast. The extent of seawater intrusion into the land varies from region to region, depending on climatological conditions. Therefore, the demarcation of saline and fresh groundwater resources is one of the main goals for sustainable groundwater development in coastal areas. This has led to an increase in exploration and the assessment of groundwater quality using sophisticated techniques (Obiefuna & Sheriff, 2011; Sherif et al., 2006).

Surface geophysical techniques are very effective in delineating the groundwater resources for sustainable management and are considered one of the easiest, suitable and economical. It is also an appropriate method for assessing the groundwater quality for domestic, agricultural, and industrial use and environmental studies (Hassan et al., 2020 & 2019; Loke et al., 2013). Such techniques are used in different environments and

sedimentary regimes worldwide (Gao et al., 2018; Telford et al., 1990). These are applied to investigate the subsurface groundwater potential, the nature of aquifers, and the quality of the groundwater in the vicinity of rivers, seas, and oceans where seawater intrusion is one of the major concerns (Todd & Mays, 2004). The electrical resistivity method has been used by various researchers to study the salinity of groundwater and is effectively used for delineating the Saline-Fresh water interface in aquifers near the coastal areas (Hasan et al., 2017; Zarroca et al., 2011).

Electrical resistivity survey also termed as vertical electrical soundings (VES). It is a 1D survey and assesses physical properties like the subsurface resistivity, porosity, saturation of water in the subsurface, and salinity. Resistivity values for saline and freshwater zones are different (Loke et. al, 2013), with an increase in the salinity of the groundwater, the resistivity values decrease; hence, this method can effectively identify zones of high salinity and demarcation of the freshwater aquifer can easily be executed, (Hamdan & Vafidis, 2013). Electrical Resistivity measurements are taken at the ground, and the resistivity is calculated. The resistivity is equal to the true resistivity values in the case of homogeneous soil only. The computed resistivity for heterogeneous layers is not the same as the true resistivity and is referred to as apparent resistivity, which is used to calculate the true resistivity of subsurface materials (Mostafa et al., 2018). Such measurements are termed Electrical Resistivity Soundings (ERS). True resistivity measurements can be directly conducted by in situ Dc resistivity meter (Priou et al., 2019; Rekapalli et al., 2015). ERS is done by using specific arrangements of arrays and is particularly helpful in areas where well data does not exist. ERS is effectively used to map the subsurface resistivity, however where similar lithologies exist, an overlap of electrical resistivity values may exist for fresh/saline water in aquifers (Hasan et al., 2020). To eliminate ambiguity, ERS data are used to estimate parameters such as Dar Zarrouk. (Henriet, 1976). D-Z characteristics, such as Longitudinal Unit Conductance (S) and Transverse Resistance (T), as well as Longitudinal and Transverse Resistivities, have been utilized in a groundwater investigations to distinguish between saline and freshwater zones (Singh et al., 2004).

## 6.2 Hydro geochemical Data

Geochemical analysis of 100 water samples was performed for major cations and anions and the trace element analysis was also carried out. Various statistical analysis was performed, and the result is given in Table 6.2 and the results are presented in this chapter. The groundwater quality is very important in assessing the suitability of water for drinking, irrigation, and domestic use. WHO standards (2017) are used to assess the suitability of water samples in the study area. The spatial distribution of the parameters studied are pH, TDS, EC, Ca, Mg, Na, Cl,  $\text{HCO}_3$ ,  $\text{NO}_3$  and  $\text{SO}_4$  and plotted as figures (4.2 to 4.12, Chapter 4). The trace metal analysis also performed on the groundwater samples and spatial distribution plotted in Figure 4.13. The parameters are categorized by the WHO limits of desired, permissible, and not permissible range.

### 6.2.1 Elemental Analysis of Groundwater Samples

In the study area the water samples have a pH value of 6.1 to 8.2, with an average of 7.5, which is within the desired WHO limits. The value of 6.1 to 6.8 indicated an alkaline nature of the water samples. The pH value of water samples exceeds in the northwestern and southwestern parts of the study area (Figure 4.2). The alkalinity is due to the presence of bicarbonate ions. The bicarbonate ( $\text{HCO}_3$ ) in the study area is from 58 to 860, with a mean value of 238.5 (Figure 4.11). The bicarbonates in water are formed due to the  $\text{CO}_2$  in water to form carbonic acid, which influence the pH of the groundwater (Azeez et al., 2000). Higher concentration of bicarbonates (Figure 4.11) is in the southeastern part of the study area, where high values are also observed in the northeast of the study area. The EC varies from 0.50 to 1992  $\mu\text{S}/\text{cm}$  of the study area. High EC (Figure 4.4) values are observed in the Southeastern parts of the study area and Southwestern part, low EC values are in the northeastern side of the study area (Figure 4.4). Two pockets identified in the southeast and southwest with high EC values fall under the category of not permissible according to

WHO standards. A TDS map (Figure 4.3) shows a distribution of 265 to 9000. High values are observed only at a few sample locations which may be a result of the leaching of salts from the surrounding soil, which decreases water quality. This may cause gastrointestinal irritation in human beings and can have a laxative effect (WHO, 2017). The concentration of ions such as Ca and Mg determines the total hardness of water. Water hardness is influenced by dissolved Ca and, to a lesser extent, Mg. It is stated as an equivalent amount of CaCO<sub>3</sub> (WHO, 2017).

Sodium is the most common cation of the study area; its concentration is from 50.7 to 1858 mg/l as shown in the map (Figure 4.5). Higher Na content is observed in south, southwest, and west of the study area. The Na content of study area is much higher than the permissible limit in drinking water set by WHO. Potassium in the samples is from 01 to 34 mg/l, with higher K values observed in southwest and west of the study area (Figure 4.6).

Ca in the study area is from 19 to 857 mg/l and an average value of 124.5 which is within the permissible limit set by WHO for drinking water. High values of Ca are in southwest of the study area (Figure 4.7). Mg is from 5.77 to 2801 mg/l with an average of 65 that is within the safe limit of WHO water standards. The high values for Mg are observed in south, southwest and the central parts of the study area (Figure 4.8).

SO<sub>4</sub> in the study area is from 44 to 4411 mg/l with an average of 295.7 and falls within the safe range of WHO. High concentration of SO<sub>4</sub> is in the west of the study area (Figure 4.9). Cl is the most abundant anion of the study area and it is from 7 to 2150 mg/l with an average value of 432 mg/l. The concentration of Cl in the study area is very high and well above the desirable limits of WHO. Very high concentration of Cl is observed in south of the study area (Figure 4.10). Nitrate in the study area is from 48 to 854 mg/l, with an average of 76.69 mg/l and is well above the permissible limits of WHO for drinking water. Very high values of Nitrate are observed from the samples collected in the central part of the study area (Figure 4.12). Figure 6.1 show the distribution of TDS and pH around the permissible limits by WHO and Figure 6.2 shows the distribution of Ca, Mg, Cl, Na,



HCO<sub>3</sub>, K, NO<sub>3</sub> and SO<sub>4</sub> around the permissible limits set by WHO.

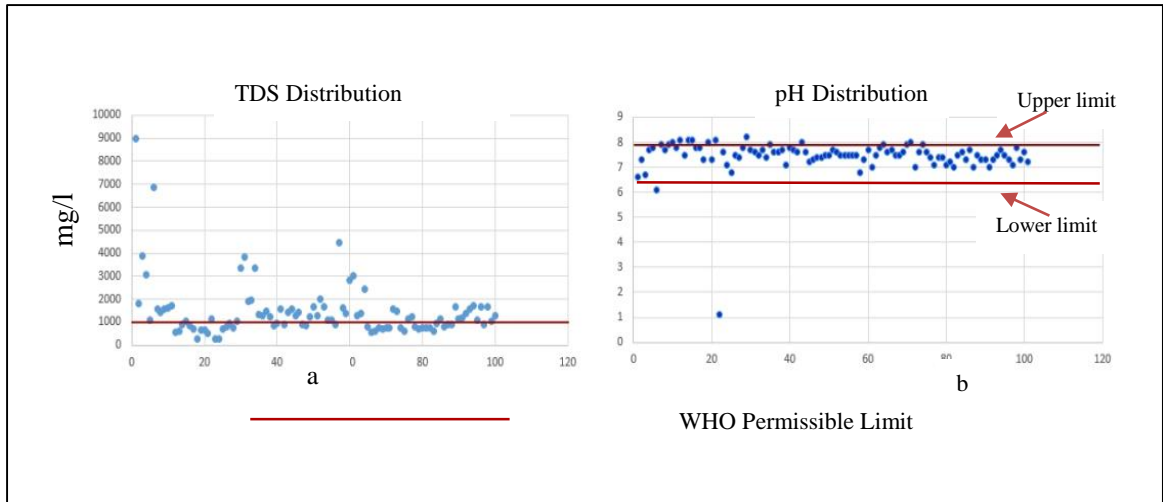


Figure 6.1 (a) TDS and the (b) pH distribution in shown is graphical form WHO Standards (WHO, 2017)

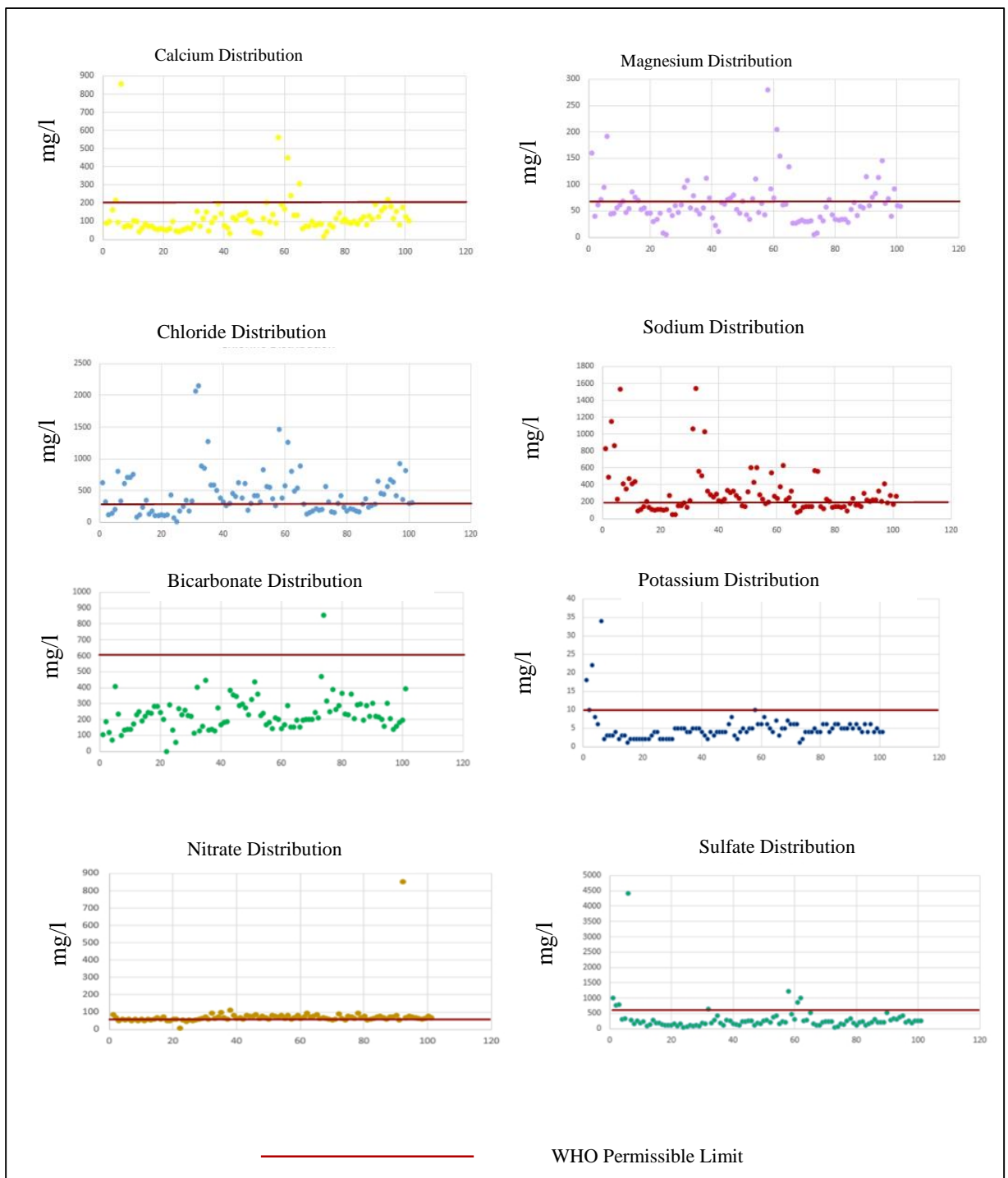


Figure 6.2 Elemental distribution in graphical form is shown (WHO, 2017).

### 6.2.2 Correlation Matrix

The correlation matrix of the major elements in groundwater samples is shown in Table 6.1. The matrix shows the relationship between the major ions in the groundwater samples of the study area.

Table 6.1 Correlation Matrix of major elements in groundwater

	Cl	HCO <sub>3</sub>	K	Mg	Na	NO <sub>3</sub>	SO <sub>4</sub>
Ca	.415	-.127	.710	.800	.432	.064	.848
Cl		.002	.178	.596	.679	.055	.306
HCO <sub>3</sub>			-.158	-.090	.111	.024	-.033
K				.492	.588	.035	.858
Mg					.425	.078	.615
Na						-.004	.614
NO <sub>3</sub>							.024

The correlation matrix shows high correlation between Ca & Mg and Ca & SO<sub>4</sub>. Very high correlation exists between K & SO<sub>4</sub>. There is a high correlation between Ca & K, Cl & Mg, Cl & Na, K & Na, Mg & SO<sub>4</sub> and Na & SO<sub>4</sub>. Whereas, Ca & Cl, Ca & Na, K & Mg, and Mg & Na are moderately correlated.

### 6.2.3 Principal Component Analysis (PCA)

The principal component analysis for the groundwater of Uthal indicates three components as shown in the Figure 6.3.

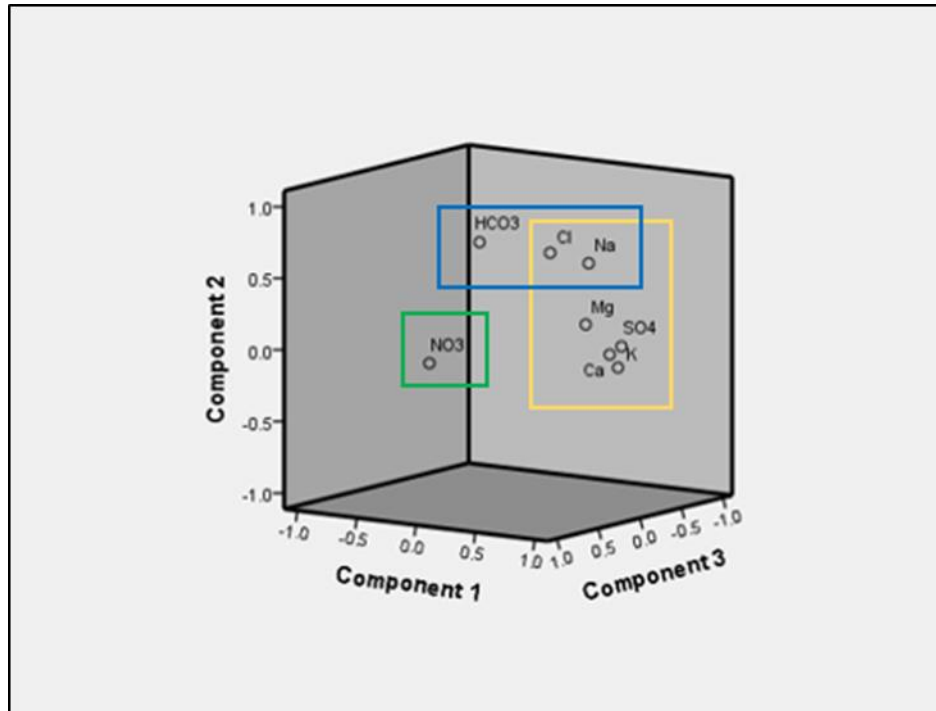


Figure 6.3 Rotated Space Diagram (PCA) shows the genetic affiliation of the major ions in the groundwater of the study area.

Three components have been identified from rotated component matrix, Component 1 shows genetic association of Ca, Mg, K, Na, Cl and SO<sub>4</sub>. The component 2 shows genetic association of HCO<sub>3</sub>, Cl and Na and the component 3 shows NO<sub>3</sub>. High values of Na and Cl is due to the high evaporation in the area and these form the dominant ionic pair as indicated by Piper Diagram and also evident from the Stiff diagrams presented in chapter 4. High values of Ca and SO<sub>4</sub> and their correlation shows these are dissolved from the sulfide mineralization which is common in the study area. High Na and low K shows the interaction of Bela Ophiolites and water through precipitation. NO<sub>3</sub> shows no correlation with the other ions and its higher concentration is in the central part of the study area, which is an agricultural area as shown in Figure 1.5. Its presence in higher concentration there is due to the use of fertilizers.

#### 6.2.4 Trace Element Analysis

Trace elements in the groundwater samples from the study area are given in Table 6.3. As, Co and Ti are below detection limits in the study area. Al in the study area is from 5 to 757  $\mu\text{g/l}$ , with an average of 63.4  $\mu\text{g/l}$ . Higher concentration of Al is observed in the northeast of the study area, with a very high value observed towards east (Figure 4.24 A). Cd in the water samples is from 0- 24, and an average of 2.8  $\mu\text{g/l}$ , which is within the permissible limits of WHO for most of the water samples. Higher concentrations of Cd are observed in samples collected from near the mountainous areas (Figure 4.24 B). Chromium in the samples range from 0.5 to 114  $\mu\text{g/l}$  and average is 1  $\mu\text{g/l}$ . Cr has a higher concentration in the eastern side near the mountains (Figure 4.24 C). Cu in water samples is in the range of 0.05 to 354  $\mu\text{g/l}$ , with an average of 64.65  $\mu\text{g/l}$  and is within the permissible limits of WHO. It has higher concentration towards the mountainous areas (Figure 4.24 D). Fe in the water samples in range of 19 to 2116  $\mu\text{g/l}$ , with an average of 328  $\mu\text{g/l}$  which is slightly higher than the WHO permissible limit. It also shows higher concentration toward the east where there is mountainous area (Figure 4.24 E). Mn has a concentration of 2 to 657  $\mu\text{g/l}$  and an average of 95  $\mu\text{g/l}$ . Mn also has higher concentration toward the mountains on the northeast of the study area (Figure 4.24 F). Ni is from 0 to 412  $\mu\text{g/l}$  with an average of 46  $\mu\text{g/l}$ . Ni is present in small concentrations with high values on the northeast (Figure 4.24 G). Pb is from 1.5 to 79  $\mu\text{g/l}$ , with an average of 17.75  $\mu\text{g/l}$  very high values are observed in the northeast of the study area where mountains are present (Figure 4.24 H). Zn is from 5 to 801  $\mu\text{g/l}$  and has an average of 62.65  $\mu\text{g/l}$ , it also shows moderately high values towards the mountains (Figure 4.24 I). From the analysis of the trace elements, it is observed that higher values of trace elements are in samples collected from near the mountains. Thus, the origin of trace elements is in the Bela Ophiolite.

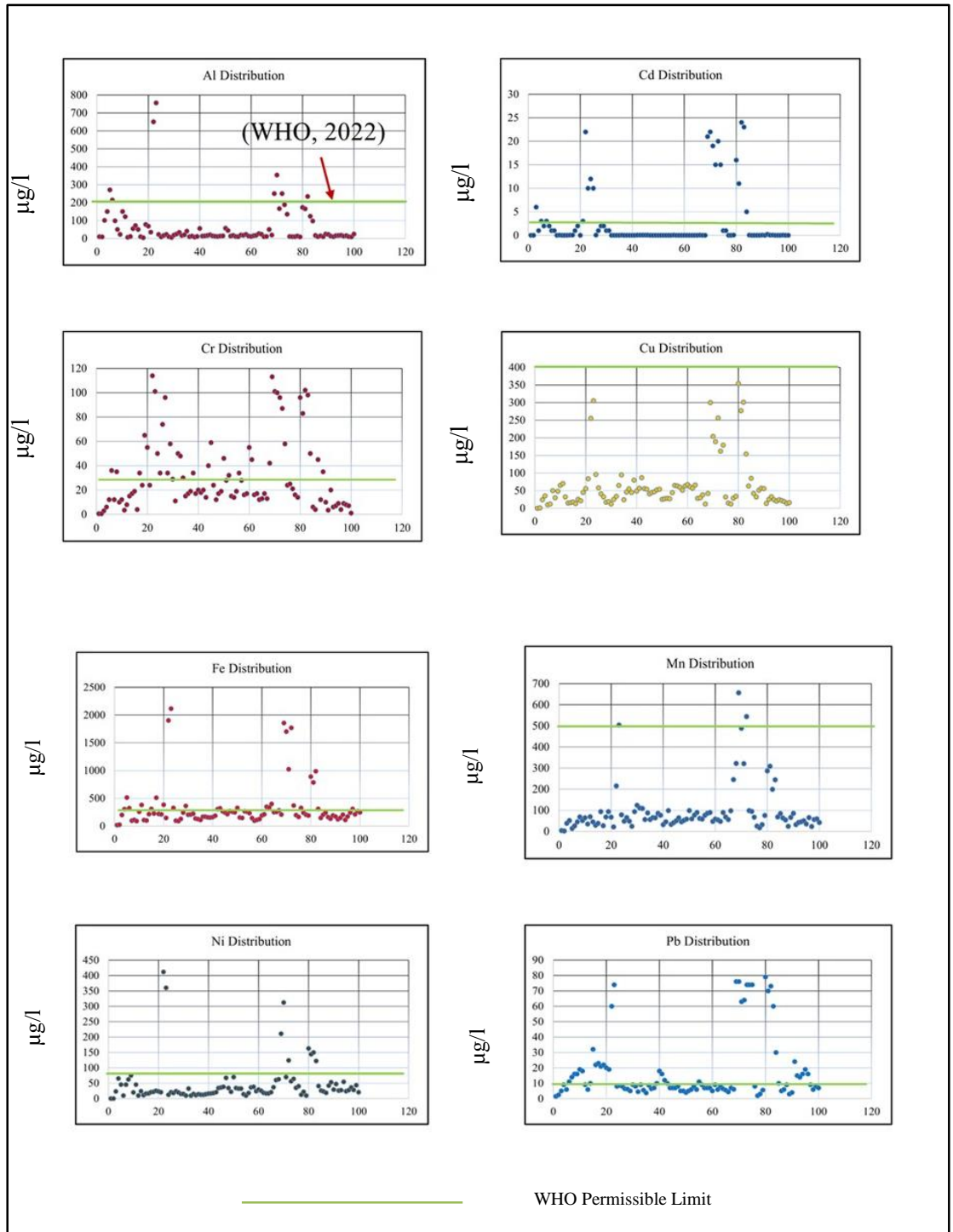


Figure 6.4 Trace Element distribution in graphical form is shown, WHO Standard (WHO, 2022). The values are given in  $\mu\text{g/l}$ .

Table 6.2 WHO drinking water permissible limits.

<b>Parameter</b>	<b>Maximum Limits</b>	<b>Minimum Limits</b>	<b>Median</b>	<b>Source</b>
pH maximum	10.5	8	8.5	WHO, 2017
pH minimum	7	5	8.5	WHO, 2017
TDS	2500 mg/l	200 mg/l	1000 mg/l	WHO, 2017
Na	400 mg/l	100 mg/l	200 mg/l	WHO, 2017
SO <sub>4</sub>	800 mg/l	50 mg/l	250 mg/l	WHO, 2017
Ca	500	30	150	WHO, 2017
Mg	1000	0.1	70	WHO, 2017
K	50	0.2	12	WHO, 2017
HCO <sub>3</sub>	600	300		WHO, 2017
NO <sub>3</sub>	75	40	50	WHO, 2017
Cd	0.15 mg/l	0.0000005	0.005	WHO, 2017
Cl	1000	20	250	WHO, 2017
Cr	0.05			WHO, 2017
Co	3.0	0.001	2.0	WHO, 2017
Pb	0.1	0.005	0.01	WHO, 2017
Mn	0.5	0.01	0.1	WHO, 2017
Ni	0.25	0.01	0.02	WHO, 2017
Fe	2	0.1	0.3	WHO, 2017
Zn	15	1	5	WHO, 2017
Ti	0.1			

Table 6.3 Minimum, Maximum and mean values of the physical parameters and major cations and anion in the water samples of the study area.

Parameters	Minimum	Maximum	Mean
pH	6.1	8.2	7.5
TDS (mg/l)	265	9000	1437
EC ( $\mu$ S/cm)	0.50	18	2.8
Na (mg/l)	50.7	1858	324
K (mg/l)	1	34	4.9
Ca (mg/l)	19	857	124.5
Mg (mg/l)	5.77	281	65
SO <sub>4</sub> (mg/l)	44	4411	295.7
Cl (mg/l)	7	2150	432
HCO <sub>3</sub> (mg/l)	58	860	238.5
NO <sub>3</sub> (mg/l)	48	854	76.7

Table 6.4 Minimum, Maximum and mean values of the trace elements of the water samples of the study area.

Parameter	Al	As	Cd	Co	Cr	Cu	Fe	Mn	Ni	Pb	Ti	Zn
Minimum	5	BDL	0	BDL	0.5	0.05	19	2	0	1.5	BDL	5
Maximum	756	BDL	24	BDL	114	354	21.16	675	412	79	BDL	801
Mean	115	BDL	BDL	BDL	32.19	64.65	28	95	46	17.75	BDL	62.65



The ion balance error (IBE) is one of the most important steps in the analysis of groundwater quality assessment. The maximum limit of the error of the cations and anions, according to Moiseenko et al. (2018), should not be more than 5%. The IBE for the analytical data of the water samples for the dissertation has a maximum value of 3%, which is within the acceptable range, and it reflects the accuracy and precision of the analytical work. For the construction of a Stiff pattern, multiple polygraphs have been formed from three parallel horizontal axes using meq/l anions and cations. Anions draw to the right while cations are plotted on the left side of the vertical zero axis. Stiff diagrams are generated for individual samples to graphically compare the concentration of selected anions and cations.

### **6.3 Rock-water Interaction**

The study area's most prevalent main cation is sodium, which is produced through the weathering of silicate and the dissolution of halite present in the area. Source of Mg in water sample is the Ophiolitic rocks in the eastern side of the study area. Major rocks of the study area consist of either limestone or has calcitic mineralization. This mineralization is of Parh Limestone, rocks of Malikhore and Kharrari Formations. Ca and Mg ions are introduced in the groundwater by the interaction of these rocks with water. Ca and Mg are mostly from the weathering of the Ophiolite in the study area and the carbonate rocks of the study area.

Clay minerals are the major source of K in groundwater as these consist of Feldspars as major mineral. Cl along with Na is the major ion in the groundwater of the study area. Na-bearing rocks are the main source of Na in water. Carbonates are abundant in the area and  $\text{HCO}_3$  enters the water due to the weathering of these rocks. Source of  $\text{SO}_4$  in the groundwater of the study area is gypsum ( $\text{CaSO}_4 \cdot 2\text{H}_2\text{O}$ ) and Anhydrite ( $\text{CaSO}_4$ ), Gypsum and Anhydrite bearing sedimentary rocks are common in the study and by chemical disintegration of these two minerals  $\text{SO}_4$  enters the groundwater. These rocks are

exposed widely in the study area. Potassium's concentration in the groundwater is less than the sodium's concentration. This is due to the weathering of silicate minerals and the halite solutions. Zn in the groundwater is contributed by the Ophiolite in the study area. Cu not abundant in the study area. The high content of Cr is also due to the ophiolitic rocks as these contain higher Cr. Fe is one of the major elements in the earth's crust and is also found in various segments of the Ophiolite. Pb is also closely associated with Fe. Fe, Cr & Mn are all associated with the Bela Ophiolite. Pillow basalts are often associated with Mn minerals. Cd is related with the sulfide phase of Bela Ophiolite. Cd is associated with Ni.

#### **6.4 Electrical Resistivity Sounding Data**

The ERS data was obtained by keeping the electrode spacing at 5.00 m and the total spread length of 300 m. For the data points, the distance MN (potential electrode spacing) was increased from 0.5 to 20 m. The distance AB/2 (current electrode spacing Figure 5.2) was increased gradually from 1.5 to 150 m. The potential drop was then measured, by sending the current through the current electrodes, across the potential electrodes. The investigation depth depends on the electrode spacing and the subsurface conductivities, with the depth being directly proportional to the spacing and inversely to the conductivity of the materials in the subsurface. The interpretation was done by repeated curve matching. Five geoelectrical layers were identified based on the resistivity method. However, due to the inhomogeneity and isotropy of the subsurface lithologies, some limitations are expected in the estimation of subsurface lithologies from the resistivity method alone. To overcome these limitations, lithology log data were collected from the drilled borehole, Well A and Well B (Figure 6.1), and correlated with the nearby ERS stations.

##### **6.4.1 Geoelectrical Layers**

The first geoelectrical layer is from the surface down to a maximum depth of 15 m in east shows a resistivity variation from 600  $\Omega\text{m}$  - 2600  $\Omega\text{m}$  (Figure 5.33). This layer is composed of surficial material with three high resistivity zones on the southeast, southwest,

and east. The thickness of this layer is 01 – 15 m (Figure 5.38). The second geoelectrical layer shows a resistivity variation from 50 - 11500  $\Omega\text{m}$  (Figure 5.34). Very high values are observed on the study area's far northwest, indicating dry surface conditions. The lower resistivity values are observed in the southeast, which is closer to the coast. In the central area, resistivity values are uniformly distributed. This layer shows the presence of unconsolidated sand. The zone indicated the presence of freshwater very near the surface in the form of small lenses. The thickness of the layer is from 01- 21 m (Figure 5.39). The third geoelectrical layer shows an almost even distribution of resistivity values from 0 - 200  $\Omega\text{m}$  (Figure 5.35), representing dry sand and clay layer. On the southwest, higher values are seen, and a small pocket in the north also has a higher resistivity value. Thickness varies from 01 - 60 m (Figure 5.40). The fourth geoelectrical layer shows resistivity variation from 75 - 100  $\Omega\text{m}$  (Figure 5.36). This layer has a thickness between 25 - 110 m (Figure 5.41) and is composed mainly of sand with fresh water. This layer forms the major water-bearing zone of the survey area. The fifth geoelectrical layer has a resistivity distribution from 48 - 90  $\Omega\text{m}$  (Figure 5.37). The lower resistivity values are observed in the southeast, indicating some amount of saline water there, whereas the rest of the area indicates the presence of a freshwater zone. The layer thickness varies from 40 - 110 m (Figure 5.42). This layer is also comprised of recent sand and clay deposits.

Table 6.5 Summary of the geoelectrical layers of study area

<b>Geoelectrical layer</b>	<b>Apparent resistivity (<math>\Omega\text{m}</math>)</b>	<b>Lithology</b>
1	600 - 2600	Unconsolidated sediments (Surficial Material)
2	5 - 11500	Unconsolidated sand
3	0 - 200	Sand and Clay (Dry)
4	75 – 100	Sand (Water bearing)
5	48 - 90	Sand & Clay (Water bearing)

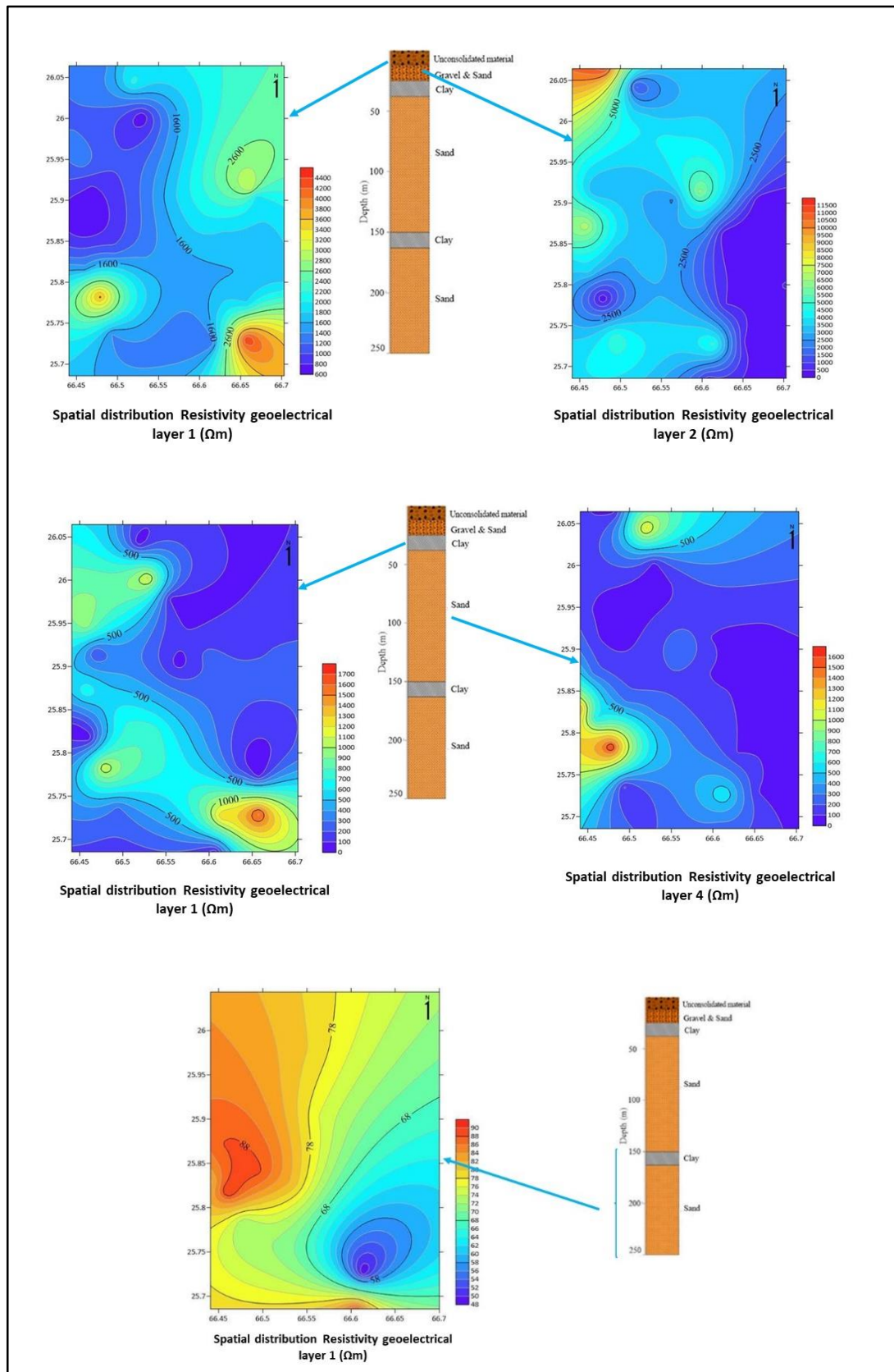


Figure 6.5 Resistivity Layers and lithologies from the well logs.

Table 6.6 Lithologies from the well log data of the study area

<b>Zone</b>	<b>Thickness</b>	<b>Lithology</b>
a	10	unconsolidated
b	40	Boulder & gravel
c	125	Sand
d	15	clay
e	95	sand

#### 6.4.2 The Dar Zarrouk (D-Z) Parameters

The geophysical methods of electrical resistivity sounding (ERS) are widely used to delineate the groundwater zones and also to demarcate the fresh/saline waters in the subsurface. The ERS data can distribute the subsurface strata into several layers each with a specific resistivity value, and delineate the fresh and saline water zones associated as done in this study (Figure 5.8 to 5.42). The five geoelectrical layers identified by the data are in the Quaternary sediments comprising of unconsolidated material, clay, sand, and gravel. As resistivity values of lithologies are similar overlapping and intermixing of resistivity values are observed. Therefore, to get a more reliable solution Dar Zarrouk (D-Z) parameters are applied for the identification of fresh/saline water zones.

The Dar Zarrouk (D-Z) parameters, Longitudinal Unit Conductance S (mho), Transverse Unit Resistance T ( $\Omega\text{m}^2$ ), Longitudinal Resistivity  $R_S$  ( $\Omega\text{m}$ ), and Transverse Resistivity  $R_T$  ( $\Omega\text{m}$ ), are helpful in providing solutions for the delineation of saline/fresh groundwater zones (Batayneh, 2013). The D-Z parameters remove the ambiguities in the ERS data interpretation where the overlapping of similar lithologies are present (Henriet, 1976; Hassan et al., 2019). These parameters delineate the groundwater conditions and the hydrological characteristics from ERS data (Batayneh, 2013; Maillet, 1947), thus can

delineate fresh/saline groundwater zones without overlapping.

The longitudinal unit conductance (S), transverse unit resistance (T), longitudinal resistance ( $R_S$ ), and transverse resistivity ( $R_T$ ) are calculated from the surface geoelectrical data (Table 5.3)

The values of longitudinal conductance (S) are between 0.1 - 1.65 mho (Figure 5.43), and the transverse unit resistance (T) is greater than 25000  $\Omega m^2$  (Figure 5.44). The longitudinal resistivity ( $R_S$ ) is from 50 - 1350  $\Omega m$  (Figure 5.45), and the transverse resistivity ( $R_T$ ) is from 22 - 1150  $\Omega m$  (Figure 5.46). The lower values of less than 2 mho for S, and greater than 8000  $\Omega m^2$  for T indicate the presence of freshwater as given by Singh et al. (2004) for the coastal aquifers and by Hasan et al. (2020). Therefore, the D-Z parameters' result shows that the groundwater zones of the study area are freshwater zones and match the ERS data results.

Table 6.7 Reference values for Dar Zarrouk parameters for fresh and saline water

<b>DZ parameter</b>	For study area	Type of water	Reference values
Longitudinal conductance (S)	0.1 - 1.65 mho	Fresh water	< 10 mhos (Batayneh et al., 2013) < 40 mhos (Singh et al., 2004)
Transverse unit resistance (T)	> 25000 $\Omega m^2$	Fresh water	6,500–8,500 $\Omega m^2$ (Batayneh et al., 2013) 2,000–8,000 $\Omega m^2$ (Singh et al., 2004)
Longitudinal resistivity ( $R_S$ )	22 - 1150 $\Omega m$	Fresh Water	>16 $\Omega m$ (Singh et al., 2004)
Transverse resistivity ( $R_T$ )	22 - 1150 $\Omega m$	Fresh water	

### 6.4.5 Subsurface Model

The integration of geoelectrical layer with the borehole data a subsurface model is generated as shown in the Figure 6.6. The model is generated from the four geometrical layers; the fifth layer was identified under a few ERS points therefore it was not used in generation of 3 D model. The layers shown in the model comprise of top unconsolidated surficial layer, the unconsolidated Sand & Gravel, Sand & Clay layer, and the water bearing Sand Layer. The water bearing zone is near the surface in vicinity of the main streams of the area. The general trend of water is from NE to SW.

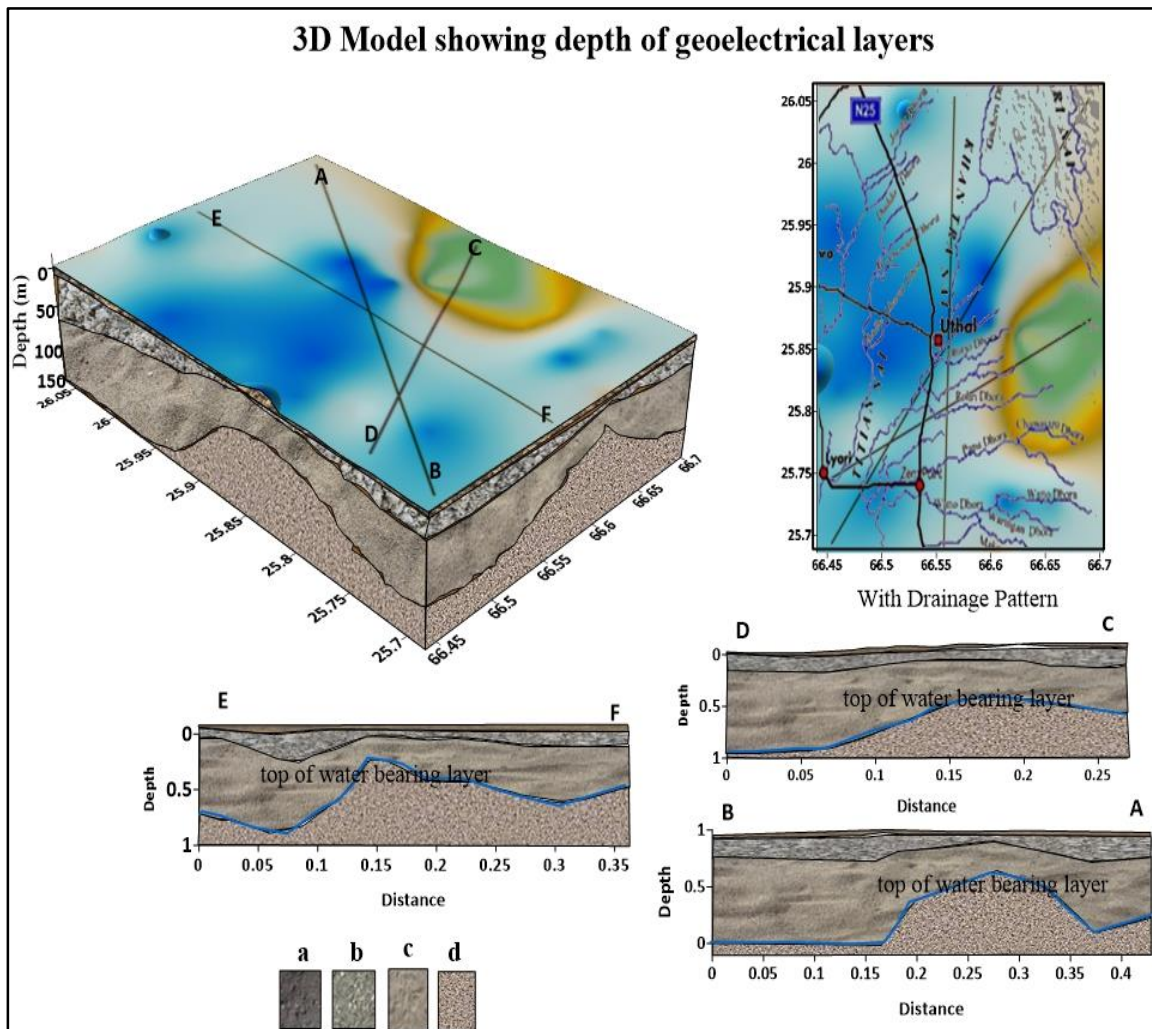


Figure 6.6 The 3D subsurface model from the geoelectrical layers and bore hole data. Four major lithologies have been identified a. Unconsolidated Surficial material b. Sand and Gravel c. Sand and Clay and d. Sand (water bearing). The blue line shows top of the water bearing layer.

The correlation between the two lithology logs from the borehole data show five layers (Figure 6.7). The layers are top unconsolidated surficial material, Unconsolidated Sand & Gravel, Sand & Clay, water bearing Sand, and Clay layer.

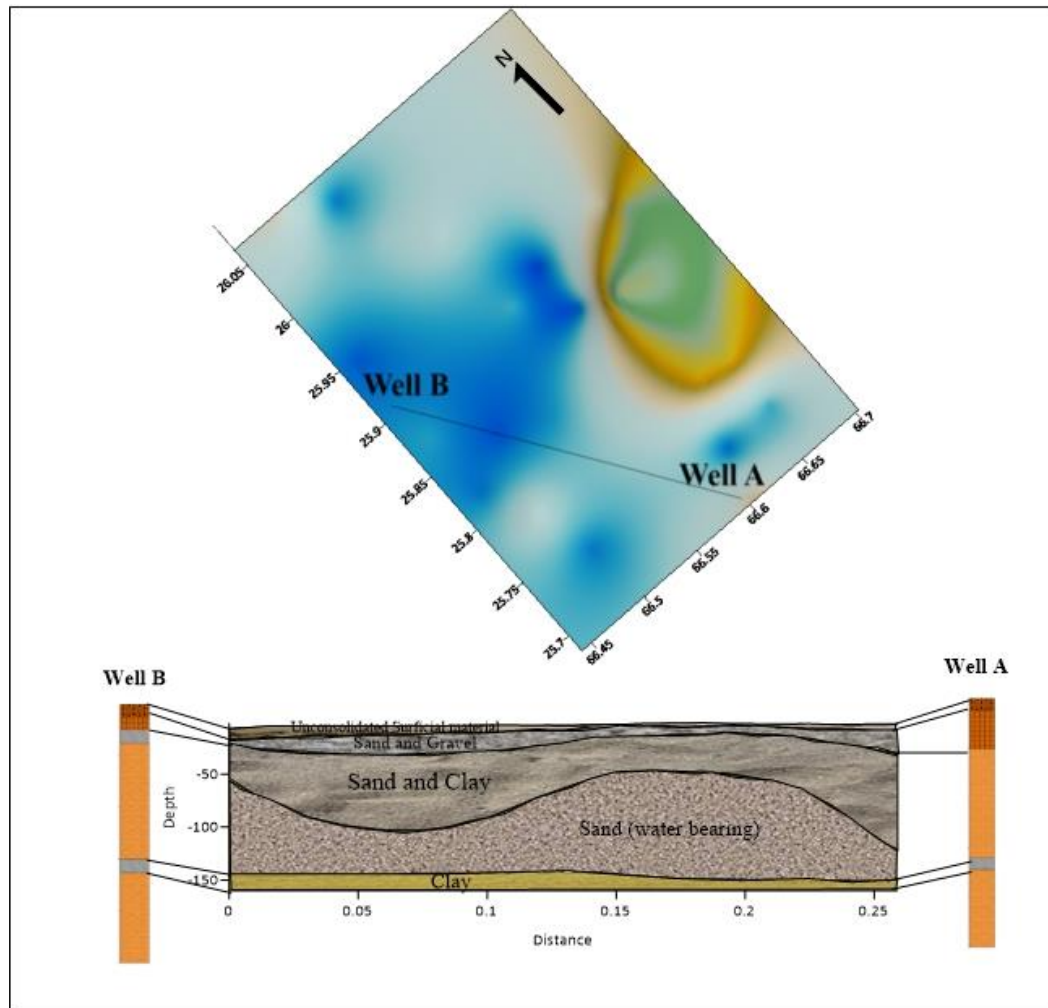


Figure 6.7 The correlation between two well logs with the lithologies identified from the resistivity data. A fifth layer comprising of Clay can be seen at a few ERS points.



## **6.5 Integration of ERS and geochemical data**

Two groundwater zones have been identified on the basis of the resistivity distribution (Table 6.5). The zones comprise of Sand and Sand & Clay. The main water bearing zone is the fourth geoelectrical layer. The fifth geoelectrical layer is present under a few ERS points. Therefore, the major water bearing zone of the area is the fourth geoelectrical layer. Integration of the resistivity distribution and major geochemical parameter distribution is also done to validate the results.

### **6.5.1 Geoelectrical layer 4 and geochemical parameters**

Main groundwater producing layer of the study area is the fourth geoelectrical layer which extends from a depth of 36 meters to a depth of 150 meters below the surface. High TDS values are reflected in the low resistivity of this layer. Resistivity in range of 500 to 1000 ohm-m is associated with a TDS of 9000 approximately. Very high resistivity of this layer is indicating a low TDS value of under 1000. Thus resistivity and TDS show an indirect relation (Figure 6.8). Resistivity of the water producing zone shows direct relation with the Ca distribution in the study area. Higher resistivity values associated with lower Ca and Lower with higher Ca concentration (Figure 6.9). Lower Na concentration in the groundwater is associated with a slightly higher resistivity of the layer. And the higher Na concentration with lower resistivity values (Figure 6.10).  $\text{HCO}_3$  concentration in the groundwater shows no direct relation with the resistivity of the main water producing zone of the study area (Figure 6.11). No direct relation between the potassium distribution and the resistivity of the layer could be observed. Thus, the concentration of K in water does not affect the resistivity (Figure 6.12). The higher resistivity values are associated with lower magnesium content in the area, similar to the association of Ca concentration with resistivity values. The total Ca and Mg in water defines the hardness of the water. Thus,

the resistivity decreases as the hardness of water increases (Figure 6.13). The resistivity of the water producing zone shows no direct relation with the  $\text{SO}_4$  concentration in water. Thus, the distribution of  $\text{SO}_4$  in water does not affect the resistivity (Figure 6.14). Lower values of Cl in groundwater are associated with the higher resistivity of the geoelectrical layer which is the main water producing zone of the study area (Figure 6.15). No relation can be observed between the spatial distribution of  $\text{NO}_3$  and groundwater resistivity. Thus the concentration of  $\text{NO}_3$  has no effect on the resistivity of water (Figure 6.16).

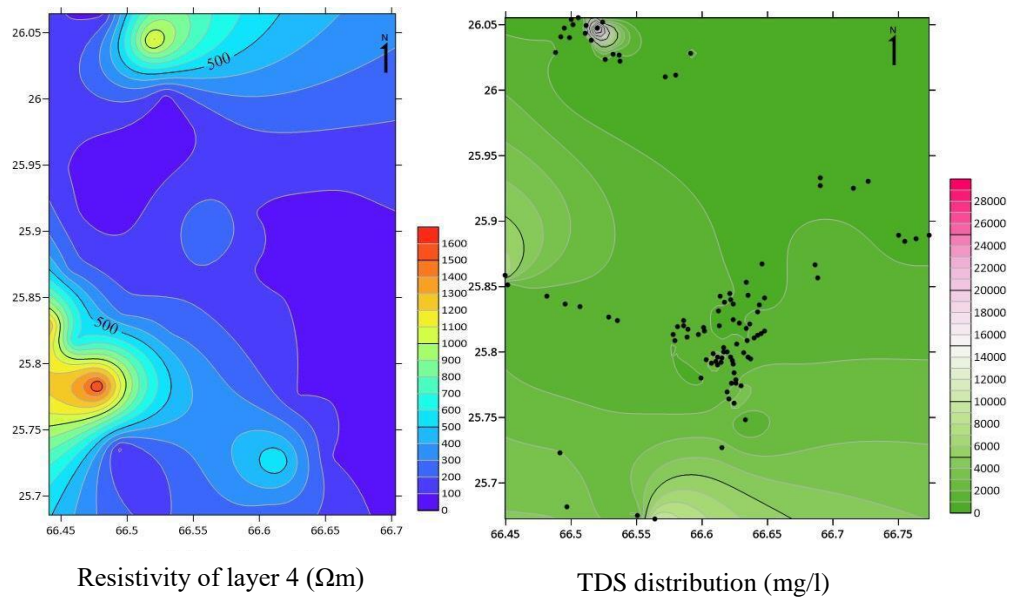


Figure 6.8 Geoelectrical layer 4 and TDS distribution of the study area

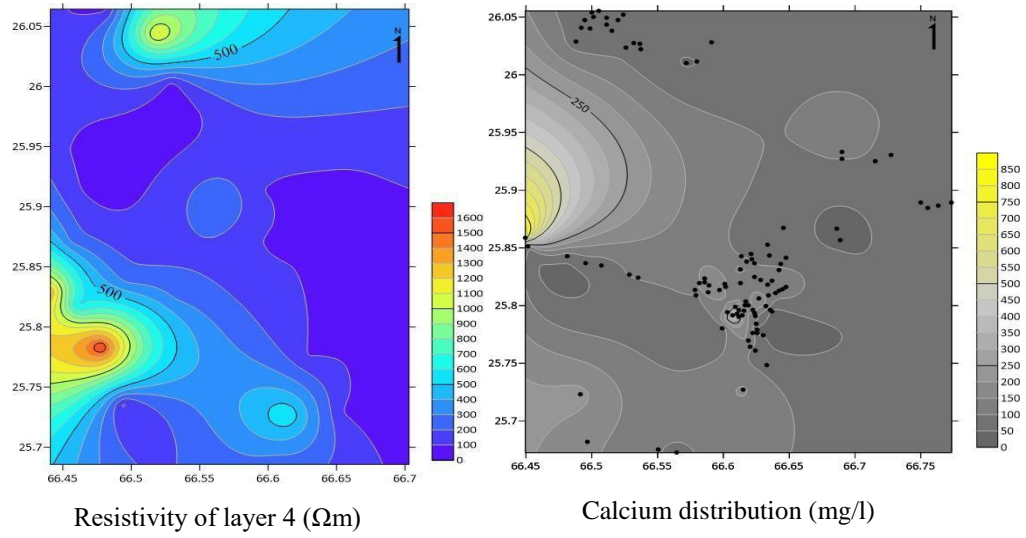


Figure 6.9 Geoelectrical layer 4 and Ca distribution of the study area

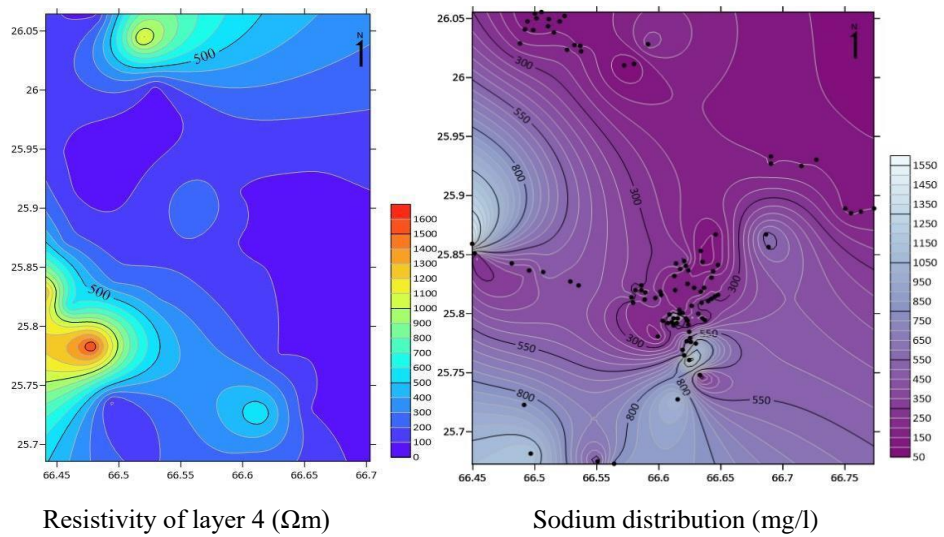


Figure 6.10 Geoelectrical layer 4 and Na distribution of the study area

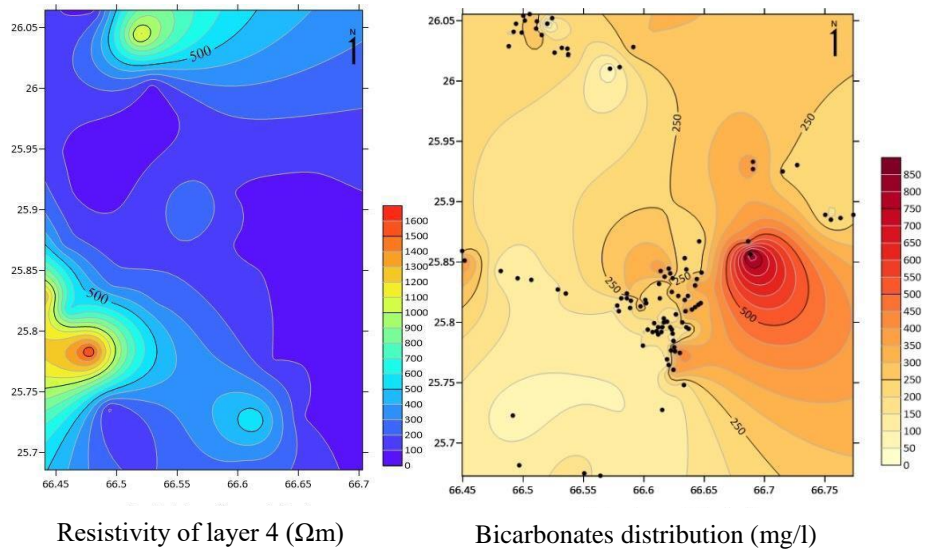


Figure 6.11 Geoelectrical layer 4 and  $HCO_3$  distribution of the study area

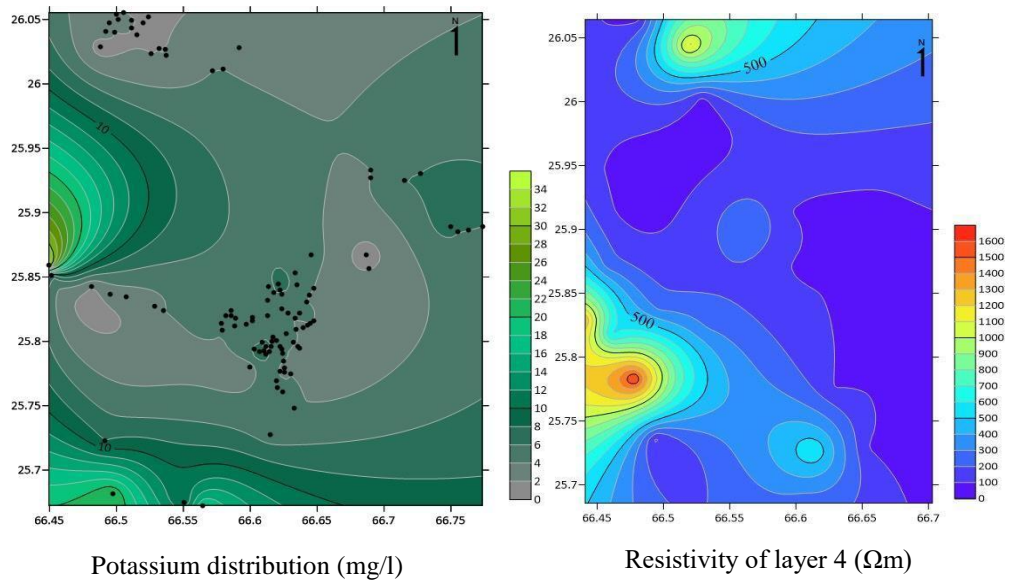


Figure 6.12 Geoelectrical layer 4 and K distribution of the study area

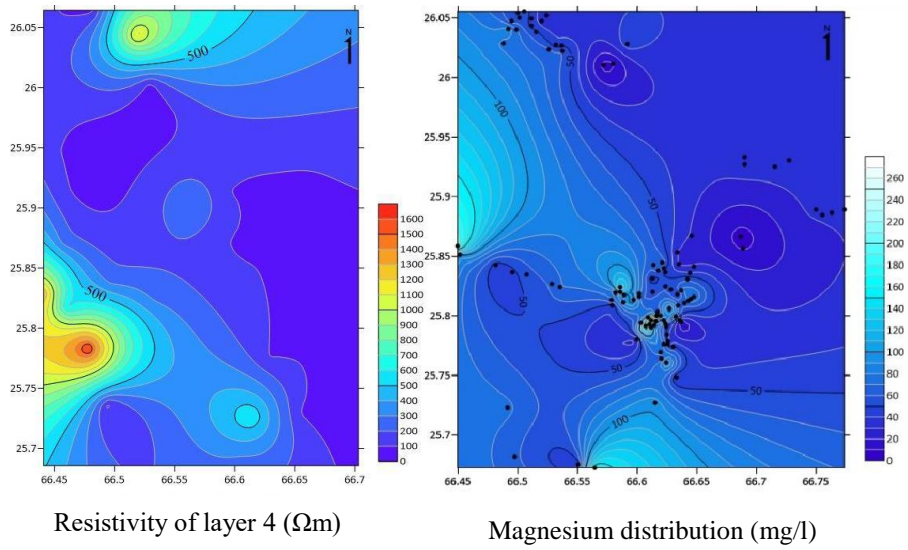


Figure 6.13 Geoelectrical layer 4 and Mg distribution of the study area

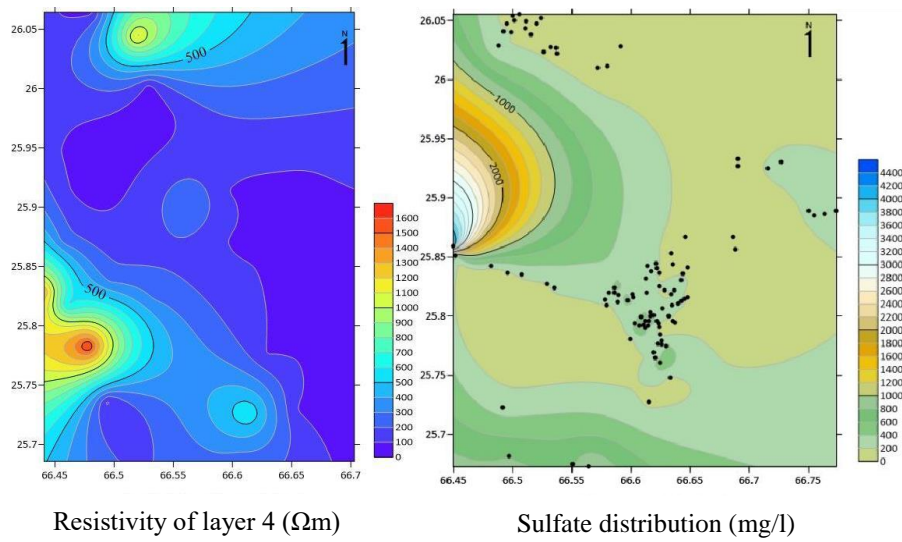


Figure 6.14 Geoelectrical layer 4 and  $SO_4$  distribution of the study area



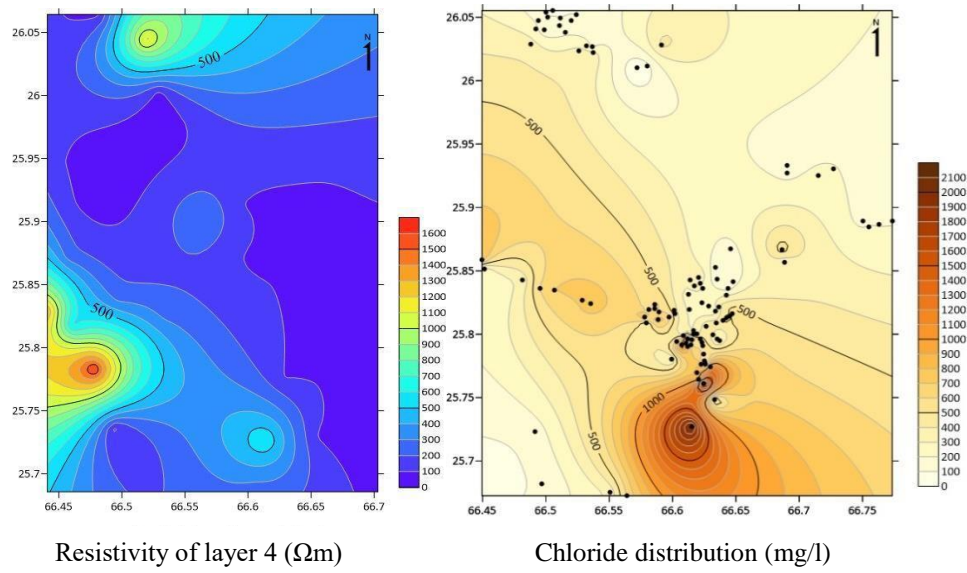


Figure 6.15 Geoelectrical layer 4 and Cl distribution of the study area

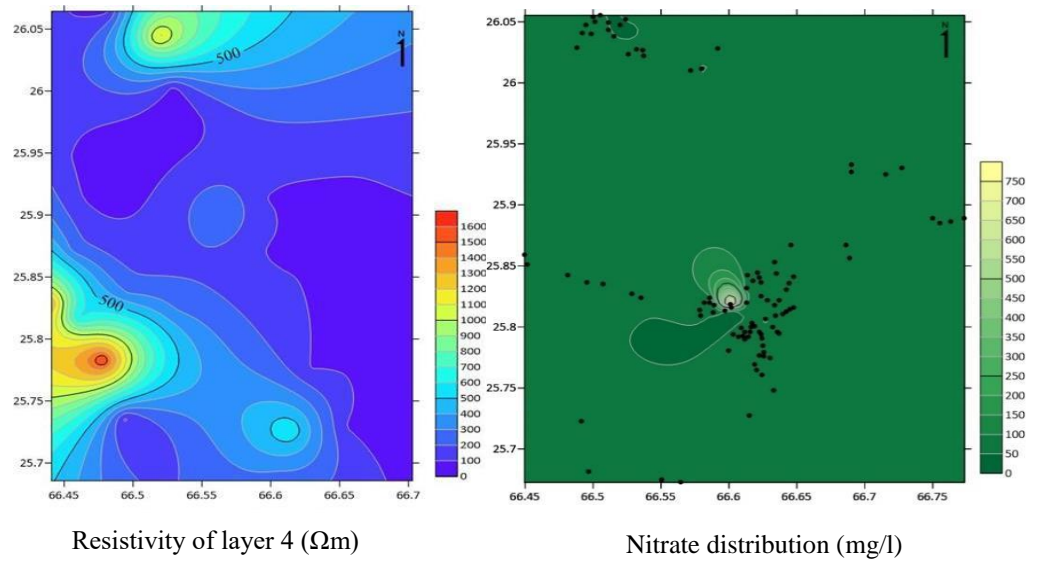


Figure 6.16 Geoelectrical layer 4 and the  $\text{NO}_3$  distribution of the study area

### 6.5.2 Geoelectrical layer 5 and geochemical parameters

The second water producing zone is identified by the fifth geoelectrical layer. The overall uniform TDS distribution is in confirmation with fresh water recourses present in the second water producing zone (Figure 6.17). Ca shows a direct relation with the resistivity distribution of this zone, with higher values of resistivity associated lower Ca concentration (Figure 6.18). Higher value of resistivity is associated with the lower  $\text{HCO}_3$  concentration and the lower resistivity with the higher  $\text{HCO}_3$  in this water producing zone (Figure 6.19).

The resistivity distribution with the spatial concentration of K in groundwater of this zone show no relationship (Figure 6.20). Lower resistivity of groundwater is associated with higher concentration of Na in water and vice versa as seen in the comparison given in Figure 6.21. The higher resistivity value of groundwater in this zone shows a lower concentration of Mg and the higher concentration of Mg (Figure 6.22) for the lower resistivity values. The total Ca and Mg in water defines the hardness of the water. Thus, the resistivity decreases as the hardness of water increases as observed in the geoelectrical layer 4. No direct relation was observed between the resistivity of the water producing zone and the spatial distribution of  $\text{SO}_4$  in water (Figure 6.23). Similar to Na, Cl concentration is higher for the zones having lower resistivity and the zones with higher resistivity indicate lower concentration of Cl in water (Figure 6.24). No relation can be observed between the spatial distribution of  $\text{NO}_3$  and groundwater resistivity (Figure 6.25)

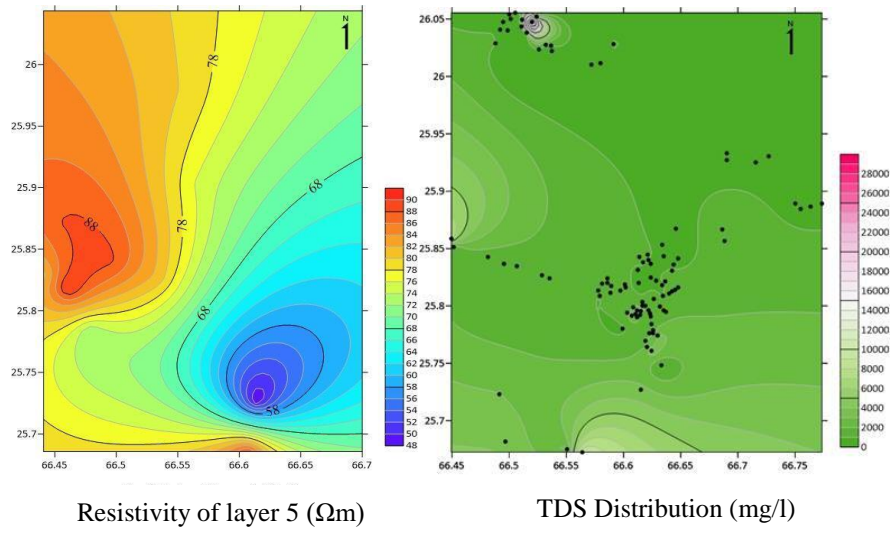


Figure 6.17 Geoelectrical layer 5 and TDS distribution of the study area

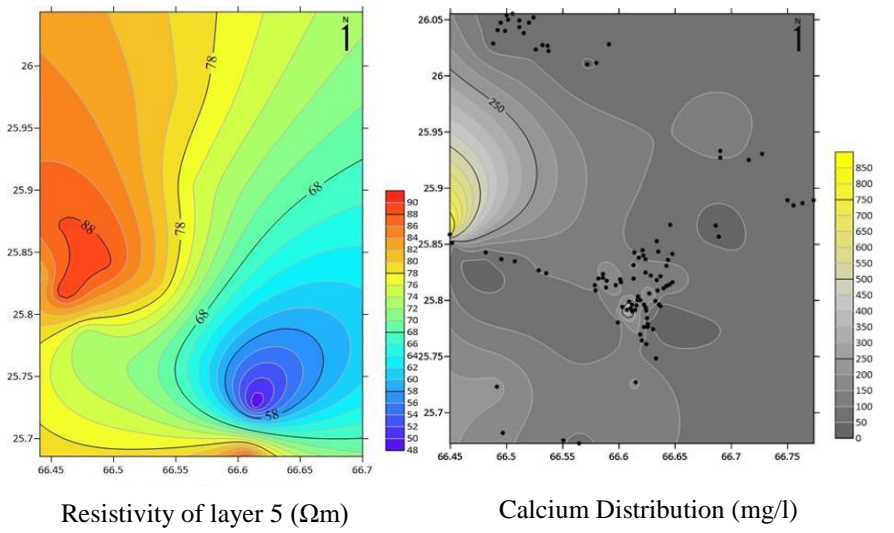


Figure 6.18 Geoelectrical layer 5 and Ca distribution of the study area



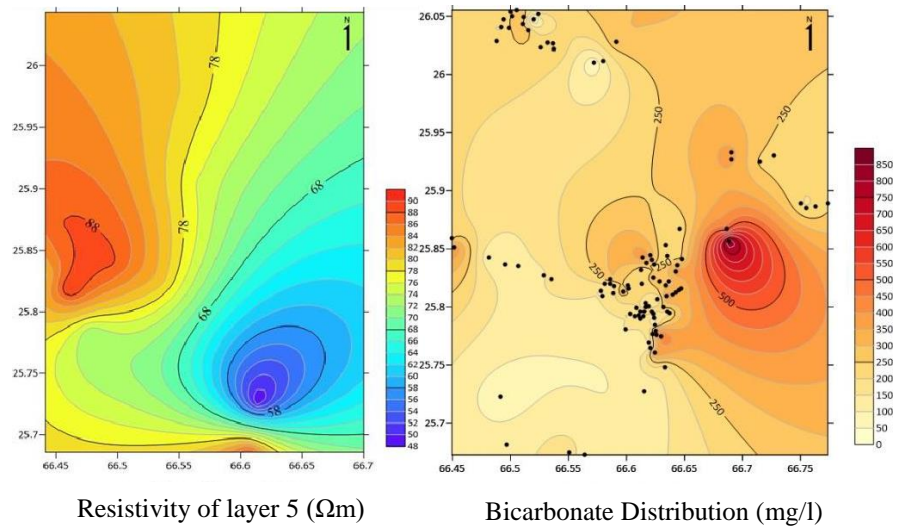


Figure 6.19 Geoelectrical layer 5 and  $\text{HCO}_3$  distribution of the study area

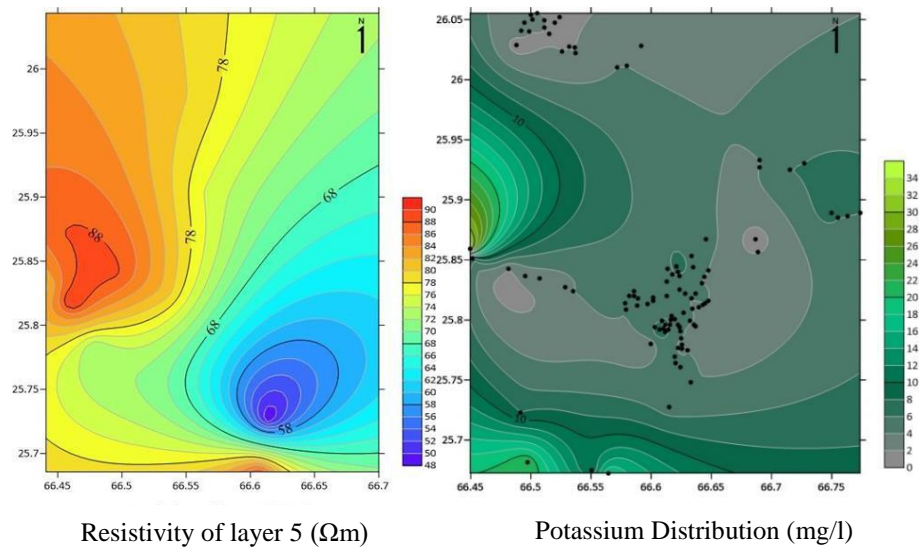


Figure 6.20 Geoelectrical layer 5 and K distribution of the study area

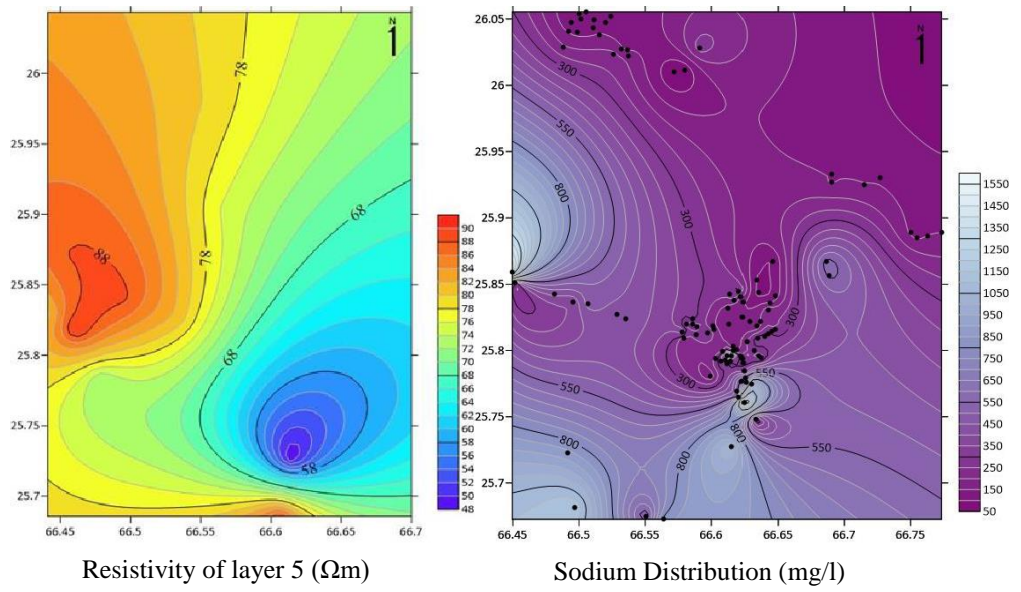


Figure 6.21 Geoelectrical layer 5 and Na distribution of the study area

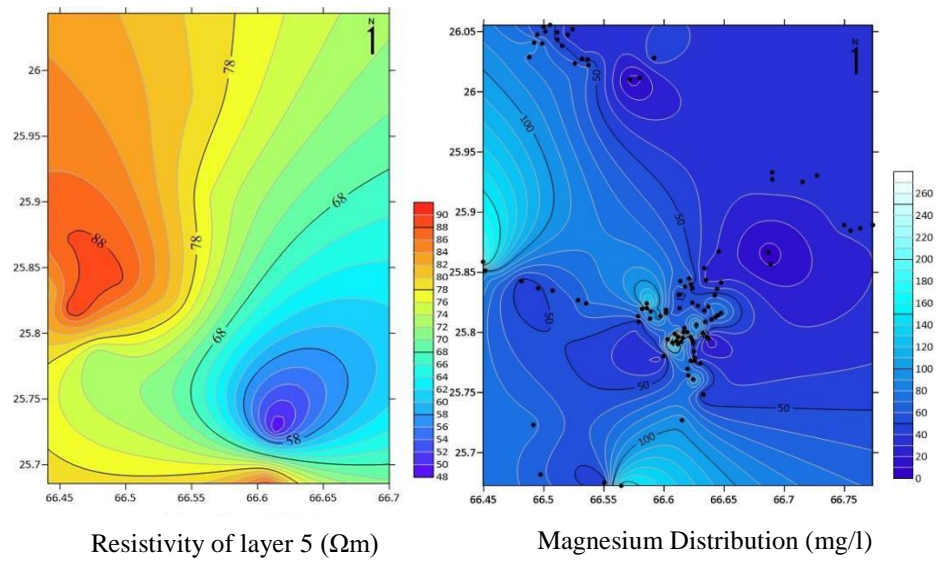


Figure 6.22 Geoelectrical layer 5 and Mg distribution of the study area

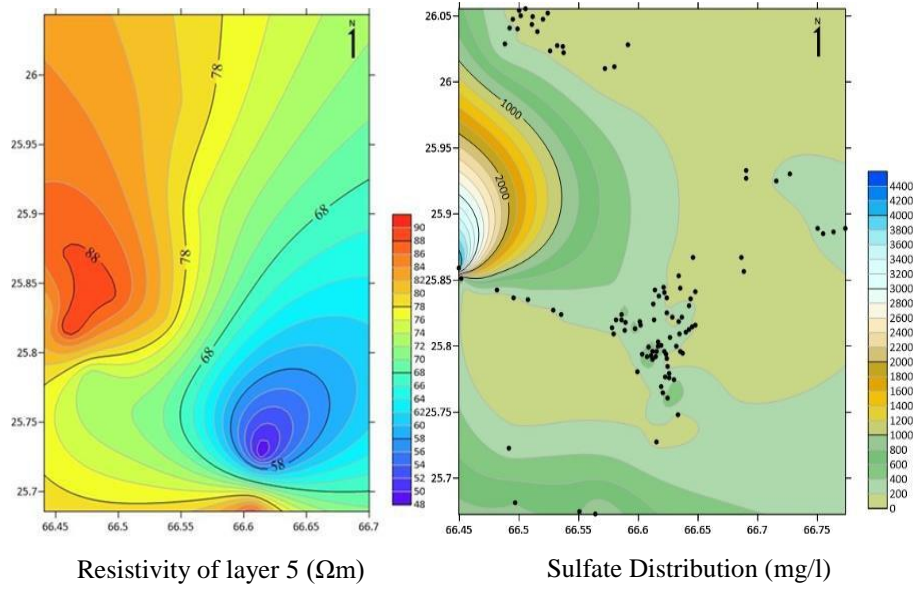


Figure 6.23 Geoelectrical layer 5 and  $\text{SO}_4$  distribution of the study area

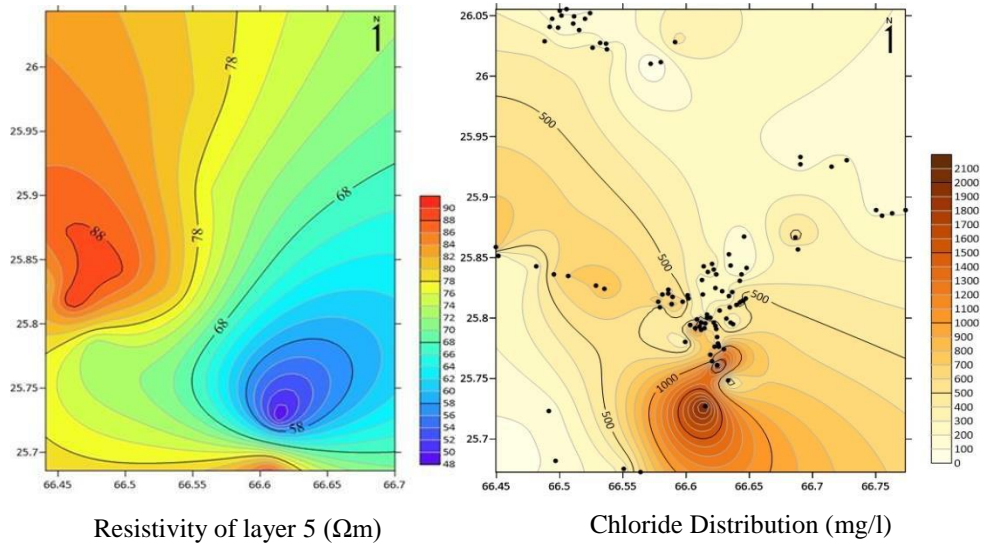


Figure 6.24 Geoelectrical layer 5 and Cl distribution of the study area

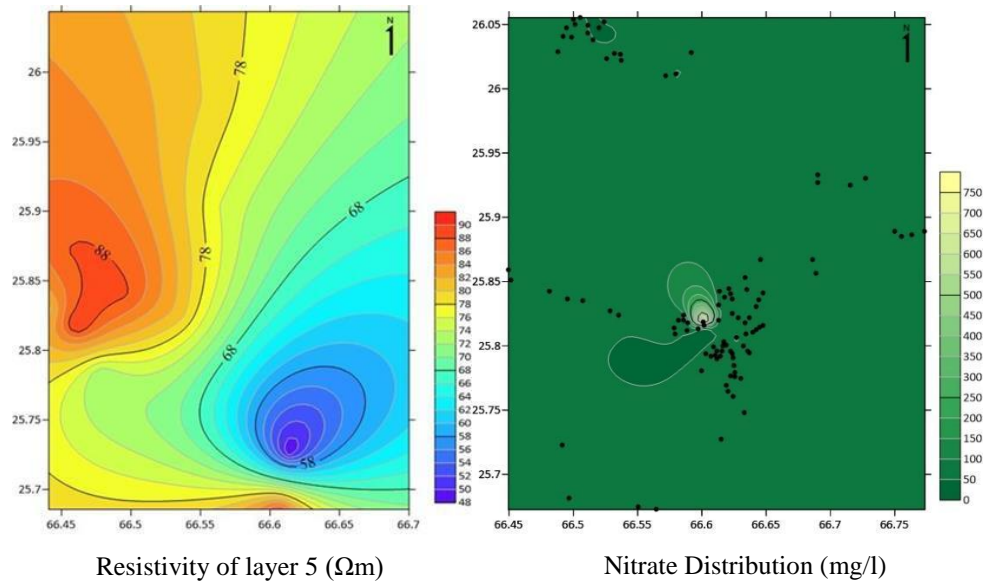


Figure 6.25 Geoelectrical layer 5 and  $\text{NO}_3$  distribution of the study area.

## 6.6 Groundwater Zones

Integration of the electrical resistivity data with the TDS values groundwater zones of different potentials have been identified for the study area as shown in the Figure 6.26

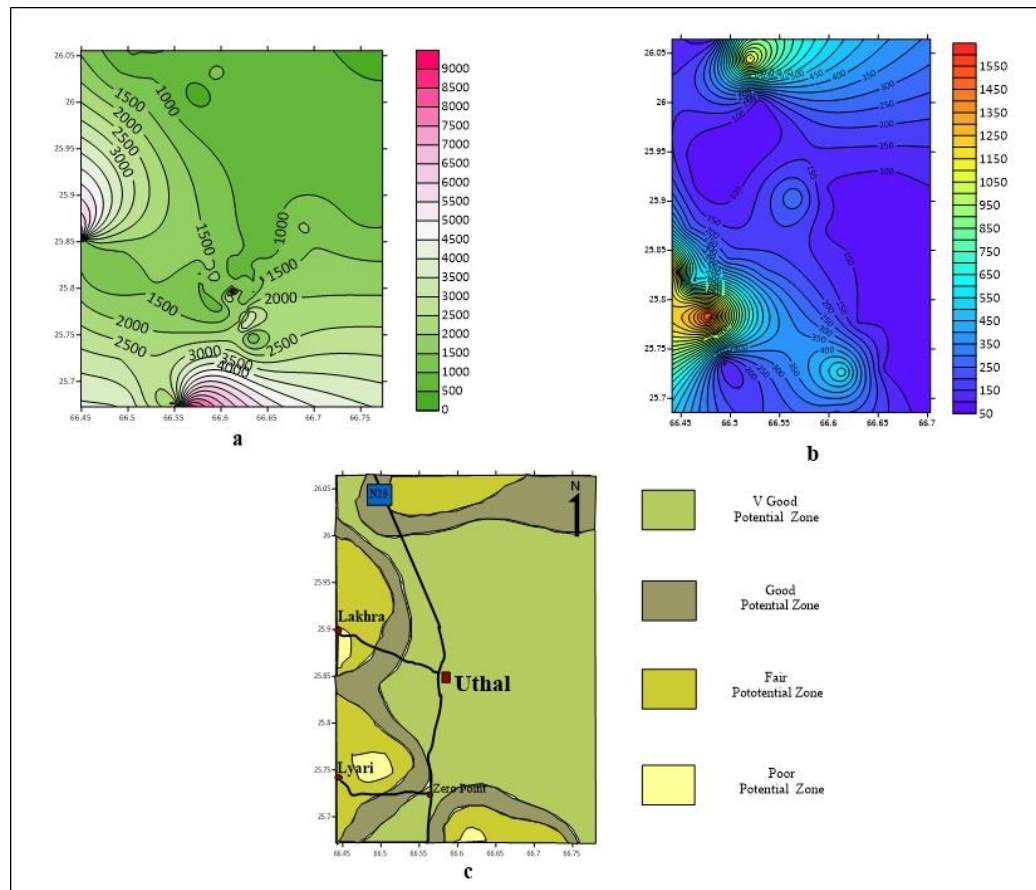


Figure 6.26 The groundwater zones (a) shows the distribution of TDS (b) resistivity distribution of fourth layer (c) the groundwater zones from the correlation of TDS and resistivity.



Four zones have been identified, namely Very Good Potential, Good Potential, Fair Potential and Poor Potential Zones. These zones divide the study area on the basis of the electrical resistivity values and the corresponding TDS values (Table 6.8).

Table 6.8 Comparison of TDS and Resistivity Values and the Groundwater Zones

<b>S.No</b>	<b>TDS (mg/l)</b>	<b>Resistivity Values (<math>\Omega</math> m)</b>	<b>Groundwater Zone</b>
1	< 500	200 -1500	Very Good Potential Zone
2	501 - 1000	100 -200	Good Potential
3	1001 - 2000	20 - 100	Fair Potential
4	> 2000	< 20	Poor Potential

## **CHAPTER 7**

### **CONCUSION**

The study area Uthal is in the Lasbela district of Balochistan, Pakistan. It lies in the semi- arid to the arid climatic zone of Pakistan. It is located at a distance of approximately 35 km from the coastal area. Uthal is in the Porali trough that lies towards the west of the western fold belt of Pakistan. The chemical composition of the groundwater in the study area is mainly controlled by the mineralogy of the rocks present in the area, the topography, and the climate of the study area. As the study area is located in the semi-arid zone, precipitation is scanty. Most of the precipitation that falls on the ground causes flash floods. Due to the vicinity of the study area to the coast, the study was undertaken to assess the quality of groundwater on the basis of the geochemical parameter and surface geophysical techniques. The population here depends on the groundwater resources for their day-to-day uses as well the crops that they grow for their livelihood. This study, therefore, presents the understanding the geochemistry of the groundwater, subsurface distribution of resistivity, identification of geoelectrical layers present in the areas and identifying of the potential groundwater zones.

The present investigation has for the first time provided the region's quantitative methodology for analyzing and integrating the geochemical and geophysical parameters in assessing the groundwater resources. Good water management practices necessitate modelling of groundwater reservoirs, monitoring and analysis of hydrofacies, and the interpretation of trending data. These parameters form a legend that can be applied to the other semi-arid to arid regions. The following conclusions have been made from the study:

1. From the surface geoelectrical data of 25 points, acquired using the Schlumberger Configuration, true resistivity of the subsurface and 3D depth model was obtained. Five geoelectrical layers were identified, with a thin (01 - 15 m) first layer consisting of unconsolidated dry surface material having true resistivity between 600 - 2600  $\Omega\text{m}$ . The second layer (01 - 21 m) consists mainly of sand with lenses of fresh water near the surface and hard rock fragments and very dry conditions towards the northwest of the study area having resistivity variation from 50 to 11500  $\Omega\text{m}$ . The third layer (01-60 m) shows an overall uniform distribution of resistivity of up to 200  $\Omega\text{m}$  and is comprised mainly of sand and clay with fresh water. The fourth layer (25 - 110 m) was the main water producing zone and had fresh water in Sand with resistivity of 75 - 100  $\Omega\text{m}$ . The last layer comprised of sand and clay (40 to 110 m) and showed a freshwater zone with resistivity in the range of 48 - 75  $\Omega\text{m}$ . The Dar Zarrouk parameters calculated from the ERS data, indicated the presence of fresh water in the area. The Longitudinal Unit Conductance (S) was from 0.5 mhos to 1.65 mhos, and T ( $> 25000 \Omega\text{m}^2$ ) and the value indicates that the area has a freshwater aquifer and seawater has not intruded. The longitudinal resistivity  $R_s$  and the transverse resistivity  $R_T$ , are from 50 - 1350  $\Omega\text{m}$  and 22 to above 1150  $\Omega\text{m}$  respectively. The results indicated that at present freshwater in the study area and saline water is present only in near-surface pockets due to dry conditions and there is no seawater in the study area. Thick fresh groundwater aquifers are of sand and sand & clay within the study area.
2. The water samples analysis for 100 sites in the study area was conducted to determine the geochemical parameters of the groundwater. The analysis was performed to determine: pH value, Total Dissolved Substances (TDS), and Electrical Conductivity



(EC). Chemical analyses were performed to determine the concentration of major cations and anions in the study area. The main cations of the area include Magnesium, Calcium, Potassium, and Sodium. The anions of the study are Chloride, Bicarbonates, Nitrate, and Sulfate. The geochemical analysis was performed according to the WHO's guidelines regarding drinking water standards. Statistical analysis was performed to determine the average values and the standard deviation. The minimum pH value for the water samples was 6.1, and maximum 8.2 that was within the permissible limit of WHO standards for drinking water. TDS was in the range of 265 – 9000 mg/l with an average of 1222 mg/l. TDS for most samples were within the permissible range by WHO standards. Na was from 50.7 – 1858 mg/l with an average of 58 mg/l and is also within the permissible range by WHO standards. K was in the range of 1 – 34 mg/l with an average of 4.07 mg/l and well within the permissible limits. Ca was in the range of 19 – 857 mg/l with an average of 124.5 mg/l and within the permissible limits. Mg had a range of 5.77 to 281 mg/l with an average of 65 mg/l and within the permissible limits. SO<sub>4</sub> was from 44 – 4411 mg/l with an average of 459 mg/l, Cl from 7 – 2150 mg/l with an average of 459 mg/l and both are within the permissible limits by WHO standards. HCO<sub>3</sub> was in the range of 58-860 mg/l with an average of 106 mg/l and within the permissible limits. The major cations and anions enter the groundwater due to the sedimentary rocks and the Bela Ophiolite exposed in the study area. Due to the weathering of sedimentary rocks exposed in the area, trace elements enter the water samples. Bela Ophiolite have high Fe, Pb & Zn, and contribute these to the water samples. Major trace metals in the groundwater samples are Aluminum (Al), Arsenic (As), Cadmium (Cd), Chromium (Cr), Cobalt (Ca), Copper (Cu), Iron (Fe), Lead (Pb), Manganese (Mn), Nickel (Ni), Titanium (Ti), and Zinc (Zn). As, Co, & Ti were below the detection limits. Cd was in the range of 0-24 µg/l with an average of 63.4 µg/l and within the permissible limits by WHO standards. Cr is from 0.5 – 114 µg/l with an average of 32.19 µg/l. Cu is from 0.05 -354 µg/l with an average of 64.65 µg/l, and Fe from 19-2116 µg/l, with an average of 328 µg/l. Both Cu and Fe are within the permissible limits by WHO for most of the water sample sites. Mn is from 2-657 µg/l with an average of 95, Ni from 0-412 µg/l, with an average of 113 µg/l, and Ni from 0 – 412 µg/l with an average of 46 µg/l. Both are within the permissible limits by WHO

standards. Pb is from 1.5 – 79  $\mu\text{g/l}$ , with an average of 17.25  $\mu\text{g/l}$ , and is slightly above the permissible limits by WHO. Zn was in the range of 5 – 801  $\mu\text{g/l}$  with an average of 130  $\mu\text{g/l}$ .

3. From the geophysical methods, the water producing zones were identified and their electrical properties determined. The freshwater zones were identified and only pockets of saline water were identified near the surface, which may be due to the dry surface conditions and high evaporation rate typical of a semi-arid region. To confirm the geoelectrical characteristic of the water bearing zones, geochemical analysis for 100 groundwater samples collected from various places in the study area was performed. The distribution of geoelectrical layers for major water bearing zones correlates with the major anions and cations, the results suggest that water bearing zones delineated by the geochemical analysis and electrical resistivity data show that saltwater has not intruded the study area. The groundwater resources are of fresh water and near the surface, saline water is due to arid conditions. From the resistivity data and the lithology logs, five geoelectrical layers comprising of top surficial unconsolidated material, unconsolidated Sand & Gravel, Sand & Clay, water bearing Sand, and Clay layers are identified. The integration of Electrical Resistivity Data and the hydrogeochemical data identified the potential of groundwater zones. The zones are marked from the correlation of TDS and the major water producing geoelectrical layer of the area. Four zones have been identified, very good potential zone with a TDS of less than 500 mg/l and resistivity from 200 to 1500  $\Omega\text{m}$ , good potential zone with a TDS of 501 to 1000 mg/l and resistivity of 100 to 200  $\Omega\text{m}$ , fair potential zone with a TDS of 1001 to 2000 mg/l and resistivity of 20-100  $\Omega\text{m}$ , and poor potential zone with TDS above 2000 mg/l and resistivity less than 20  $\Omega\text{m}$ . Most of the central part of the study area falls in very good to good potential zone. The fair and poor potential zones are limited to the south and southwest of the study area.

## **RECOMMENDATIONS**

The current study has provided the quantitative legend of the area. This legend can be quantified and applied to surrounding semi-arid to arid of the area. This is valid for reservoir modeling and changes in hydrofacies and trend analysis for good water management practices. A detailed study with well log (piezometers) data and the pumping test values should be carried out for the study area. The pumping test data for the study area would give detailed aquifer parameters for further groundwater modelling and monitoring.

With the detail modeling, monitoring and good pumping practices, authorities to ensure the availability of freshwater for the domestic and agricultural uses of the area.

## REFERENCE

- Addison, M. J., Rivett, M. O., Phiri, P., Mleta, P., Mblame, E., Wanangwa, G., & Kalin, R. M. (2020). Predicting groundwater vulnerability to geogenic fluoride risk: A screening method for Malawi and an opportunity for national policy redefinition. *Water*, 12(11), 3123.
- Ahmed, A. M., & Sulaiman, W. N. (2001). Evaluation of groundwater and soil pollution in a landfill area using electrical resistivity imaging survey. *Environmental management*, 28(5), 655-663.
- Ahmed, K., Shahid, S., Demirel, M. C., Nawaz, N., & Khan, N. (2019). The changing characteristics of groundwater sustainability in Pakistan from 2002 to 2016. *Hydrogeology Journal*, 27(7), 2485-2496.
- Ahmed, W., Zeb, M. J., Mahmood, Z., Khan, S., & Waseem, M. (2021). Geoelectrical and magnetic survey of Tatta Pani thermal spring: a case study from Kotli District, Jammu and Kashmir, Pakistan. *Geomechanics and Geophysics for Geo-Energy and Geo-Resources*, 7(2), 1-22.
- Ahsan, S., N., , Malick, K., A. , & Khan, A. (2000). Litho-Microfacies of Loralai Formation, Kharrari Nai Section, Lasbela District Balochistan, Pakistan; . *Karachi Univ. Jour. Science*, , 28(2):-107.
- Ahsanullah. ( 1971). *Report on Landform and Drainage Basins in Karachi Region. Master Plan for Karachi Metropolitan Region, Karachi Development Authority, Karachi.*
- Aizebeokhai, A. P. (2010). 2D and 3D geoelectrical resistivity imaging: Theory and field design. *Scientific Research and Essays*, 5(23), 3592-3605.
- Akaa, M. U., Ekpab, M. M., Okorohb, D. O., Oguamac, B. E., & Ibuota, J. C. (2020). . Investigation Of Stability Of Engineering Projects Using Seismic Refraction Technique. *Geological Behavior (GBR)*, 4(2), 84-88.
- Akbar, F., Khan, G. D., Khan, M. J., Haq, I., Khan, S., & Saleh, A. (2014). Seasonal Variations in Soil Conditions, Its Classification and Mapping of Dry Sub Tropical Region of Uthal, District Lasbela.
- Akhter, G., & Hasan, M. (2016). Determination of aquifer parameters using geoelectrical sounding and pumping test data in Khanewal District, Pakistan. *Open Geosciences*, 8(1), 630-638.
- Alam, K., & Ahmad, N. (2014). Determination of aquifer geometry through geophysical methods: A case study from Quetta Valley, Pakistan. *Acta Geophysica*, 62(1), 142-163.
- Almasri, M. N. (2008). Assessment of intrinsic vulnerability to contamination for Gaza coastal aquifer, Palestine. *Journal of Environmental Management*, 88(4), 577-593.
- Anomohanran, O. (2013). Geoelectrical investigation of groundwater condition in Oleh, Nigeria. *International Journal of Research Reviews in Applied Science*, 15, 145-151.
- Anselin, L., & Getis, A. (1992). Spatial statistical analysis and geographic information

- systems. *The Annals of Regional Science*, 26(1), 19-33.
- Anwar, M. (1991). Revised nomenclature and stratigraphy of Ferozabad, Alozai and Mona Jhal Groups of Balochistan (Axial Belt), Pakistan. *Acta Mineral. Pakistan*, 5, 46-61.
- Aouiti, S., Hamzaoui Azaza, F., El Melki, F., Hamdi, M., Celico, F., & Zammouri, M. (2021). Groundwater quality assessment for different uses using various water quality indices in semi-arid region of central Tunisia. *Environmental Science and Pollution Research*, 28(34), 46669-46691.
- Arsène, M., Wassouo Elvis, B. W., Daniel, G., Théophile, N.-M., Kelian, K., & Daniel, N. J. (2018). Hydrogeophysical investigation for groundwater resources from electrical resistivity tomography and self-potential data in the Méiganga area, adamawa, Cameroon. *International Journal of Geophysics*, 2018.
- Arslan, H., Cemek, B., & Demir, Y. (2012). Determination of seawater intrusion via hydrochemicals and isotopes in Bafra Plain, Turkey. *Water resources management*, 26(13), 3907-3922.
- Asadi, E., Isazadeh, M., Samadianfard, S., Ramli, M. F., Mosavi, A., Nabipour, N., Shamshirband, S., Hajnal, E., & Chau, K.-W. (2019). Groundwater quality assessment for sustainable drinking and irrigation. *Sustainability*, 12(1), 177.
- Atta, M. I., Zehra, S. S., Dai, D.-Q., Ali, H., Naveed, K., Ali, I., Sarwar, M., Ali, B., Iqbal, R., & Bawazeer, S. (2023). Amassing of heavy metals in soils, vegetables and crop plants irrigated with wastewater: Health risk assessment of heavy metals in Dera Ghazi Khan, Punjab, Pakistan. *Frontiers in plant science*, 13, 1080635.
- Baby, S. N. (2012). *The Potential of Open-source Internet GIS as an In-house and Outreach Communication Interface in Regional Environmental Management: Exemplification from Phillip Island*, Victoria Monash University].
- Bahammou, Y. A., Benamara, A., Ammar, A., Hritta, D., Dakir, I., & Bouikbane, H. (2021). Application of vertical electrical sounding resistivity technique to explore groundwater in the Errachidia basin, Morocco. *Groundwater for Sustainable Development*, 15, 100648.
- Bailey, D., & Bilderback, T. (1997). Alkalinity control for irrigation water used in nurseries and greenhouses. *Hort. Info. Lflt*, 558.
- Bajjali, W. (2018). Introduction to GIS. In *ArcGIS for Environmental and Water Issues* (pp. 1-10). Springer.
- Baloch, M., Ames, D., & Tanik, A. (2015). Hydrologic impacts of climate and land-use change on Namnam Stream in Koycegiz Watershed, Turkey. *International Journal of Environmental Science and Technology*, 12(5), 1481-1494.
- Banerjee, P., & Prasad, B. (2020). Determination of concentration of total sodium and potassium in surface and ground water using a flame photometer. *Applied Water Science*, 10(5), 1-7.
- Barcelona, M. J. (1985). *Practical guide for ground-water sampling* (Vol. 600). Robert S. Kerr Environmental Research Laboratory, Office of Research and ....
- Bashir, E., Naseem, S., Akhtar, T., & Shireen, K. (2009). Characteristics of ultramafic rocks and associated magnesite deposits, Nal Area, Khuzdar, Balochistan, Pakistan. *Journal of Geology and Mining Research*, 1(2), 034-041.
- Bashir, E., Shahid, N., & Salma, H. (2007). Hydrogeochemistry of the Winder River and adjoining tributaries, Balochistan, Pakistan. *Chinese Journal of Geochemistry*,

26(3), 259-266.

- Bashir, I., Naseem, S., Nadeem, S., Sheikh, S. A., & Shirin, K. (2004). Petrography, Mineralogy And Geochemistry Of Baran Lak Magnesite And Associated Rocks, Khuzdar, Baluchistan, Pakistan. *Journal Of Himalayan Earth Sciences*, 37.
- Bashir, M. T., Ali, S., & Bashir, A. (2012). Health effects from exposure to sulphates and chlorides in drinking water. *Pakistan Journal of medical and health sciences*, 6(3), 648-652.
- Batayneh, A. T. (2006). Use of electrical resistivity methods for detecting subsurface fresh and saline water and delineating their interfacial configuration: a case study of the eastern Dead Sea coastal aquifers, Jordan. *Hydrogeology Journal*, 14(7), 1277-1283.
- Batayneh, A. T. (2013). The estimation and significance of Dar-Zarrouk parameters in the exploration of quality affecting the Gulf of Aqaba coastal aquifer systems. *Journal of Coastal Conservation*, 17(3), 623-635.
- Bauman, P. (2005). 2-D resistivity surveying for hydrocarbons—A primer. *CSEG Recorder*, 30(4), 25-33.
- Bear, J., Cheng, A. H.-D., Sorek, S., Ouazar, D., & Herrera, I. (1999). *Seawater intrusion in coastal aquifers: concepts, methods and practices* (Vol. 14). Springer Science & Business Media.
- Béjar-Pizarro, M., Guardiola-Albert, C., García-Cárdenas, R. P., Herrera, G., Barra, A., López Molina, A., Tessitore, S., Staller, A., Ortega-Becerril, J. A., & García-García, R. P. (2016). Interpolation of GPS and geological data using InSAR deformation maps: Method and application to land subsidence in the alto guadalentín aquifer (SE Spain). *Remote Sensing*, 8(11), 965.
- Bender, F., K. (1995). Geological Framework” In Bender, F.K. and Raza, H.A. (Eds.). *Geology of Pakistan. Gebruder Borntraeger, Berlin, Germany.*, pp 11-22
- Best, A. G., & Ross, S. L. (1977). *River Pollution Studies*.
- Bhattacharya, P., & Bundschuh, J. (2015). Groundwater for sustainable development-cross cutting the UN sustainable development goals. *Groundwater for Sustainable Development*, 1(1-2), 155-157.
- Bilotta, G. S., & Brazier, R. E. (2008). Understanding the influence of suspended solids on water quality and aquatic biota. *Water research*, 42(12), 2849-2861.
- Bobachev, C. (2002). IPI2Win: A windows software for an automatic interpretation of resistivity sounding data. *Moscow State University*, 320.
- Boothroyd, R. J., Williams, R. D., Hoey, T. B., Barrett, B., & Prasojo, O. A. (2021). Applications of Google Earth Engine in fluvial geomorphology for detecting river channel change. *Wiley Interdisciplinary Reviews: Water*, 8(1), e21496.
- Bosch, M., & McGaughey, J. (2001). Joint inversion of gravity and magnetic data under lithologic constraints. *The Leading Edge*, 20(8), 877-881.
- Bouaroudj, S., Menad, A., Bounamous, A., Ali-Khodja, H., Gherib, A., Weigel, D. E., & Chenchouni, H. (2019). Assessment of water quality at the largest dam in Algeria (Beni Haroun Dam) and effects of irrigation on soil characteristics of agricultural lands. *Chemosphere*, 219, 76-88.
- Brindha, K., Pavelic, P., Sotoukee, T., Douangsavanh, S., & Elango, L. (2017). Geochemical Characteristics and Groundwater Quality in the Vientiane Plain, Laos. *Exposure and Health*, 9(2), 89-104. <https://doi.org/10.1007/s12403-016->

- Burke, F., Hamza, S., Naseem, S., Nawaz-ul-Huda, S., Azam, M., & Khan, I. (2016). Impact of cadmium polluted groundwater on human health: winder, Balochistan. *Sage Open*, 6(1), 2158244016634409.
- Burke, F., Huda, S., Hamza, S., & Azam, M. (2005). Disparities in agricultural productivity in Balochistan-A GIS perspective. *Pakistan Geographical Review*, 60(1), 27-34.
- Byrne, C., Krogager, M., Kragholm, K., Pareek, M., Mohr, G., Ringgren, K., Wissenberg, M., Folke, F., Gislason, G., & Koeber, L. (2022). Association between serum potassium levels and short-term mortality in out-of-hospital cardiac arrest survivors. *European Heart Journal: Acute Cardiovascular Care*, 11(Supplement\_1), zuac041. 082.
- Calvete, J. J., Petras, D., Calderón-Celis, F., Lomonte, B., Encinar, J. R., & Sanz-Medel, A. (2017). Protein-species quantitative venomics: looking through a crystal ball. *Journal of Venomous Animals and Toxins including Tropical Diseases*, 23.
- Canobbio, S., Azzellino, A., Cabrini, R., & Mezzanotte, V. (2013). A multivariate approach to assess habitat integrity in urban streams using benthic macroinvertebrate metrics. *Water science and technology*, 67(12), 2832-2837.
- Cardona, A., Carrillo-Rivera, J., Huizar-Alvarez, R., & Graniel-Castro, E. (2004). Salinization in coastal aquifers of arid zones: an example from Santo Domingo, Baja California Sur, Mexico. *Environmental Geology*, 45(3), 350-366.
- Cardoso, L. H., & Bacellar, L. d. A. P. (2021). Assessment of geoelectrical configurations using reduced physical models for the structural mapping of rock mass and fractured aquifers. *Journal of Applied Geophysics*, 191, 104368.
- Castells, M. (1999). *Information technology, globalization and social development* (Vol. 114). UNRISD Geneva.
- Cataldo, A., Persico, R., Leucci, G., De Benedetto, E., Cannazza, G., Matera, L., & De Giorgi, L. (2014). Time domain reflectometry, ground penetrating radar and electrical resistivity tomography: a comparative analysis of alternative approaches for leak detection in underground pipes. *Ndt & E International*, 62, 14-28.
- Chen, L., Liu, Y., Hu, Z., Gao, S., Zong, K., & Chen, H. (2011). Accurate determinations of fifty-four major and trace elements in carbonate by LA-ICP-MS using normalization strategy of bulk components as 100%. *Chemical Geology*, 284(3-4), 283-295.
- Clesceri, L. s., Greenberg, A. E., & Eaton, A. D. (1988). *Standard methods for examination of water and wastewater*, .
- Cox, D. R., Newton, A. M., & Huuse, M. (2020). An introduction to seismic reflection data: acquisition, processing and interpretation. In *Regional Geology and Tectonics* (pp. 571-603). Elsevier.
- DAR. (2000). *Directorate of agriculture research (DAR) wayaro, Lasbela*
- Das, S., & Nag, S. (2015). Deciphering groundwater quality for irrigation and domestic purposes—a case study in Suri I and II blocks, Birbhum District, West Bengal, India. *Journal of earth system science*, 124(5), 965-992.
- Davraz, A., & Batur, B. (2021). Hydrogeochemistry characteristics of groundwater and health risk assessment in Yalvaç–Gelendost basin (Turkey). *Applied Water Science*, 11(4), 1-21.

- DCR. (2017). *District Census Report of Lasbela, Government of Pakistan* <https://www.pbs.gov.pk/content/final-results-census-2017>
- DeJong, K. A., & Subhani, A. (1979). Note on the Bela ophiolites with special reference to the Kanar area. *Geodynamics of Pakistan*, 263-269.
- Dong, D., Zhao, X., Hua, X., Liu, J., & Gao, M. (2009). Investigation of the potential mobility of Pb, Cd and Cr (VI) from moderately contaminated farmland soil to groundwater in Northeast, China. *Journal of Hazardous Materials*, 162(2-3), 1261-1268.
- Dronova, I., Kislik, C., Dinh, Z., & Kelly, M. (2021). A review of unoccupied aerial vehicle use in wetland applications: Emerging opportunities in approach, technology, and data. *Drones*, 5(2), 45.
- Ebong, E. D., Akpan, A. E., Emeka, C. N., & Urang, J. G. (2017). Groundwater quality assessment using geoelectrical and geochemical approaches: case study of Abi area, southeastern Nigeria. *Applied Water Science*, 7(5), 2463-2478.
- Ebraheem, A. A. M., Senosy, M. M., & Dahab, K. A. (1997). Geoelectrical and Hydrogeochemical studies for delineating ground-water contamination due to salt-water intrusion in the northern part of the Nile Delta, Egypt. *Groundwater*, 35(2), 216-222.
- Edmunds, W. M. (2012). Limits to the availability of groundwater in Africa. *Environmental Research Letters*, 7(2), 021003.
- Edwards, L. (1977). A modified pseudosection for resistivity and IP. *Geophysics*, 42(5), 1020-1036.
- Ekwok, S. E., Akpan, A. E., Kudamnya, E. A., & Ebong, E. D. (2020). Assessment of groundwater potential using geophysical data: a case study in parts of Cross River State, south-eastern Nigeria. *Applied Water Science*, 10(6), 1-17.
- Elbarbary, S., Araffa, S. A., El-Shahat, A., Zaher, M. A., & Khedher, K. M. (2021). Delineation of water potentiality areas at Wadi El-Arish, Sinai, Egypt, using hydrological and geophysical techniques. *Journal of African Earth Sciences*, 174, 104056.
- Essa, K. S., Mehane, S. A., Soliman, K. S., & Diab, Z. E. (2020). Gravity profile interpretation using the R-parameter imaging technique with application to ore exploration. *Ore Geology Reviews*, 126, 103695.
- Fajana, A. O. (2021). Geohazard characterization of subsurface materials using integrated geophysical methods for post foundation studies: a case study. *Modeling Earth Systems and Environment*, 7(1), 403-415.
- Farid, A., Khan, G., Khan, M., Abdul, R., & Muhammad, H. (2014). Geochemical classification of groundwater quality and its mapping in a dry sub climate (a case study of Lasbela Region). *Journal of Environment and Earth Science*, 4(7), 50-54.
- Farid, H. U., Mahmood-Khan, Z., Ali, A., Mubeen, M., & Anjum, M. N. (2017). Site-Specific Aquifer Characterization and Identification of Potential Groundwater Areas in Pakistan. *Polish Journal of Environmental Studies*, 26(1).
- Faryadi, Q. (2012). The magnificent effect of magnesium to human health: a critical review. *International Journal of Applied*, 2(3), 118-126.
- Fatmi, A., Hyderi, I., & Anwar, M. (1990). Occurrence of the Lower Jurassic Ammonoid genus *Bouleiceras* from the surghar range with a revised nomenclature of the Mesozoic Rocks of the Salt Range and Trans Indus Ranges (Upper Indus Basin).



- Geological Bulletin Punjab University*, 25, 38-46.
- Fatmi, A., & Rawson, P. F. (1993). The first Early Cretaceous ammonite faunas from Baluchistan. *Cretaceous research*, 14(1), 91-100.
- Fetter, C. W. (2001). *Applied Hydrogeology Fetter Fourth Edition*.
- Fitriani, R., Muhammad, J., & Rini, A. S. (2020). Investigation of the distribution of aquifers and groundwater quality in the Village of Rimbo Panjang, Kampar District. *Science, Technology & Communication Journal*, 1(1), 8-15.
- Frassetto, L., Morris Jr, R. C., & Sebastian, A. (1997). Potassium bicarbonate reduces urinary nitrogen excretion in postmenopausal women. *The Journal of Clinical Endocrinology & Metabolism*, 82(1), 254-259.
- Friedman, N. (2004). Inferring cellular networks using probabilistic graphical models. *Science*, 303(5659), 799-805.
- Frohlich, R. K., & Urish, D. W. (2002). The use of geoelectrics and test wells for the assessment of groundwater quality of a coastal industrial site. *Journal of Applied Geophysics*, 50(3), 261-278.
- Fulai, L., Ma, W., Meng, F., & Diao, H. (2021). Geochemical characteristics and geological significance of Daohugou Formation at Ningcheng County of Inner Mongolia, Eastern China. *Geological Journal*, 56(4), 2223-2239.
- Gao, Q., Shang, Y., Hasan, M., Jin, W., & Yang, P. (2018). Evaluation of a weathered rock aquifer using ERT method in South Guangdong, China. *Water*, 10(3), 293.
- Garofalo, F., Foti, S., Hollender, F., Bard, P., Cornou, C., Cox, B. R., Ohrnberger, M., Sicilia, D., Asten, M., & Di Giulio, G. (2016). InterPACIFIC project: Comparison of invasive and non-invasive methods for seismic site characterization. Part I: Intra-comparison of surface wave methods. *Soil Dynamics and Earthquake Engineering*, 82, 222-240.
- Ghani, M., Atif, M., Saeed, M., RASHEED, M. U., Abbas, S. A., Jan, I. U., Sami, M., & AZIZ, M. M. (2022). Geo-electrical sounding for subsurface lithological investigation and modeling for groundwater exploration in Sheikhmanda Kili region, Northern Quetta, Pakistan. *HIMALAYAN GEOLOGY*, 43(1 A), 40-50.
- Ghoraba, S. M. (2015). Hydrological modeling of the Simly Dam watershed (Pakistan) using GIS and SWAT model. *Alexandria Engineering Journal*, 54(3), 583-594.
- Gnos, E., Khan, M., Mahmood, K., Khan, A. S., Shafique, N. A., & Villa, I. M. (1998). Bela oceanic lithosphere assemblage and its relation to the Reunion hotspot. *Terra Nova-Oxford*, 10(2), 90-95.
- Gopalakrishnan, T., Kumar, L., & Mikunthan, T. (2020). Assessment of spatial and temporal trend of groundwater salinity in Jaffna Peninsula and its link to paddy land abandonment. *Sustainability*, 12(9), 3681.
- Gorgoglione, A., Bombardelli, F. A., Pitton, B. J., Oki, L. R., Haver, D. L., & Young, T. M. (2018). Role of sediments in insecticide runoff from urban surfaces: Analysis and modeling. *International journal of environmental research and public health*, 15(7), 1464.
- Gorgoglione, A., Gioia, A., & Iacobellis, V. (2019). A framework for assessing modeling performance and effects of rainfall-catchment-drainage characteristics on nutrient urban runoff in poorly gauged watersheds. *Sustainability*, 11(18), 4933.
- Gupta, N. K. (2021). Progresses in Solar Still Technology with Phase Change Material. IOP Conference Series: Materials Science and Engineering,

- Gupta, P. K., Gupta, P., & Gupta, P. (2007). *Methods in environmental analysis: water, soil and air*. Agrobios Jodhpur, India.
- Haghnazar, H., Johannesson, K. H., González-Pinzón, R., Pourakbar, M., Aghayani, E., Rajabi, A., & Hashemi, A. A. (2022). Groundwater geochemistry, quality, and pollution of the largest lake basin in the Middle East: Comparison of PMF and PCA-MLR receptor models and application of the source-oriented HHRA approach. *Chemosphere*, 288, 132489.
- Haiyan, L., Gao, D., Wu, J., Zhao, D., & Zhang, L. (2021). Determination method of water gushing runoff zones in the open pit mining area. *Bulletin of Engineering Geology and the Environment*, 80(5), 3953-3971.
- Hamdan, H. A., & Vafidis, A. (2013). Joint inversion of 2D resistivity and seismic travel time data to image saltwater intrusion over karstic areas. *Environmental Earth Sciences*, 68(7), 1877-1885.
- Hamza, S. (2011). *The Influence of Ophiolitic and Sedimentary Rocks on Cultivated and Wild Vegetation of Winder Agriculture Farms, Balochistan, Pakistan*.
- Hamza, S. (2019). *Spatial Analysis of Groundwater Quality of Uthal (Balochistan) with reference to Pb* (NRPU#5250).
- Haq, F., Naeem, U. A., Gabriel, H. F., Khan, N. M., Ahmad, I., Rehman, H. U., & Zafar, M. A. (2021). Impact of Urbanization on Groundwater Levels in Rawalpindi City, Pakistan. *Pure and Applied Geophysics*, 178(2), 491-500.
- Hasan, M., Shang, Y., Akhter, G., & Jin, W. (2018). Geophysical assessment of groundwater potential: a case study from Mian Channu Area, Pakistan. *Groundwater*, 56(5), 783-796.
- Hasan, M., Shang, Y., Akhter, G., & Khan, M. (2017). Geophysical investigation of fresh-saline water interface: A case study from South Punjab, Pakistan. *Groundwater*, 55(6), 841-856.
- Hasan, M., Shang, Y., Jin, W., Shao, P., Yi, X., & Akhter, G. (2020). Geophysical Assessment of Seawater Intrusion into Coastal Aquifers of Bela Plain, Pakistan. *Water*, 12(12), 3408.
- He, F. J., & MacGregor, G. A. (2008). Beneficial effects of potassium on human health. *Physiologia plantarum*, 133(4), 725-735.
- Henriet, J. (1976). Direct applications of the Dar Zarrouk parameters in ground water surveys. *Geophysical prospecting*, 24(2), 344-353.
- Hinze, W. J. (1990). The role of gravity and magnetic methods in engineering and environmental studies. In *Geotechnical and Environmental Geophysics: Volume I: Review and Tutorial* (pp. 75-126). Society of Exploration Geophysicists.
- HSC. (1960). Reconnaissance Geology of part of West Pakistan, a Colombo Plan cooperative project. *Hunting Survey Corporation, Government of Canada, Toronto*.
- Huda, S. N. U., & Burke, F. (2012). *Social and economic inequality and Sindh and Balochistan: A welfare theme in geography*. LAP LAMBERT Academic Publishing.
- Hunt, A. (2021). Soil formation, vegetation growth, and water balance: A theory for Budyko. *Hydrogeology, chemical weathering, and soil formation*, 67-80.
- Hussain, Y., Ullah, S. F., Akhter, G., & Aslam, A. Q. (2017). Groundwater quality evaluation by electrical resistivity method for optimized tubewell site selection in

- an ago-stressed Thal Doab Aquifer in Pakistan. *Modeling Earth Systems and Environment*, 3(1), 1-9.
- Islami, N., Irianti, M., Fakhrudin, F., Azhar, A., & Nor, M. (2020). Application of geoelectrical resistivity method for the assessment of shallow aquifer quality in landfill areas. *Environmental Monitoring and Assessment*, 192(9), 1-16.
- Jayeoba, A., & Oladunjoye, M. A. (2015). 2-D electrical resistivity tomography for groundwater exploration in hard rock terrain. *International Journal of Science and Technology*, 4(4), 156-163.
- Jha, M. K., Shekhar, A., & Jenifer, M. A. (2020). Assessing groundwater quality for drinking water supply using hybrid fuzzy-GIS-based water quality index. *Water Research*, 179, 115867.
- Jiang, W., Sheng, Y., Liu, H., Ma, Z., Song, Y., Liu, F., & Chen, S. (2022). Groundwater quality assessment and hydrogeochemical processes in typical watersheds in Zhangjiakou region, northern China. *Environmental Science and Pollution Research*, 29(3), 3521-3539. <https://doi.org/10.1007/s11356-021-15644-1>
- JICA, J. I. C. A. (1987). *Report of Coperative mineral exploration in Khuzdar area of Balochistan*.
- Jorstad, L., Jankowski, J., & Acworth, R. (2004). Analysis of the distribution of inorganic constituents in a landfill leachate-contaminated aquifer: Astrolabe Park, Sydney, Australia. *Environmental Geology*, 46(2), 263-272.
- Juanah, M. S., Ibrahim, S., Sulaiman, W. N. A., & Latif, P. A. (2013). Groundwater resources assessment using integrated geophysical techniques in the southwestern region of Peninsular Malaysia. *Arabian Journal of Geosciences*, 6(11), 4129-4144.
- Kabata-Pendias, A. (2010). *Trace Elements in Soils and Plants*. CRC Press.
- Kachholz, F., & Tränckner, J. (2021). A model-based tool for assessing the impact of land use change scenarios on flood risk in small-scale river systems—part 1: Pre-processing of scenario based flood characteristics for the current state of land use. *Hydrology*, 8(3), 102.
- Kadri, I. (1995). *Petroleum Geology of Pakistan: sedimentary basins and their evolution*. Pakistan Petroleum Limited, 32, 965.
- Kahlowan, M. A., & Majeed, A. (2003). Water-resources situation in Pakistan: challenges and future strategies. *Water Resources in the South: present scenario and future prospects*, 20, 33-45.
- Kazmi, A. H., & Jan, M. Q. (1997). *Geology and tectonics of Pakistan*. Graphic publishers.
- Kazmi, I. A., AH Abbasi. (2008). *Stratigraphy and Historical Geology of Pakistan*. Published by Department and National Centre of Excellence in Geology, University of Peshawar, Pakistan, 524p.
- Khair, S. M., Mushtaq, S., Culas, R. J., & Hafeez, M. (2012). Groundwater markets under the water scarcity and declining watertable conditions: The upland Balochistan Region of Pakistan. *Agricultural Systems*, 107, 21-32.
- Khair, S. M., Mushtaq, S., & Reardon-Smith, K. (2015). Groundwater Governance in a Water-Starved Country: Public Policy, Farmers' Perceptions, and Drivers of Tubewell Adoption in Balochistan, Pakistan. *Groundwater*, 53(4), 626-637.
- Khan, M., Gnos, E., Mahmood, K., & Khan, A. (1999). The metamorphic rocks associated with the Bela Ophiolite. *Acta Mineralogica Pakistanica*, 10, 37-44.
- Khan, S. (2019). Climate classification of Pakistan. *International Journal of Economic and*

- Environmental Geology*, 10(2), 60-71.
- Khan, S., Rana, T., Gabriel, H., & Ullah, M. K. (2008). Hydrogeologic assessment of escalating groundwater exploitation in the Indus Basin, Pakistan. *Hydrogeology Journal*, 16(8), 1635-1654.
- Kleine, D., & Unwin, T. (2009). Technological revolution, evolution and new dependencies: What's new about ICT4D? *Third World Quarterly*, 30(5), 1045-1067.
- Kliengchuay, W., Worakhunpiset, S., Limpanont, Y., Meeyai, A. C., & Tantrakarnapa, K. (2021). Influence of the meteorological conditions and some pollutants on PM10 concentrations in Lamphun, Thailand. *Journal of Environmental Health Science and Engineering*, 19(1), 237-249.
- Kmet, L. M., Cook, L. S., & Lee, R. C. (2004). Standard quality assessment criteria for evaluating primary research papers from a variety of fields.
- Kozmutza, C., & Picó, Y. (2009). To address accuracy and precision using methods from analytical chemistry and computational physics. *Environmental monitoring and assessment*, 151, 59-75.
- Kubier, A., Wilkin, R. T., & Pichler, T. (2019). Cadmium in soils and groundwater: a review. *Applied Geochemistry*, 108, 104388.
- Kut, K. M. K., Sarswat, A., Bundschuh, J., & Mohan, D. (2019). Water as key to the sustainable development goals of South Sudan—a water quality assessment of eastern Equatoria state. *Groundwater for Sustainable Development*, 8, 255-270.
- Legault, J. M. (2015). Airborne electromagnetic systems—state of the art and future directions. *CSEG Recorder*, 40(6), 38-49.
- Leghouchi, E., Laib, E., & Guerbet, M. (2009). Evaluation of chromium contamination in water, sediment and vegetation caused by the tannery of Jijel (Algeria): a case study. *Environmental monitoring and assessment*, 153(1), 111-117.
- Liu, X., Wang, X., Wright, G., Cheng, J. C., Li, X., & Liu, R. (2017). A state-of-the-art review on the integration of Building Information Modeling (BIM) and Geographic Information System (GIS). *ISPRS International Journal of Geo-Information*, 6(2), 53.
- Loke, M., Chambers, J., Rucker, D., Kuras, O., & Wilkinson, P. (2013). Recent developments in the direct-current geoelectrical imaging method. *Journal of applied geophysics*, 95, 135-156.
- Madrid, Y., & Zayas, Z. P. (2007). Water sampling: Traditional methods and new approaches in water sampling strategy. *TrAC Trends in Analytical Chemistry*, 26(4), 293-299.
- Maillet, R. (1947). The fundamental equations of electrical prospecting. *Geophysics*, 12(4), 529-556.
- Malkani, M. S. (2015). Stratigraphy, mineral potential, geological history and paleobiogeography of Balochistan Province, Pakistan. *Sindh University Research Journal-SURJ (Science Series)*, 43(2).
- Malkani, M. S. (2020). Revised stratigraphy and mineral resources of Balochistan Basin, Pakistan: An update. *Open Journal of Geology*, 10(07), 784.
- Maqsood, H., Ahmed, S., & Ahmed, S. (2013). Assessment of weather indicators for possible climate change. *Environmentally sustainable development (ESDev)*. Abbottabad, Pakistan.

- Marschner, H. (1995). Mineral nutrition of higher plants 2nd edn. *Institute of Plant Nutrition University of Hohenheim: Germany*.
- Mathivanan, M., Sabarathinam, C., Viswanathan, P. M., Senapathi, V., Nadesan, D., Indrani, G. G., Malaimengu, G., & Kumar, S. S. (2022). Mobilization and health risk assessment of fertilizer induced uranium in coastal groundwater. *Environmental research*, 203, 111791.
- Mehmood, Qaisar Mahmood, W., Awais, M., Rashid, H., Rizwan, M., Anjum, L., Muneer, M. A., Niaz, Y., & Hamid, S. (2020a). Optimizing groundwater quality exploration for irrigation water wells using geophysical technique in semi-arid irrigated area of Pakistan. *Groundwater for Sustainable Development*, 11, 100397.
- Mehmood, Zahid, Khan, N. M., Sadiq, S., Mandokhail, S.-u. J., & Ashiq, S. Z. (2020b). Assessment of subsurface lithology, groundwater depth, and quality of UET Lahore, Pakistan, using electrical resistivity method. *Arabian Journal of Geosciences*, 13(6), 1-7.
- Mertzanides, Y., Tsakmakis, I., Kargiotis, E., & Sylaios, G. (2020). Electrical resistivity tomography for spatiotemporal variations of soil moisture in a precision irrigation experiment. *International Agrophysics*, 34(3).
- Mitasova, H., Drake, T. G., Bernstein, D., & Harmon, R. S. (2004). Quantifying rapid changes in coastal topography using modern mapping techniques and geographic information system. *Environmental & Engineering Geoscience*, 10(1), 1-11.
- Mohamaden, M., Hamouda, A., & Mansour, S. (2016). Application of electrical resistivity method for groundwater exploration at the Moghra area, Western Desert, Egypt. *The Egyptian Journal of Aquatic Research*, 42(3), 261-268.
- Mokoena, P., Manyama, K., van Bever Donker, J., & Kanyerere, T. (2021). Investigation of groundwater salinity using geophysical and geochemical approaches: heuningnes catchment coastal aquifer. Western Cape Province, South Africa. *Environmental Earth Sciences*, 80(5), 1-18.
- Mondal, N., Singh, V., & Ahmed, S. (2013). Delineating shallow saline groundwater zones from Southern India using geophysical indicators. *Environmental monitoring and assessment*, 185(6), 4869-4886.
- Mostafa, M., Anwar, M. B., & Radwan, A. (2018). Application of electrical resistivity measurement as quality control test for calcareous soil. *HBRC journal*, 14(3), 379-384.
- Mostafa, M. G., Uddin, S., & Haque, A. (2017). Assessment of hydro-geochemistry and groundwater quality of Rajshahi City in Bangladesh. *Applied Water Science*, 7(8), 4663-4671.
- Mouratidis, I., Dimopoulos, G., Astaras, T., & Savvidis, S. (2010). Sustainable water resources management through the use of GIS technologies. *Global NEST Journal*, 12(2), 140-151.
- Mthembu, P. P., Elumalai, V., Senthilkumar, M., & Wu, J. (2021). Investigation of Geochemical Characterization and Groundwater Quality with Special Emphasis on Health Risk Assessment in Alluvial Aquifers, South Africa. *International Journal of Environmental Science and Technology*, 18(12), 3711-3730. <https://doi.org/10.1007/s13762-021-03129-0>
- Muchingami, I., Hlatywayo, D., Nel, J., & Chuma, C. (2012). Electrical resistivity survey for groundwater investigations and shallow subsurface evaluation of the basaltic-

- greenstone formation of the urban Bulawayo aquifer. *Physics and Chemistry of the Earth, Parts A/B/C*, 50, 44-51.
- Murdoch, P. S., Baron, J. S., & Miller, T. L. (2000). POTENTIAL EFFECTS OF CLIMATE CHANGE ON SURFACE-WATER QUALITY IN NORTH AMERICA 1. *JAWRA Journal of the American Water Resources Association*, 36(2), 347-366.
- Mussett, A. E., & Khan, M. A. (2000). *Looking into the earth: an introduction to geological geophysics*. Cambridge University Press.
- Mustafa, D., & Qazi, M. U. (2007). Transition from karez to tubewell irrigation: development, modernization, and social capital in Balochistan, Pakistan. *World Development*, 35(10), 1796-1813.
- Mustafa, N., Ashraf, A., Ahmad, B., Iqbal, B., & Naz, R. (2013). Spate irrigation potential and distribution of watersheds of rodkahi areas of Pakistan using geoinformatics. *Research Desk*, 2(4), 300-316.
- Nakamura, Y., Watanabe, H., Tanaka, A., Yasui, M., Nishihira, J., & Murayama, N. (2020). Effect of increased daily water intake and hydration on health in Japanese adults. *Nutrients*, 12(4), 1191.
- Narejo, A. A., Shar, A. M., Fatima, N., & Sohail, K. (2019). Geochemistry and origin of Mn deposits in the Bela ophiolite complex, Balochistan, Pakistan. *Journal of Petroleum Exploration and Production Technology*, 9(4), 2543-2554.
- Naseem, S. (1996). Genesis of manganese ore deposits Of Lasbela area, Balochistan Pakistan.
- Naseem, S., Hamza, S., & Bashir, E. (2010). Groundwater Geochemistry of Winder Agricultural Farms, Balochistan, Pakistan and Assessment for Irrigation Water Quality.
- Naseem, S., Hamza, S., & Bashir, E. (2012). Assessment of geochemistry of soils for agriculture at Winder, Balochistan, Pakistan. *Water quality, soil and managing irrigation of crops, InTech-Open Access Publisher, Croatia*, 73-94.
- Naseem, S., Hamza, S., Bashir, E., & Ahmed, S. (2005). Distribution of Mn in the fruits and wild flora of Winder area, Balochistan, Pakistan and its impact on Human Health. *Editorial Advisory Board e*, 18(4), 689-699.
- Naseem, S., Hamza, S., Bashir, E., Tajnees, P., & Talpur, M. M. A. (2013). Trace element geochemistry of groundwater of Winder, Balochistan, Pakistan and its appraisal for irrigation water quality. *British Journal of Applied Science and Technology*, 3(1), 182-198.
- Naseem, S., Hamza, S., Nawaz-ul-Huda, S., & Bashir, E. (2014). Geochemistry of Cd in groundwater of Winder, Balochistan and suspected health problems. *Environmental Earth Sciences*, 71(4), 1683-1690.
- Nielsen, D. M., & Nielsen, G. (2006). *The essential handbook of ground-water sampling*. CRC Press.
- Ntengwe, F. (2006). Pollutant loads and water quality in streams of heavily populated and industrialised towns. *Physics and Chemistry of the Earth, Parts A/B/C*, 31(15-16), 832-839.
- Obiefuna, G., & Sheriff, A. (2011). Assessment of shallow ground water quality of Pindiga Gombe Area, Yola Area, NE, Nigeria for irrigation and domestic purposes. *Research Journal of Environmental and Earth Sciences*, 3(2), 131-141.

- Oh, H.-J., Kim, Y.-S., Choi, J.-K., Park, E., & Lee, S. (2011). GIS mapping of regional probabilistic groundwater potential in the area of Pohang City, Korea. *Journal of Hydrology*, 399(3-4), 158-172.
- Oldham, R. D. (1892). Report on the Geology of Thal-Chotli and part of the Mari country. *Records of Geological Survey of India*, 25, 18-29.
- Pal, A., Pal, M., Mukherjee, P., Bagchi, A., & Raha, A. (2018). Determination of the hardness of drinking packaged water of Kalyani area, West Bengal. *Asian Journal of Pharmacy and Pharmacology*, 4(2), 203-206.
- Palacky, G. (1987). Clay mapping using electromagnetic methods. *First Break*, 5(8).
- Patel, S., Park, H., Bonato, P., Chan, L., & Rodgers, M. (2012). A review of wearable sensors and systems with application in rehabilitation. *Journal of neuroengineering and rehabilitation*, 9(1), 1-17.
- Paul, M., Negahban-Azar, M., Shirmohammadi, A., & Montas, H. (2020). Assessment of agricultural land suitability for irrigation with reclaimed water using geospatial multi-criteria decision analysis. *Agricultural Water Management*, 231, 105987.
- Peña-Arancibia, J. L., Stewart, J. P., & Kirby, J. M. (2021). Water balance trends in irrigated canal commands and its implications for sustainable water management in Pakistan: Evidence from 1981 to 2012. *Agricultural Water Management*, 245, 106648.
- Piper, A. M. (1944). A graphic procedure in the geochemical interpretation of water-analyses. *Eos, Transactions American Geophysical Union*, 25(6), 914-928.
- Pla, J. M., Ghiglieri, G., & Uras, G. (2014). Seawater intrusion and coastal groundwater resources management. Examples from two Mediterranean regions: Catalonia and Sardinia. *Contributions to science*, 171-184.
- Prasad, B., & Narayana, T. (2004). Subsurface water quality of different sampling stations with some selected parameters at Machilipatnam Town.
- Priou, J., Lecieux, Y., Chevreuil, M., Gaillard, V., Lupi, C., Leduc, D., Rozière, E., Guyard, R., & Schoefs, F. (2019). In situ DC electrical resistivity mapping performed in a reinforced concrete wharf using embedded sensors. *Construction and Building Materials*, 211, 244-260.
- Qadeer, R. (2004). Pollutants in drinking water: Their sources, harmful effects and removal procedures. *Journal of the Chemical Society of Pakistan*, 26(3), 293-327.
- Qureshi, A. S. (2018). Challenges and opportunities of groundwater management in Pakistan. *Groundwater of South Asia*, 735-757.
- Rahman, A.-u. (1996). Groundwater as source of contamination for water supply in rapidly growing megacities of Asia: Case of Karachi, Pakistan. *Water Science and Technology*, 34(7-8), 285-292.
- Rahman, M. M., & Woobaidullah, A. S. M. (2020). Groundwater resources exploration in a Hillock Valley at Lada refugee camp, Teknaf using electrical resistivity soundings. *Arabian Journal of Geosciences*, 13(2), 1-9.
- Randhir, T. (2012). Water for Life and Ecosystem Sustainability. *J Earth Sci Climate Change* 3: e107. doi: 10.4172/2157-7617.1000 e107 Page 2 of 2 Volume 3• Issue 1• 1000e107 J Earth Sci Climate Change ISSN: 2157-7617 JESCC, an open access journal 4. Postel S, Richter BD (2003) Rivers for life: Managing Water for People and Nature. In: Island Press: Washington, DC.
- Rashid, M. u., Ahmad, W., Zeb, M. J., Haider, N., Khan, A., & Khan, S. (2019).

- Determination of Underground Structure and Migration of Hot Plumes Contaminating Fresh Water Using Vertical Electrical Survey (VES) and Magnetic Survey, A Case Study of Tattapani Thermal Spring, Azad Kashmir. *International Journal of Economic and Environmental Geology*, 10(1), 84-92.
- Ray, R. K., & Mukherjee, R. (2008). Reproducing the piper trilinear diagram in rectangular coordinates. *Groundwater*, 46(6), 893-896.
- Reedman, J. (2012). *Techniques in mineral exploration*. Springer Science & Business Media.
- Rehman, F., Harbi, H. M., Azeem, T., Naseem, A. A., Ullah, M. F., ur Rehman, S., Riaz, O., & Abuelnaga, H. S. (2021). Shallow geophysical and hydrological investigations to identify groundwater contamination in Wadi Bani Malik dam area Jeddah, Saudi Arabia. *Open Geosciences*, 13(1), 272-279.
- Rekapalli, R., Sarma, V., & Phukon, P. (2015). Direct resistivity measurements of core sample using a portable in-situ DC resistivity meter in comparison with HERT data. *Journal of the Geological Society of India*, 86(2), 211-214.
- Riveros-Perez, E., & Riveros, R. (2018). Water in the human body: An anesthesiologist's perspective on the connection between physicochemical properties of water and physiologic relevance. *Annals of medicine and surgery*, 26, 1-8.
- Robinson, E. S. (1988). Basic exploration geophysics.
- Rusydi, A. F. (2018). Correlation between conductivity and total dissolved solid in various type of water: A review. IOP conference series: earth and environmental science, Safdar, H., Amin, A., Shafiq, Y., Ali, A., Yasin, R., Shoukat, A., Hussan, M. U., & Sarwar, M. I. (2019). A review: Impact of salinity on plant growth. *Nat. Sci*, 17(1), 34-40.
- Sajid, F., Musa, K. B., & Syed, A. A. (2012). Water pollution: Major issue in urban areas. *International journal of water resources and environmental engineering*, 4(3), 55-65.
- Samouëlian, A., Cousin, I., Tabbagh, A., Bruand, A., & Richard, G. (2005). Electrical resistivity survey in soil science: a review. *Soil and Tillage research*, 83(2), 173-193.
- Sarwar, G. (1992). Tectonic setting of the Bela Ophiolites, southern Pakistan. *Tectonophysics*, 207(3-4), 359-381.
- Schmutz, M., Ghorbani, A., Vaudelet, P., & Blondel, A. (2014). Cable arrangement to reduce electromagnetic coupling effects in spectral-induced polarization studies. *Geophysics*, 79(2), A1-A5.
- Shah, S. (2009). Stratigraphy of Pakistan (memoirs of the geological survey of Pakistan). *The Geological Survey of Pakistan*, 22.
- Shailaja, G., Kadam, A., Gupta, G., Umrikar, B., & Pawar, N. (2019). Integrated geophysical, geospatial and multiple-criteria decision analysis techniques for delineation of groundwater potential zones in a semi-arid hard-rock aquifer in Maharashtra, India. *Hydrogeology Journal*, 27(2), 639-654.
- Sharma, P. V. (1997). *Environmental and engineering geophysics*. Cambridge university press.
- Sharma, S., & Baranwal, V. (2005). Delineation of groundwater-bearing fracture zones in a hard rock area integrating very low frequency electromagnetic and resistivity data. *Journal of Applied Geophysics*, 57(2), 155-166.
- Sherif, M., El Mahmoudi, A., Garamoon, H., Kacimov, A., Akram, S., Ebraheem, A., &



- Shetty, A. (2006). Geoelectrical and hydrogeochemical studies for delineating seawater intrusion in the outlet of Wadi Ham, UAE. *Environmental geology*, 49(4), 536-551.
- Sikandar, P., Bakhsh, A., Ali, T., & Arshad, M. (2010). Vertical electrical sounding (VES) resistivity survey technique to explore low salinity groundwater for tubewell installation in Chaj Doab. *Journal of Agricultural Research (03681157)*, 48(4).
- Singh, S. K., Bharose, R., Nemčić-Jurec, J., Rawat, K. S., & Singh, D. (2021). Irrigation water quality appraisal using statistical methods and WATEQ4F geochemical model. In *Agricultural Water Management* (pp. 101-138). Elsevier.
- Singh, U., Das, R., & Hodlur, G. (2004). Significance of Dar-Zarrouk parameters in the exploration of quality affected coastal aquifer systems. *Environmental Geology*, 45(5), 696-702.
- Singha, S. S., Pasupuleti, S., Singha, S., Singh, R., & Venkatesh, A. (2019). A GIS-based modified DRASTIC approach for geospatial modeling of groundwater vulnerability and pollution risk mapping in Korba district, Central India. *Environmental Earth Sciences*, 78(21), 1-19.
- Smith, R. A., Schwarz, G. E., & Alexander, R. B. (1997). Regional interpretation of water-quality monitoring data. *Water resources research*, 33(12), 2781-2798.
- Soetan, K. O., Olaiya, C. O., & Oyewole, O. E. (2010). The importance of mineral elements for humans, domestic animals and plants-A review. *African journal of food science*, 4(5), 200-222.
- Stanly, R., Yasala, S., Oliver, D. H., Nair, N., Emperumal, K., & Subash, A. (2021). Hydrochemical appraisal of groundwater quality for drinking and irrigation: a case study in parts of southwest coast of Tamil Nadu, India. *Applied Water Science*, 11(3), 1-20.
- Stiff, H. A. (1951). The interpretation of chemical water analysis by means of patterns. *Journal of petroleum technology*, 3(10), 15-13.
- Stollar, R. L., & Roux, P. (1975). Earth Resistivity Surveys—A Method for Defining Ground-Water Contamination a. *Groundwater*, 13(2), 145-150.
- Storz, H., Storz, W., & Jacobs, F. (2000). Electrical resistivity tomography to investigate geological structures of the earth's upper crust. *Geophysical prospecting*, 48(3), 455-472.
- Sun, Q., Jackson, C. A., Magee, C., & Xie, X. (2020). Deeply buried ancient volcanoes control hydrocarbon migration in the South China Sea. *Basin Research*, 32(1), 146-162.
- Swigart, J., Heo, J., & Wolf, D. (2021). Soil contamination assessments from drilling fluids and produced water using combined field and laboratory investigations: A case study of Arkansas, USA. *International Journal of Environmental Research and Public Health*, 18(5), 2421.
- Tarussov, A., Vandry, M., & De La Haza, A. (2013). Condition assessment of concrete structures using a new analysis method: Ground-penetrating radar computer-assisted visual interpretation. *Construction and Building Materials*, 38, 1246-1254.
- Telford, W. M., Telford, W., Geldart, L., & Sheriff, R. E. (1990). *Applied geophysics*. Cambridge university press.
- Tiwari, A. K., Suozzi, E., Fiorucci, A., & Lo Russo, S. (2021). Assessment of groundwater geochemistry and human health risk of an intensively cropped alluvial plain, NW

- Italy. *Human and Ecological Risk Assessment: An International Journal*, 27(3), 825-845.
- Todd, D. K., & Mays, L. W. (2004). *Groundwater hydrology*. John Wiley & Sons.
- Tooth, S. (2015). Google Earth as a resource. *Geography*, 100(1), 51-56.
- Valley, S. (2009). Groundwater availability of the Central Valley aquifer, California. *US Geological Survey professional paper*.
- Van Calster, B., Wynants, L., Riley, R. D., van Smeden, M., & Collins, G. S. (2021). Methodology over metrics: current scientific standards are a disservice to patients and society. *Journal of Clinical Epidemiology*, 138, 219-226.
- Van Steenberg, F. (1995). The frontier problem in incipient groundwater management regimes in Balochistan (Pakistan). *Human ecology*, 23(1), 53-74.
- Van Steenberg, F. (1996). Land, water and ethnicity: social organization and resource management in irrigated communities in Balochistan. In: Karachi: Oxford University Press.
- Van Steenberg, F., Kaisarani, A. B., Khan, N. U., & Gohar, M. S. (2015). A case of groundwater depletion in Balochistan, Pakistan: Enter into the void. *Journal of Hydrology: Regional Studies*, 4, 36-47.
- Vasantry, B. M., Bhaskarrao, P. J., Mukund, B. A., Baburao, G. R., & Narayan, P. S. (2017). Comparative study of Wenner and Schlumberger electrical resistivity method for groundwater investigation: a case study from Dhule district (MS), India. *Applied Water Science*, 7(8), 4321-4340.
- Viles, H. (2016). Technology and geomorphology: Are improvements in data collection techniques transforming geomorphic science? *Geomorphology*, 270, 121-133.
- Vine, F. J., & Kearey, P. (1990). *Global tectonics*. Blackwell.
- Vredenburg, E. W. (1909). *Report on the Geology of Sarawan, Jhalawan, Mekran and the State of Las Bela, Considered Principally from the Point of View of Economic Development*. Geological survey of India.
- Wada, Y., Van Beek, L. P., Van Kempen, C. M., Reckman, J. W., Vasak, S., & Bierkens, M. F. (2010). Global depletion of groundwater resources. *Geophysical research letters*, 37(20).
- Wandrey, C. J., Law, B., & Shah, H. A. (2004). *Sembar Goru/Ghazij composite total petroleum system, Indus and Sulaiman-Kirthar geologic provinces, Pakistan and India*. US Department of the Interior, US Geological Survey Reston, VA, USA.
- Watto, M. A., Muger, A. W., Kingwell, R., & Saqab, M. M. (2018). Re-thinking the unimpeded tube-well growth under the depleting groundwater resources in the Punjab, Pakistan. *Hydrogeology Journal*, 26(7), 2411-2425.
- Wesch, C., Elert, A. M., Wörner, M., Braun, U., Klein, R., & Paulus, M. (2017). Assuring quality in microplastic monitoring: About the value of clean-air devices as essentials for verified data. *Scientific Reports*, 7(1), 1-8.
- WHO. (2017). World Health Organization Guidelines for drinking-water quality: first addendum to the fourth edition.
- WHO. (2022). *Guidelines for drinking-water quality: incorporating the first and second addenda*. World Health Organization.
- Williams, M. D. (1959). 19. Stratigraphy of the Lower Indus Basin, West Pakistan. 5th World petroleum congress,
- Wilson, S., Ingham, M., & McConchie, J. (2006). The applicability of earth resistivity

- methods for saline interface definition. *Journal of hydrology*, 316(1-4), 301-312.
- Woodward, J. (1959). Stratigraphy of the jurassic system, Indus Basin. Stand. *Vacuum Oil Co*, 2-13.
- Xiao, Y., Hao, Q., Zhang, Y., Zhu, Y., Yin, S., Qin, L., & Li, X. (2022). Investigating sources, driving forces and potential health risks of nitrate and fluoride in groundwater of a typical alluvial fan plain. *Science of the Total Environment*, 802, 149909.
- Yang, Q., Wang, C., & Zeng, T. (2021). A method of water change monitoring in remote image time series based on long short time memory. *Remote Sensing Letters*, 12(1), 30-39.
- Zarroca, M., Bach, J., Linares, R., & Pellicer, X. M. (2011). Electrical methods (VES and ERT) for identifying, mapping and monitoring different saline domains in a coastal plain region (Alt Empordà, Northern Spain). *Journal of Hydrology*, 409(1-2), 407-422.
- Zhang , M, Y., Wang, W. Y., & Xiong, S. Q. (2020a). Research on the vertical recognition ability of gravity and magnetic data of point (line) source model with given survey accuracy. *Chinese Journal of Geophysics*, 63(11), 4220-4231.
- Zhang, Qiying, Xu, P., & Qian, H. (2020c). Groundwater quality assessment using improved water quality index (WQI) and human health risk (HHR) evaluation in a semi-arid region of northwest China. *Exposure and health*, 12(3), 487-500.
- Zhang, C. (2007). *Fundamentals of environmental sampling and analysis*. John Wiley & Sons.
- Zhang, C., Quan, J., Liu, Z., Xu, Z., Pang, X., & Zhang, Y. (2019). Geochemical characteristics and geological significance of meta-volcanic rocks of the Bainaimiao Group, Sonid Right Banner, Inner Mongolia, China. *Journal of Earth Science*, 30(2), 272-285.
- Zhang , J., Zeng, Z., Zhao, X., Li, J., Zhou, Y., & Gong, M. (2020b). Deep mineral exploration of the Jinchuan Cu–Ni sulfide deposit based on aeromagnetic, gravity, and CSAMT methods. *Minerals*, 10(2), 168.
- Zhang, J., Zhou, J., Zhou, Y., Zeng, Y., Ji, Y., Sun, Y., & Lei, M. (2021). Hydrogeochemical characteristics and groundwater quality assessment in the plain area of Yarkant River Basin in Xinjiang, PR China. *Environmental Science and Pollution Research*, 28(24), 31704-31716.
- Zhao, M., Liu, X., & Sun, Z. (2021). Development of decision support tool for clustering urban regional risk based on R-ArcGIS Bridge. *Applied Soft Computing*, 110, 107621.
- Zhou, Y., Li, P., Xue, L., Dong, Z., & Li, D. (2020). Solute geochemistry and groundwater quality for drinking and irrigation purposes: a case study in Xinle City, North China. *Geochemistry*, 80(4), 125609.
- Zohdy, A. A. (1989). A new method for the automatic interpretation of Schlumberger and Wenner sounding curves. *Geophysics*, 54(2), 245-253.

